Bulletin
of
The Geological Society of America

VOLUME 61 June 1950 NUMBER 6

CONTENTS

Pages

Conjugate sets of en echelon tension fractures in the Athens limestone at Riverton, Virginia. By Vincent E. Shainin 509–518

Genesis of some Adirondack garnet deposits. By S. Benedict Levin 519–566

Flow of heat in the Front Range, Colorado. By Francis Birch 567–630

Index to Volume 60 (January–June) 631–634

Subscription $15 per year.

Publication Office: Mt. Royal & Guilford Aves., Baltimore 2, Md.

Communications for publication should be addressed to The Geological Society of America, Dr. H. R. Aldrich, Secretary, 419 West 117th Street, New York 27, N. Y.

NOTICE.—Four weeks notice of change of address is necessary. In accordance with the rules established by the Council, claims for non-receipt of the preceding number of the Bulletin must be sent to the Secretary of the Society within three months of the date of the receipt of this number in order to be filled gratis.

Entered as second-class matter in the Post-Office at Baltimore, Md., under the Act of Congress of July 16, 1894.

Accepted for mailing at special rate of postage provided for in Section 1103 Act of October 3, 1917, authorized on July 8, 1918.

PAPERS IN PRESS FOR FORTHCOMING ISSUES

STUDIES OF HEAVY DETRITAL MINERALS. By C. Osborne Hutton

Separates of this paper will be available at 75 cents per copy. Remittance should accompany order.

TECTONIC SCARPS AND FAULT VALLEYS. By C. A. Cotton

COMPARISON OF FIELD AND LABORATORY MEASUREMENTS OF SEISMIC VELOCITIES IN SEDIMENTARY ROCKS By Charles W. Oliphant

STRATIGRAPHY AND STRUCTURE OF THE OAK HILL SUCCESSION IN VERMONT. By Verne H. Booth

VARIATION OF ELASTIC MODULI OF IGNEOUS ROCKS WITH PRESSURE AND TEMPERATURE. By D. S. Hughes and H. J. Jones

ORIGIN OF THE FILLED-SINK STRUCTURES AND CIRCLE DEPOSITS OF MISSOURI. By J Harlen Bretz

AIRBORNE MAGNETOMETER AND GEOLOGICAL RECONNAISSANCE SURVEY IN NORTHWESTERN MAINE. By Patrick M. Hurley and James B. Thompson

BULLETIN OF THE GEOLOGICAL SOCIETY OF AMERICA
VOL. 61, PP. 509–517, 8 FIGS., 2 PLS. JUNE 1950

CONJUGATE SETS OF EN ECHELON TENSION FRACTURES IN THE ATHENS LIMESTONE AT RIVERTON, VIRGINIA

By Vincent E. Shainin

CONTENTS

	Page
Abstract	509
Introduction	509
Problem	509
Method of field study and acknowledgments	510
Belts of en echelon fractures and their geological setting	510
Strain axes	513
Third dimension	513
Orientation of axes	514
General statement	514
Local strain axes in limestone containing en echelon fractures	514
Regional, overall axes of strain	515
Analysis of stresses	515
Anomalous curvature of fractures	516
Description	516
Riedel's experiment	516
Discussion	516
References cited	516

ILLUSTRATIONS

Figure	Page
1. Conjugate shear planes and conjugate rows of en echelon tension fractures	510
2. Index map showing location of Riverton	511
3. Geological map and sections of the northern part of Riverton, Virginia	512
4. Trends of rows of en echelon tension fractures at Riverton	513
5. Tension fractures showing two forms of curvature	513
6. Block diagram of Riverton showing mutual relations of structural features	514
7. Rectangular cement prism compressed in Daubrée's experiment	515
8. Origin of "anomalous" curvature in en echelon fractures	516

Plate	Facing page
1. Rows of en echelon tension fractures in Athens limestone	514
2. Rows of en echelon tension fractures in Athens limestone	515

Abstract

At Riverton, Virginia, in the Athens limestone are conjugate sets of en echelon tension fractures which demonstrate that division of the strained rock mass into wedge-shaped units precedes shearing.

The lower Ordovician argillaceous Athens limestone at Riverton, Virginia, exhibits pinnate tension fractures aligned, en echelon, in fairly straight rows. Some rows contain as many as 50 fractures. The rows of conjugate sets trend east-west and northwest-southeast. The shearing couple origin of echelon fractures suggests that the trend of each row may be considered as the trace of a plane of incipient shearing. Some shear fractures parallel the trend of a row. The direction of greatest shortening (the greatest stress axis) bisects the acute angle between the conjugate incipient shear planes.

The axis of elongation of the incipient shear planes is essentially horizontal, while the axis of elongation of the folds and thrust faults of the area is essentially vertical. However, the axes of shortening practically coincide, which suggests that the direction of greatest stress was essentially the same.

Two hypotheses are advanced: (1) There were two periods of compressive stress, each accompanied by a different direction of elongation. A modification of this hypothesis postulates that the similarity in orientation of the least strain axes at Riverton is a local coincidence and that a regional survey might show a change in the direction of these axes. (2) As in the deformation of a prism in Daubrée's classic experiment, two sets of conjugate shears developed simultaneously as the result of one compressive stress. Direction of elongation for one set of shears, however, was normal to that for the other.

Introduction

Problem

En echelon tension fractures have been described many times (Hurst, 1942; Sherrill, 1929; Cloos, 1932; Lopez, 1942; Riedel, 1929; Lagally, 1929; Chamberlain, 1919; Foley, 1926;

Hancock, 1918 and others). Abundant experimental evidence, supported by field observations, shows that such fractures are formed by a shearing motion in which the opposing forces

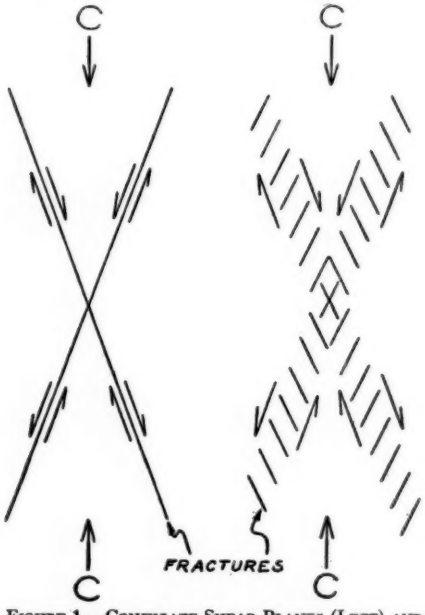

FIGURE 1.—CONJUGATE SHEAR PLANES (LEFT) AND CONJUGATE ROWS OF EN ECHELON FRACTURES (RIGHT)
C = direction of compression.

produce a rotational strain, causing tensional rupture normal to the direction of maximum elongation (Fig. 1).

Joints that formed as a result of shearing have also been studied in great detail, and many intersecting shear joints have been described. However, the writer knows of no description of conjugate sets of en echelon tension fractures.

The Lower Ordovician Athens limestone in the Folded Appalachians near Riverton, Virginia (Fig. 2), contains numerous belts of en echelon, calcite-filled tension fractures aligned in two intersecting directions similar to the pattern formed by conjugate shear planes (Fig. 1; Pl. 1). When the belts of fractures are plotted on a geologic map (Fig. 3) their orientation, with reference to the fold axes, simulates that expected for conjugate shear planes.

The belts of en echelon tension fractures are the traces of planes of shearing strain, and the existence of such belts is noteworthy *per se*, because it shows that the division of the strained rock mass into wedge-shaped units precedes actual shearing. In some instances a shear fracture, parallel to and within the belt, has offset the tension fractures. The surfaces of shearing are vertical and their traces on the topographic surface are from an inch to 3 feet long. The shears are not uncommon; typical ones are shown in Plates 1 and 2.

Method of Field Study and Acknowledgments

A total of 4 weeks were spent in the field in 1942 and 1943. A base map of the area, on a scale of 200 feet to the inch (Fig. 3), was prepared from a mosaic of aerial photographs having a scale of approximately 500 feet to the inch. The geologic data were mapped by chain and compass traverses.

Mr. Edward I. Williams, president of the Riverton Lime and Stone Co., Inc., has kindly permitted publication of geological information collected by the writer while serving the company in the field. An outline of the structural geology of Riverton has been published (Shainin, 1943). The writer owes a debt of gratitude to Professor Walter H. Bucher, who gave a great deal of helpful discussion, criticism, and advice in the preparation of the manuscript. Professors Robert Balk, Marland P. Billings, Joseph M. Trefethen, Weston S. Evans, and Hamilton Gray, have provided numerous helpful suggestions. Mrs. Patricia S. Clabaugh, of the U. S. Geological Survey, discussed many details of the manuscript with the writer, and she is responsible for numerous improvements. Not all of the critics named are in complete agreement with the interpretations of the writer, who accepts full responsibility for the views presented here.

William Bell and Raymond Santmeyers assisted in the field, and Mr. E. L. Cameron assisted in the photography.

BELTS OF EN ECHELON FRACTURES AND THEIR GEOLOGIC SETTING

Riverton, Virginia, is underlain by strongly folded and faulted Paleozoic sediments. The

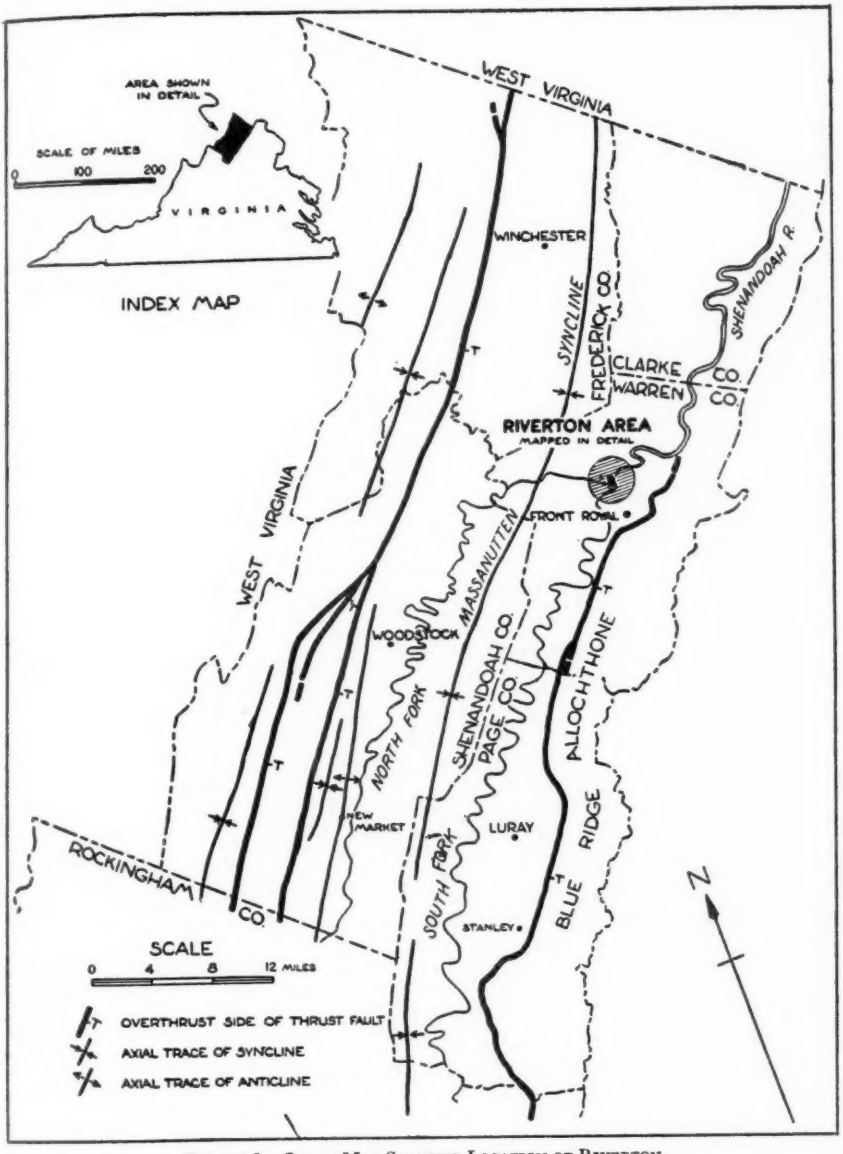

FIGURE 2.—INDEX MAP SHOWING LOCATION OF RIVERTON

Appalachian Revolution, to which the major structures of the area owe their origin, occurred at the close of the Paleozoic era and produced crustal shortening from southeast to northwest. Riverton lies on the southeast limb of the Massenutten syncline, about 3 miles west of the northern end of the Blue Ridge thrust fault (Fig. 2).

The sets of tension fractures, are found in the Athens formation, a fine-grained, black,

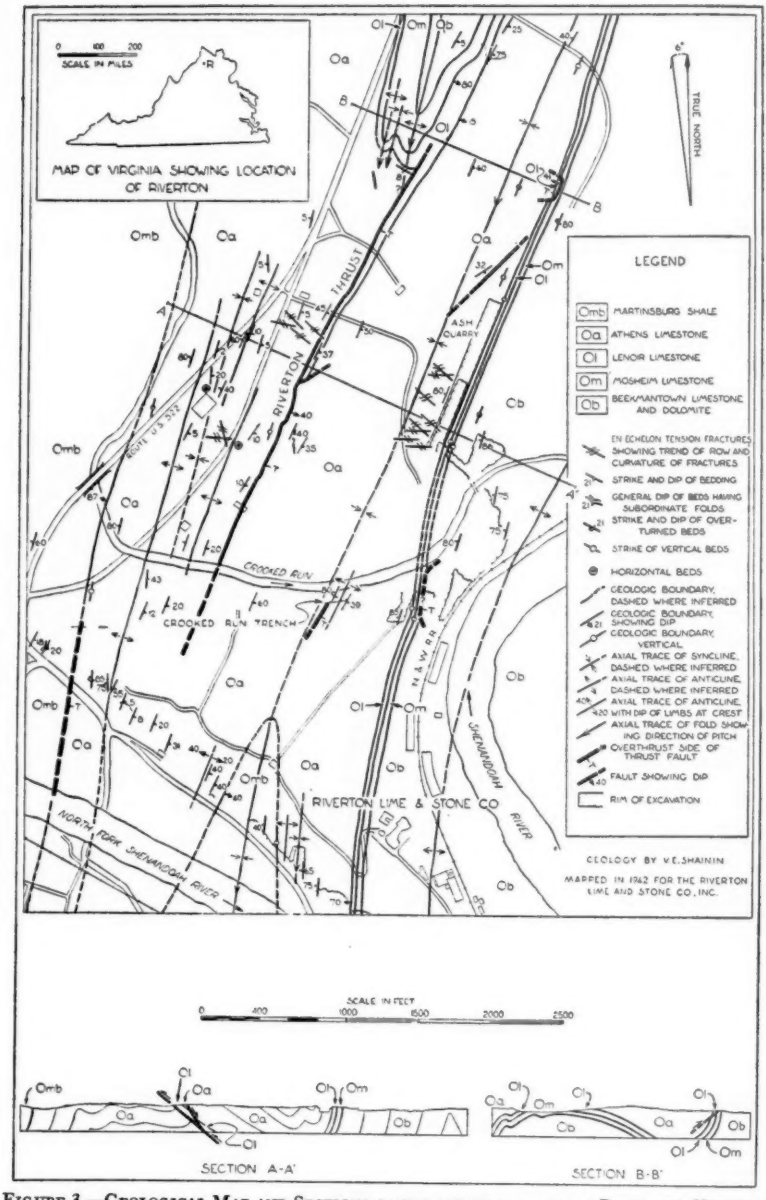
MAP OF VIRGINIA SHOWING LOCATION OF RIVERTON
SCALE IN MILES
TRUE NORTH
LEGEND
Omb MARTINSBURG SHALE
Oa ATHENS LIMESTONE
Ol LENOIR LIMESTONE
Om MOSHEIM LIMESTONE
Ob BEEKMANTOWN LIMESTONE AND DOLOMITE
EN ECHELON TENSION FRACTURES SHOWING TREND OF ROW AND CURVATURE OF FRACTURES
STRIKE AND DIP OF BEDDING
GENERAL DIP OF BEDS HAVING SUBORDINATE FOLDS
STRIKE AND DIP OF OVERTURNED BEDS
STRIKE OF VERTICAL BEDS
HORIZONTAL BEDS
GEOLOGIC BOUNDARY, DASHED WHERE INFERRED
GEOLOGIC BOUNDARY, SHOWING DIP
GEOLOGIC BOUNDARY, VERTICAL
AXIAL TRACE OF SYNCLINE, DASHED WHERE INFERRED
AXIAL TRACE OF ANTICLINE, DASHED WHERE INFERRED
AXIAL TRACE OF ANTICLINE, WITH DIP OF LIMBS AT CREST
AXIAL TRACE OF FOLD SHOWING DIRECTION OF PITCH
OVERTHRUST SIDE OF THRUST FAULT
FAULT SHOWING DIP
RIM OF EXCAVATION
RIVERTON THRUST
ASH QUARRY
CROOKED RUN
CROOKED RUN TRENCH
RIVERTON LIME & STONE CO
SHENANDOAH RIVER
NORTH FORK SHENANDOAH RIVER
GEOLOGY BY V.E. SHAININ
MAPPED IN 1942 FOR THE RIVERTON LIME AND STONE CO., INC.
SCALE IN FEET
SECTION A-A'
SECTION B-B'

FIGURE 3.—GEOLOGICAL MAP AND SECTIONS OF THE NORTHERN PART OF RIVERTON, VIRGINIA

thin-bedded limestone, interbedded with brown or gray shale. The fractures cut layers of high calcium content, 1–10 inches thick, and also the less common, and usually thinner, argillaceous beds.

As many as 50 or more fractures occur in

fairly straight belts (Pl. 1). Sixty-six belts were chosen at random. Trends fall into two groups: east-west and northwest-southeast (Fig. 4); the angle between the groups averages about 40°.

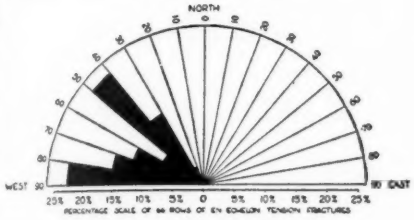

FIGURE 4.—TRENDS OF ROWS OF EN ECHELON TENSION FRACTURES AT RIVERTON

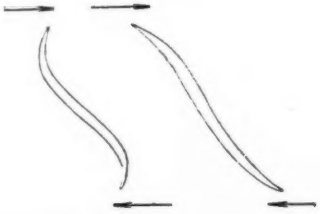

FIGURE 5.—TENSION FRACTURES SHOWING TWO FORMS OF CURVATURE

The majority of the fractures in the Riverton area are similar in form to the fracture on the right, i.e., they are curved at the ends in directions opposite from those that would result from the action of frictional drag.

The individual fractures are from half an inch to 7 inches long, and up to 2 inches wide. Most of them are filled with calcite, and some show vugs along the middle of the calcite-filling. The majority are curved at the ends in directions opposite from those that would result from the action of frictional drag (Fig. 5; Pl. 2, fig. 2). The fractures are essentially vertical (for a detailed discussion of their attitude, see "Strain Axes; Third Dimension"). Although five formations composed of chemical and detrital sediments make up the stratigraphic column in the Riverton area, the tension fractures were observed only in the Athens limestone. This localization may be due to certain physical characteristics of the rocks, the detailed study of which is beyond the scope of this paper. Partial chemical analyses of the Athens limestone are listed in Table 1.

The other formations mapped in the Riverton area (Fig. 3), are also Ordovician. The overlying Martinsburg formation is a fine-grained, arenaceous, graptolitic shale. The underlying rocks, progressively older, include the Lenoir, a very coarse-grained, gray-black carbonaceous limestone; the Mosheim, a fine-grained dove-colored limestone; and the Beekmantown formation, composed of fine- to medium-grained limestone and dolomite.

TABLE 1. PARTIAL ANALYSES OF ATHENS LIMESTONE*

Sample No.	SiO_2	Iron Oxides and Al_2O_3	CaO	MgO	Loss on Ignition	Total
1	17.94	6.50	40.04	1.58	33.41	99.46
2	15.66	6.04	41.64	1.48	34.56	99.38
3	18.46	7.64	38.94	2.26	32.13	99.43
4	20.74	7.32	37.74	1.64	31.93	99.37
5	15.04	6.34	40.86	2.46	34.88	99.58
6	15.04	6.60	41.06	1.96	35.00	99.66
7	16.26	7.40	39.48	2.18	34.10	99.42
8	15.36	7.52	40.06	1.70	34.88	99.52
9	13.40	5.72	42.74	1.70	35.87	99.43
10	13.60	5.32	42.94	1.62	35.82	99.30
11	16.08	6.86	39.26	2.84	34.39	99.43
12	12.92	5.88	42.14	2.42	36.04	99.40
13	10.64	4.88	43.44	2.76	37.63	99.35
14	6.34	3.18	47.52	2.36	39.00	99.40

* Each analysis represents a composite sample taken for a distance of 10 feet across strike. Analyses by E. L. Cameron.

The conjugate rows of en echelon fractures were observed only in the area covered by the map in Figure 3, although large areas of Warren, Page, Shenandoah and Frederick counties were examined in reconnaissance mapping.

STRAIN AXES

Third Dimension

In Riverton no difficulty is encountered in obtaining a satisfactory three-dimensional picture of the attitude in space of the thrust faults and folds. However, satisfactory three-dimensional measurements of the planes of shearing strain (along which the en echelon fractures occur) are lacking in most cases. The rows of tension fractures at Riverton usually occur on flat, low-lying outcrops of the Athens

limestone, flush with the ground, which is, in most cases, practically horizontal. It is usually impossible to obtain a three-dimensional view of the fractured zone, but in practically every instance in which a vertical section through

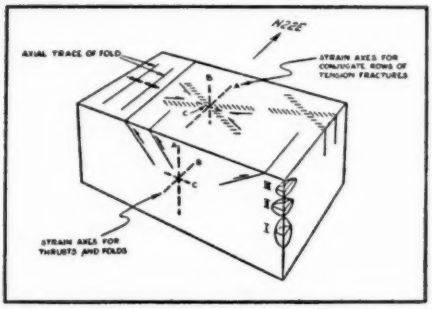

FIGURE 6.—BLOCK DIAGRAM OF RIVERTON SHOWING MUTUAL RELATIONS OF STRUCTURAL FEATURES

Figures I, II and III show forms assumed by triaxial strain ellipsoid for points at center of block (I), just below the surface (II) and on the surface of the block (III).

Scale of rows of tension fractures is exaggerated. A = Greatest strain axis. B = Intermediate strain axis. C = Least strain axis.

the zone of fracturing does occur, the fractures appear as vertical surfaces that strike in the direction of their traces at the surface (Fig. 6). Exceptions undoubtedly exist, which make postulations as to the precise orientation of the principal strain axes in space inaccurate. Actually the size of the observed angle in the horizontal plane would vary inversely with deviation of the planes of shearing strain from the vertical. As a result the size of the observed angle described here must be regarded as a minimum. It will be assumed, however, that the zones of shearing strain are practically vertical planes, and that the conclusions are based on close approximations of the true strain axes. References made to the horizontal or vertical attitude of axes should be understood as meaning "essentially" horizontal, or "essentially" vertical. While this inaccurate three-dimensional picture makes precise calculations impossible, it permits important qualitative observations on various phases of the deformation.

Orientation of Axes

General statement.—The orientation of the strain axes of the planes of shearing strain differs from that of the strain axes of the folds and thrust faults in that the direction of elongation in the former case is essentially horizontal, while in the latter it is essentially vertical. However, the direction of shortening practically coincides in the two orientations (Fig. 6).

Local strain axes in limestone containing en echelon fractures.—A total of 66 belts of tension fractures were studied, and their trends plotted (Fig. 4).

The planes of shearing strain vary widely in strike, but (1) the majority fall into two groups with strikes of N40°–50°W and N80°–90°W; (2) the acute angle between the conjugate sets invariably faces the direction of greatest shortening (the least strain axis and axis of maximum compressive stress). Without exception, the rows of fractures are aligned so that the components of differential movement are directed toward the vertex of the acute angle and away from the vertex of the obtuse angle (Figs. 1, 6). In most cases the actual direction of movement along the shear planes is not visible, since the shearing surfaces are seldom exposed.

The principal strain axes for these rows of fractures are oriented with the direction of shortening (least strain axis or C), and the direction of elongation (greatest strain axis or A) in the horizontal plane, and the intermediate strain axis (mean strain axis or B) in the vertical plane (Fig. 6).

PLATE 1.—ROWS OF EN ECHELON TENSION FRACTURES IN ATHENS LIMESTONE

FIGURE 1. LOOKING NORTH 31° WEST

Note slight "anomalous" curvature.

FIGURE 2. LOOKING NORTH 10° WEST

Note slight offset of calcite-filled fractures along a shear parallel to the row in right center.

FIGURE 3. LOOKING SOUTH 60° EAST

FIGURE 4. LOOKING NORTH 40° WEST

Note slight offset of fractures along shear parallel to trend of row.

FIGURE 1

FIGURE 2

FIGURE 3

FIGURE 4

ROWS OF EN ECHELON TENSION FRACTURES IN ATHENS LIMESTONE

FIGURE 1

FIGURE 2

FIGURE 3

ROWS OF EN ECHELON TENSION FRACTURES IN ATHENS LIMESTONE

Regional, overall axes of strain.—In the case of the folds and thrusts of the Riverton area, while the direction of greatest shortening was practically identical with the shortest strain axis of the incipient shear planes (en echelon belts), the direction of greatest elongation (A axis) was vertical and the intermediate strain axis (B axis) horizontal. Inclined conjugate shear planes (thrust faults) with their line of intersection in the horizontal plane, parallel to B, were formed (Fig. 6).

The planes of shearing in which elongation is vertical may be recognized in the following thrust faults of the area (Fig. 3):

(1) The Riverton thrust, shown on the geological map, strikes N25E and dips about 40° SE.
(2) The small thrust bounded by tear faults northeast of Ash Quarry strikes N20E and dips about 40°NW.
(3) Imbricate thrust fault structure exposed in the face of Crooked Run Trench shows seven small thrusts, all dipping SE. The surface of only one fault is exposed; it strikes N40E and dips 40° SE.

Figure 3 also shows the local fold axes. Although these folds have moderate, even steep pitches, the average pitch of folds in the Riverton area is about 5° toward the southwest.[1]

Analysis of Stresses

Parker (1942) has described essentially vertical conjugate shear joints in the northern Folded Appalachians in which, locally, the direction of shortening coincides with that of folds in the vicinity. In one place the axis of elongation for the joints is horizontal, parallel to the axial traces of the folds, while elongation is vertical in the case of the folds. Tracing the same sets of conjugate joints over a large area, however, shows a regional swing of the joints independent of the folding. Parker believes that the jointing occurred before the folding and that any relation in orientation between the two is a local coincidence.

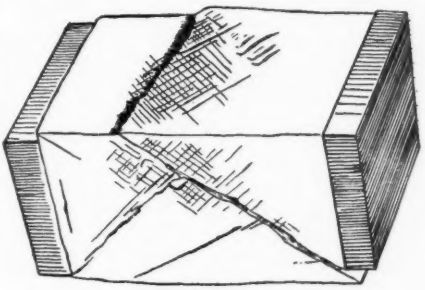

Figure 7.—Rectangular Cement Prism Compressed in Daubrée's Experiment

Compression was from left and right. Note fracture pattern on surface of block. Drawing by Joe Hoare, provided through courtesy of Professor W. H. Bucher.

Such may be true at Riverton; the similarity in orientation of the strain axes for the conjugate rows of en echelon fractures and the strain axes for the folds and thrusts may be purely coincidental, and these features may have been formed by two compressive forces active at different geologic times.

A second hypothesis postulates one period of compression during which local horizontal release may have been responsible for the horizontal direction of elongation attending formation of the fracture belts.

An experiment by Daubrée (1879) (Fig. 7)

[1] Because of this pitch, the A strain axis pitches approximately 85° to the northeast and the B axis 5° southwest. This deviation from the true vertical and horizontal, however, is probably not in excess of any deviation to be expected in the case of the shear planes' axes. It is quite possible, in fact, that if the latter axes do "tilt" away from the ideal vertical and horizontal positions, they tilt in the same direction as the fold and thrust axes.

Plate 2.—Rows of En Echelon Tension Fractures in Athens Limestone

Figure 1. En Echelon Tension Fractures, Looking Due East

Note offset of some fractures along shear parallel to and within the row.

Figure 2. Rows of En Echelon Tension Fractures Showing Anomalous Curvature Looking South 73° West

Figure 3. Small, Secondary Fractures Adjacent to the Second and Third Tension Fractures from the Bottom

Coalescence at a later stage may produce "anomalous" curvature. Note vug in center of lowermost fracture. Looking North 78° East.

suggests that more than one orientation of strain axes may be present in a deformed block as the result of a single compressive force. Bucher (Personal communication) analysed the deformation of Daubrée's block and recognized two main types of fractures:

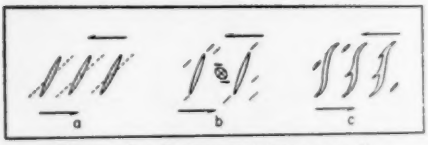

FIGURE 8.—ORIGIN OF "ANOMALOUS" CURVATURE IN EN ECHELON FRACTURES

After Bucher and Riedel. Drawn by Patricia Sutton Clabaugh. a. Gaping of the fractures as the result of rotation. Dashed lines represent original position of the fractures. b. Formation of secondary fractures, as the result of new strain set-up within rhombs between primary fractures. c. Coalescence of primary and secondary fractures.

(1) large-scale conjugate shear planes. (2) small-scale conjugate shear planes, with the direction of elongation normal to that of the first set.

A comparison of Figure 6 with Figure 7 shows the similarity in orientation and relative magnitude of fractures at Riverton and in Daubrée's experiment. (The size of the rows of tension fractures in Figure 6 is exaggerated.)

ANOMALOUS CURVATURE OF FRACTURES

Description

Many of the tension gashes at Riverton are curved fractures, and in the majority of cases the ends of the gashes curve toward the direction from which the movement occurred. This curvature is the antithesis of that which should form as a function of normal frictional drag, and for that reason has been here called anomalous. The following hypothesis is suggested to explain its origin.

Riedel's Experiment

Riedel (1929) covered two adjacent boards with a layer of especially prepared clay and watched the development of strain and rupture therein when the two boards were moved in opposite directions. En echelon tension fractures formed on the surface of a wedge-shaped zone above the contract, making angles of 45° to 47° with the line of displacement between the two boards (Fig. 8a). As the displacement between the boards increased the fractures were accordingly rotated, so that they eventually made angles of up to 60° with the direction of motion. At about this, time, according to Riedel, along the margins of the zone new fractures were formed, at the original angle of 45° to 47° to the direction of motion (Fig. 8b). Ultimately the entire zone became a mass of jumbled blocks.

Discussion

The part of Riedel's experiment which deals with the formation of secondary fractures is pertinent to the problem of "anomalous" curvature in the tension fractures at Riverton. The writer discussed Riedel's experiment with Professor Bucher who analyzed the stress-strain relationship as follows (Personal communication): After the tension fractures have come into existence, the entire stress-strain relationship changes; each individual rhomb between adjacent fractures reacts as a unit to the movement still in progress. This motion tends to rotate the fractures and also to create a new strain set-up within any individual rhomb, whereby zones of tension and the resulting fractures make approximately the same angle with the line of displacement as in the original rupture. Several such tension gashes at angles to each other would run together and eventually have the appearance of regular tension fractures curving in the "wrong" direction, as do those at Riverton (Fig. 8c).

The lack of this anomalous curvature along some of the belts of fractures can only be explained as due to less total movement, or greater resistance to rupture of those particular zones. In other words, only primary fractures were formed, which would exhibit normal frictional drag curvature if never supplemented by the secondary gashes (Fig. 5).

REFERENCES CITED

Bucher, Walter H. (1921) *The mechanical interpretation of joints*, Jour. Geol., vol. 28, no. 8, p. 707–730.

Chamberlain, R. T. (1919) *A peculiar belt of oblique faulting*, Jour. Geol., vol. 27, no. 8, p. 602–613.

Cloos, E. (1932) *"Feather" joints as indicators of the direction of movements on faults, thrusts, joints and magmatic contacts*, Nat. Acad. Sci., Pr., vol. 18, p. 387–395.

Daubrée, A. (1897) *Études synthétiques de géologie experimentale*, Paris.

Foley, L. L. (1926) *The origin of the faults in Creek and Osage counties, Oklahoma*, Am., Assoc. Petrol. Geol., Bull., vol. 10, no. 3, p. 293–303.

Hancock, E. T. (1918) *Geology and oil and gas prospects of the Lake Basin field, Montana*, U. S. Geol. Survey, Bull., 691, p. 101–147.

Hurst, M. E. (1942) *Gold Deposits at Porcupine, Ontario; Ore Deposits as Related to Structural Features*, Princeton Univ. Press, p. 196–199.

Lagally, M. (1929) *Versuch einer Theorie der Spaltenbildung in Gletschern*, Zeitschr. f. Gletscherkunde, vol. 17, p. 285–301.

Lopez, V. M. (1942) *Chuquicamata, Chile; Ore Deposits as Related to Structural Features*, Princeton Univ. Press, p. 126–128.

Parker, J. M. III (1942) *Regional systematic jointing in slightly deformed sedimentary rocks*. Geol. Soc. Am., Bull., vol. 53, no. 3, p. 381–408.

Riedel, W. (1929) *Zur Mechanik geologischer Brucherscheinungen* (*Ein Beitrag zum Problem der Fiederspalten*), Centralblatt für Mineralogie, Geologie und Palaontologie, Abteilung B. Jahrgang 1929, p. 354–368.

Shainin, V. E. (1943) *New application of en echelon tension fractures to geological stress-strain analysis* (Abstract), Geol. Soc. Am., Bull., vol. 54, p. 1826–1827.

Sherrill, R. E. (1929) *Origin of the en echelon faults in north central Oklahoma*, Am. Assoc. Petrol. Geol., Bull., vol. 13, p. 31.

UNIVERSITY OF MAINE, ORONO, MAINE

Manuscript received by the Secretary of the Society, April 21, 1949

BULLETIN OF THE GEOLOGICAL SOCIETY OF AMERICA
VOL. 61, PP. 519-565, 2 PLS., 20 FIGS. JUNE 1950

GENESIS OF SOME ADIRONDACK GARNET DEPOSITS

By S. Benedict Levin

CONTENTS

	Page
Abstract	520
Introduction	520
Acknowledgments	521
Regional geologic setting	521
Geologic column	521
Anorthosite and gabbro	521
Syenite and granite	523
Habitat of the garnet	523
Habit of the garnet	524
Local setting of the Barton deposit	525
Location and geologic setting	525
Local structure	525
Garnet composition	528
Methods	528
Composition	533
Compositional variation	534
In different facies	534
Within one facies	534
In individual garnets	535
Between textural types	535
Anorthosite-gabbro series	536
General discussion	536
Primary features	536
Primary minerals	537
Plagioclase	537
Pyroxene	539
Olivine	540
Modification of the primary features	540
General statement	540
Early stage of coronation (C type garnet)	540
Granulation and recrystallization of the augite	542
Advanced stage of garnet corona formation	543
Stage of poikiloblastic anhedral garnet (P type)	543
Stage of megascopic, non-poikilitic garnet porphyroblasts (X type)	545
Stage of giant, hornblende-sheathed garnets (XH type)	546
Syenite and syenitic hybrids	549
Primary facies of the syenite	549
Features of transitional facies	549
Syenite-gabbro and syenite-anorthosite hybrids	551
Garnetiferous meta-anorthosite facies	551
Petrography	551
Garnet in meta-anorthosite	552
Origin of the Barton deposit	553
Introduction	553
Hypothesis 1. Modification of Grenville inclusion	553
Hypothesis 2. Primary magmatic segregation	554
Alternate hypotheses of regional or contact metamorphism	555
Hypothesis 3. Post-syenite regional metamorphism	555
Hypothesis 4. Double contact metamorphism	557
Hypothesis 5. Proposed hypothesis	559
Loci and causes of large garnet growth	559
Rimmed versus rimless garnets	560
Corona garnet origin	560
Regional significance	561
Other Adirondack deposits	561
General statement	561
Deposits of Anorthosite-gabbro derivation	561
General description	561
Coronated gabbro as a deposit of abrasive garnet	562
Dark-ore type deposits	562
Light-ore type deposits	563
References cited	565

ILLUSTRATIONS

Figure	Page
1. Regional geologic map of the Adirondacks	522
2. Modal composition diagram, members of the anorthosite-gabbro series	523
3. Southeastern Adirondack garnet localities, geologic setting	526
4. Areal geologic map, Gore Mountain district	527
5. Structure plan, Barton mine	527
6. Structure sections, Barton mine	528
7. N/G and N/a_0 fields of Adirondack garnets	529
8. Detailed plots, N/G and N/a_0 fields, garnets of anorthosite-gabbro derivation	530
9. Composition variation diagram, garnets of anorthosite-gabbro derivation	535
10. Variation in composition and physical properties across a diameter of one large Barton garnet	535
11. Composition diagram, primary and secondary minerals of the anorthosite-gabbro series	536
12. Micrographs of primary anorthosite, Gore Mountain	537
13. Micrographs of primary gabbro, Gore Mountain	538

Figure Page
14. Micrographs of meta-gabbro, Gore Mountain ... 541
15. Micrographs of coronated gabbro, Gore Mountain ... 542
16. Modes of gabbro and meta-gabbro facies ... 545
17. Bulk compositions of gabbro and meta-gabbro facies ... 545
18. Variation in composition of total feldspar in syenite and syenite hybrids ... 550
19. C, P, X, XH series of garnet types in gabbroic facies, southeastern Adirondacks ... 559
20. Schematic section across Barton deposit, illustrating occurrence of garnet types in relation to the syenite-gabbro intrusive contact ... 560

Plate Facing page
1. Hornblende-rimmed garnets of the Barton deposit ... 526
2. Large garnet crystals from Barton deposit ... 527

TABLES

Table Page
1. Precambrian rocks of the eastern Adirondacks ... 521
2. Garnets of anorthosite-gabbro derivation, Barton mine and vicinity, Gore Mountain district ... 531
3. Garnets of anorthosite-gabbro derivation, various Adirondack localities ... 532
4. Garnets in Grenville facies, southeastern Adirondacks ... 533
5. Composition and physical properties, XH type garnet B110, Barton mine ... 534
6. Physical properties of garnet end-members ... 534
7. Compositional comparison of C type and XH type garnets in gabbroic facies, Gore Mountain ... 536
8. Modes of gabbro and meta-gabbro facies ... 541
9. Bulk compositions of gabbro and meta-gabbro facies ... 546
10. Composition and properties of rim hornblende B110h, Barton mine ... 548
11. Modes of syenite and syenite hybrid facies ... 559

Abstract

New mineralogic and petrographic data, derived from study of a number of garnet-rich deposits in the southeastern Adirondacks, are presented, with particular emphasis on the Barton deposit at Gore Mountain. This deposit, long the world's largest producer of abrasive garnet and widely known for its giant hornblende-sheathed garnets, has been ascribed to various primary and secondary modes of genesis. The new data indicate that the Barton ore is an extreme metagabbro facies whose large garnets were derived by progressive recrystallization growth from microscopic corona garnet during the peripheral metamorphism of the gabbro by intrusive syenite magma. The progressive changes from corona garnet (C type) to very small poikiloblasts (P type), to megascopic non-poikilitic porphyroblasts (X type), and finally to very large hornblende-sheathed crystals (XH type) are traced petrographically and compositionally. These basic garnet types, representing different degrees of recrystallization growth of the original, probably deuteric, corona garnet, are recognized in many gabbroic and anorthositic facies as well as in hybrid facies of syenite-gabbro and syenite-anorthosite derivation. Because of this genetic relationship, garnet composition and textural type facilitate the petrogenetic interpretation of a number of garnetiferous facies and deposits, and throw new light on certain old petrologic problems of the Adirondack province.

Chemical analyses, specific gravities, optical and x-ray diffraction data, micrometric modes, micrographs, maps, and graphs are presented.

Introduction

The genesis of the numerous and locally rich garnet deposits of the southeastern Adirondacks has long been studied without reference to the microscopic and small megascopic garnet so extensive in the gabbroic and anorthositic facies of that region. In a field and laboratory study, interrupted by the war and recently concluded, new mineralogic and petrographic data were gathered which indicate a genetic relationship between the different types of garnet and throw light simultaneously on the origin of certain of the garnet-rich deposits and on the petrogenesis of garnetiferous facies.

The most interesting among the many local concentrations of garnet is the Barton deposit on Gore Mountain, the world's largest producer of abrasive garnet and the only Adirondack deposit being worked at the time of this investigation. The deposit is widely known for its spectacular giant red garnet crystals, several inches to 3 feet in diameter and enclosed in distinctive shells of coarse black hornblende. Because of its particular geologic and economic interest and its association with garnetiferous gabbro and anorthosite, and with syenite, study

was begun at the Barton deposit and subsequently extended to other Adirondack deposits and garnetiferous facies localities.

Garnet is so widespread in the rocks of the region that it has figured significantly in a number of fundamental premises in Adirondack petrology. The problem of the genesis of the different garnet types consequently cannot be divorced from some of the broader considerations of igneous and metamorphic history of the Adirondacks; conversely, the interpretations reached in the present study bear directly on certain of the petrogenetic theories particularly those which rest rather heavily upon the thesis that garnet was a primary magmatic mineral in the parental magma of the gabbro-anorthosite series.

Acknowledgments

The generous assistance given by so many persons in the course of this study is gratefully acknowledged by the author. The investigation of the Barton deposit was first suggested in 1941 by the late Dr. Philip Krieger and by Professor C. P. Berkey. Field work was facilitated by the permission of the Barton Mines Corporation, and many pleasant and fruitful hours were spent in the field with Mr. Frank C. Hooper, former manager of the Barton mine and pioneer garnet operator in the Adirondacks. Dr. Medora H. Krieger assisted materially by helpful discussions of the areal geology and by the loan of thin sections. Dr. Ralph Holmes and Dr. Paul F. Kerr guided the earlier x-ray diffraction work. Most of the mineralogic and petrographic work was done in the laboratories of the Department of Geology, Columbia University; specific gravity determinations and refractometry were carried out in the laboratories of the Department of Geology and Geography, Hunter College.

For constructive criticism and helpful discussions the author is indebted especially to Dr. A. F. Buddington, Dr. C. H. Behre, Jr., and Dr. Robert Balk.

Above all, sincerest appreciation and thanks to Professor S. J. Shand. His repeated help in chemical analysis and frank, friendly criticism and guidance in petrology were a constant source of stimulation and inspiration.

Regional Geologic Setting

Geologic Column

The Adirondack region is structurally an asymmetrical dome from which the early Paleozoic sediments have been stripped, exposing the Precambrian igneous and metamorphic rocks over an area approximately 120 miles in diameter. The eastern half of the province is surmounted by mountains rising three to four thousand feet above the general upland level. In this eastern half, the larger igneous masses occur and garnet is prominent.

Table 1.—Pre-cambrian Rocks of the Eastern Adirondacks

Diabase: Dikes of diabase, lamprophyre, etc. (minor).
Syenite-Granite Series: Chiefly quartz-pyroxene-syenite, quartz - pyroxene - hornblende - syenite, and hornblende-biotite-granite; locally shonkinitic or monzonitic; hybrid facies or migmatites.
Anorthosite-Gabbro Series: Core (Marcy) and border (White face) types of anorthosite, grading thru gabbroic anorthosite and anorthositic gabbro to gabbro, mafic gabbro, and magnetite-ilmenite bodies; norite; amphibolite; meta-anorthosite and meta-gabbro.
Grenville Series: Limestone and marble gneiss; amphibolitic gneiss; mixed gneisses and schists (migmatites); quartzite and quartzitic gneiss.

Into the old Grenville sedimentary rocks the parent magma or magmas of the anorthosite-gabbro series and those of the syenite-granite series were intruded, accompanied by intensive and extensive folding, syntexis, and general dynamo-thermal metamorphism (Table 1).

Anorthosite and Gabbro

The anorthosite occurs as one very large massif (Fig. 1), with smaller bodies to the northeast and southwest. The core of the main massif and minor portions of the smaller bodies are composed of the so-called Marcy type or *core* facies of anorthosite, a massive, very coarse, dark bluish-gray rock made up of plagioclase crystals and up to 15 per cent of dark minerals. Much of the border of the massif

(and most of each smaller body) is composed of the grayish-white, medium-grained Whiteface or *border* facies, which contains a higher proportion of the dark accessories and is generally foliated (gneissoid). The more mafic character of the border facies is here regarded as a primary variation, its foliation as a secondary, metamorphic feature.

Gabbro, in the eastern and southeastern Adirondacks, occurs as irregular, round, or elongate bodies, several hundred feet to 3 or more miles long, located for the most part around the periphery of the anorthosite massif. Gabbros wholly within anorthosite are few and small; the largest gabbro bodies occur along the contact between anorthosite and the surrounding syenite. Most of the gabbros occur in syenite or in Grenville metasediment, or partly in Grenville and partly in syenite. Gabbro, to judge from the exposures, occupies a very much smaller volume than anorthosite, but is much more abundant than the related modal extremes with which both are associated, namely, meta-peridotite or meta-pyroxenite (now ortho-amphibolite), and magnetite-ilmenite ore (Fig. 2).

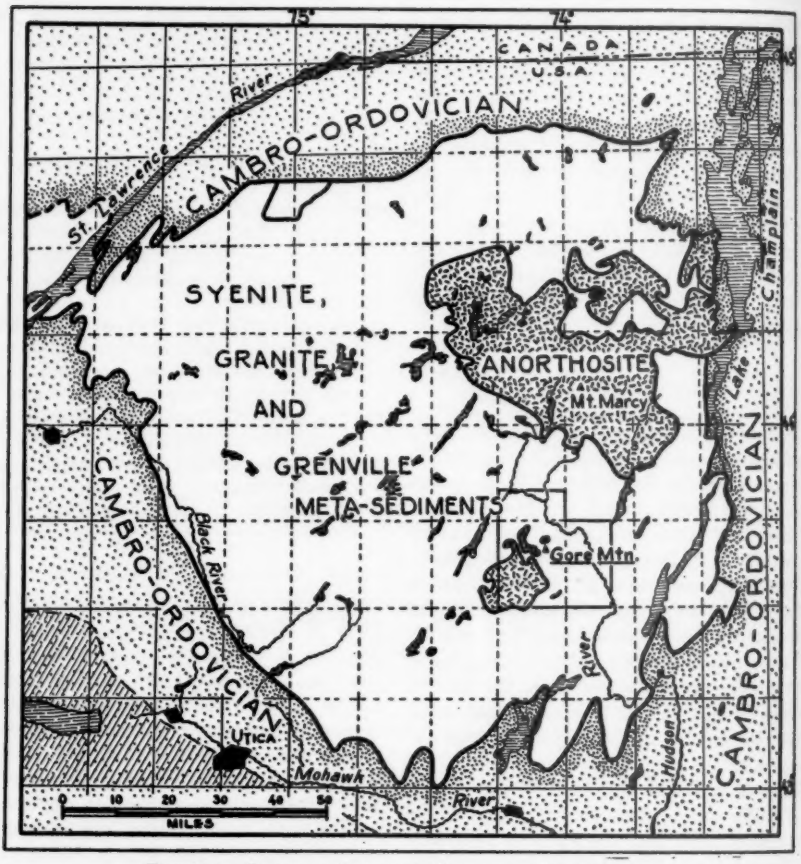

FIGURE 1.—REGIONAL GEOLOGIC MAP OF THE ADIRONDACKS

From maps by Balk, Buddington, and others, and publications of the New York State Museum. Area covered by map Figure 3 outlined.

The term metagabbro is generally used to designate more or less reconstituted, generally amphibolitic gabbro. Its use is restricted here to those facies which exhibit only relics of the primary mineralogic and textural features of the original gabbro, but which, on the evidence of those relics and of transitional facies, are known or reliably inferred to have been derived from gabbro by reconstitution without material change in bulk composition. The term gabbro is used for those facies which, even though texturally and modally somewhat modified from the original, are still largely characterized by the primary textures and mineral assemblage. The term meta-anorthosite will be used here for anorthosite facies related to primary ophitic or protoclastic anorthosite by transitional facies and relic features but lacking, for the most part, the characteristics of the parental type.

The primary facies of the gabbros and the bulk of the anorthosite (Marcy type) are composed largely of the same minerals—intermediate plagioclase feldspar and pyroxene—in varying proportions. Because of the textural and mineralogical similarities and gradational relationships observed in the field, the anorthositic and gabbroic members are now generally accepted as closely consanguineous and broadly contemporaneous, the products of crystal fractionation from a common magma. At some localities the syngenetic relationship of smaller gabbro bodies to surrounding or associated anorthosite is unmistakably indicated; elsewhere, sharply discordant gabbro dikes in anorthosite clearly establish the locally epigenetic status of some of the gabbro.

Syenite and Granite

The syenites and granites constitute a mineralogically gradational series characterized by a variation in quartz content, in soda-potash ratio, and in color index (from leucocratic to shonkinitic). Quartz-pyroxene syenites and hornblende granites of medium to coarse grain and massive to gneissoid structure are abundant in the eastern Adirondacks.

The age relationship of the syenite-granite series to the anorthosite-gabbro series is still controversial. At some localities the intrusion of syenite into anorthosite and into gabbro is satisfactorily established, but elsewhere the field relationships have been interpreted both as indicative of consanguineity and essential contemporaneity (Balk, 1931, p. 383, 402) and as indicative of a later and unrelated intrusion

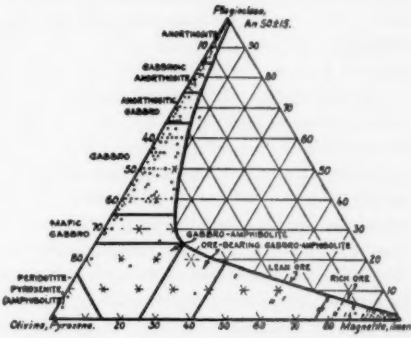

FIGURE 2.—MODAL COMPOSITION DIAGRAM, MEMBERS OF THE ANORTHOSITE-GABBRO SERIES

From modes by Miller, Buddington, Stephenson, Levin, and others.

of syenite into gabbro and anorthosite (Buddington, 1939, Table 48). The "transition rocks", which occur where rocks of the two series meet and exhibit some of the features of each, have correspondingly been interpreted by some, especially Balk (1931), as due to incomplete differentiation of syenite and anorthosite from a common magma, and by others (Miller, 1929; Buddington, 1939) as due to partial syntexis of anorthosite by later intrusive syenitic fluids. The present writer believes that the syenite-granite series in the southeastern Adirondacks represents a distinct intrusive sequence which followed so closely upon the consolidation of the anorthosite-gabbro series that partial assimilation of still hot anorthosite and gabbro was thermally feasible. If the syenite-granite series is consanguineous with the anorthosite-gabbro series, that relationship is not convincingly disclosed at the present level of exposure in the southeastern Adirondacks.

HABITAT OF THE GARNET

Garnet is ubiquitous in eastern and southeastern Adirondacks. It is found, though in

widely varying proportions, in the gabbros and anorthosites, in facies mapped as members of the syenite-granite series, in anorthosite-to-Grenville skarns, in Grenville mixed gneisses, and in amphibolites of diverse origins. Garnet is essentially absent from the igneous rocks of the western and northwestern Adirondacks, although it does occur there in certain Grenville siliceous gneisses and amphibolites.

One explanation of this regional difference is implied in Buddington's (1939, p. 251 et seq.) descriptions of the metamorphic zones in the Adirondack region. In the western zone, metamorphism was less intense, cataclastic textures more prominent, and recrystallization less extensive. In the east, deformation and recrystallization were more intensive and more extensive. The relative predominance of granoblastic over cataclastic textures hardly tells the whole story, however, for garnet is found as a significant accessory, in the eastern Adirondacks, in portions of some rocks in which recrystallization of the primary minerals had not occurred or had reached only an incipient stage. Nevertheless, it is a useful empirical generalization that garnet is more ***prominent*** in the more thoroughly metamorphosed rocks and in the more mafic types (metagabbro, amphibolites, and gabbroic anorthosite) than in syenite, granite, and undeformed anorthosite.

Habit of the Garnet

Several different modes of occurrence of Adirondack garnet have been noted. These habits may be tabulated as follows:

A. In rocks of the gabbro-anorthosite series.
   1. As microscopic, anhedral, or subhedral individuals, sparsely scattered through primary facies of the rocks. Embryonic corona (C) type.
   2. As microscopic, granular aggregates, so grouped as to form narrow "rims" or "coronas", in unmodified or only slightly recrystallized gabbro and (the more mafic facies of) anorthosite. C type.
   3. As microscopic to megascopic, scattered, individual poikiloblasts, with characteristic sponge-like structure and abundant enclosures of the associated minerals, occurring in largely or partly reconstituted facies. P type.
   4. As megascopic, small to medium sized (about ¼–1 inch diameter), subhedral to euhedral, scattered individual porphyroblasts, without inclusions of the associated minerals, occurring in wholly reconstituted, granoblastic, amphibolitic facies. X type.
   5. As medium to very large (up to 3 feet in diameter), spherical or dodecahedral, isolated, individual porphyroblasts, enclosed in shells of coarse hornblende, occurring in wholly reconstituted, coarsely granoblastic, amphibolitic facies. XH type.
   6. As granular aggregates forming narrow borders around Grenville quartzitic xenoliths in anorthosite (Elizabethtown; Kemp, 1910, p. 34). Rare.

B. In rocks of the syenite-granite series, as field-classified; hybrids in some cases:
   1. As microscopic, subhedral to euhedral individuals, very sparsely scattered in "normal" foliated syenite and in granite.
   2. As microscopic to very small megascopic, subhedral, granular aggregates grouped to form narrow "rims" or "coronas", in coarse, granoblastic, mafic (amphibolitic or dioritic) facies of the syenite, and in normal granoblastic quartz-pyroxene syenite.
   3. As small (less than a quarter inch), irregular to round, anhedral individuals with sponge-like structure, enclosing associated minerals, occurring in coarse granoblastic amphibolitic or dioritic facies of the syenite. P type.
   4. As small to medium (¼–1½ inches), subhedral to euhedral nonpoikilitic individuals, isolated, or in small lenticular clusters cumulatively forming a prominent lineation, in well foliated granoblastic mafic "syenite"-gneiss. X type.
   5. As medium to large (1–3 inches, approximately), subhedral to euhedral, isolated individuals, not poikilitic, in massive granoblastic mafic "syenite", the larger garnets being enclosed in a shell of coarse hornblende. XH type.

C. In Grenville limestone—silicated marble gneiss (skarns):
   1. As fine- to medium-grained, granular aggregates with green granular clinopyroxene and coarse calcite (with or without wollastonite), in close association with anorthosite or gabbro, S type.
   2. As fine- to medium-grained, granular aggregates with green granular clinopyroxene and coarse calcite, in close association with syenite or syenitic gneisses. S type.

D. In Grenville mixed gneisses of various compositions:
   1. As small to very large (½ inch to 3 feet, ap-

proximately), nearly spherical, isolated, poikiloblastic, with or without hornblende shells, in dark hornblende-biotite-feldspar gneisses and in dark amphibolitic gneisses and schists, generally near syenite or syenitic gneisses.

2. As massive granular aggregates of anhedral garnet and clinopyroxene, occurring as large lenticular masses in pyroxene-quartz-feldspar gneisses. (Johnsburg eclogite type). E type.
3. As small (up to ¼ inch), subhedral, isolated or scattered individuals in various quartzitic and feldspathic grey gneisses.

E. In later basic dikes.

1. As fine-grained individuals or small clusters in diabase dikes cutting gabbro and anorthosite.

Several of these types of occurrences, particularly A4, A5, B4, B5, C1, C2, D1, and D2, are locally represented by deposits which have been mined for abrasive garnet. No one mode of genesis will satisfactorily account for all occurrences, but study of the garnets and their petrographic settings indicates that several of these types are genetically related as sequential stages of an over-all progressive program of metamorphism. The relationship is particularly well brought out by various petrographic facies exposed near the two outstandingly productive deposits, the Barton mine on Gore Mountain and the Hooper mine at Thirteenth Lake.

The significant garnet types encountered in this area are the corona C type, the poikiloblast P type, the larger nonpoikilitic porphyroblasts of X type, and the very large hornblende-rimmed porphyroblasts of XH type.

Local Setting of the Barton Deposit

Location and Geologic Setting

The Barton deposit is located[1] at 4340.8–7403, at an elevation of 2600 feet, on the north slope of Gore Mountain, about 6 miles by road south of the village of North River (Fig. 3, B; Fig. 4). The geology in the vicinity of the mine has been described by Krieger (1937).

The deposit lies along the contact between a body of gabbro on the north and a body of syenite on the south, along the periphery of an outlier of anorthosite and gabbro.

The anorthosite is now largely meta-anorthosite and the gabbro is part metagabbro; the two are here consanguineous and essentially contemporaneous, although the gabbro may have completed its consolidation slightly later. Both are garnetiferous.

The syenite in this area is discordantly intrusive into the anorthosite-gabbro series which it has peripherally metamorphosed and partially assimilated, with the development of hybrid facies along and near the contacts. Normal syenite in this district is free of garnet. The facies exposed in the area northwest of the large anorthosite mass and designated by Krieger (1937) "Low grade garnet rock", is here interpreted as a hybrid facies of syenite-anorthosite. Certain peripheral garnetiferous facies, designated "garnet gneiss deposits" on Krieger's map, are interpreted here as meta-anorthosite and syenitic hybrids of meta-anorthosite.

The garnet "ore" of the Barton deposit consists of very large hornblende-sheathed garnets (Pl. 1) set in a coarse, dark matrix of hornblende and plagioclase. This is the so-called "dark ore" (matrix color index about 70 to 75) comprising the bulk of the deposit. Along the southern edge of the deposit is a narrow zone of "light ore", consisting of large garnets in a feldspathic matrix (color index 20 to 50).

Local Structure

The mine is an open pit or quarry which in 1941 was 50 to 250 feet wide by approximately 2000 feet long in an east-west direction (Fig. 5). The floor rose in four steps of 20 to 40 feet each, forming five horizontal benches or levels, the lowest being at the west end. Quarry depth, or side wall heights varied between about 25 feet and 90 feet because of irregular topography. According to Krieger (1937, p. 110), the deposit occurs as a lens which "dips" (plunges?) 7° to 9° to the west. The bottom of the workings, and the limits of the deposit at the surface, suggested such an attitude, but there were no indications that the lower limits of the deposit had actually been exposed. Along the strike, beyond the eastern end of known ore,

[1] Map positions are given in abbreviated form; e.g. 4340.8–7403 for 43° 40.8′ north latitude, 74° 3′ west longitude, as measured on U. S. Geological Survey topographic maps of scale 1/62,500.

at the surface, is a garnetiferous syenite-gabbro hybrid, and at the western end the ore grades into syenite-gabbro-anorthosite primary (Marcy) anorthosite there. A complex variety of mixed facies is found there where syenite, anorthosite, and gabbro meet. Field

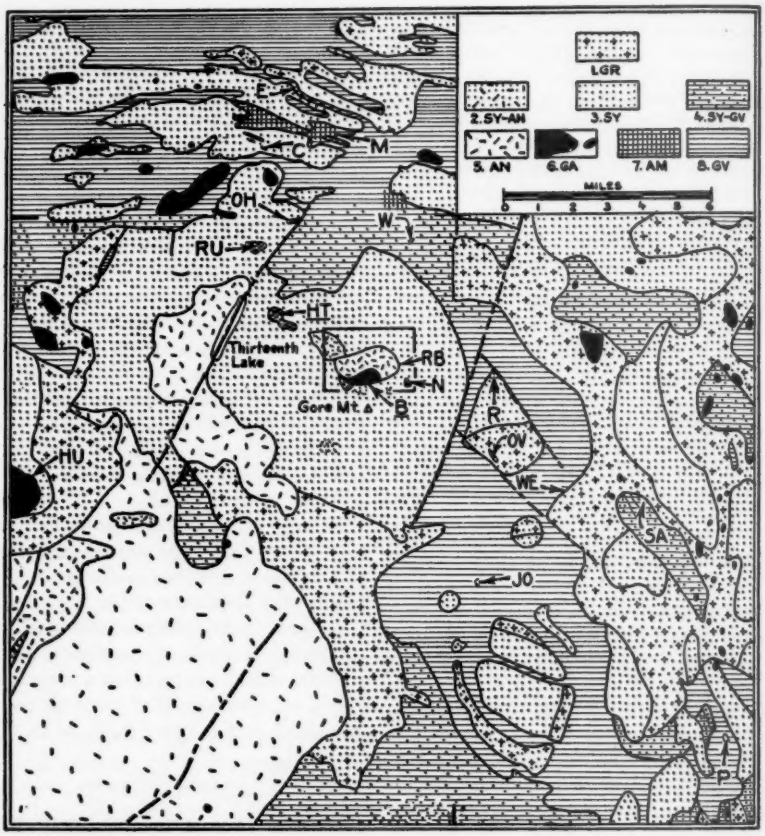

FIGURE 3.—SOUTHEASTERN ADIRONDACK GARNET LOCALITIES, GEOLOGIC SETTING

From quadrangle geologic maps by Krieger (Thirteenth Lake, 1937), Miller (North Creek, 1914), and Balk (Newcomb 1932). Rock types: 1 granite, 2 syenite-anorthosite hybrid, 3 syenite, 4 syenite-Grenville mixed gneisses, 5 anorthosite and meta-anorthosite, 6 gabbro and meta-gabbro, 7 amphibolites (Grenville), 8 Grenville meta-sediments. Garnet localities indicated by initial letters. Area of map Figure 4 outlined.

hybrid locally carrying very small megascopic and microscopic garnet.

At the western end of the mine, a capping of syenite extended over the deposit onto the gabbro, and apparently also overlaps the and petrographic evidence indicate that anorthosite formerly extended into the area south of the Barton deposit but was cut out and partly assimilated by the syenite magma.

Foliation, presumably primary, is moder-

PLATE 1.—HORNBLENDE-RIMMED GARNETS OF THE BARTON DEPOSIT

FIGURE 1. RIMMED GARNETS IN BARTON DARK ORE

XH type garnets, 4 to 6 inches diameter, in the north wall, level 3 of the Barton Mine.

FIGURE 2. TYPICAL XH TYPE GARNET WITH HORNBLENDE RIM

Near spherical garnet individual, 8 inches diameter, in Barton dark ore.

FIGURE 1

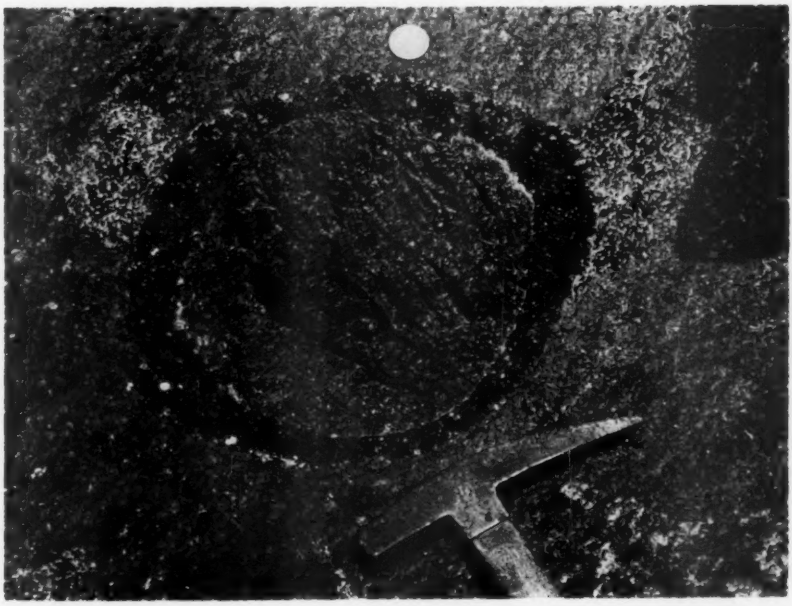

FIGURE 2

HORNBLENDE-RIMMED GARNETS OF THE BARTON DEPOSIT

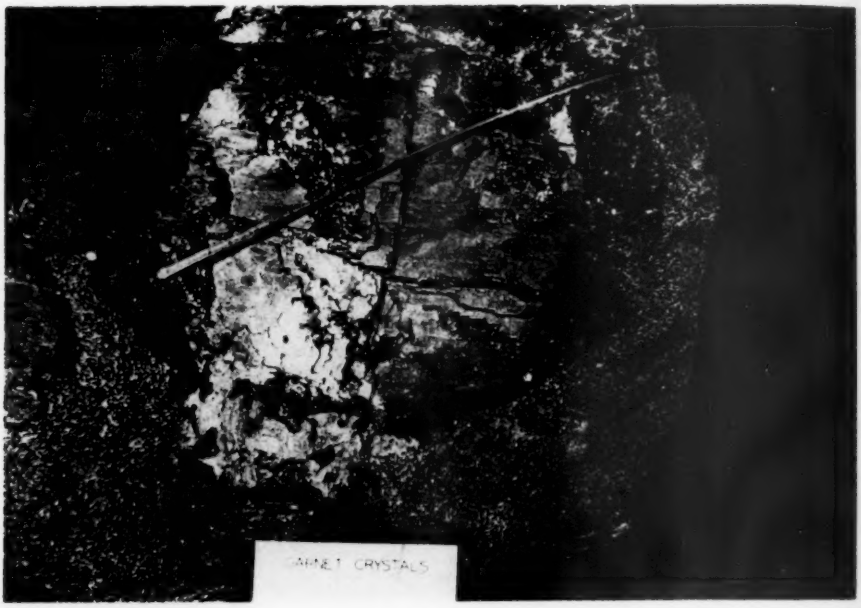

FIGURE 1

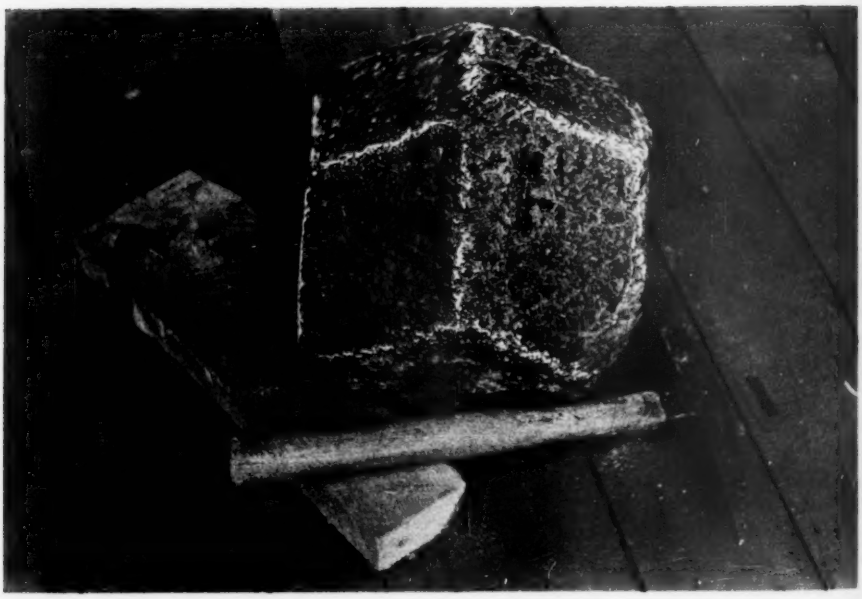

FIGURE 2

LARGE GARNET CRYSTALS FROM BARTON DEPOSIT

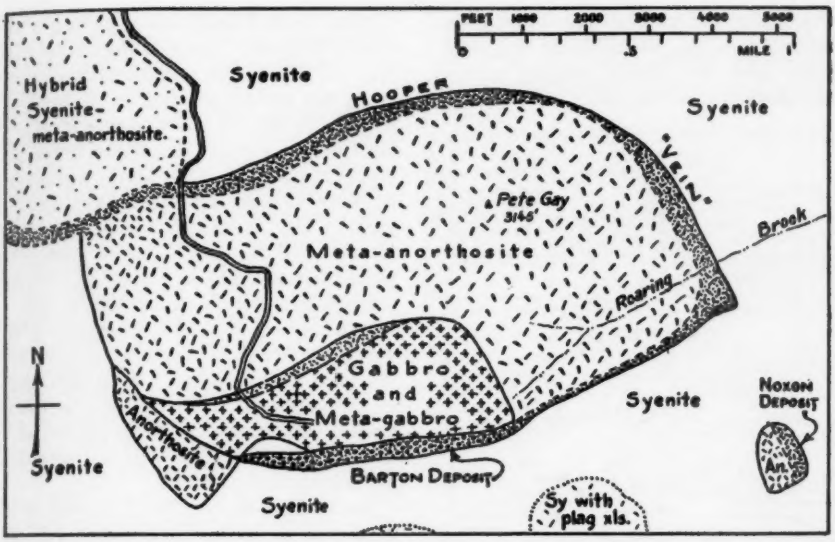

FIGURE 4.—AREAL GEOLOGIC MAP, GORE MOUNTAIN DISTRICT
From map by Krieger (1937), with slight modifications.

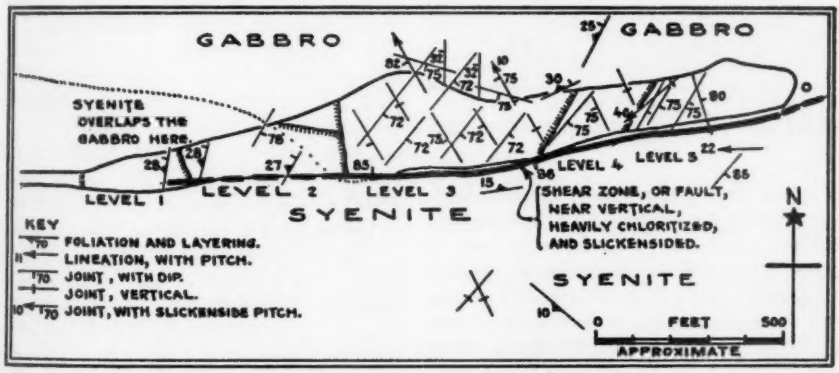

FIGURE 5.—STRUCTURE PLAN, BARTON MINE (1941)

ately developed in the syenite and is near horizontal, dipping 10° to 15° in one direction or another with considerable irregularity. At the contact, top of the southern rim of the quarry, the syenite dips gently northward, but at much too low an angle for it to have passed below the gabbro, unless the latter has been downthrown at least 100 feet on the north side of the fault, which seems unlikely.

Foliation is absent in the least modified facies

PLATE 2.—LARGE GARNET CRYSTALS FROM BARTON DEPOSIT

FIGURE 1. LARGE CRYSTAL WITH IRREGULAR RIM

This 19 inch garnet (B71–75), on display at Columbia University, shows well developed fracture system, hornblende rim of irregular thickness, and late plagioclase between garnet and rim. One crystal of this size weighs over 500 pounds.

FIGURE 2. SOLID GARNET DODECAHEDRON

The edges of this 10 inch crystal were outlined with chalk when photographed. The specimen is in the possession of Mr. Frank C. Hooper and Dr. M. H. Krieger.

of the gabbro and is not generally evident in the metagabbro facies, including the ore, of the quarry north wall. Modal banding, however, was apparent at several places, especially (Fig.

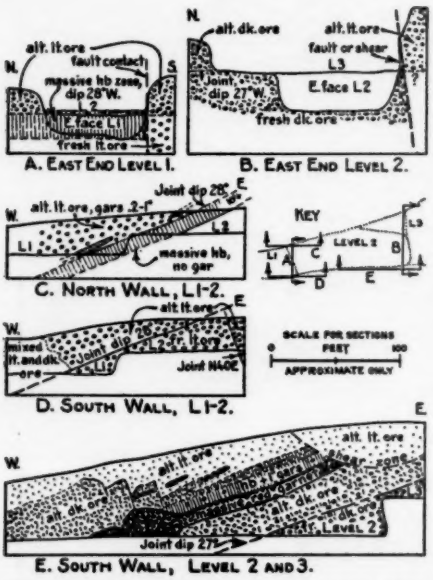

FIGURE 6.—STRUCTURE SECTIONS, BARTON MINE (1941)

6) in the south wall of Level 2, where fresh garnet ore of the normal type ("dark ore") is overlain successively by a layer or zone of altered dark ore, a zone of dominantly massive red garnet, a zone of hornblende-rich matrix with small (1 inch) red garnets, another zone of altered dark ore, and finally altered "light ore". The fresh "dark ore" here is the same coarse, hornblende-rich, metagabbro ore facies which constitutes the bulk of the deposit; the "light" ore is modified syenite, a hybrid consisting of xenolithic garnet and hornblende in a feldspathic matrix.

The intrusive, almost breccia-like, contact of the light ore (syenite-hybrid) and the dark ore facies is well shown on the south wall of Level 2 (Fig. 6E). The intruding syenite magma here pried up a 1-foot thick band of dark ore and stoped xenoliths of the dark (metagabbro) ore. The syenite hybrid at this point itself contains sufficient xenocrystic garnet to be minable ("light ore").

Extensive and closely spaced jointing is well developed in the vicinity of the Barton mine (Fig. 5). No study of relative abundance was made, but the NE-trending set of joints appears to be the more prominently developed. Both sets are found in the syenite, in the gabbro, in the ore, and in the nearby anorthosite. Evidence of local movement, along the NE joints at least, is found in the slight local displacement of the two halves of large hornblende-rimmed garnets. The displacement amounts to a movement, on the NW. side, of half an inch to 4 inches in a direction S. 40°W., with pitch 40°SW; it is observable only where the joint passes through a very large single crystal of garnet. In the medium- to coarse-grained granoblastic matrix of the ore, as in the syenite and the gabbro, displacement along the joints is not observed.

Summarizing the structural features of the vicinity of the Barton deposit: the syenite displays primary foliation, near horizontal; the gabbro and the primary anorthosite are not foliated, but modal banding is present in some of the metagabbro; the intrusive contact of syenite against ore-facies is also a locus of later shearing; two sets of near-vertical joints with NE and NW strikes are prominently developed, and a third set, seen only in the ore, dips gently W. and NW. parallel to the banding or layering; this last set of joints guided solutions responsible for later alteration at the west end of the deposit. The northeast-striking set corresponds to that found by Balk (1932) to be dominant in the Newcomb quadrangle to the north. The diagonal system of steep NE and NW joints is well developed in the Barton garnets and has a direct bearing upon their economic value.

GARNET COMPOSITION

Methods

Data were obtained on the composition and variation in composition of the Barton XH type garnets, as well as of the other types in this and other localities, and in various petrographic facies (Figs. 7, 8; Tables 2, 3, 4). The compositions of over 60 different garnet specimens were determined or estimated from carefully controlled measurements of refractive index N, and specific gravity G, combined

with partial chemical analyses for total manganese and for ferrous iron, and supplemented in many cases by the determination of the lattice constant a_0.

The specific gravity was determined on micro-picked clean material 30 to 100 mesh in size, using a micro-pycnometer with toluene, and eliminating entrapped air by gentle vacuum boiling, at about 30 mm. Hg pressure, and room temperature. The results in most cases were reproducible within a G value of ±.005.

The refractive index was determined by the immersion method, with thermal variation, in specially prepared high index liquids (methylene iodide base) which were concurrently checked, for index and temperature coefficient, on a temperature controlled Abbé type refractometer. The mounted specimens were observed while in a micro-oven on the microscope stage, using a sodium-arc light source. The results are reliable within an N value of ±.001.

Total Mn was determined colorimetrically after fusion with Na_2CO_3, solution, and oxidation to permanganate (by means of potassium periodate), allowance being made for color due to Fe^{3+} ion. Calibrated potassium permanganate solution was used as a standard. Only very small amounts of manganese were found, and the results, expressed as weight per cent MnO, are believed to be accurate to ±.05.

Ferrous iron was determined on garnet which was handpicked at 20 to 40 mesh under stereoscopic microscope, treated with HCl to remove limonite and pyrite films, crushed to minus 100 mesh in steel mortar, probed with small magnet to remove steel splinters, and finally ground 3–5 minutes in an agate mortar. A modification of the Pratt method was used, involving gentle boiling in a mixture of warm 1:1 H_2SO_4 and 40 per cent HF for a predetermined period, followed by rapid titration in boiled-out, borated water, with standardized $KMnO_4$ solution. Multiple determinations indicate a reliability of about ±.1 expressed as weight per cent FeO.

The lattice constant a_0 was determined by x-ray diffraction analysis of finely ground powder using either filtered Fe K alpha or filtered Cu K alpha radiation in a Debye type camera of 57.3 mm. radius, having equivalent dispersion of 1 millimeter per degree of the double Bragg angle 2θ. Several diffraction patterns were made in a Phragmén type focusing camera using the back region from $2\theta = 91°$ to $2\theta = 164°$. In all cases 4 or 6 distinct and indexed lines in the back region were measured and the

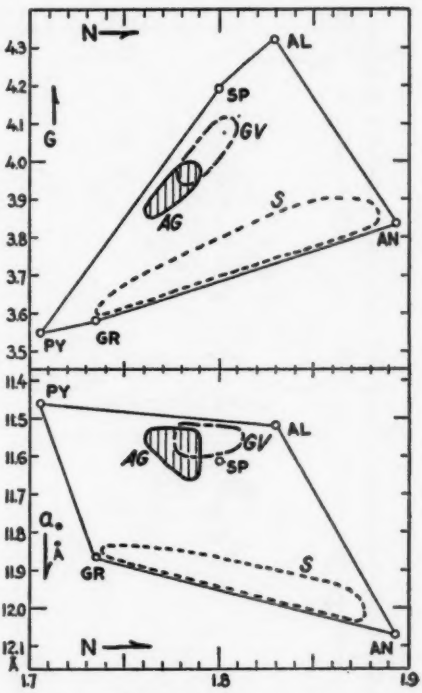

FIGURE 7.—N/G AND N/a_0 FIELDS OF ADIRONDACK GARNETS

Refractive index N plotted against specific gravity G and lattice constant a_0 (in Angstrom units, 1947 wave-lengths). AG: field of anorthosite-gabbro series garnets. S: field of skarn garnets from contact zones of anorthosite, syenite, or granite with Grenville limestone. GV: field of garnets in Grenville amphibolitic-biotitic facies.

a_0 determined by a Bradley-Jay extrapolation to $\sin^2\theta = 1$. The results are reliable to ±.001 Angstrom unit.

As a base of reference for evaluating the routine reliability of the physical techniques and instruments used, one typical specimen of garnet (XH type, B 110) from the Barton deposit was selected for more complete chemical analysis and physical measurement (Table 5). The material analyzed was a portion of a single garnet crystal 2.3 inches in diameter and hornblende-sheathed. The specimen was

taken from Level 3 of the quarry, roughly at the plan-center of the deposit. The material for analysis was very carefully micro-picked and cleaned and was microscopically pure.

trometer-goniometer, using sodium-arc light. Similarly, particular care was taken in the determination of the specific gravity and the lattice constant of this reference sample.

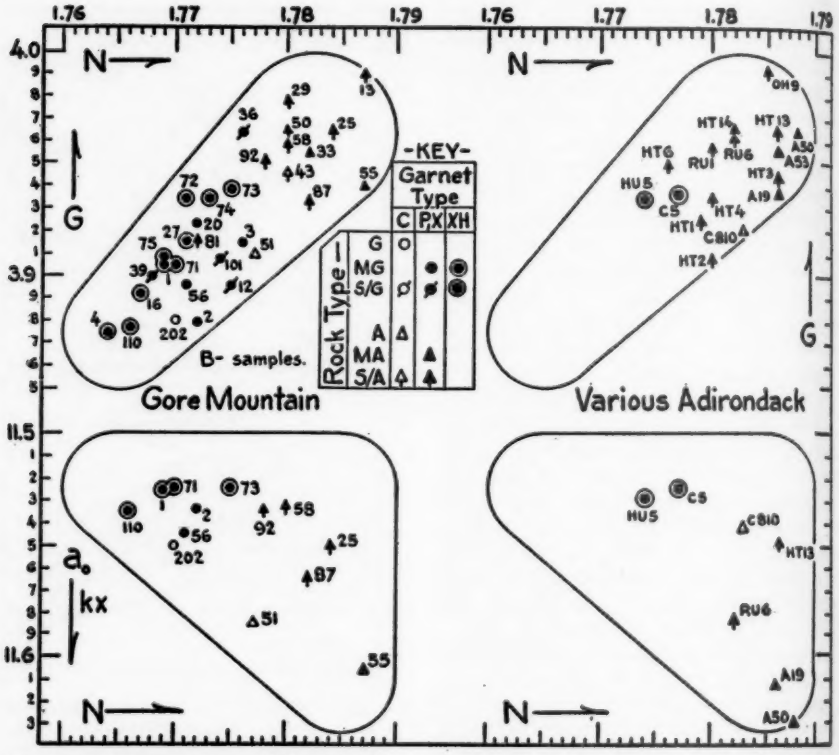

FIGURE 8.—DETAILED PLOTS, N/G AND N/a_0 FIELDS, GARNETS OF ANORTHOSITE-GABBRO DERIVATION
Data of Tables 2 and 3. Lattice constants plotted in kx units (1931 wavelengths).

Silica and alumina were determined in duplicate and ferrous iron and manganese were run several times for check.

Material for physical analysis was taken from the same vial as that for chemical analysis. The refractive index was determined by two independent methods. First, multiple immersion measurements were made by thermal variation in the same liquids used for the other specimens. Then the index was measured by minimum deviation on minute wedges ground from 2 mm. flawless grains of garnet taken from the same part of the specimen; prism angle and deviation were measured on a spec-

The close agreement between the physical properties as measured and as calculated from analyzed composition provides independent checks on the reliability of the techniques and on the validity of utilizing measured physical properties in estimating the composition of other specimens.

The values used, in this study, for the various end-members (or molecules, or minals) of the body-centered cubic mineral garnet, $A_3^{2+}B_2^{3+}(SiO_4)_3$, are given in Table 6. The N values are those of Ford (1915), confirmed by Fleischer (1937) on newer reliable analyses. The G and a_0 values are those of Fleischer

TABLE 2.—GARNETS OF ANORTHOSITE-GABBRO DERIVATION, BARTON MINE AND VICINITY, GORE MOUNTAIN DISTRICT

No.	Rock	Gar	G	N	a_0	MnO	FeO	PY	AL	SP	GR	AN
B202	G	C				.49	17.8	*41	39	1	14	5
B 3	MG	P	3.915	1.776	—	.81	23.2	34	49	2	14	1
B 2	MG	P, X	3.879	1.772	11.533	.65	21.6	38	46	1	13	2
B 20	Ore	P, X	3.923	1.772	—	—	—	38	46	1	13	2
B 4	Ore	XH	3.875	1.764	—	.35	19.1	43	40	1	14	2
B110	Ore	XH	3.877	1.766	11.534	.38	19.6	42	41	1	14	2
B110								*43	40	1	14	2
B 16	Ore	XH	3.892	1.767	—	.34	20.4	41	42	1	14	2
B 1	Ore	XH	3.905	1.769	11.525	.35	21.2	41	44	1	12	2
B 27	Ore	XH	3.916	1.771	—	—	—	38	46	1	13	2
B 71	Ore	XH	3.905	1.770	11.524	.30	21.1	42	44	1	10	3
B 72	Ore	XH	3.934	1.771	—	.37	21.8	40	46	1	10	3
B 73	Ore	XH	3.938	1.775	11.524	.67	23.3	37	49	1	11	2
B 74	Ore	XH	3.934	1.773	—	.58	22.8	38	48	1	10	3
B 75	Ore	XH	3.908	1.769	—	.44	21.2	42	44	1	10	3
B 39	S/G	X	3.900	1.768	—	—	—	40	43	1	12	4
B101	S/G	X	3.908	1.774	—	.60	21.5	40	45	1	11	3
B 12	S/G	X	3.896	1.775	—	.59	22.0	38	46	1	11	4
B 36	S/A	X	3.963	1.776	—	.81	24.2	33	52	2	11	2
B 43	S/A	C	3.946	1.780	—	.63	22.7	34	48	1	13	4
B 50	S/A	X	3.964	1.780	—	.73	23.8	32	50	2	13	3
B 29	S/A	X	3.978	1.780	—	.79	24.6	31	52	2	12	3
B 33	S/A	X	3.954	1.782	—	.59	23.6	31	50	1	14	4
B 25	S/A	X	3.965	1.784	11.550	.61	23.6	31	51	1	11	6
B 13	S/A	X	3.990	1.787	—	.97	26.3	25	57	2	13	3
B 26	S/A	X	3.945	—	—	—	—	—	—	—	—	—
B 14	S/A?	X	4.074	1.802	11.592	1.20	28.5	8	64	3	21	4
B 51	A	C	3.91c	1.777	11.585	—	—	31	44	2	19	6
B 55	MA	P, X	3.940	1.787	11.606	.52	24.7	13	54	1	30	2
B 59	MA	X	—	1.787	—	—	—	—	—	—	—	—
B 58	S/A	P, X	3.959	1.780	11.532	.88	24.0	33	51	2	11	3
B 92	S/A	X	3.950	1.778	11.534	.56	23.9	33	51	1	12	3
B 81	S/A	X	3.916	1.772	—	.53	22.7	32	48	1	18	1
B 87	S/A	X	3.932	1.782	11.565	.67	23.4	27	50	1	18	4
B 56	MG	P, X	3.896	1.771	11.544	.48	21.5	35	45	1	17	2

Specific gravity followed by c indicates determination by Clerici solutions instead of by micropycnometry.

MnO and FeO given in weight per cent; garnet compositions given in mol per cent; those starred calculated from the data of complete chemical analyses. Equivalent composition of B202 calculated from Shand's 1945 analysis.

Values of lattice constant a_0 in kx units based on 1931 wavelengths.

(1937) based on relatively recent and reliable chemical analyses and on x-ray diffraction data. All are extrapolated values; pure pyrope, for example, is not known. Other combinations of divalent and trivalent ions, including Cr^{3+} and Mn^{3+}, are theoretically possible on the basis of ionic radii, but in the Adirondacks as in most other regions the five "molecules" listed

TABLE 3.—GARNETS OF ANORTHOSITE-GABBRO DERIVATION, VARIOUS ADIRONDACK LOCALITIES

No.	Rock	Gar	G	N	a_0	MnO	FeO	PY	AL	SP	GR	AN
HU 5	MG	XH	3.935	1.774	11.529	.50	22.9	36	49	1	12	2
HT 1	S/A	X	3.924	1.779	—	.79	23.2	31	49	2	16	2
HT 2	S/A	X	3.907	1.780	—	.80	24.2	28	52	2	15	3
HT 3	S/A	X	3.943	1.786	—	.81	25.4	27	54	2	13	4
HT 4	S/A	X	3.934	1.780	—	.65	23.4	30	50	1	14	5
HT 6	S/A	X	3.949	1.776	—	.61	24.0	29	51	1	13	4
HT13	S/A	X	3.964	1.786	11.548	.72	25.3	27	54	2	13	4
HT14	S/A	X	3.965	1.782	—	.67	24.5	28	52	1	13	4
OH 9	S/A	X	3.991	1.785	—	1.05	26.0	20	56	2	22	0
RU 1	S/A	X	3.957	1.780	—	.70	24.3	21	52	2	25	0
RU 6	S/A	X	3.963	1.782	11.582	.56	24.0	20	52	1	25	2
C 5	S/G	XH	3.938	1.777	11.523	.42	23.3	38	49	1	8	4
C810	A	C	3.92c	1.783	11.541	—	—	44	42	1	0	13
A 19	MA	P, X	3.937	1.786	11.612	1.10	24.0	11	53	2	32	2
A 50	MA	P, X	3.964	1.788	11.630	.49	25.4	4	56	1	39	0
A 51	MA?	P, X	4.122	1.810	—	1.46	30.3	7	66	3	23	1
A 52	MA	P, X	—	1.796	—	—	—	—	—	—	—	—
A 53	MA	P, X	3.956	1.786	—	.70	24.6	10	53	1	33	3

Localities:
HU Humphrey Mountain (4338.5–7414.3).
HT Hooper Thirteenth Lake, North River Garnet Co. (4342.5–7406.2).
OH Old Hooper deposit (4344.9–7405.3).
RU Ruby Mountain (4344.2–7406.5).
C5 Crehore deposit (4346.7–7406.5).
C810 Garnet rim from anorthositic magnetite-ilmenite ore, Lake Sanford.
A19 Along U. S. Highway 9, near Schroon River (4357–7345).
A50, 51, 53 Columbia University collection specimens A343, 17754, and C167 respectively, all labelled anorthosite gneiss from near Schroon River.

Rock types: A, anorthosite; MA, meta-anorthosite.
G, gabbro; MG, meta-gabbro.
S/A and S/G, syenite-anorthosite and syenite-gabbro hybrids.

Garnet types: C, corona; P, poikiloblasts; X, porphyroblasts; XH, large hornblende-rimmed porphyroblasts.

account for over 99 per cent of each garnet specimen.

Since the fundamental differences between various garnet specimens are the variations in the proportions of the proxying divalent and trivalent ions, and since garnet molecules as such do not occur in the lattice, the compositions are properly expressed in ionic or atomic percentages, without implying the specific association of certain trivalent ions with certain divalent ions. But the physical properties are related to the structure as a whole, which may be treated statistically as a solid solution of the purest possible lattices or ionic combinations—as a solution of all possible end-members. The five listed in Table 6 are chosen both on the empirical basis of occurrence and on the basis of theoretical considerations of lattice stability as related to ionic radii. The various garnet specimens may thus be designated in two ways: e.g.,

$$(Mg_{40}Fe_{40}Mn_8Ca_{12})_3(Al_{92}Fe_8)_2(SiO_4)_{300}$$

for compositional considerations; and its equivalent $PY_{40}AL_{40}SP_8GR_{10}AN_2$, primarily for considerations of physical properties.

TABLE 4.—GARNETS IN GRENVILLE FACIES, SOUTHEASTERN ADIRONDACKS

No.	Rock	Gar	G	N	a_0	MnO	FeO	PY	AL	SP	GR	AN
Skarn facies												
E 3	S/GV	G	3.687	1.766	11.832	.42	4.7	0	10	1	76	13
P 8	S/GV	G, P	3.762	1.85	11.968	.11	1.8	0	4	0	27	69
P 9	S/GV	G, P	3.815	—	—	.09	1.8	0	4	0	17	79
Amphibolitic facies												
M 1	GVAM	P	3.983	1.789	—	.54	26.7	36	56	1	2	5
M 7	GVAM	P	4.046	1.795	11.507	.96	29.6	28	64	2	2	4
M15	GVAM	P	3.967	1.788	—	.73	27.5	33	58	2	2	4
M19	GVAM	P	4.056	1.792	—	.99	28.9	30	62	2	3	3
R 3	GVAM	P, X	4.097	1.805	—	1.45	29.8	18	66	3	4	9
R 7	GVAM	XH	4.021	1.788	—	.90	27.3	28	59	2	10	1
R 8	GVAM	P	3.980	1.788	—	.80	26.1	30	55	2	10	3
R10	GVAM	P	3.962	1.779	—	.66	24.8	35	52	1	12	0
W 1	GVAM	G, P	4.020	1.790	—	.85	27.4	—	58	2	—	—
W 6	GVAM	G, P	4.016	1.795	—	1.54	27.7	—	60	3	—	—
W16	GVAM	G, P	4.006	1.790	—	.80	27.1	—	59	2	—	—
WE4	GVAM	P, X	3.987	1.785	—	.96	26.0	30	56	2	10	2
Eclogitic type facies												
JO2	GV	G	3.951	1.781	11.557	.60	24.4	25	53	1	19	2

Localities: E Pete Gay Eddy on the Hudson.....(4348.0–7405.2)
P Parker deposit.....(4332.0–7351.0)
M Black Mountain Pond area.....(4347.1–7404.2)
R Rexford deposit.....(4341.0–7358.7)
W Washout, north shore of Hudson.....(4344.3–7401.2)
WE Weverton crossroads.....(4338.0–7356.6)
JO Johnsburg deposit.....(4336.0–7359.2)
Locality latitudes and longitudes given in degrees, minutes, and tenths of a minute, from quadrangle maps.

Rock types: S/GV syenite-Grenville skarn.
GVAM Grenville amphibolitic facies.

Garnet types: G granular; P poikiloblastic; X porphyroblastic individuals, megascopic; XH large porphyroblasts with hornblende rim.

Composition

The garnets, regardless of textural type or host facies, are all approximately 85 to 65 per cent pyralmandite and 15 to 35 per cent lime garnet. The major compositional variation is the Mg^{2+}/Fe^{2+} ratio (ionic), which ranges between about 45/40 and 15/50, equivalent to from 1.12 to .30. As the magnesium content drops both Fe^{2+} and Ca^{2+} increase, roughly in proportion to their general abundance (Fig. 9). To what extent the relative abundance of the Mg^{2+}, Fe^{2+}, and Ca^{2+} ions in the 8-co-ordination lattice positions reflects their relative availability at the time and place of garnet formation is not known. However, the more magnesium-rich (pyropic) garnets occur in the more mafic facies (gabbro and its metamorphic derivatives), while the less pyropic and disproportionately calcic garnets are found in the less mafic (anorthositic) facies.

With one exception (B14), all of the specimens, whether from the Barton ore, from the gabbro or metagabbro, from the anorthosite or meta-anorthosite, or from the hybrid facies

TABLE 5.—COMPOSITION AND PHYSICAL PROPERTIES, XH TYPE GARNET B110, BARTON MINE

	Wt. per cent	Ions		Ratios	
SiO_2	39.29	Si^{4+}	.655	656	2.96
TiO_2	0.05	Ti	.001		
Al_2O_3	22.12	Al^{3+}	.434		
Cr_2O_3	0.00	Cr	.000	444	2.00
Fe_2O_3	0.73	Fe	.010		
FeO	19.63	Fe^{2+}	.273		
MnO	0.38	Mn	.005	675	3.04
MgO	11.48	Mg	.287		
CaO	6.16	Ca	.110		
H_2O-	0.03			"Molecular" weight: 450.9	
	99.87			Analyst: S. B. L.	

Formula:
$(Mg_{43}Fe_{40}Mn_1Ca_{16})_3(Al_{89}Cr_0Fe_2)_2(Si_3O_{12})_{100}$
Equivalent: $PY_{43}AL_{40}SP_1GR_{16}AN_2$
Specific gravity, G:
3.877 ± .005 measured at 26°C.
3.880 calculated.
Lattice constant, a_0:
11.534 ± .001 kx at 22°C, λ 1.93208 kx.
11.532 calculated.
Refractive index, N:
1.7658 ± .0001, at 25°C, λ 5893 A.
1.764 calculated.
Dispersion (N_{Tl}-N_{Li}): 0.0095 at 25°C.
Indentation hardness: 1250 ± 50 (Knoop number), on 210 surface.
Notes:

1. Calculated G based on molecular weight from chemical analysis and on a_0 as measured; $G = 1.65\ WZ/a_0^3$, where Z = 8 mols/cell.
2. Calculated a_0 based on Fleischer's (1937) values for lattice constants of end-members, applied to above chemical analysis.
3. Calculated N based on Ford's (1915) average values for the index of end-members, applied to above chemical analysis.
4. N measured by minimum deviation on 2 mm wedge ground to 22°18′. Also measured by immersion with thermal variation and high-index refractometer control: N 1.766 ± .001 (25°C).
5. Chromatic dispersion interpolated from N values measured by minimum deviation at λ 5400A, 5893A, and 6800A.
6. Garnet color: red in hand specimen; pink at 60 mesh; pale pink in thin section.

with syenite, fall within one small N/G field and one correspondingly small N/a_0 field (Fig. 7, AG; Fig. 8). The close agreement of G, N, MnO, and FeO, as determined for these representative garnets, indicates that all fall within the rather restricted compositional range noted above. This is further confirmed by those cases for which the determination of the lattice constant a_0 permitted a mathematical computation of the composition with an accuracy of approximately ±1 molecular per cent.

TABLE 6.—PHYSICAL PROPERTIES OF GARNET END-MEMBERS

General formula: $A_3B_2(SiO_4)_3$

Name		A^{2+}ion	B^{3+}ion	N	G	a_0(kx)*
Pyrope.....	PY	Mg	Al	1.705	3.554	11.440
Almandite...	AL	Fe	Al	1.830	4.325	11.495
Spessartite...	SP	Mn	Al	1.800	4.196	11.590
Grossularite..	GR	Ca	Al	1.735	3.582	11.840
Andradite...	AN	Ca	Fe	1.895	3.838	12.045

* Values of lattice constant a_0 increase by .023 on conversion to Ångstrom units.

Compositional Variation

In different facies.—On the basis of the data cited it appears that in the genetically related facies of the anorthosite-gabbro series, that is, in the gabbro, metagabbro, anorthosite, meta-anorthosite, syenite-gabbro hybrids, and syenite-anorthosite hybrids, the garnets constitute a single continuous series having a relatively limited compositional range. The only facies dependence noted is, as already mentioned, that the less pyropic garnets are found in the anorthositic facies, the more pyropic in the gabbroic facies. The variations in ferrous iron and in calcium are apparently inversely related to the Mg variation, but the Ca variation is probably also related to the anorthite content of the primary plagioclase in the primary facies; i.e. garnets in anorthosite are disproportionately richer in lime than are those in gabbro.

Within one facies.—The best sampling within any one facies is that in the Barton ore itself which, on the evidence of petrographic gradation, bulk composition, and field relationships, is independently interpreted as a metamorphic facies of the gabbro. In this ore, the large garnets vary from Mg 35 to 45 atomic per cent (of total divalent cations), with corresponding variation in ferrous iron and lime.

The Mn^{2+} remains approximately 1 per cent, as usual throughout the district, although in detail it varies with the Fe^{2+} content.

The sampling in other facies, especially in primary gabbro and anorthosite, leaves much

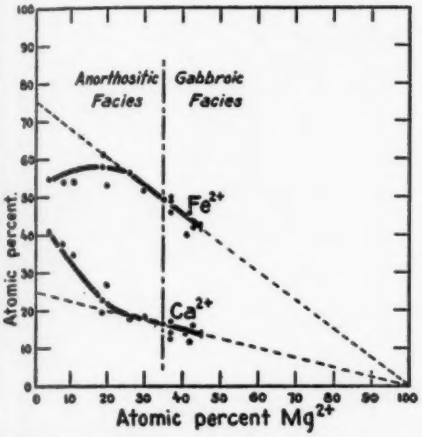

FIGURE 9.—COMPOSITION VARIATION DIAGRAM, GARNETS OF ANORTHOSITE-GABBRO DERIVATION

to be desired. But in microscopic examination significant differences in composition are detectable, by the accustomed observer, as variations in garnet color; since many more specimens were examined, in addition to those analyzed, without detecting any major color variations, it is concluded that the compositional variation in the other facies is of the same order of magnitude as in the Barton ore. B-14 is an exception; under the binocular microscope it is notably darker than all other specimens in its vicinity, and proves to be much richer in iron and measurably richer in manganese.

In individual garnets.—In the very many garnets examined, no zonal color variation was noted and no peripheral optical anisotropism (such as characterizes some skarn garnets). That the large garnets of the Barton ore are nevertheless compositionally zoned is indicated by an analytical traverse across a diameter of the 19-inch garnet (Pl. 2, Fig. 1) now on display in the Department of Geology, Columbia University. Five samples (B 71–75)were taken at approximately quarter-radius intervals along a diameter of a near-great circle section. The data (Table 2; Fig. 10) show that this giant individual, evidently a single crystal, became slightly but progressively poorer in Fe^{2+} as

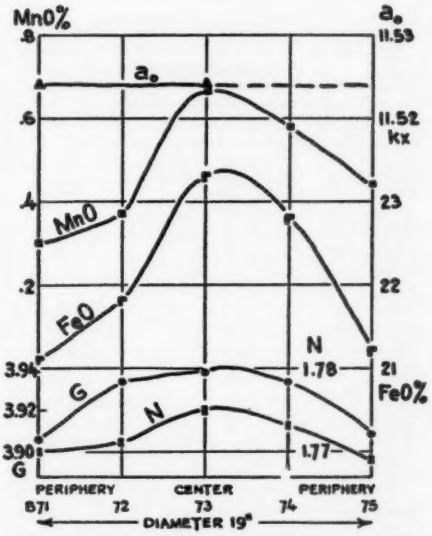

FIGURE 10.—VARIATION IN COMPOSITION AND PHYSICAL PROPERTIES ACROSS A DIAMETER OF ONE LARGE BARTON GARNET, XH TYPE

it grew larger. The Mg^{2+}/Fe^{2+} ratio ranges from 37/49 at the center, to 42/44 at the periphery (i.e., .75 to .95), while the lime content remains essentially constant.

The crystallization trend of ferro-magnesian minerals in basic magmas, as a rule, is such as to yield progressively smaller Mg/Fe ratios rather than larger. This zoning, therefore, does not support the view that the garnets are direct magmatic products, unless they grew from periphery toward the center rather than centrifugally; and there is no evidence of centripetal growth.

Between textural types.—The difficulty of separating adequate amounts of clean garnet of the corona (C) and the poikiloblastic (P) types limits the possibilities of comparing the compositions of garnets of the four major textural types (C, P, X, XH) in facies of the anorthosite-gabbro series. The data (Table 2; Fig. 8) indicate, however, that the compositional differences between representatives of

the different types is not greater than the compositional variation within any one type. There is no significant compositional dependence on textural type.

TABLE 7.—COMPOSITIONAL COMPARISON, C TYPE AND XH TYPE GARNETS IN GABBROIC FACIES, GORE MOUNTAIN

	C type (B202) Near Barton mine	XH type (B110) Barton mine
SiO_2.....	41.30	39.29
TiO_2.....	.15	.05
Al_2O_3.....	19.78	22.12
Fe_2O_3.....	1.80	.73
FeO.....	17.80	19.63
MnO.....	.49	.38
MgO.....	10.60	11.48
CaO.....	6.98	6.16
H_2O-.....	.54	.03
Total...	99.44	99.87
Analyst:	S. J. Shand (1945, p. 257)	S. B. L.
Equivalent:	$Mg_{41}Fe_{39}Mn_3Ca_{19}$ $Al_{95}Fe_5$	$Mg_{48}Fe_{40}Mn_1Ca_{16}$ $Al_{98}Fe_2$

The close correspondence in composition between representative specimens of the two extreme textural types is shown by the chemical analyses (Table 7) of one corona garnet (C type) and one hornblende-sheathed megacrystal (XH type). The C type garnet is from the gabbro, about 150 feet north of the Barton quarry; the XH type is a typical specimen from the Barton ore.

ANORTHOSITE-GABBRO SERIES

General Discussion

The rocks of this district are characterized by so many gradationally related textural and mineralogical variations that it is difficult to establish distinct types or facies among them. However, it is possible to characterize any variant satisfactorily in terms of the parental type or primary facies from which it was evidently derived, and the kind and degree of modification which it has undergone.

The major part of the Barton garnet deposit, the so-called "dark ore", is an extreme variant of the primary parental facies of the gabbro, of which it forms a peripheral portion; the "light ore", along the southern margin is a hybrid variant of the syenite. The genesis of the deposit is best described by tracing the courses of modification, beginning with the primary (magmatic) textures and mineral assemblages (Fig. 11).

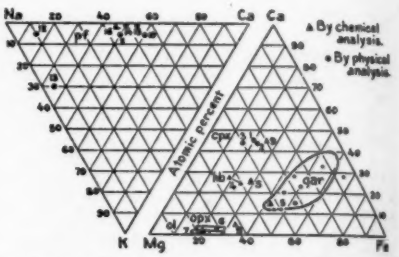

FIGURE 11.—COMPOSITION DIAGRAM, PRIMARY AND SECONDARY MINERALS OF THE ANORTHOSITE-GABBRO SERIES

All Gore Mountain except 8 and 9

1. Primary augite in anorthosite.
2. Primary augite in gabbro.
3. Recrystallized augite in gabbro.
4. Metamorphic hornblende in meta-gabbro.
5. Deuteric and metamorphic garnet in gabbroic and anorthositic facies.
6. Secondary hypersthene in meta-gabbro.
7. Primary olivine in gabbro.
8. Hypersthene in anorthosite, Mt. Marcy (Leeds).
9. Augite in anorthosite, Mt. Marcy (Leeds).
10. Primary plagioclase in anorthosite.
11. Primary plagioclase in gabbro.
12. Late interstitial feldspar in anorthosite.
13. Late interstitial feldspar in anorthosite.
14. Recrystallized plagioclase in meta-gabbro.
15. Recrystallized plagioclase, meta-anorthosite.
16. "Rim" plagioclase in XH facies meta-gabbro.

S. Shand's (1945) analysis of Gore Mountain gabbro.

Primary Features

Extensive bodies of purely primary facies are rare in this district. The original character of the undeformed anorthosite is best preserved in the area of anorthosite at the western end of the gabbro body.

The rock is massive, coarse, very dark bluish to greenish black, and consists largely (90 per cent or more) of tabular plagioclase crystals,

very many over an inch long. Thin sections reveal, at low magnifications, that the only other component mineral of volumetric consequence is augite, and that it bears a completely ophitic relationship to the euhedral plagioclase crystals. The clino-pyroxene completely occupies the triangular or polygonal (actually polyhedral) interstices between the plagioclase crystals, and on a micro-scale exhibits uniformity of optical orientation over considerable areas, including (for most mesostatic individuals) several interstices not visibly connected in the plane of the section. Another textural feature apparent at low magnifications is the fairly well developed preferred orientation of the closely packed plagioclase crystals (Figs. 12A, B).

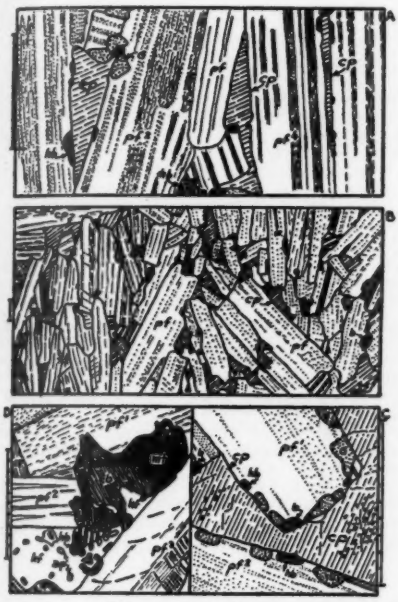

Scale bar in each case represents 1 mm.

A. Primary, ophitic anorthosite, Gore Mountain. Scale 35/1. Closely packed crystals of "dusty" plagioclase (pf) with mesostatic clinopyroxene (cp). Accessory garnet (G), hornblende (hb), and biotite (b) are secondary (deuteric).

B. Anorthosite, Gore Mountain. Scale 3/1. Same as A; showing preferred orientation.

C. Anorthosite, Gore Mountain. Scale 25/1. Portions of two primary plagioclase crystals (pf^1 and pf^2) and an area of mesostatic clinopyroxene (cp) are shown. Along the plagioclase-augite boundaries, but entirely on the plagioclase side, are minute grains of garnet (G) and occasional grains of hornblende (hb) and biotite (b). Except for faint wedging of twin lamellae in the plagioclase and several cracks in the augite there is no evidence of deformation.

D. Anorthosite, Gore Mountain. Scale 17/1. An irregular grain of magnetite-ilmenite (black mt) is surrounded by deep red-brown biotite (b), which has replaced slightly wedge-twinned primary plagioclase (pf) and possibly also some late interstitial potash feldspar (kf) with associated twinned albite-oligoclase. A grain of hornblende (hb) and several minute prisms of apatite (ap) are seen in the potash feldspar.

FIGURE 12.—MICROGRAPHS OF PRIMARY ANORTHOSITE, GORE MOUNTAIN

The primary gabbro is best represented by the medium-grained, massive, dark-green to greenish-black rock found in parts of the core of the Gore Mountain gabbro body. Even these least modified parts have the characteristic brown speckled appearance of weathered Adirondack gabbro, due to the surface oxidation of small rosette-like clusters of ferromagnesian minerals. Wholly unmodified gabbro is evidently to be found only on a micro-scale, in thin sections. These reveal the very close textural and mineralogical similarity of the primary gabbro and primary anorthosite, the gabbro differing chiefly in the less close packing and smaller size (0.5 to 8 mm.) of its plagioclase crystals, the correspondingly greater prominence of mesostatic augite, and the presence of 3 to 15 per cent of olivine anhedra embedded in the augite. Magnetite-ilmenite, apatite, and spinel appear as minor accessories in the primary facies, and garnet, hypersthene, hornblende, and biotite appear locally where reconstitution had begun. Orientation of the plagioclase crystals is relatively poorly developed in much of the primary gabbro (Fig. 13A).

Primary Minerals

Plagioclase.—The primary plagioclase is distinctive. It uniformly presents a roughly rectangular cross-section with dimensional ratio between 2.5 and 5.0; the direction of dimen-

sional elongation lies in the twin composition plane (010). Albite twinning is universally well developed, with distinct broad and narrow lamellae. Pericline twinning also occurs, and

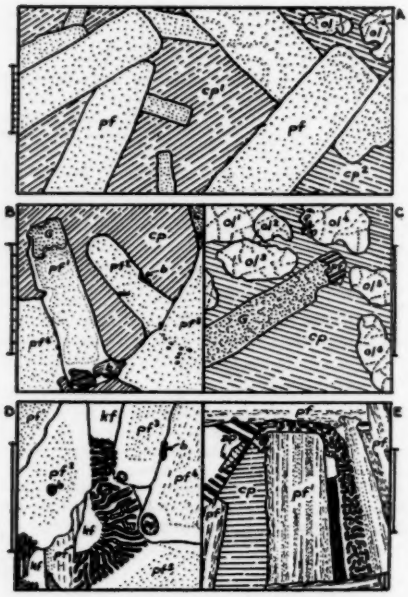

Scale bars represent 1 mm.

A. Primary ophitic gabbro, Gore Mountain. Scale 10/1. Composite micrograph. Loosely packed crystals of "dusty" plagioclase (pf) with mesostatic clinopyroxene (cp^1 and cp^2) enclosing anhedra of fresh olivine (ol).

B. Gabbro (B52), Gore Mountain. Scale 17/1. Several primary plagioclase crystals (pf^1 etc.), with inclusion-free peripheries, are shown with a single continuous individual of mesostatic clinopyroxene (cp). One end of crystal pf^1 is replaced by garnet (G) without evidence of contribution from or effect upon the adjacent augite. The other end of this crystal (pf^1) is partly replaced by biotite (b).

C. Gabbro (B63), Gore Mountain. Scale 17/1. Similar to B, but representing a more advanced metasomatic replacement of the plagioclase (pf) by garnet (G), which now occupies all but the tip of the original crystal. The mesostatic augite (cp) encloses six rounded grains of olivine (ol).

D. Gabbro, Gore Mountain. Scale 17/1. Vermicular intergrowth of clinopyroxene with late interstitial potash feldspar, in primary gabbro.

E. Gabbro, Gore Mountain. Scale 13/1. Vermicular clinopyroxene intergrown with late interstitial feldspar and optically continuous with mesostatic clinopyroxene.

FIGURE 13.—MICROGRAPHS OF PRIMARY GABBRO, GORE MOUNTAIN

combination albite-carlsbad twins are not uncommon. Where other evidence of deformation is lacking, the twin lamellae are straight.

The crystals are generally 1–40 mm. or more in length, the size variation being seriate. Larger sizes (5–40 mm) predominate in the anorthosite, smaller sizes (1–8 mm.) in the gabbro.

Although it is the most abundant and petrologically most important mineral in the Adirondack anorthosite-gabbro series, the primary plagioclase has never been directly analyzed chemically. Clean separation from its dark micro-inclusions is evidently not feasible. In the present study a considerable number of optical determinations were made, chiefly by direct measurement (on the universal stage) of the maximum extinction angle in the zone normal to 010. This was supplemented in a number of cases by measurement of the optic angle 2V, and by measurement and stereographic plotting of the elements of the optical indicatrix for comparison with Duparc-Reinhard plots. Composition determination by measurement of refractive index on cleavage fragments in mechanically fractionated powders was used only for those wholly recrystallized facies in which the presence of no more than one type of plagioclase was assured. Each of these methods gives only the anorthite (An) percentage, the remainder being albite (Ab) plus orthoclase (Or).

The measurements indicate that the primary plagioclase of the anorthosite at Gore Mountain ranges from An_{32} to An_{56}, with An_{45} predominant, and that of the gabbro between An_{40} and An_{46}, with An_{43} most common. Careful search failed to disclose any evidence of compositional zoning. Even the inclusion-free border extinguishes optically with the corresponding internal twin lamellae.

In the ophitic anorthosite and gabbro of the Gore Mountain district no antiperthite or perthite was found, but rather rare interstitial areas (.5–1.0 mm.) of clear feldspar with refractive indices lower than 1.54 do occur. Some

of this interstitial feldspar is twinned and some is not, and the two types may be found side by side in the same interstice. Universal stage measurements show that one is albite-oligoclase ($2V_x = 80°-84°$, An 8–12), and the other anorthoclase ($2V_x = 50°$). But the amount of interstitial potash-rich feldspar observed, in the considerable number of thin sections studied, is much too small to account for more than a small fraction of the normative potash feldspar. It is therefore concluded that, while a small amount (a fraction of 1 per cent) of potash feldspar occurs interstitially, considerably more (about 3–7 per cent) occurs in solid solution in the primary plagioclase.

A universal and characteristic feature of the *primary* plagioclase is the presence of minute inclusions (crystallites of spinel, possibly also pyroxene, hornblende, and rutile) in such profusion as to render the feldspar dark (in anorthosite) or nearly opaque (in gabbro) in thin section, at low magnifications. The peripheral zone of each plagioclase is generally inclusion-free but, apart from this feature, distributional zoning of the inclusions is exceedingly rare. The clear periphery is often lacking where plagioclase abuts against plagioclase, and the intercrystal boundary may be marked by a string (in section) of small green spinels larger than the internally included spinels. Adjacent to pyroxene or magnetite or garnet the plagioclase is generally clear of inclusions.

Pyroxene:—The primary pyroxene in both the anorthosite and the gabbro in the vicinity of Gore Mountain is a clinopyroxene, an augite. It is labelled primary because it is the only pyroxene found in ophitic relationship with the primary plagioclase, and the only one which can be traced into those portions of the gabbro or anorthosite where definitely secondary textures and secondary mineral assemblages are absent. Its primary nature is further indicated by the fact that, in the gabbro, rounded but otherwise unaltered grains of olivine occur wholly enclosed in single individuals of the augite.

The augite is colorless in thin section but locally clouded with small black plate-like inclusions (magnetite-ilmenite?) which preferentially lie in the (100) plane. This plane is also the locus of very thin lamellae of orthopyroxene, presumably exsolved. The lamellae are identifiable by analogy with similar lamellae optically continuous with larger areas of recognizable hypersthene developed at the periphery of primary augite where incipient recrystallization is in evidence.

The augite is wholly xenomorphic toward the plagioclase, its grain shape being determined entirely by the interstitial spaces. Between the closely packed and roughly parallel plagioclase crystals of the anorthosite the clinopyroxene commonly appears as plates, but triangular and polygonal sections of augite are the rule in primary gabbro. At low magnifications, and with the universal stage it becomes apparent that many such mesostatic areas of augite, not connected in the plane of the section, are identically oriented (in three dimensions) and represent parts of larger individuals up to 10 mm. or more in size.

The composition of the primary clinopyroxene is estimated, from optical measurements, to be approximately $Ca_{45}Mg_{35}Fe_{20}$ ($2V_x = 54°-56°$, $Z \wedge \dot{c} = 45°-49°$) in the anorthosite, and slightly richer in iron, $Ca_{44}Mg_{34}Fe_{22}$, ($2V_x = 53°-54°$, $Z \wedge \dot{c} = 49°-56°$) in the gabbro. The measured extinction angles are quite high, but this condition is believed to be due to the presence of Ti, Al, and Fe^{3+} ions in the lattice. Winchell (1933, pt. II, p. 230) cites an augite in which the presence of 0.58 TiO_2, 5.24 Al_2O_3, and 2.02 Fe_2O_3 is responsible for an increase of nearly 4° in the extinction angle over that of pure theoretical Ca-Mg-Fe augite. That such ions are present in the augite of the Adirondack anorthosite-gabbro series is indicated by Leeds' (1878, p. 79) analysis of "diallage" from Mt. Marcy anorthosite; his analysis may be recast to 89.5 per cent (by weight) of $Ca_{44}Mg_{29}Fe_{27}$, plus 7.4 per cent Al_2O_3, 2.2 per cent Fe_2O_3, and 0.6 per cent TiO_2.

A feature of paragenetic significance is the occasional occurrence of primary vermicular clinopyroxene in an intergrowth association with interstitial anorthoclase and soda plagioclase, the feldspars which have been independently interpreted as "late stage". The clinopyroxene vermiculae in Figure 13D are in optical orientation with each other but yield no clue to their relationship with the mesostatic primary clinopyroxene of this rock. In the

example shown in 13E, however, the vermicular pyroxene is optically continuous with the larger area of primary mesostatic augite, with which both the vermicular pyroxene and its associated alkali feldspar are evidently contemporaneous. The feature may be regarded as corroborative evidence of the later crystallization of the mesostatic augite as compared with the primary plagioclase.

Olivine:—Olivine is an essential mineral (3–15 per cent) in the primary gabbro facies at Gore Mountain. Its occurrence in the gabbro does not appear to support the suggested (Buddington, 1939, p. 55, 215, and Table 48) dual classification of Adirondack gabbros into a saturated group and an undersaturated group having implicitly somewhat different origins—the former closely consanguineous with the anorthosite and the latter considerably less so, if at all. The Gore Mountain gabbro is definitely undersaturated, yet it is closely consanguineous with the associated anorthosite. Moreover, olivine also occurs, even though rarely, in the anorthosite itself.

Optic angle measurements by universal stage indicate range in composition of the olivine, from Fe_{17} to Fe_{27} in different specimens ($2V_x$ ave. 84°–88°). In the undisturbed mesostatic pyroxene the olivine anhedra are fresh except for minor iron-oxide-stained cracks. Some of these cracks are restricted to the olivine; others extend into the augite; none enter the primary plagioclase.

The olivine occurs exclusively as rounded, somewhat oval, anhedra, 0.2 to 3 mm. in diameter, wholly embedded in the mesostatic augite. Within single interstitial triangles of (continuous) mesostatic augite, two or more close but unattached olivine anhedra commonly have different optical orientation. This circumstance, coupled with the facts that the olivine grains in the mesostatic augite are, in general, fresh and unaltered, and that their boundaries against the pyroxene are sharp and well knit, suggests the absence of peritectic or reaction relationship between these two minerals. Resorption of the (earlier-formed) olivine had evidently stopped when crystallization of the mesostatic augite took place. The paragenetic relationship of olivine to primary plagioclase is less certain; the two are not commonly found in contact, but neither appears to display xenomorphism towards the other.

Modification of the Primary Features

General Statement.—Modification of their primary textural and mineralogical features began, in part, before the gabbro and anorthosite were completely consolidated; it continued during and immediately after the final consolidation, and was either prolonged or renewed by the invading syenitic magma. The features now observed should theoretically be classifiable as magmatic, deuteric, and metamorphic, but such clear-cut classification is, in fact, not feasible. Certain features at each extreme can be labelled, with some conviction, magmatic or metamorphic, but many of the intermediate features fit into one pigeon-hole as well as into another. This suggests that the magmatic, deuteric, and metamorphic processes may have graded progressively into each other without marked interruption. Effective continuity of this kind would have been achieved presumably if the syenitic intrusion followed closely upon the consolidation of the anorthosite and gabbro, while the latter were still hot. Such a history is compatible with field relationships and with independent petrographic evidence of the partial selective assimilation of gabbro and anorthosite by the syenitic magma, since the problem of heat requirement for such assimilation is thereby minimized. Progressive deviation from the parental types is best traced first in the gabbro, then in the anorthosite.

Early stage of coronation (C type garnet).—The earliest modification of the primary features of essentially undeformed ophitic gabbro and anorthosite is recorded petrographically as a selective and progressive metasomatic replacement of primary plagioclase by garnet. A high degree of localization of the garnet to those intergranular boundaries where primary mesostatic augite lies adjacent to the plagioclase, marks these occurrences as representative of the incipient stage in the development of the so-called garnet coronas. Close examination discloses that, without exception, the emplacement of the garnet is accomplished wholly at the volumetric expense of the plagioclase, and that the immediately adjacent py-

roxene is not involved. The micrograph (Fig. 12C) of a typical case is especially instructive in this connection. Any doubt as to the entirely passive role played by the contiguous pyroxene replacing the primary plagioclase, suggests either that the same environment favored the simultaneous growth of the anhydrous silicate, garnet, and the hydroxyl-bearing silicates, bio-

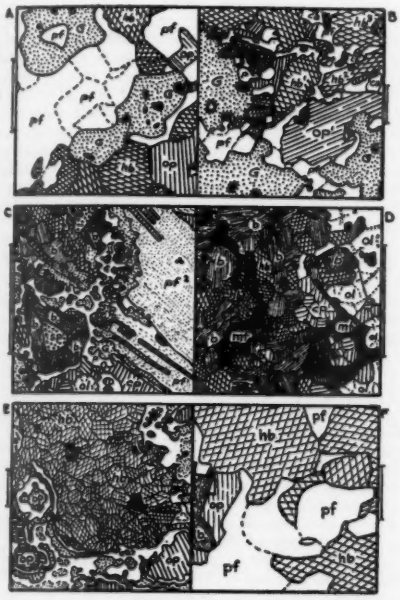

Scale bars represent 1 mm.

A. Metagabbro, north edge of Barton deposit. Scale 11/1. Wholly granoblastic. Irregular poikiloblasts of garnet (G) with inclusions of hornblende and plagioblase; anhedra of hornblende (hb), clear plagioclase (pf), and orthopyroxene (op).

B. Metagabbro, north edge of Barton deposit. Scale 6/1. Coarse, granoblastic facies, with poikiloblast (P type) garnet (G) in matrix of hornblende (hb), clear plagioclase (pf), and hypersthene (op).

C. Gabbro, Gore Mountain. Scale 17/1. Primary dusty plagioclase (pf) replaced peripherally and along cleavages by corona garnet (G); primary mesostatic augite (cp) in part recrystallized to granular aggregate of augite; primary olivine (ol). Cluster of biotite (b) with spinel (sp) core, and associated hornblende (hb).

D. Gabbro, Gore Mountain. Scale 17/1. Aggregates of secondary (deuteric) biotite (b), hornblende (hb), and ilmenite-magnetite (mt), with primary olivine (ol) and recrystallized augite (cp).

E. Metagabbro, north of Barton deposit. Scale 6/1. Traces of residual olivine (ol) and corona garnet (dotted) associated with granoblastic hornblende (hb), hypersthene (op), and clear plagioclase.

F. Barton ore matrix. Scale 8/1. Coarse granoblastic hornblende (hb) with clear anhedral plagioclase (pf) and minor hypersthene (op) and biotite (b).

FIGURE 14.—MICROGRAPHS OF METAGABBRO, GORE MOUNTAIN

in this early stage of garnet formation is dispelled by other cases (Figs. 13B, 13C). In some instances garnetization has progressed from one end of the crystal inward along (010) cleavages by selective replacement of one set of twin lamellae. Plagioclase crystals pf^1 and pf^2 (Fig. 14C) show this type of replacement. The usual distribution of the garnet, however, is in general along those peripheral portions of the plagioclase which bound the mesostatic augite.

Plagioclase-to-plagioclase boundaries, as a rule, are not garnetized. Figure 15B illustrates a mature stage of coronation: the garnet surrounds the triangular interstice occupied by the (recrystallized) augite but is not found along the inter-plagioclase boundaries between crystals pf^1 and pf^2, or between pf^2 and pf^3.

The association of biotite and hornblende with the garnet (Fig. 12C) in this early stage and in a manner indicating that the three minerals were essentially contemporaries in tite and hornblende, or that there was a fine balance between the conditions favorable to the one and those favorable to the others. Magnetite with more or less ilmenite is also found in close association, particularly with a deep red-brown biotite in facies exhibiting slight to moderate modification of the primary features. The magnetite, or magnetite-ilmenite, occurs generally as grains of highly irregular shape suggestive of deuteric formation rather than by free crystallization in a melt or solution. It displays no tendency to replace primary plagioclase but is found in interstitial locations, which suggests that locally it may have replaced mesostatic augite (Fig. 12D).

A direct genetic relationship between the magnetite and the biotite is strongly indicated by the very common occurrence of magnetite at the core of biotite clusters. It would appear either that the magnetite grains were in part responsible for the localization of the biotite.

or that both were formed by and from the same solutions—the biotite first, then the magnetite. Less prominent at this early stage, but increasing as modification progressed, is the occurrence of irregular grains (up to .3 mm.) of deep-green spinel in close association with the magnetite or actually taking its place at the core of biotite clusters (Fig. 14C).

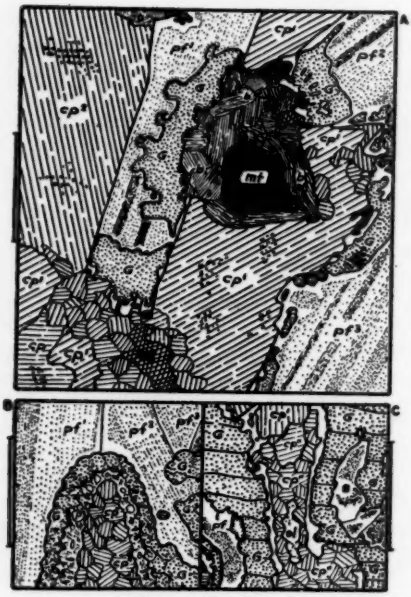

Scale bars represent 1 mm.

A. Gabbro (B52), Gore Mountain. Scale 17/1. Each of three primary plagioclase crystals (pf^1, pf^2, pf^3) is partly replaced by corona stage garnet (G). A portion of the mesostatic clinopyroxene (cp) is recrystallized to a granular mosaic of small (.2 mm), clear grains of augite in which a grain of hornblende (cross-hatched) has also formed. An irregular grain of magnetite (mt) is sheathed in deep red-brown biotite (b) which replaces plagioclase and possibly augite. The garnet, biotite, hornblende, and magnetite are secondary, probably deuteric.

B. Gabbro (B201), Gore Mountain. Scale 17/1. Three crystals of primary plagioclase (pf^1, pf^2, pf^3) are unmodified except for local replacement by corona garnet (G). An originally continuous triangular interstitial augite is represented by a granular mosaic of small, clear grains of recrystallized augite (cp″). Between the augite mosaic and the garnet corona is a mixed zone of intergrown clear plagioclase and clear augite with minor hornblende.

C. Gabbro (B15), Gore Mountain. Scale 17/1. Only two small areas (pf) of primary "dusty" plagioclase survive, the remainder being extensively replaced by corona stage garnet (G). One fragment of primary augite (cp′) survives, the remainder of the mesostatic individual being recrystallized to a mosaic of clear, fine-grained augite (cp″), enclosing a residual grain of olivine (ol). Between the (cp″) aggregate and the garnet corona is a very narrow, discontinuous moat of clear, fine-grained plagioclase.

FIGURE 15.—MICROGRAPHS OF CORONATED GABBRO, GORE MOUNTAIN

Since these features are found in the least deformed portions of the anorthosite and gabbro bodies, but are not found in the definitely metamorphosed peripheral portions next to syenite, they are attributed to the earliest processes operative in the consolidated rock after crystallization of the essential minerals —to the so-called deuteric processes.

Granulation and recrystallization of the augite. —Earliest deformation of the primary gabbro is manifested by the fracturing, granulation, and recrystallization of the primary mesostatic clinopyroxene. Examination of suites of gabbro and metagabbro specimens discloses all gradations, from those in which the mesostatic pyroxene is only slightly fractured to those in which each originally continuous area of mesostatic pyroxene is now represented by a granular aggregate of clear, recrystallized augite, the individual grains having random optical orientation. The recrystallization is from augite to augite, the major changes being in grain size and shape and in the elimination of inclusions. Optical determinations indicate only minor differences in composition between the primary clinopyroxene ($2V = 53\frac{1}{2}°$, $Z \wedge \dot{c} = 52°$) of the gabbro and its recrystallization derivative ($2V = 53°$, $Z \wedge \dot{c} = 42\frac{1}{2}°$). These two pyroxenes are nevertheless readily distinguishable because of the smaller grain size (.1–.5 mm.), the absence of inclusions, and the lack of orthopyroxene lamellae in the recrystallized product. In this stage (Fig. 15) the olivine grains characteristically survive, apparently unchanged, through the granulation and recrystallization of the augite; the minute, opaque, schiller-type inclusions of the primary augite are characteristically eliminated during the recrystallization, as are the orthopyroxene lamellae. The hypersthene grains which develop along the periphery of partly granulated primary augite, or within the granular aggregates of recrystal-

lized augite, are probably derived from those lamellae.

It is not clear whether the recrystallization of the primary augite was deuteric or an exomorphic process superimposed upon the coronation program. Since in the definitely exomorphic portions of the gabbro modification of the augite consisted of complete reconstitution, its simple recrystallization in the remainder of the gabbro may have been endomorphic.

Advanced stage of garnet corona formation.—Metasomatic replacement of plagioclase by garnet evidently continued during the granulation and recrystallization of the pyroxene until the garnet, entirely of the corona or rimming type, constituted 20 to 25 per cent of the rock by weight. The modified gabbro at this stage (Fig. 15 B, C) consists of: (1) irregular areas of residual primary plagioclase; (2) mosaic aggregates of recrystallized augite, with residual fragments of primary mesostatic augite; (3) residual grains of primary olivine embedded in the granulated pyroxene; (4) abundant garnet of the corona type; (5) a few per cent of biotite and hornblende; (6) traces of hypersthene, magnetite-ilmenite, spinel, and apatite. In mode (Table 8, Fig. 16) and in bulk composition (Table 9, Fig. 17) as well as in texture the facies of this stage reveal their close relationship to the less reconstituted and to the more reconstituted facies with which they are associated.

Relics of the primary ophitic texture are readily found even in facies in which nearly half of the primary plagioclase is replaced by garnet and nearly all of the pyroxene is recrystallized. From the residual areas of primary plagioclase the outlines of the original crystals can be traced, and the original triangular or polygonal areas of mesostatic clinopyroxene are also traceable in the shape and disposition of the granular aggregates of recrystallized augite.

The sharp, and generally straight, boundary between the mesostatic pyroxene and the corona garnet becomes less distinct in later states of coronation. As granulation of the primary pyroxene proceeds, that boundary becomes irregular and is commonly characterized by a narrow zone of mixed garnet and clinopyroxene, with a considerable amount of fine-grained, clear plagioclase (Fig. 15B) and, in some cases, minute scattered grains of hornblende. In other, more advanced cases, the boundary zone is cleared of both pyroxene and garnet, and a narrow moat-like zone of clear plagioclase is formed as small twinned anhedra (Fig. 15C). The exact derivation of this plagioclase zone is not clear, but it is not a corona mineral in the sense that the garnet is.

Stage of poikiloblastic anhedral garnet (P type).—From the central part of the Gore Mountain gabbro toward its southern periphery, one traces relics of the primary mineralogy and textures to within 10 or 20 feet of the Barton garnet deposit. From there on the mineralogical and textural changes are rapid and striking; they are certainly directly related to the intrusion of the syenite magma and are metamorphic in the orthodox sense.

Within this relatively short distance, the last vestiges of ophitic texture and of the primary grain sizes and shapes are eliminated and the coronated gabbro gives way to a wholly reconstituted granoblastic metagabbro. In place of the corona type of garnet one finds highly irregular but nevertheless individualized garnets, 1–3 mm. in size, containing many large inclusions of all the associated minerals. These poikiloblastic garnets (P type) have clearly resulted from a grain-growth recrystallization in which the substance of the more widely scattered and generally finer-grained corona garnet contributed to and was consumed in the growth of larger but fewer garnet individuals. This recrystallization was accomplished without significant change in the chemical composition of the garnet. Moreover, the total amount of garnet in the rock is essentially unchanged (column 5, Table 8).

Concurrently with this very significant change and within the same narrow transition zone, the olivine and the clinopyroxene of the gabbro disappear (Figs. 14A, B). In their place hornblende develops abundantly and orthopyroxene appears as sizeable, discrete grains. The last traces of primary plagioclase disappear, yielding by recrystallization a new and distinctive but less abundant generation of plagioclase.

The new or secondary plagioclase is water-clear, being entirely free of inclusions, and

occurs as sub-equant anhedra 0.5–2.0 mm. in size. The secondary plagioclase is distinctly different in appearance from its primary antecedent, but the compositional range of the plagioclase as irregular anhedra ranging in size from 0.2 mm. to as much as 5 mm. No diopsidic lamellae were observed. The grains are strongly pleochroic from deep pink (X′) to

TABLE 8.—MODES OF GABBRO AND META-GABBRO FACIES

	1	2	3	4	5	6	7	8	9	10
pf:1	58	37.1	34.0	15.7	—	—	—	—	—	—
pf:2	—	—	—	6.0	25.4	36.9	19	20	13	1
ol	10	12.8	6.7	3.6	—	—	—	—	—	—
cpx:1	32	13.0	17.5	20.6	—	—	—	—	—	—
cpx:2	—	10.0	10.0	12.0	—	—	—	—	—	—
opx:2	—	—	—	—	9.7	10.1		7		12
hb	—	tr	5.0	17.2	39.4	42.2	70	61	76	80
bio	—	4.8	.4	.1	tr	tr		1		6
gar C	—	21.1	26.0	24.2	—	—	—	—	—	—
P	—	—	—	—	22.2	10.8	11	—	—	—
X	—	—	—	—	—			—	—	—
XH	—	—	—	—	—	—	—	11	11	—
mt	tr	.9	.3	.6	1.7	tr	tr	—	—	1
sp	tr	.3	tr	tr	tr	tr	tr	—	—	—
ap	tr	tr	.1	tr	tr	tr	—	—	—	—

Legend. pf:1 and pf:2, primary and recrystallized plagioclase; cpx:1 and cpx:2, clinopyroxene, primary and recrystallized; ol, olivine; opx:2, orthopyroxene; hb, hornblende; bio, biotite; gar, garnet, C, P, X, and XH textural types; mt, magnetite and ilmenite; sp, spinel; ap, apatite; pyrite is a minor or trace accessory in several of these facies.

Modes are given in weight per cent.

1. Hypothetical garnet-free primary gabbro; calculated mode.
2. Corona-garnet facies (B201); 150 ft. north of Barton mine.
3. Corona-garnet facies (B 15); north edge Barton mine.
4. Corona-garnet facies (B201a); about 150 feet north of level 3 of Barton mine.
5. Poikiloblastic-garnet facies of metagabbro (B3); north edge of Barton mine. 1.6% calcite omitted.
6. Poikiloblastic and non-poikioblastic crystals garnet facies of metagabbro (B2); north side of Barton deposit.
7. P and X garnet facies similar to 6 above; mode by electromagnetic and Clerici fractionations; north side of Barton deposit. (B2a).
8. Barton ore, typical "dark" ore, XH facies metagabbro. (B110); level 3, Barton mine; mode by combination of fractionation and micrometric analysis.
9. Barton ore; total mode calculated from (a) matrix mode, by fractionation, (b) average garnet content from mine and mill data, and (c) hornblende rim proportions, by measurements.
10. Amphibolite facies (B200); Barton mine.

secondary plagioclase is An_{42} to An_{46}, essentially the same as that of the primary phase. Albite twinning is well developed, and for the most part the lamellae are straight, but evidence of deformation is found in the occurrence of some bent and wedged twin lamellae.

The orthopyroxene in this facies occurs intimately intergrown with the hornblende and pale greenish gray (Z′); most exhibit parallel extinction, but many, as measured in the plane of the section, extinguish at as much as 10° or more from the cleavage. This circumstance may account for the reported presence of "clinohypersthene" in this metagabbro. Universal stage measurements of these grains nevertheless confirm the geometric identity of the optical

indicatrix Z direction with the crystallographic c axis. The optic angle $2V_x$ ranges from 68° to 77°, indicating a composition in the range $Mg_{76}Fe_{24}$ to $Mg_{68}Fe_{18}$. The reliability of the 2V values for composition determination is, however, uncertain because of the possibility of residual strain (Hess and Phillips, 1940, p. 280); the composition is therefore best estimated from the refractive index, Ng = 1.704, which indicates $Mg_{71}Fe_{29}$.

The hornblende occurs as irregular anhedra of medium to coarse grain (1–5 mm)., with the usual well developed cleavage. Coal black in hand specimen, the hornblende is strongly pleochroic light brown or green-brown to dark brown in this section. It is occasionally twinned, with (100) as the composition plane, and is remarkably uniform optically, having a large optic angle, $2V_x$ = 94°, and small extinction angle, $Z \wedge \dot{c}$ = 16°. Small blades of biotite and small irregular grains of magnetite are associated with the hornblende.

The presence in this metagabbro of H_2O, F, and CO_2 in combined form, in the hornblende, in the biotite, and in the traces of carbonate, suggests introduction of volatiles into the gabbro during its peripheral metamorphism by the syenite magma. However, there is no other evidence of significant addition of material to (or removal from) the gabbro; as nearly as can be estimated, the new mineral assemblage is practically equivalent in total bulk composition to that of the corona-bearing gabbro (Table 9, Columns 2, 3).

Stage of megascopic, non-poikilitic garnet porphyroblasts (X type).—The individualized but very small (1–3 mm.), irregular, and characteristically poikilitic garnets of the preceding stage grade within a few feet into clear, red, spherical or dodecahedral crystals ranging up to about 1″ in diameter. These garnets, free of inclusions, are set well apart from each other in a coarse-grained matrix of black (in hand specimen) hornblende and white plagioclase. This facies is the northern edge of the Barton deposit and is mined as garnet ore.

Approximate modes representing the transition between this stage and the preceding one are given in columns 6 and 7 of Table 8. The matrix mineral assemblage, as seen in thin section, is essentially as in the last stage, consisting of coarse (1–5 mm.) hornblende anhedra (green to brown and strongly pleochroic); clear, sub-equant, 0.5–2 mm. grains of secondary plagioclase; minor, small, irregular grains of strongly pleochroic hypersthene; occasional

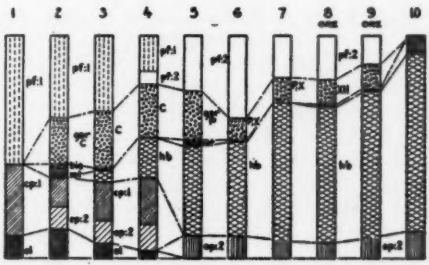

FIGURE 16.—MODES OF GABBRO AND METAGABBRO FACIES, GORE MOUNTAIN
Data of Table 8.

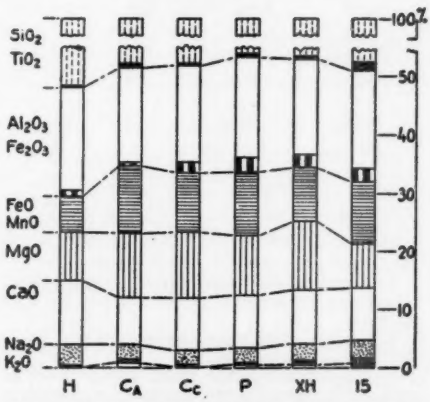

FIGURE 17.—BULK COMPOSITIONS OF GABBRO AND METAGABBRO FACIES, GORE MOUNTAIN

H: hypothetical garnet-free primary gabbro, calculated.

C_A: corona garnet facies, by chemical analysis.

C_C: corona garnet facies, as calculated from mode and mineral analyses.

P: poikiloblastic garnet facies.

XH: Barton dark ore XH garnet facies.

15: Buddington's (1939) average of 15 Adirondack meta-gabbros for comparison.

small blades of red-brown biotite. Neither lineation nor foliation is observed either in thin section or in the rock in place. The texture of the matrix in which the garnet porphyroblasts occur is xenoblastic granular.

The differences between the modes of B2 and B2a (columns 6 and 7) are due partly to the methods used and partly to normal varia-

tion in mineral proportions in these relatively coarse-grained facies. Mode B2 was made micrometrically using a Hurlbut integrating counter, with mechanically driven stage, to record linear traverses at 1 mm. intervals. For B2a 21.59 grams (equivalent to the mass of 324 thin sections) of 30 to 40 mesh crushed sample was fractionated, first with Clerici heavy liquid to separate the garnet, and then by electromagnet to separate the plagioclase from the other ferro-magnesians. The powder loss was slight, and would at most increase the plagioclase figure by 2 per cent.

TABLE 9.—BULK COMPOSITIONS OF GABBRO AND METAGABBRO FACIES

	1	2	3	4	5
SiO_2	47.73	47.5	46.1	46.3	47.30
TiO_2	.65	.3	.6	.7	1.76
Al_2O_3	16.39	16.8	17.2	16.2	16.55
Fe_2O_3	.54	1.5	2.3	2.2	2.21
FeO	11.17	10.2	10.9	9.4	10.24
MnO	.16	.1	.1	.1	.19
MgO	11.07	11.6	10.4	11.8	7.53
CaO	8.04	9.0	9.0	9.2	9.09
Na_2O	2.53	2.2	2.5	2.7	2.95
K_2O	.48	.7	.3	.6	.83
H_2O+	.96	.1	.6	.8	.57
P_2O_5	.28	tr	tr	—	.31
Other.....	—	—	—	—	.36
Total.....	100.00	100.0	100.0	100.0	99.89

1. Corona-garnet facies. Shand's (1945) chemical analysis, recomputed to 100. North of the Barton mine.
2. Corona-garnet facies, as computed from mode and mineral compositions.
3. Poikiloblastic-garnet facies, Barton mine; as computed from modes and mineral compositions; CO_2 subtracted.
4. Barton ore (XH garnet facies); as computed from mode and mineral compositions.
5. Buddington's (1939, p. 221) average of 15 Adirondack metagabbros, for comparison.

The most significant changes which mark the increase in size of the garnet at this stage are its expulsion of foreign inclusions, its development of the spherical or, less commonly, dodecahedral shape, and finally, the apparent reduction in total amount of garnet. The amount of garnet (11 per cent) found in the transition specimen B2 by linear micrometric analysis agrees with that found by fractionation (B2a), and both agree with the average garnet content of the ore as indicated by Barton mill data, (10–12 per cent garnet, according to Mr. F. C. Hooper, former manager, Barton Mines). It is not known whether the difference between the 11 per cent of garnet (in the XH and X facies) and the 22–25 per cent (in the P and C facies) represents a reduction during metamorphism or a difference in amounts of deuteric garnet originally present in the core of the gabbro as compared with the periphery.

Stage of giant, hornblende-sheathed garnets (XH type).—The culmination of the recrystallization growth of the garnet is represented by the giant individuals of the Barton garnet ore. Deep red, extraordinary in size, framed in a shell (in section a rim) of coal-black hornblende, and set in a salt-and-pepper matrix of hornblende and plagioclase, these garnets make a spectacular showing in the walls and faces of the Barton quarry. The main body of the deposit, including the bulk of the ore, is comprised of this facies, which differs from the X facies in only two respects: (1) the garnets are larger; and (2) they are surrounded by hornblende shells. The composition and properties of this garnet are essentially the same as those of the garnet of all the previously described facies of the Gore Mountain gabbro.

SIZE OF THE GARNETS: Most of the garnets are 4–6 inches in diameter. The observed size range is 1–20 inches or more, but exceptional single garnets 3 feet in diameter, and over 1½ tons in weight, are reported to have been quarried here. Size distribution is seriatal both in the deposit as a whole and locally; within any small area of exposure, such as a square yard, the size range is quite narrow. Moreover, smaller garnets are in general more closely spaced than are the larger ones, and the matrix between garnets is completely devoid of fine or microscopic garnet. There is thus reason for believing that the garnet content in this facies

is somewhat uniform and that the local growth of larger crystals is compensated by their reduction in number per cubic yard of rock.

SHAPE OF THE GARNETS: A roughly spherical shape characterizes the majority of the garnets, but many dodecahedra are found (Pl. 2, fig. 2). Less common are the highly irregular garnets whose shapes suggest fragmentation and partial resorption of garnet locally during the period of large garnet growth. One 6-inch spherical garnet was found to contain, as a core, two 1-inch dodecahedra from which it broke away readily because of an intervening film of chlorite. All others, however, were found to be visibly uniform and homogeneous throughout. Except for occasional crystals of biotite and hypersthene, the garnets are free of megascopic inclusions. A universal and economically important feature of the garnet is its well developed close fracturing, which is co-ordinate with the regional joint system.

HORNBLENDE SHELL OR RIM: In cross-sectional exposure each garnet is surrounded by a rim which, in the third dimension, is a shell of roughly uniform thickness, concentric with the periphery of the garnet. The shell is composed of xenoblastic grains of coarse (3–25 mm.) hornblende, optically very similar to that of the matrix. In fact, the shell is not sharply bounded externally; it grades, though rather abruptly, into the hornblende-plagioclase matrix. Only megascopically can the effective outer boundary of the shell be located. The inner boundary is sharp megascopically and is, in many cases, separated from the garnet by a thin, irregular, discontinuous shell of glassy plagioclase ("rim plagioclase"), which appears to be associated with veinlets of late glassy plagioclase containing occasional large (1–4 inch) crystals of pyroxene (hypersthene). Composition and physical properties of the rim hornblende are given in Table 10.

MATRIX: The matrix between the sheathed garnets is coarse, xenomorphic granular hornblende and plagioclase with orthopyroxene (hypersthene) and minor biotite. The average mode, as determined by linear micrometric analyses on thin sections of typical specimens, is given in the next column.

Ore matrix, mode

Mineral	*Wt.%*	*Composition*
hb	62.5	Optically same as rim hornblende
pf	27.0	$Or_{.5}Ab_{49.5}An_{50}$
op	9.3	$Mg_{71}Fe_{29}$, Ng′ on (110) = 1.704
bio	1.2	Not determined

The plagioclase, as in the preceding facies, is anhedral, water-clear, 1–2 mm. in size, and albite-twinned. Its composition, which has considerable bearing on the genesis of the deposit, was determined by analysis of a fractionated sample of typical matrix plagioclase, and by numerous optical measurements. It is evidently slightly more calcic (An_{50}) than the primary plagioclase (An_{45}) of the gabbro.

Matrix plagioclase

SiO_2	55.24	
Al_2O_3	28.17	Analysis recast: $Or_{.5}Ab_{49.5}An_{50}$
Fe_2O_3	.65	plus 3% femags.
		Maximum extinction angle, by U-stage:
MgO	.20	X′∧ (010) = 27° – 28°; An_{49-50}
CaO	9.75	N′p on (010) = 1.554; An_{50}
Na_2O	5.86	Optics: S. B. L.
K_2O	.09	
H_2O	.17	
	100.13	

Analyst: S. J. Shand.

The hornblende occurs as anhedra, .5–5 mm. in diameter, with optical properties very similar to those of the rim hornblende. The hypersthene is found as strongly pleochroic, rounded anhedra 0.2 mm.–1 x 3 mm.; many grains give evidence of peripheral alteration to hornblende or to biotite.

MODE OF THE GARNET ORE: Accurate determination of the mode of so very coarse a facies is not feasible by petrographic methods, but for the purposes of comparison with other facies of the gabbro an approximate mode is computed by combining available data. Taking the average garnet content as 11 per cent (from mine and mill data), and the average weight ratio of rim hornblende to garnet as 1.37 (independently determined), the weight of the hornblende shells is 1.37 x 11 per cent = 15 per cent. The garnets and their shells together

TABLE 10.—COMPOSITION AND PHYSICAL PROPERTIES OF RIM HORNBLENDE B110h, BARTON MINE

	Wt.	Mol	
	per cent		
SiO_2	43.50	725	G = 3.172 ± .005 (20°C).
TiO_2	1.12	014	
Al_2O_3	13.15	129	Ng = 1.676 ± .002 (λ5893):
Fe_2O_3	3.39	021	Np = 1.658 ± .002
FeO	9.38	130	Ng-Np = .018
MnO	0.09	001	$2V_x$ = 95° ± .5 (λ5893).
MgO	14.25	356	$Z \wedge c$ = 16° ± .5
CaO	10.58	189	
Na_2O	2.53	041	Absorption: Z > Y > X.
K_2O	0.68	007	Color: in thin section, olive green, light brown, brown; at 60 mesh, green; in hand specimen, black.
H_2O^+	1.15	064	
H_2O^-	0.12		
F	0.30	016	
	100.24		Analyst: S. B. L.
−O=F	.12		
	100.12		Structure type: $X_{0-1}A_2B_5C_8Y_{24}$

Ionic ratios		Structural account					Electrical	
		X	A	B	C	Y	(+)	(−)
K^{1+}	.12	.12					0.12	
Na	.72	.72					0.72	
Ca^{2+}	1.65	.02	1.63				3.30	
Mn	.01		.01				0.02	
Fe	1.14		.36	.78			2.28	
Mg	3.12			3.12			6.24	
Fe^{3+}	.37			.37			1.11	
Al	2.26			.61	1.65		6.78	
Ti^{4+}	.12			.12			0.48	
Si	6.35				6.35		25.40	
O^{2-}	22.74					22.74		45.58
OH^{1-}	1.12					1.12		1.12
F^{1-}	.14					.14		.14
		.86	2.00	5.00	8.00	24.00	46.45	46.84

thus constitute 11 per cent plus 15 per cent, or 26 per cent of the ore. The remainder, 74 per cent, is matrix, whose micrometric mode has been given above. By equating the matrix mode to 74 per cent, the total ore mode is computed as follows (Table 8, column 8):

TABLE 10.—COMPOSITION AND PHYSICAL PROPERTIES OF RIM HORNBLENDE B110h, BARTON MINE

	Wt.	Mol	
	per cent		
SiO_2	43.50	725	G = 3.172 ± .005 (20°C).
TiO_2	1.12	014	
Al_2O_3	13.15	129	Ng = 1.676 ± .002 (λ5893):
Fe_2O_3	3.39	021	Np = 1.658 ± .002
FeO	9.38	130	Ng-Np = .018
MnO	0.09	001	$2V_x$ = 95° ± .5 (λ5893).
MgO	14.25	356	$Z \wedge \dot{c}$ = 16° ± .5
CaO	10.58	189	
Na_2O	2.53	041	Absorption: Z > Y > X.
K_2O	0.68	007	Color: in thin section, olive green, light brown, brown; at 60 mesh, green; in hand specimen, black.
H_2O^+	1.15	064	
H_2O^-	0.12		
F	0.30	016	
	100.24		Analyst: S. B. L.
−O=F	.12		
	100.12		Structure type: $X_{0-1}A_2B_5C_8Y_{24}$

Ionic ratios		Structural account					Electrical	
		X	A	B	C	Y	(+)	(−)
K^{1+}	.12	.12					0.12	
Na	.72	.72					0.72	
Ca^{2+}	1.65	.02	1.63				3.30	
Mn	.01		.01				0.02	
Fe	1.14		.36	.78			2.28	
Mg	3.12			3.12			6.24	
Fe^{3+}	.37			.37			1.11	
Al	2.26			.61	1.65		6.78	
Ti^{4+}	.12			.12			0.48	
Si	6.35				6.35		25.40	
O^{2-}	22.74					22.74		45.58
OH^{1-}	1.12					1.12		1.12
F^{1-}	.14					.14		.14
		.86	2.00	5.00	8.00	24.00	46.45	46.84

thus constitute 11 per cent plus 15 per cent, or 26 per cent of the ore. The remainder, 74 per cent, is matrix, whose micrometric mode has been given above. By equating the matrix mode to 74 per cent, the total ore mode is computed as follows (Table 8, column 8):

Modes, weight per cent

Ore matrix			Garnet & Shell	Total ore	Mineral Composition
hb	62.5	46.2	15.0	61.2	As analyzed
pf	27.0	20.0		20.0	As analyzed
op	9.3	6.9		6.9	$Mg_{71}Fe_{29}$
bio	1.2	0.9		0.9	Not determined
gar			11.0	11.0	As analyzed
	100.0	74.0	26.0	100.0	

No precision can be claimed for this mode, but the close agreement with the mode of the transitional (small garnet) facies B2a (Table 8, column 7) independently obtained by fractionation, indicates sufficient reliability for use in evaluating the hypotheses of garnet ore genesis.

BULK CHEMICAL COMPOSITION OF THE ORE: Using the computed ore mode, and mineral compositions as analyzed, or as indicated by optical determinations, the approximate bulk composition of typical ore facies was computed. The results (Table 9, column 4) may be compared with the bulk compositions of the poikiloblastic garnet facies and the corona garnet facies as similarly computed, and with the composition of a specimen of the corona garnet facies as analyzed by Shand. The agreement is very close except for slight but not unexpectable variations in magnesia and in ferrous-ferric iron. These three facies (C, P, XH) have essentially the same composition in spite of their different mineral assemblages and quite different textures. The hypothesis that the garnet ore is simply a highly reconstituted facies of the Gore Mountain gabbro, based at first upon the existence of complete mineral and textural gradation between primary gabbro and the garnet ore, is thus supported by the evidence of their bulk chemical composition.

SYENITE AND SYENITIC HYBRIDS

Primary Facies of the Syenite

The southern edge of the garnet deposit, against the syenite, presents a complex array of facies and structural details whose significance is better understood by approaching from the syenite side rather than from the gabbro side.

The syenite at Gore Mountain, as elsewhere in the eastern Adirondacks, is quite variable in amount of quartz and in the relative amounts of the several ferromagnesian constituents. But the character of the feldspar present, and the habits of the dark minerals, are distinctive enough so that any significant departure from the local primary facies is recognizable. The mode of a typical specimen of the unmodified syenite, from an exposure 400 feet south of the Barton mine, is given in Column 1, Table 11. The fresh rock is pale olive green to gray green, medium-grained, and moderately foliated; weathered surfaces are a characteristic light buff or tan, faintly spotted or streaked. In thin section the bulk of the rock is observed to be composed of orthoclase microperthite occurring as anhedral grains, 0.5–2 mm. in diameter, with abundant "guttate" and spindle-shaped blebs of non-twinned plagioclase inclusions. A small but variable amount of plagioclase is present as individual clear anhedra, many of which are albite-twinned; the extinction angles indicate a composition between about An_{10} and An_{25}. The quartz occurs as irregular, sometimes elongate, anhedra (0.5–1.5 mm). Hornblende anhedra (0.5–2 mm.) tend to be elongate, and almost invariably exhibit embayed outlines against feldspar, but straight boundaries against other hornblende grains. The hornblende is deep green and strongly pleochroic. The clinopyroxene likewise is green, and highly irregular in shape. Dark schiller-type inclusions in the form of plates extending across some of the augite grains, and projecting beyond the embayed boundaries into the surrounding feldspar, give evidence of selective resorption. Irregular grains of magnetite, small prisms of apatite, and traces of hypersthene and titanite complete the mineral assemblage. Garnet is absent.

Features of Transitional Facies

In exposures nearer to and finally immediately adjacent to the garnet deposit, several striking changes in the syenite are noted (Table 11, Fig. 18). The plagioclase increases in

amount, and becomes more calcic, and more coarse; from an original 3 or 4 per cent the plagioclase increases to 80 per cent and even more, meanwhile changing progressively from An_{20} to An_{33}. Clear of intergrowths at An_{33}, it becomes locally antiperthitic at An_{27}, and clears again to a single phase as the An content increases. Concurrently with these progressive changes in plagioclase composition and amount, the original, dominant, orthoclase microperthite diminishes in amount, becomes nonperthitic, finally disappears; with it goes the quartz.

Within a few feet of the contact with the garnet deposit, but still within the syenitic rock, xenolithic constituents appear. Small shreds and angular masses of coarse black hornblende up to several feet long become increasingly prominent, and with them are found numerous deep-red garnets 1–3 inches in diameter. Many of the garnets are euhedral; almost all are rimless. In composition these garnets are essentially the same as those of the

TABLE 11.—MODES OF SYENITE AND SYENITIC HYBRID FACIES

	1	2	3	4	5	6
kf	61.9	69.3	1.1	0	5	0
pf	3.7	16.4	65.3	80	45	75
qtz	14.7	.5	10.2			
hb	10.4	9.3	—			
cpx	5.3	—	—			
opx	tr	—	14.3			
mt	2.9	4.1	4.8			
ap	1.1	.2	1.7			
tit	tr	.2	tr			
gar	—	—	2.6			
	100.0	100.0	100.0			
kf:	Orthoclase perthitic	Orthoclase perthitic	Orthoclase clear	None	Orthoclase clear	None
pf:	An_{20} clear	An_{23} clear	An_{27} antiperthitic	An_{40} clear	An_{45} clear	An_{52} clear

Modes in weight per cent.
1. Primary syenite (B10); 400 feet south of Barton mine.
2. Matrix of slightly contaminated syenite (B14), from along the south side of the mine; contains few garnet xenocrysts, 1–3 inches diameter, rimless.
3. Matrix of syenite hybrid (B9) from syenite-ore contact; large garnet xenocrysts not included in mode.
4. to 6. Feldspars in the matrix of syenite hybrids (B25, 13, 34) containing different amounts of xenolithic hornblende and rimless garnet xenocrysts ½–3 inches diameter; from syenite-ore contact, south side of Barton mine.

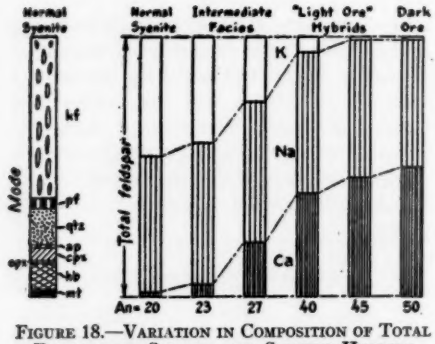

FIGURE 18.—VARIATION IN COMPOSITION OF TOTAL FELDSPAR IN SYENITE AND SYENITE HYBRIDS

South side of Barton mine. Numbers at base of bars indicate composition of the modal plagioclase (in mol per cent anorthite) in each facies. Perthitic "potash" feldspar: kf. Plagioclase: pf.

garnet deposit proper. Most of the garnets are embedded directly in the matrix of this hybrid facies, which consists dominantly of coarse (2–7 mm.), clear, anhedral plagioclase, An_{45} to An_{32}, and coarse hornblende; but many garnets are wholly in the hornblende masses or partly in hornblende and partly in the plagioclase matrix. The present author agrees with Krieger (1937, p. 110) that the syenite appears to have separated the garnets from their hornblende rims; the larger garnets, originally enclosed in shells of hornblende, were partly "shelled" during incorporation in the syenite. The hornblende, in this hybrid rock, is apparently the same as that in the adjacent meta-gabbro.

From the progressive change in the feldspar composition, the angular character of the xenolithic hornblende, and the unresorbed profiles of the garnet in the hybrid rock, it appears that the syenite magma was selective in its assimilation of the ore facies metagabbro. While the garnet and the hornblende of the metagabbro remained unassimilated, the plagioclase was evidently thoroughly made over, combined with the feldspathic content of the syenite magma, and then crystallized out as a new feldspar. The composition of the new feldspar was thus determined by the compositions and relative amounts of assimilated plagioclase and potential feldspar of the uncontaminated magma.

The product of this partial and selective assimilation is a coarse-grained, garnetiferous hornblende-plagioclase rock of dioritic or soda gabbroic character, depending upon the amount of meta-gabbro locally incorporated and the extent of diffusion in the magma. The same, or very similar, rock type, found in numerous other adirondack localities in syenite, but without visible connection with gabbro or metagabbro, has been variously interpreted by earlier investigators.

Syenite-gabbro and Syenite-anorthosite Hybrids

There are several other facies in which mineralogic and textural relics of ophitic anorthosite and gabbro occur. These are found chiefly at the western end of the Barton mine where syenite, gabbro, metagabbro, and anorthosite meet.

In the layered facies, at the western end of Level 1, a weathered, light-colored facies grades down-dip into fresh, dark-green, syenite-anorthosite hybrid carrying 5–25 per cent of angular hornblende patches or hornblende-rimmed pyroxene patches. Large (up to 50 x 75 mm.), tabular crystals of labradorite (An_{55}), dark blue in hand specimen, and Carlsbad-twinned in many cases, are found in this facies of widely varying color index. The crystals are identical with the plagioclase of the primary anorthosite, and, in the hybrid, are believed to be xenocryst relics. In dominantly hornblendic matrix, the plagioclase crystals are commonly framed by red corona garnet. In dominantly feldspathic matrix, vestiges of the primary ophitic texture of the gabbro and of the anorthosite are represented by the triangular patches of granular mosaic pyroxene and derivative hornblende; the aggregate in many cases is framed from the matrix by corona-stage garnet. Where many such aggregates have survived in a cream-buff matrix of anhedral plagioclase, the rock presents a characteristic hieroglyphic appearance. The features of each hybrid facies thus reflect not only the original composition of the invaded rock, but also the degree of metamorphic reconstitution undergone by that rock before hybridization.

In the syenite half a mile south and southeast of the Barton mine, on the slopes of Gore Mountain, according to Krieger's map, there are areas of syenite in which large labradorite crystals occur. The view (Balk, 1932, p. 21; Krieger, 1937, p. 52, 56) that these crystals, rather than being surviving xenocrysts, were indigenous in the syenite magma is not supported by the evidence of the hybrid facies at the western end of the Barton mine.

Garnetiferous Meta-anorthosite Facies

Petrography

The facies comprising most of the larger anorthositic body of the Gore Mountain area was described by Krieger (1937, p. 44) as largely Whiteface type: a light gray-white, medium-grained, dominantly (80–85 per cent) feldspathic, somewhat foliated rock, locally variable in color and texture, and grading into gabbroic anorthosite.

This rock bears no outward resemblance to the Marcy type in hand specimen or outcrop, except for the local occurrence of large plagioclase crystals. In thin section, however, relics of primary, dark, euhedral plagioclase, mesostatic clinopyroxene, and ophitic texture are locally preserved in a xenoblastic granular matrix. In spite of their extensive obliteration in this area, the local small-scale survival of these primary mineralogical and textural features reveals clearly that the parental type from which the present facies was derived was a normal ophitic anorthosite. It has here undergone extensive granulation and recrystallization of a type more intense than that which produced the so-called protoclastic structure characteristic of much of the core facies anorthosite of the main Adirondack massif.

In the resulting meta-anorthosite of the Gore Mountain area the history of protoclastic deformation and granoblastic reconstitution is revealed especially by the feldspar. The early stages are represented by residual plagioclase crystals exhibiting all degrees of strain, fracture, and granulation. An extensive recrystallization of plagioclase into plagioclase accompanied and followed the deformation. The secondary plagioclase which resulted is dominant and distinctive; in sharp contrast with the primary crystals, it occurs as small (.5–2 mm) anhedra completely clear of inclusions. (In hand specimen the secondary plagioclase is characteristically dull white and medium-grained, as compared with the dark-blue or greenish, coarse-grained primary type.) The well developed twin lamellae of the clear anhedra are generally straight, but the occurrence of a small percentage of bent or wedged lamellae indicate a chronological overlap of deformation and recrystallization. Minute blebs and tablets of antiperthitic potash feldspar in some of the secondary plagioclase indicate that exsolution was also a phase of the recrystallization process.

The proportions of residual (primary) and recrystallized plagioclase in the meta-anorthosite at Gore Mountain are extremely variable. Of two specimens taken from the western part of the body, along the Gore Mountain road near the north and south borders, one showed no residual primary plagioclase, the other showed an estimated 5 per cent. A specimen from Pete Gay (elev. 3145 feet), nearer the center of the body, contains approximately equal amounts of primary and recrystallized plagioclase. Primary mesostatic augite is not common, being preserved only between surviving euhedral plagioclase crystals. But all stages of granulation, recrystallization, and metasomatic replacement of the primary clinopyroxene are represented here, as in the gabbro. In many roughly polygonal aggregates of granular recrystallized augite, representing former mesostatic areas, alteration to orthopyroxene or replacement by hornblende, magnetite, and biotite is far advanced. Hypersthene is the dominant pyroxene in some specimens, but its petrographic setting leaves little doubt concerning its metamorphic origin as a phase of the reconstitution of augite.

Garnet In Meta-anorthosite

Garnet is a prominent accessory in all facies of the meta-anorthosite, and is locally abundant. Both the corona and the poikiloblastic stages of development are represented. Corona-garnet, as in the gabbro, is restricted to those spots where primary plagioclase has survived. But, since primary plagioclase survives in all but the recrystallized peripheral portions of the gabbro mass, corona-garnet is the characteristic type in most of the gabbro, whereas in the almost completely recrystallized anorthositic body the garnet occurs characteristically as irregular, small (1–5 mm.), poikiloblastic individuals scattered through the matrix of medium-grained, anhedral, white plagioclase. Somewhat larger non-poikilitic porphyroblasts (X type) occur more locally. In the less exclusively feldspathic facies, the garnet is commonly associated with the other ferro-magnesian constituents, chiefly hornblende with magnetite, biotite, and hypersthene, and occasionally with recrystallized augite.

This association of individual garnet (porphyroblasts) with the other ferromagnesian minerals locally takes the form of rounded masses or clumps up to 2 or 3 inches in diameter (Krieger, 1937, p. 45). More commonly, however, a crude alinement of the dark minerals into short and irregular sub-parallel streaks

or lenticular clusters gives the meta-anorthosite a poorly developed, gneissoid foliation, here interpreted as secondary.

Origin of the Barton Deposit

Introduction

The possible origins of the garnet of the Gore Mountain area were discussed in detail by Krieger (1937, p. 100–120), who reported that the evidence was insufficient and inconclusive. In the light of the additional evidence now available the subject is reviewed here and four earlier hypotheses are re-evaluated:

Hypothesis 1. The Barton deposit is a highly modified Grenville inclusion.

Hypothesis 2.—The Barton deposit is a primary peripheral facies of the gabbro, the product of flow segregation (of the garnet and associated dark minerals) in the parental magma.

Hypothesis 3.—The Barton XH garnets as well as the associated garnet types (including corona garnet) in the gabbroic and anorthositic facies, and in the contiguous (syenitic) facies, are all *in situ* products of post-syenite regional metamorphism.

Hypothesis 4.—The Barton deposit is a reconstituted peripheral portion of the gabbro, its metamorphism induced by the intruding syenitic magma, and the XH garnets are *in situ* products of that metamorphism. But the "light ore" zone, between the Barton ("dark") ore proper and the syenite, is a surviving band of an older, pre-syenite hybrid, the consolidation product of a syntectic magma formed when anorthosite magma intruded and assimilated the peripheral portion of the gabbro. The X type garnets grew in that syntectic magma and are thus magmatic, indigenous in the hybrid facies, pre-syenite in age, and older than the XH garnets of the contiguous Barton ore.

Hypothesis 1. Modification of Grenville Inclusion

This hypothesis, that the Barton garnet ore represents a highly modified or wholly reconstituted lenticular inclusion of Grenville rock, the original having been caught up either in the syenite magma or in the gabbro-anorthosite-syenite magma, depending upon one's view of Adirondack petrogenesis, was originally advanced by W. J. Miller (1912; 1914, p. 81). He subsequently rejected it (1938, p. 399), but it is still accepted by some.

Since no relic structural or textural features indicate a metasediment, this hypothesis must stand or fall on the chemical evidence of mineral phases and bulk composition. The presence of garnet, a common and prominent product of contact metamorphism, probably first suggested this hypothesis. The garnet, then, should reflect compositionally the nature of the modified rock. Consideration of a limestone inclusion is eliminated at once; in that case the garnets would be the lime-rich grossularite-andradite variety rather than pyralmandite. Similarly, a siliceous (quartzitic) inclusion is ruled out by the high percentage of magnesium component in the Barton garnets.

It is not feasible, however, on the sole basis of garnet composition, to eliminate the possibility of derivation from a Grenville amphibolitic lens. In the present study many garnet specimens were collected, especially in the Newcomb, North Creek, and Thirteenth Lake quadrangles, from Grenville metasediments and hybrid facies; some 15 of these were selected for partial analysis. Omitting two obviously skarn garnets, the N/G field of the others overlaps the iron-rich end of the N/G field of garnets from anorthosite-gabbro facies. The plots of several specimens from amphibolitic Grenville facies fell within the field of the anorthosite-gabbro garnets. But in spite of this indicated compositional overlap, a structural distinction exists between garnets in definite anorthosite-gabbro settings and those in definite Grenville amphibolitic setting: the former, when larger than about 1 inch in diameter, are non-poikilitic; the latter, when larger than about 1 inch, almost always contain abundant inclusions, usually of quartz and feldspar, and are quite irregular. Structurally the Barton garnets bear no resemblance to the garnets of definitely Grenville amphibolites.

The bulk composition of the Barton ore does not rule out the possibly of derivation from a Grenville amphibolite. But since the ore is compositionally equivalent to the associated gabbro and grades into it, there is no

need for assuming the former presence of a Grenville amphibolite.

Conclusions with respect to this first hypothesis are: (1) The ore could not have been derived from an inclusion of Grenville limestone or sandstone or quartzite. (2) The ore probably could have been derived from an amphibolite having the bulk composition of the gabbro, but there is no positive evidence of such derivation, and the habit of the Barton garnets argues against it. (3) The completely gradational relationship between the ore and the gabbro points to a genetic relationship quite independent of any Grenville involvement.

Hypothesis 2. Primary Magmatic Segregation

Others have variously implied and suggested that the garnetiferous amphibolitic peripheral facies of Adirondack gabbroic bodies is the product of flow segregation of primary ferromagnesian minerals in a parental magma from which gabbro, anorthosite, and syenite were differentiated. A corollary of this hypothesis is that the texture and mineral assemblage of the massive, ophitic facies which forms the core of the gabbro bodies are secondary, the products of subsequent recrystallization. Balk (1931, p. 352–4; 1932 p. 19, 56, 67) has been the chief advocate of this viewpoint, although he did not specifically apply it to the Barton deposit.

The hypothesis implies an approximate equivalence in bulk composition between the core and the peripheral facies of the gabbro, as well as a textural and mineralogical gradation between them. For the southern periphery of the Gore Mountain gabbro body, these conditions have been confirmed by the present study. There is no structural discontinuity between the Barton dark ore and the gabbro; there is a continuous gradation, mineralogically and texturally, between the ophitic gabbro and the dark ore; and the coronated ophitic facies and the dark ore, as well as the intermediate granoblastic metagabbro, have essentially the same bulk composition. This, however, simply confirms the genetic relationship of the ophitic gabbro and the Barton dark ore as varietal extreme facies of the same body. It does not establish which is the original and which the derivative or reconstituted facies.

The ophitic texture is regarded by the present writer, and would probably be accepted by most petrologists, as strong presumptive evidence that the core facies is the primary one. This distinctive texture is found widely in basic igneous rocks where there is no evidence of subsequent metamorphism, and, conversely, the xenomorphic amphibolitic facies—in rocks of this composition—is almost universally associated with a metamorphic history. But there is more direct evidence on this point.

Of the three major constituents of the core facies, two (the augite and the olivine) are characteristically igneous in origin, while the third (plagioclase of euhedral habit and An_{65} composition) is not characteristically metamorphic. Moreover, two of the major constituents of the peripheral facies (the hornblende and the garnet) are more characteristically secondary than primary.

From the fact that XH type garnets of the Barton deposit are more nearly subhedral to euhedral than are any of the other minerals (except some hypersthene crystals), it is inferred that their morphological habit, as well as their large size, must be attributed either to early growth in a magma, or to superior force of crystallization under metamorphic conditions. The specific gravity (4) of these giant garnets is nearly half again as great as that (say 2.7) of any (gabbroic) magma in which they may have occurred, and they are massive enough to have been subject to gravitational segregation in any but an unusually viscous magma. Yet there is no evidence of gravitational segregation or clustering of the Barton garnets; in fact, the larger are the more distantly spaced from each other.

Further pertinent evidence is the nature of the slight compositional zoning of the large (XH) garnets. Since in the crystallization of femic magmas there is generally a progressive increase in the Fe/Mg ratio, one might expect that the large garnets, if magmatic in origin, and if zoned at all, would have peripheral zones relatively rich in Fe. Actually, there is a slight but progressive decrease in the Fe/Mg ratio from the center outwards. Furthermore, their morphology indicates normal centrifugal growth.

In summary, the lack of gravitational segre-

gation and the inverse Fe/Mg ratio of the large Barton garnets, together with the mode and texture of the facies in which they occur, as compared with the ophitic gabbro, argue against a magmatic origin.

Alternative Hypotheses of Regional or Contact Metamorphism

Hypotheses 3 and 4 both treat the large hornblende-rimmed garnets (XH type) of the Barton dark ore as *in situ* products of the metamorphic reconstitution of gabbro. They disagree on three points: (1) the character of that metamorphism, whether contact or regional; (2) the time of metamorphism, whether pre-syenite, syenite, or post-syenite; (3) the origin of the X type garnet in the "light ore" facies, and whether contemporary with or older than the XH garnets of the contiguous dark ore.

The determination of the genetic order in the sequence of garnet types is critical in the evaluation of these hypotheses. The present study has shown that the C, P, and X, and XH type garnets, in the coronated ophitic gabbro, in the granoblastic metagabbro, and in the dark ore, respectively, constitute a continuously gradational textural series, characterized by increasing grain size and progressively more euhedral habit, and by a narrow range of compositional variation. It is inferred from these observations that the four textural types of garnets represent a parental type and its progressive derivatives.

The XH type is not primary; location and petrographic evidence indicate that these very large garnets represent the most advanced stage of metamorphic garnet growth. The corona C type (1) is restricted to the ophitic facies or to residual-ophitic portions of otherwise recrystallized facies; and (2) was developed exclusively by replacement of primary plagioclase. It is therefore inferred (1) that the corona garnet is secondary in origin; (2) that it is, however, most closely related to the primary facies; (3) that, on the direct evidence, the corona garnet could be either deuteric or meta-morphic; but (4) that, in either case, the corona garnet is the parental type.

Hypothesis 3. Post-syenite Regional Metamorphism

In his Adirondack memoir (1939, p. 250–323), Buddington reported, in effect, as follows: (1) In those igneous rocks, including ortho-gneisses, which retain essentially their texture of magmatic crystallization, no garnet occurs. (2) In the western Adirondack region, where the metamorphism was largely or wholly cataclastic, no garnet is found in any of the igneous rocks. (3) In the south-central region and in the north-central region (around the northwestern end of the anorthosite massif), where recrystallization was a major feature of the metamorphism, garnet is prominent in gabbroic and anorthositic facies, and present though sparse in syenite and syenite-related granite; but it does not occur at all in facies classified by him as belonging to the younger granite series. Moreover, he noted (p. 298) that in the most intensely metamorphosed facies the garnet occurs "as disseminated euhedral crystals in contrast to the garnet coronas of an earlier stage".

From the available evidence Buddington concluded: (1) that garnet formation was a regional phenomenon and related primarily to regional metamorphism; (2) that the difference between corona garnet and the larger, more euhedral, porphyroblasts is simply a matter of variation in metamorphic intensity; (3) that there was essentially only one period of garnet formation, a period of post-syenite pre-younger-granite regional metamorphism.

The unusually large, hornblende-rimmed garnets he attributes to the more favorable conditions found locally along the contact zones between two rock masses of different character, perhaps an appropriate combination of rock composition, of pressure, stress, and temperature, and the adequacy of solutions for the transfer of material. Application of this hypothesis to the Barton and other deposits in the southeastern Adirondacks encounters several difficulties.

It is by no means clear that such favorable conditions are localized along the contact zones between two rock masses of different character, unless one refers explicitly to the intrusive character of an intrusive contact. And in that

case, what more favorable time than the time of intrusion? Why should the conditions be considered more favorable during some later and unrelated period of regional metamorphism?

In the southeastern Adirondacks the garnet-rich facies (other than in the Grenville) occur where syenite magma intruded members of the anorthosite-gabbro series; the garnet deposits are found either along the intrusive contacts or in the hybridized relic bodies of gabbro or gabbroic anorthosite. The XH type garnets, which evidently represent the most advanced stage, are restricted to the syenite-gabbro contacts, both at the Barton mine and at Humphrey Mountain some 10 miles distant; the Barton deposit as a whole is essentially co-extensive with the syenite-gabbro contact.

It may be argued that the gabbro or anorthosite, contact-metamorphosed by the syenite magma or hybridized by it, provided precisely the favorable setting required for later development of garnet by regional metamorphism. But there is no evidence for such an interpretation in this region. In the north-central region (Santa Clara, Nicholville, Stark quadrangles) Buddington's interpretation of garnet age is based in large part on the frequent occurrence of corona garnet in syenite and its absence from the later granite; it is evidently also based upon an implied assumption that the corona and porphyroblast garnets in the gabbroic and anorthositic facies are products of the same (regional) metamorphic program which was responsible for the corona garnet in the syenite. To the present writer this assumption seems unwarranted in any case, and particularly inapplicable in the southeastern region, where the syenite is garnet-free and there is no evidence of post-syenite garnet. In the southeast it is more in keeping with the available evidence to interpret the preferential localization along syenite-gabbro and syenite-anorthosite contacts as genetically related to the direct metamorphic influence of the intruding syenite magma.

The problem of the age relationship of garnet to syenite in the southeastern Adirondacks is more directly approached by consideration of the garnet in the Barton light ore. According to hypothesis 3 the garnets in this facies, and those in the other facies, are *in situ* products of post-syenite regional metamorphism. The present study leads instead to the conclusion that the garnets were not indigenous in this facies, but are xenocrysts which had grown and were growing as porphyroblasts in a gabbroic matrix until hybridization took place.

That the light ore is a hybrid facies resulting from partial assimilation of metagabbro by syenite magma is inferred from these observations: (1) There is no structural discontinuity between the normal syenite and the light ore; (2) There is a structural discontinuity between light ore and dark ore; tongues of the former project irregularly into the latter and large angular fragments of the dark ore occur in the light ore along and near the contact; (3) The light ore is quite different from the syenite in composition but there is a continuous modal and textural gradation between them; (4) There is especially a continuous gradation in total feldspar composition from the normal syenite (approximately $K_{44}Na_{33}Ca_{23}$) into the light ore (approximately $K_{1}Na_{33}Ca_{46}$), and the direction of this variation is that which would result from the incorporation of metagabbroic feldspar.

That the assimilative process was selective, affecting primarily the feldspar, and leaving fragments of coarse black hornblende as xenoliths is inferred from these observations: (1) It is the feldspar which shows the very marked and progressive compositional gradation. (2) The hornblende of the hybrid facies is optically and texturally like that of the dark ore, and unlike that of the normal syenite. (3) The hornblende of the hybrid facies (unlike that in the syenite) occurs in large, angular, and irregular, polycrystalline masses. (4) There is no evidence of resorption of the garnet.

Finally, it is inferred that the large garnet individuals (X, and some XH) which occur in the hybrid facies are xenocrysts, because (1) they are identical in habit and in composition with the garnet prophyroblasts of the contiguous dark ore and metagabbro; (2) they are associated with and in some cases occur in the hornblende patches independently interpreted as xenolithic; (3) there are no garnets in the normal syenite in this area, not even corona garnets.

If these garnets are xenocrysts in the syenitic hybrid, they cannot be post-syenite. And if (as appears to be the case) they are congenetic with the garnet porphyroblasts in the (metagabbroic) dark ore, then the latter also can not be post-syenite. It may perhaps be argued that if these garnets are xenocrysts in the syenitic hybrid their formation must have antedated the intrusion of the syenite magma. But the evidence requires only that the garnets shall have attained the X stage of growth before the assimilative process took place. Moreover, there is, in the opinion of the writer, no evidence of any post-gabbro pre-syenite metamorphism which, in the Gore Mountain area, could account for the development of the porphyroblast garnet.

The evaluation of hypothesis 3 may be summarized as follows. The evidence supports the view that the P, X, and XH garnets in the gabbroic (and anorthositic) facies are congenetic, contemporary, and metamorphic, and that they developed *in situ*. The evidence indicates that the porphyroblast garnets in the syenitic hybrid facies are contemporary with the corresponding garnets in the gabbroic and anorthositic facies, but not that those in the hybrid developed *in situ*. The view that the responsible metamorphic program was regional in character and the localization of large garnets only incidentally preferential is not supported; the evidence favors contact metamorphism. The evidence does not support the view that the garnets are post-syenite in age. Corona garnet does not occur in the syenite of the southeastern Adirondacks, and the evidence from this area throws no light on the origin and age of corona garnet in syenite elsewhere. The view that the corona garnet (in members of the anorthosite-gabbro series) is congenetic and contemporary with the porphyroblast garnet is neither confirmed nor refuted by the direct evidence examined thus far; but the view that the larger porphyroblast garnets resulted from the locally more intense metamorphic recrystallization is confirmed.

Hypothesis 4. Double Contact Metamorphism

Miller (1938) drew a major genetic distinction between garnets without hornblende envelopes and those with. He arrived at the general conclusions (1) "that the garnets without hornblende envelopes were produced where anorthosite magma reacted with or assimilated metagabbro inclusions"; and (2) "that the garnets with conspicuous hornblende envelopes were produced by dynamo-thermal action of quartz-syenite magma upon border portions of gabbro bodies, and upon inclusions of it in the syenite, no anorthosite having been involved in their genesis".

According to this hypothesis, the first type of garnet (the X type of the present report) is evidently magmatic, since (p. 401): "The material of the garnets was produced by the reaction between the anorthosite magma and the metagabbro, and conditions in the cooling syntectic magma were favorable for the growth of the large variably euhedral garnets". The distinction between the X and the XH garnets is thus two-fold; the X garnets are magmatic and attributable to the assimilation of gabbro by anorthosite magma; the XH garnets are metamorphic and attributable to the contact metamorphism of gabbro by syenite magma. The genetic distinction is based primarily upon observations of field occurrence and facies association. Miller offered no explanation as to why the one process should produce rimless garnets while the other yields hornblende-rimmed garnets.

The distinctions made by Miller are not substantiated. The essential identity of composition and habit of the two sets of garnets indicate a very similar if not a common genetic process, and compositionally similar environments. That the X and XH garnets at the Barton deposit are congenetic, contemporary, and metamorphic is especially compellingly shown by the evidence of the close and continuously gradational relationship between XH garnet in the Barton dark ore and the associated X garnet on the metagabbro side of the mine. The only difference between these types, apart from the rim, is their size; in the gabbroic facies all the garnet porphyroblasts larger than a certain size (about 1 inch diameter) developed rims.

Particularly significant in hypothesis 4 is the sequence of events at the Barton deposit. Miller recognized there two transitional hybrid facies

between the syenite proper and the mine rock proper (dark ore):

A. Syenite proper; no garnet.
B. Basic syenite hybrid; hornblende-poor (1–3%); 2–3% garnet, rimless and "little".
C. Dioritic hybrid; hornblende-rich (30% approx.); 10% garnet, rimless, size up to 1" diameter.
D. Mine rock, gabbroic or gabbro-dioritic; hornblende-rich; garnet-rich; garnets rimmed with hornblende, and 2–24 inches diameter.

The sequence of events was outlined by Miller (1938, p. 406) as follows:

". . . the southern border portion of the body of gabbro was more or less intimately cut and assimilated by the anorthosite magma, producing a syntectic rock [i.e. the light ore, facies C] rich in fairly large garnets without hornblende envelopes. . . . conditions in the cooling syntectic magma were favorable for the growth of the large, variably euhedral garnets. . . . Then came the great intrusion of quartz syenite magma which, on the south, cut out all the true anorthosite and variably digested or assimilated most of the then existing garnet-bearing syntectic rock [facies C], producing a new syntectic rock [facies B] with numerous small garnets, and leaving a band of the older garnetiferous syntectic rock [facies C], a few yeards wide, next to the mine". It was at this same time "by metamorphism, induced by the rise of the great body of quartz syenite magma" that the "mine rock [i.e. the dark ore, facies D], with its large hornblende-enveloped garnets, was produced along the southern side of the body of gabbro . . . little if any material was added to the gabbro by the syenite magma, and so the nature of the metamorphism was largely or wholly dynamo-thermal".

This dual hypothesis, which Miller applied also to other garnet deposits in this area, is in keeping with his view that the gabbro differentiated out of the parent magma first, as a crystal cumulate, leaving a residual anorthosite magma capable of intruding some of the already consolidated gabbro. The present author does not accept this view. It is true that the occurrence of anorthosite xenoliths and of individual xenocrysts of plagioclase in the syenite area south of the Barton mine suggest that the gabbro body may originally have been bounded on the south by anorthosite, prior to the syenite intrusion. But there is no direct evidence for regarding the anorthosite-gabbro contact as intrusive, and no compelling reason for resorting to such an involved dual hypothesis when a single intrusion (the syenite magma) with its attendant contact metamorphism and peripheral hybridization can account satisfactorily for the observed features.

One item of field evidence not mentioned by Miller appears to support his interpretation of the role of an anorthositic magma. On the north side of the gabbro body, along its contact with the meta-anorthosite, Krieger mapped a narrow zone, or lens, identified as "garnet gneiss". Specimens from that zone were found by the present author to consist of small garnets set in a matrix typical of meta-rock of the anorthosite-gabbro series,—that is, consisting largely of granoblastic plagioclase and hornblende, but containing relics of the primary ophitic texture and the primary mineralogy. The garnets are red and approximately spherical; most are less than an inch in diameter and rimless, but a few are 2–3 inches in diameter and have embryonic rims of coarse hornblende. A typical specimen of the garnet (B56) is identical in composition with the garnets of the Barton deposit. The plagioclase of the matrix ranges between An_{43} and An_{57}, corresponding as well with the plagioclase of the anorthosite as with that of the gabbro. But the relatively high color index (proportion of dark minerals) of this crudely foliated rock ally it more closely with the metagabbro than with the meta-anorthosite.

The mineralogy, petrography, and setting of this garnetiferous zone, in the absence of contiguous syenite, thus appear to indicate some such genetic relationship between anorthosite and the development of garnet megacrystals along the gabbro border as Miller suggested. But the absence of contiguous syenite may be deceptive; 6 or 8 feet more of erosion would have removed the patch of syenite hybrid which overlies the metagabbro at the western end of the Barton mine, and syenite may once have overlapped to the northern border of the gabbro. Moreover, the assumption that the anorthosite was intruded after emplacement of the gabbro is not warranted, in this area at least. General considerations make it much more probable that the gabbro is syngenetic in the anorthosite and, if anything, that the gabbro consolidated somewhat later.

Hypothesis 5. Proposed hypothesis

Loci and causes of large garnet growth.—This hypothesis is intended to apply specifically to garnet in the gabbroic and anorthositic rocks and in syenitic hybrids of these facies, in the southeastern Adirondacks. It is not meant to apply to corona garnet in normal syenite or granite.

The growth of garnet porphyroblasts in facies of the anorthosite-gabbro series was induced by the rise and intrusion of the magmas of the syenite-granite series. Because of the magnitude of those magmas, as evidenced by the geographic extent of the syenite and associated granite, they evidently exerted regional as well as contact metamorphic influence. Hence, although garnet porphyroblasts are widespread in their occurrence in metagabbro and meta-anorthosite, they are especially prominently developed, and exceptionally large, along the intrusive contacts of syenite against gabbroic and anorthositic bodies, where the intensity of metamorphic conditions was particularly high. The progressive variation in size and morphologic development in the gradational series of garnet types (Fig. 19), such as occur in the gabbroic facies at the Barton deposit, must be attributed to this local variation in metamorphic intensity.

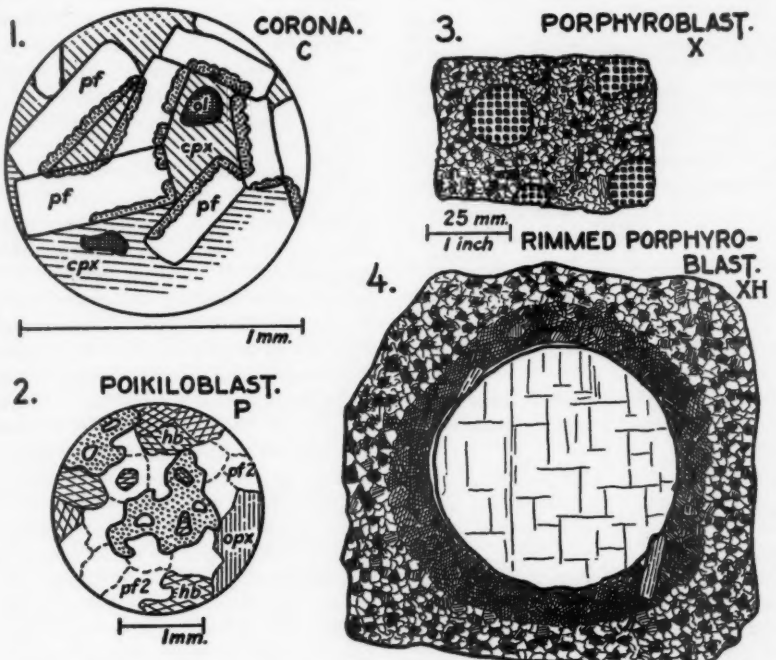

FIGURE 19.—C, P, X, XH SERIES OF GARNET TYPES IN GABBROIC FACIES, SOUTHEASTERN ADIRONDACKS

In addition to the thermo-dynamic localization of the larger porphyroblasts along or near the intrusive contacts, there appears to be preferential localization related to facies composition: garnet is more abundantly and more prominently developed in facies of gabbro or gabbroic-anorthosite composition than in the more purely anorthositic facies where garnet is only sparsely developed, or absent. This apparent facies localization may represent a direct compositional control, so that garnets grew only in those facies, or local portions of a rock body capable of supplying, for example, the necessary Fe and Mg; or it may represent

an indirect control, such as that exercised by the presence of some feature whose earlier localization was related to the facies differences. The present writer favors the second alternative and believes that the controlling feature was the

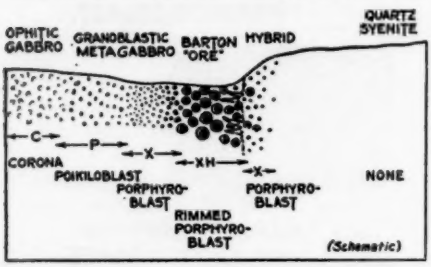

FIGURE 20.—SCHEMATIC SECTION ACROSS BARTON DEPOSIT, ILLUSTRATING OCCURRENCE OF GARNET TYPES IN RELATION TO SYENITE-GABBRO INTRUSIVE CONTACT

presence of pre-existing corona garnet, more extensively developed in gabbro than in anorthosite.

An important phase of the program of intrusion and metamorphism attributable to the syenite magma was the hybridization effected through the partial assimilation of small bodies (or of peripheral zones of larger bodies) of gabbroic and anorthositic rock. Though difficult to reconcile with geo-chemical principles, the evidence indicates that the assimilative process was selective; that the plagioclase was more susceptible of assimilation, the hornblende and garnet much less so, if at all; and that consequently hybridization of metagabbroic (hornblende-rich) facies was limited to narrow peripheral zones, while hybridization of anorthositic (plagioclase-rich) facies was more extensive and thorough.

It is significant that, in some cases at least, garnets had attained an advanced stage of porphyroblastic growth before assimilation finally overtook the rock in which they were growing. In the resulting hybrid facies, these garnets survived as xenocrysts, without further growth, while their congenetic equals in the adjacent gabbroic facies continued their growth to a more advanced stage.

At Gore Mountain (Fig. 20), according to the hypothesis advocated here, the Barton ore proper (the dark ore) is a highly reconstituted peripheral portion of the gabbro, its metamorphism induced by the intrusion of the syenite magma. The XH, X, and P type garnets, in the dark ore and in the adjacent metagabbro, developed *in situ* at that time, the products of progressive recrystallization starting from the corona garnet as an initial stage. The most advanced stages of garnet growth (X and XH) were attained near the contact where metamorphic conditions were most intense.

The narrow zone of light ore is a hybrid facies, the product of partial assimilation, by the syenite magma, of peripheral metagabbro whose garnets had already reached the large prophyroblast X stage of growth. In this hybrid facies they are xenocrysts, originally congenetic with the porphyroblast garnets (X and XH) on the gabbro side of the contact.

Rimmed versus rimless garnets.—Substantiating evidence has already been cited for all but two of the features of this hypothesis. The first has to do with the genetic distinction between the hornblende-rimmed garnets (XH) and the rimless ones (X),—that is, with the origin of the hornblende rims. The detailed argument on this point is left for a later paper. The distinction is not a major genetic one, and in any event a comparison of the XH garnets of the dark ore with the X garnets of the light ore, as made by Miller, can not reveal their relationship. The true relationship is brought out by a comparison of XH garnets with X garnets in the same, i.e. metagabbroic facies. It then becomes clear that the critical difference is size of the garnet, and that whether an individual garnet porphyroblast develops a rim, or not, depends only upon the size attained by the garnet individual and the hornblende content of the matrix in which it grows. The rim is the hornblende displaced by the garnet in the course of its growth in a hornblende-rich matrix; the larger it grows the more rim it accumulates.

Corona garnet origin.—The second feature concerns the origin of the corona garnet in the gabbro. The direct evidence indicates quite clearly that the corona C garnet was the initial stage, and that the more advanced types (P, X, XH) developed by progressive recrystallization of corona garnet. The textural difference

between the four types undoubtedly reflects the local variation in intensity, or duration of metamorphic conditions. If the corona garnet is a product of the same metamorphic program which produced the P, X, and XH types, then its distribution must represent the locus of the least intense conditions capable of developing garnet in these facies. But if it is an earlier endomorphic (i.e. deuteric) product of post-consolidation metasomatism in the gabbro, then it must have survived as such only where later metamorphic influences were incapable of recrystallizing it. In either case, the corona garnet can not be post-syenite as proposed by Buddington (1939, and in recent personal communications); it is either essentially contemporaneous with the porphyroblast (P, X, XH) types and with the emplacement of the syenite, or it is older. The distinction does not affect the interpretation of later events in the genesis of the garnet deposits, except that prior localization of an earlier corona garnet would control the subsequent localization of garnet-rich deposits.

This question of the origin and relative age of the corona garnet in the gabbro and anorthosite has received much attention because of its bearing on several fundamental aspects of Aridondack petrology. Roesler and Kemp (Kemp, 1920, p. 38–47) attributed the garnet coronas to reaction between pyroxene and feldspar during dynamic metamorphism, but did not specify the age. Alling (Kemp and Alling, 1925, p. 58) concluded that the corona garnet in gabbro is the magmatic product of peritectic reaction between the pyroxene and its surrounding magma; later (1936, p. 267–73) he elucidated the possible peritectic process of coronation. Shand (1945, p. 262, and in personal communications) questioned the deuteric formation of garnet coronas and favored a metamorphic origin. The writer nevertheless believes that the petrographic and chemical evidence points strongly toward a deuteric origin under conditions which especially favored the development of corona garnet in the more gabbroic facies of the anorthosite-gabbro series. Detailed argument will be presented in a separate paper.

Regional significance.—The same igneous and metamorphic processes, more or less, must have operated throughout the petrographic province, their effectiveness differing only in degree from one part of the province to another. Any hypothesis valid for the garnetiferous facies of the southeastern Adirondacks should be applicable in principle to corresponding facies elsewhere in the province. The hypothesis here proposed does not take into account some of the garnet features reported (Buddington, 1939) from the area around the northwestern end of the anorthosite massif, especially the corona garnet in syenite; it may need extension or modification when details of those occurrences become available. The hypothesis, however, has been satisfactorily applied to a considerable number of garnet occurrences besides the Barton deposit.

Other Adirondack Deposits

General Statement

The many garnet deposits and garnetiferous facies of the eastern Adirondacks fall into the following categories:

1. Deposits of anorthosite-gabbro derivation
   (a) Coronated gabbro.
   (b) Dark-ore type.
   (c) Light-ore type.
2. Deposits of Grenville derivation
   (a) Anorthosite-Grenville skarn type.
   (b) Syenite-Grenville skarn type.
   (c) Amphibolitic Grenville type.
   (d) "Eclogitic" type.

Grenville-associated garnetiferous facies were examined only incidentally primarily to establish criteria for distinguishing between facies of anorthosite-gabbro derivation and those of Grenville derivation where unequivocal identification is lacking. In general, this distinction was not difficult to make.

Deposits of Anorthosite-Gabbro Derivation

General description.—If the processes of corona garnet formation, contact metamorphic reconstitution and recrystallization, and hybridization here visualized for the Barton deposit are correct, one may expect to find other gabbro bodies similarly coronated and peripherally reconstituted; some small bodies

of coarse, amphibolitic metagabbro which contain large garnet porphyroblasts and grade through a zone of hybrid rock into surrounding normal syenite; some large or protected bodies of anorthosite peripherally reconstituted into more-or-less garnetiferous meta-anorthosite, surrounded by syenite-anorthosite hybrid; and small, or extensive but thin, bodies of anorthosite largely assimilated into a more-or-less garnetiferous syenite-anorthosite hybrid passing by gradual transition into the surrounding syenite.

Many examples of such facies occur, and among them considerable variation is noted in size of the garnet porphyroblasts, in the proportion of hornblende to feldspar in the matrix (its color index), and in the composition of the feldspar. These variations are related to three significant genetic factors: (1) variation in composition (gabbroic to anorthositic) of the primary facies; (2) variation in degree of metamorphic reconstitution effected prior to hybridization; (3) variation in degree and extent of hybridization.

It is convenient qualitatively to classify the anorthosite-gabbro derived deposits into three types: (a) coronated gabbro; (b) dark-ore type, consisting of garnet porphyroblasts in a richly hornblendic matrix; (c) light-ore type, consisting of garnet porphyroblasts in a highly feldspathic matrix. The second type is, of course, essentially metagabbro. The light ore may be either a syenitic hybrid facies or a meta-anorthosite originally of somewhat gabbroic character.

Coronated gabbro as a deposit of abrasive garnet.—Until recently deposits of fine-grained garnet have had little or no commercial value, regardless of the richness of the deposit. But with changing industrial requirements and the expanded use of garnet powders in the fine grinding or polishing of glass and other products, the recovery and cleaning of garnet fines by flotation processes becomes feasible, and rich deposits of fine-grained garnet may eventually be exploitable. It is worth noting that much of the *Gore Mountain gabbro* is coronated and that the (corona) garnet content of the gabbro, in weight per cent, is approximately twice as great as the porphyroblast garnet content of the Barton dark ore.

Dark ore type deposits.—The fairly large Humphrey Mountain deposit (HU, at 4338.5–7414.3) (Krieger, 1937; Miller, 1938) is situated along the contact between syenite and the body of gabbro which caps Humphrey Mountain. The geologic setting is the same as at the Barton deposit and the garnets are quite comparable in habit and composition, although not quite as large. Garnets (of XH type) constitute 10 to 15 per cent of the ore. A typical specimen has the composition $(Mg_{35}Fe_{48}Mn_1Ca_{16})_3$ $(Al_{100}Fe_0)_2$. Corona garnet is abundantly developed in the contiguous ophitic gabbro. Light-ore facies were not observed here but the feldspar of the contiguous syenite indicates that some hybridization occurred. The normal syenite of this area does not contain garnet.

The deposit is definitely of dark-ore type. The present author agrees with Miller that this deposit is simply a highly reconstituted peripheral facies of the gabbro, a product of contact metamorphism attributable to the syenite magma.

The Ruby Mountain deposits (RU, 4344.2–7406.5) on the southwest slopes of Ruby Mountain, in an area of foliated syenite, are a number of irregular bodies of dark, coarse rock carrying 4 to 10 per cent of scattered, red, rimless garnet porphyroblasts up to 3 inches in diameter. The matrix is a coarse-grained, granoblastic assemblage of black hornblende (up to 40 per cent) and white plagioclase (An_{50}); it is partly massive and partly foliated. This dark, garnet-rich facies grades through a more feldspathic garnet-poor facies of hybrid character into the surrounding normal syenite; there are no distinct facies boundaries. A typical specimen of the garnet has the composition $(Mg_{30}Fe_{52}Mn_1Ca_{17})_3$ $(Al_{100})_2$.

There is, in this case, no visibly associated gabbro or anorthosite; but the evidence (only a portion is detailed here) points compellingly to a gabbro-anorthosite derivation for these deposits, unmistakeably dark ore type. Miller (1938, p. 402) ascribed to the Ruby Mountain deposits a dual origin, but the observed features are equally well accounted for by regarding the bodies as xenolithic masses of gabbro or gabbroic anorthosite which had become caught up in the syenite magma, peripherally hybridized, and internally reconstituted.

The Crehore deposit (C, 4346.7–7406.5), at the east base of Casey Mountain in the Newcomb quadrangle, is a small garnet deposit in which the American Glue Company once opened a pit about 150 feet long by 30 feet wide. The deposit is a lenticular body of garnetiferous plagioclase-amphibole rock enclosed in well-foliated syenite. The garnets, some 5–10 per cent of the ore, are red, round, up to 4 inches in diameter, and have well developed hornblende rims. A typical specimen has the composition $(Mg_{37}Fe_{49}Mn_1Ca_{13})_3$ $(Al_{98}Fe_2)_2$. The matrix is a medium- to coarse-grained, granoblastic, crudely foliated aggregate of hornblende (47 per cent) and plagioclase (An_{44}). The boundaries of this deposit are more distinct than those at Ruby Mountain, but the wall rocks are hybrid rather than normal syenite, as indicated by the composition (An_{29}) of their feldspar, their high hornblende content, and the local presence of garnets; the wall rocks are of light-ore type.

Balk (1932) interpreted the Crehore body as a primary gabbro-amphibolite, the result of magmatic flow segregation of the normal dark constituents in the parental magma of the gabbro-anorthosite-syenite suite. But neither the garnet nor the particular type of hornblende found in the deposit is a normal constituent of the syenite, and the feldspar (An_{44}) is quite different from that in the syenite. The observed features, in good agreement with those of gabbro-derived deposits, appear to support Miller's contention (1938, p. 408) that the Crehore body is a metagabbro inclusion in syenite, and that the garnets are metamorphic rather than magmatic.

The Old Hooper deposit (OH, 4344.9–7405.3) is well exposed in the walls of an old water-filled quarry at the base of a ridge 1 mile northeast of Ruby Mountain, directly against the Thirteenth Lake fault (Krieger, 1937, p. 114; Miller, 1938, p. 407). It is another garnetiferous hornblende-plagioclase body of variable character and indefinite boundaries against the syenite in which it is enclosed. Here too there is no visibly associated gabbro or anorthosite, although both occur in the district. But the mineralogical, modal, and textural evidence, together with the general setting, as compared with other deposits, strongly indicate metamorphic derivation from a mafic member of the anorthosite-gabbro series. In the crudely foliated, coarse, granoblastic matrix of the deposit, black hornblende varies from less than 5 to more than 80 per cent, plagioclase (An_{30}) from about 8 to 85 per cent, pyroxene from 2 to 35 per cent. Garnet, of P and X types, with some XH, varies from a few per cent up to 35 per cent, and is spotty in habit and distribution. A typical specimen of X type has the following approximate composition: $Mg_{19}Fe_{56}Mn_2Ca_{23}$.

Light-ore type deposits.—The Hooper Thirteenth Lake deposit (HT, 4342.5–7406.2) is the outstanding example of the light-ore type with prominent X type garnet. It was a major producer of abrasive garnet for about 20 years before 1928 (North River Garnet Co.). It occupies a summit 1 mile east of Thirteenth Lake and is well exposed in a quarry some 300 feet in diameter and 10 to 100 feet deep (Krieger 1937, p. 104–8; Miller, 1938).

The ore is typically a medium-coarse-grained, light-colored (highly feldspathic), buff-weathering rock whose well developed foliation is emphasized by streaks rich in dark minerals, principally hornblende. The garnets, deep red and 1–3 inches in diameter, stand out prominently like dark knots in a board. They are almost universally regular in shape, either spherical or dodecahedral, and they do not have hornblende rims. They are preferentially located in the dark folia as seen in outcrop section, and arranged along flow lines as seen in the plane of the foliation. Garnet constitutes 5–15 per cent of the entire rock.

Analysis of one representative specimen of the garnet indicates a composition of $(Mg_{36}Fe_{64}Mn_2Ca_{18})_3(Al_{99}Fe_1)_2$ and partial analysis of seven typical specimens shows that the compositional range is not great. The average composition is very close to that of 10 analyzed garnets (P and X types) from syenite-anorthosite hybrid at Gore Mountain, and not very different from the composition of garnet porphyroblasts in Gore Mountain meta-anorthosite.

Plagioclase (An_{50-54}) constitutes 70–85 per cent of the ore matrix, in which it occurs only as clear anhedra; hornblende accounts for 10–20 per cent, hypersthene and augite each

1–5 per cent, and magnetite and biotite each 1–3 per cent. No orthoclase or perthite was found. Thus the modal composition of the Hooper mine rock corresponds to that of some of the light ore syenite hybrid at the Barton Mine or possibly to gabbroic meta-anorthosite, while its appearance in outcrop suggests a syenitic facies.

As mapped and described by Krieger, the deposit occurs in a general area of syenite, from which it is separated by an irregular aureole, some 500 to 1000 feet wide, of "low-grade garnet rock", a feldspathic gneissic facies which grades on the one hand into the garnet-rich mine rock and on the other hand into the surrounding, essentially garnet-free, moderately foliated, normal syenite. This intermediate facies comprising the aureole contains occasional residual crystals of primary plagioclase; it is also more feldspathic than the mine rock, consisting very largely of granoblastic andesine.

According to Miller (1938, p. 401), the mine-rock (garnet ore) is an anorthosite-metagabbro hybrid, and the garnets are magmatic in origin, having grown in the hybrid magma resulting from the assimilation of metagabbro by anorthosite magma. The anorthosite which then surrounded the mine-rock hybrid was in turn subjected to peripheral assimilation during the later intrusion of syenite magma, resulting in the aureole which grades centrally into the anorthosite-metagabbro hybrid (the mine rock), and peripherally through an irregular zone of syenite-anorthosite hybrid into the syenite proper.

The Hooper ore and the surrounding facies of the aureole are genetically related to the anorthosite-gabbro series. But the evidence does not require a two-intrusion history, nor support the hypothesis of magmatic origin of the X type garnets. The garnet composition and habit, and the character of the matrix, are very similar to the corresponding features of the "light ore" at the Barton deposit. It is therefore suggested that the Hooper deposit is a peripherally hybridized gabbroic meta-anorthosite with garnets produced by metamorphic recrystallization of pre-existing corona garnet.

The deposit and its aureole probably represent a xenolith of once more extensive gabbroic anorthosite; the more gabbroic portions were richer in corona garnet, and from this the larger porphyroblasts grew during the recrystallization and plastic deformation accompanying the rise of the syenite magma. The outer periphery of the aureole is undoubtedly a syenite-anorthosite hybrid as suggested by Miller.

Metamorphism and partial hybridization of some of the (especially gabbroic) peripheral portions of the Gore Mountain anorthosite body, and of its outlying xenoliths, have yielded a discontinuous zone of garnetiferous, amphibolitic foliated meta-anorthosite which Krieger (1937, p. 102) referred to as "Garnet gneiss" and as the "Hooper vein". A representative specimen (B58), from near the Gore Mountain road, consists of typical secondary plagioclase (clear, anhedral, sub-equant, 0.5–1.5 mm., An_{48}); anhedral, dark-green, hornblende (1–2 mm.); and garnet. Partial determinations of the garnet place it in the anorthosite-garnet compositional field. Non-poikilitic garnets 1 inch to 3 or 4 inches in diameter are abundant in this facies, and the larger ones are surrounded by embryonic hornblende shells similar to those at the Barton deposit.

Presumably the same garnetiferous zone is exposed in Rooring Brook at the eastern end of the meta-anorthosite body. The mineral assemblage, texture, and structure are the same but the rock resembles somewhat the foliated, amphibolitic, hybrid syenite in contact with the Barton deposit. The plagioclase composition, however, is An_{55}, and no micro-perthite or other potash feldspar, or quartz is present. Plotted garnet determinations (e.g. B92) fall in the anorthosite-gabbro garnet field.

Half a mile farther southeast is the so-called Noxon garnet deposit, probably a further extension of the same zone, since it occupies the corresponding peripheral position relative to the small xenolithic body of anorthosite with which it occurs. (The narrow diabase dike mentioned by Krieger (1937, p. 103) does not separate the garnet deposit from the anorthosite, but cuts across both.) The facies here is identical with that "hieroglyphic" rock found at the western end of the Barton deposit, where syenite invaded and partially assimilated ophitic anorthosite. In a matrix of gray-green

plagioclase, weathering cream colored, are (1) wedgeshaped and polygonal ferromagnesian patches, 5–25 mm. long, (locally pseudomorphously altered to chlorite), whose outlines are emphasized by frames of half a mm. granular red garnet; (2) angular shreds of black hornblende; (3) individualized garnets, spherical to dodecahedral, 3–50 mm. in diameter, rimless in the plagioclase matrix but with thin plagioclase rim when set in hornblende. The smaller garnets are poikilitic, the larger non-poikilitic. Distribution of the larger garnets (¼–2 inches) is spotty, amounting locally to an estimated 10 per cent of the rock. Of two garnets determined (B81 and B87), one falls in the gabbro-garnet field and the second in the anorthosite-garnet field. The garnets are easily cobbed out from their matrix, just as at the Hooper deposit near Thirteenth Lake.

The garnet-rich rock grades, on one side, through a crudely banded, amphibolitic, syenitic facies into normal syenite, and on the other into the small body of primary ophitic anorthosite identical with that at the western end of the Barton mine. In thin section, the dark "hieroglyphic" patches are seen to be granular aggregates of the hornblende and orthopyroxene, with garnet and traces of clinopyroxene. The matrix plagioclase is clear, anhedral, subequant, An_{44}. Microperthite and orthoclase are absent.

By their structural position, gradational relationships, petrographic features, and garnet types, these occurrences (Roaring Brook and Noxon) are closely allied to the mixed garnet ore at the western end of the Barton deposit. They are evidently hybrid facies resulting from metamorphism and partial assimilation of the periphery of the anorthosite by syenite magma. By analogy the remainder of the "Hooper Vein" is judged to have the same origin, although elsewhere indications of contact metamorphism are stronger and those of hybridization weaker.

References Cited

Alling, H. L. (1936) *Interpretative Petrology*, McGraw-Hill Book Co., New York.

Balk, R. (1931) *Structural geology of the Adirondack anorthosite*, Min. Petr. Mitt., Bd. 41, H. 3–6, p. 308–434.

—— (1932) *Geology of the Newcomb quadrangle*, N. Y. State Mus., Bull. 290.

Buddington, A. F. (1939) *Adirondack igneous rocks and their metamorphism*, Geol. Soc. Am., Mem. 7.

—— and Whitcomb, L. (1941) *Geology of the Willsboro quadrangle*, N. Y. State Mus., Bull. 325.

Fleischer, M. (1937) *The relation between chemical composition and physical properties in the garnet group*, Am. Mineral., vol. 22, p. 751–759.

Ford, W. E. (1915) *A study of the relations existing between the chemical, optical, and other physical properties of members of the garnet group*, Am. Jour. Sci., ser. 4, vol. 40, p. 33–49.

Hess, H. H. and Phillips, A. H. (1940) *Optical properties and chemical composition of magnesian orthopyroxenes*, Am. Mineral., vol. 25, p. 271–285.

Kemp, J. F. (1920) *Geology of the Mount Marcy quadrangle*, N. Y. State Mus., Bull. 229–230.

—— and Alling, H. L. (1925) *Geology of the Ausable quadrangle*, N. Y. State Mus., Bull. 261.

—— and Reudemann, R. (1910) *Geology of the Elizabethtown and Port Henry quadrangles*, N. Y. State Mus., Bull. 138.

Krieger, M. H. (1937) *Geology of the Thirteenth Lake quadrangle*, N. Y. State Mus., Bull. 308.

Leeds, A. R. (1878) *Notes on the lithology of the Adirondacks*, N. Y. State Mus., 30th Ann. Rept., p. 79–109.

Miller, W. J. (1912) *The garnet deposits of Warren County, New York*, Econ. Geol., vol. 7, p. 493–501.

—— (1914) *Geology of the North Creek quadrangle*, N. Y. State Mus., Bull. 170.

—— (1929) *Significance of newly found Adirondack anorthosite*, Am. Jour. Sci., ser. 5, vol. 18, p. 383–400.

—— (1938) *Genesis of certain Adirondack garnet deposits*, Am. Mineral., vol. 23, p. 399–408.

Shand, S. J. (1945) *Coronas and coronites*, Geol. Soc. Am., Bull. vol. 56, p. 247–266.

Stephenson, R. C. (1945) *Titaniferous magnetite deposits of the Lake Sanford area, New York*, A.I.M.E. Tech. Pub. No. 1789.

Winchell, A. N. (1933) *Elements of optical mineralogy, Pt. II*, John Wiley & Sons, New York.

Micro-Optical Section, Signal Corp Engineering Laboratories, Fort Monmouth, New Jersey

Manuscript Received by the Secretary of the Society, May 28, 1948

Abstract
Introduc
Acknowl
Notation
Field stu
Descri
Measu
Tur
Surfac
Geologic
Thermal
Histor
Theory
lutio
Calcul
Tun
Two-d
Two-d
Chang
Gen
Loc
Vari
Effe
Effe

Figure

1. Topo
tio
2. Temp
agg
geo
3. Obse
cal
4. Mea
alti
5. Block
lut
Da
6. Corre
ous
7. Refer
gra
8. Corre
rec
ner
tio
9. Corre
rec
mil
10. Corre
rec
mil
11. Corre
rec
lio

BULLETIN OF THE GEOLOGICAL SOCIETY OF AMERICA
VOL. 61, PP. 567-630, 16 FIGS. JUNE 1950

FLOW OF HEAT IN THE FRONT RANGE, COLORADO

BY FRANCIS BIRCH

CONTENTS

	Page
Abstract	568
Introduction	568
Acknowledgments	570
Notation and abbreviations	571
Field studies	571
Description of Adams Tunnel	571
Measurement of temperature in the Adams Tunnel	575
Surface temperature	577
Geologic history	580
Thermal gradient	582
Historical review	582
Theory of thermal effects of topographic evolution	584
Calculation of corrected gradient, Adams Tunnel	590
Two-dimensional solution, Adams Tunnel	596
Two-dimensional solution, Moffat Tunnel	597
Change of gradient with depth	599
General statement	599
Local radioactivity	599
Variation of conductivity with depth	599
Effect of incorrect allowance for erosion	599
Effect of glaciation	599
Thermal conductivity	600
Introduction	600
Method of measurement	601
Sampling	602
Variation of conductivity with rock type	603
Variation of conductivity with location	607
Density	608
Flow of heat	608
Discussion	612
Introduction	612
Distribution of radioactivity	612
Estimated radioactivity of root	614
Other hypotheses	618
General statement	618
Mechanical compression	619
Initial heat of a nonradioactive root	620
Subcrustal currents	621
Magma	621
Concluding remarks	622
References cited	623
Appendix A. Validity of approximate treatment of topography	625
Appendix B. Effect of departures from assumed conditions	628

ILLUSTRATIONS

Figure	Page
1. Topographic map of Rocky Mountain National Park	572
2. Temperatures, profile (tenfold vertical exaggeration), structure (true scale), and geologic reconnaissance map	573
3. Observed temperatures as function of vertical cover	577
4. Mean annual air temperature as function of altitude	579
5. Block diagram showing "two-cycle" evolution of the Front Range, after W. M. Davis	581
6. Correction function $E(R/\sqrt{4kt})$ for various times t (k = 0.02 cm²/sec)	587
7. Reference diagram for discussion of topographic correction	589
8. Corrected temperature as function of corrected depth, with topography permanently as at present (steady-state solution)	593
9. Corrected temperature as function of corrected depth, for linear evolution in 4 million years	593
10. Corrected temperature as function of corrected depth, for linear evolution in 1 million years (20 points)	593
11. Corrected temperature as function of corrected depth for linear evolution in 1 million years (71 points)	595
12. Surface profile and observed temperatures for Moffat Tunnel, after Van Orstrand	597
13. Corrected temperature as function of corrected depth for Moffat Tunnel (steady-state solution)	598
14. Diagram of apparatus for measurement of relative conductivity	601
15. Diagram illustrating several schemes of compensation for a mean altitude of 3 kilometers	616
16. Combinations of a uniform field with the field of a line doublet	626

Table	Page
1. Principal occurrences of water	574
2. Original rock temperatures	575
3. Variations of rock and air temperatures with time	576
4. Mean annual temperatures	578
5. Rate of decrease of mean annual soil temperature with altitude	580
6. Correction functions for surface change proportional to time	587
7. Theoretical temperatures at various points during uplift and erosion	589
8. Weights of rings for various depths	591
9. Mean surface altitudes for rings	592
10. Details of correction for Station 37	592
11. Condensed results for selected stations	594

Table		Page
12.	Corrected temperatures and depths for intermediate stations, by interpolation.	594
13.	Parameters of least-squares straight lines.	596
14.	Data for the Moffat Tunnel	598
15.	Thermal conductivity and density	604
16.	Composition and conductivity	607
17.	Variation of conductivity and density with rock type	607
18.	Variation of conductivity and density along the tunnel	608
19.	Corrected gradients and flow of heat in mountains	609
20.	Flow of heat in various regions	610
21.	Radioactivity and heat production of rocks	613
22.	Heat production from uranium and thorium for granitic and intermediate rocks.	614
23.	Gravity anomalies in Colorado	615
24.	Estimated mean heat production	617
25.	The quantity $erfc\ L/\sqrt{4kt}$ for various values of L and t	618
26.	Characteristics of several schemes of compensation	619
27.	Strains and strain rates for different durations of crushing	620

Abstract

Modern conceptions of the structure of the earth's crust and of the distribution of radioactivity lead to an expectation of a greater flow of heat to the surface in mountains than in lowlands. An exceptional opportunity for testing this expectation is provided by the data obtained by the geologists of the Bureau of Reclamation during the construction of the Alva B. Adams Tunnel under Rocky Mountain National Park. This tunnel, 13 miles long, at a mean altitude of 8300 feet, passes under the Continental Divide, more than 12,000 feet above sea level. Some 70 observations of temperature have been reduced with the purpose of finding the flow of heat.

Corrections have been applied for the topography on several different hypotheses regarding the physiographic history. The corrected vertical gradient of temperature lies between 24°C/km, on the assumption that the present topography has persisted indefinitely, and 20°C/km, on the assumption that the surface features have been derived from an old-age surface by erosion and by uplift of 7000 feet uniformly distributed over the last million years. If the time of evolution is taken as 4 million years, the corrected gradient is 22°C/km. An uncertainty of about 1°C/km results from lack of reliable data concerning the surface temperature.

Thermal conductivity has been measured in the laboratory for 123 samples of rock from the tunnel; these rocks are chiefly granites, gneisses, and schists. The variations of conductivity with rock type and with position along the tunnel are found to be insignificant; the mean value of conductivity is 0.008 cal/cm·sec·deg.

The heat flow is then computed as between 1.6 and 1.9 microcal/cm²·sec, with a "best value" of 1.7 microcal/cm²·sec. This is believed to differ significantly from the best values for a "normal" sea-level crust, which fall close to 1.1 microcal/cm²·sec. With conventional assumptions as to thickness and density of the layers of the normal crust, the difference of heat flow may be accounted for in terms of mountain roots having a mean radioactivity of the same order as that of granites or intermediate rocks. The observed heat flow is consistent with the doctrine of mountain roots and with an approximately uniform distribution of radioactivity throughout the "granitic" layer. A few of the other possible interpretations are briefly discussed.

Introduction

Of the various schemes of compensation proposed to account for the observed deficiency of the gravitational attraction of mountains, Airy's conception of mountain "roots" possesses the clearest physical and geological interpretation. It is evidently important to determine to what extent this conception agrees with the ideas of mountain and continental structure derived from other branches of geophysics. Byerly (1939) and Gutenberg (1943) have examined the seismological evidence and reached conclusions generally favorable to the existence of mountain roots, although the data are scanty and quantitatively inconclusive. A third form of inquiry is suggested by modern theory regarding the earth's heat.

Since the work of Rayleigh (1906) it has been clear that the radioactivity of a relatively thin layer of ordinary rocks would currently generate the heat known to be escaping from the earth. With typical values, the maximum permissible thickness of "average granite" is about 30 km. Jeffreys (1929) has used the determinations of the rate of radioactive heat production for granite and basalt to find the normal thicknesses of the individual layers consistent with observations of the flow of heat to the surface. Jeffreys assumes that: (1) the basaltic layer is twice as thick as the granitic layer; (2) heat production is uniform throughout each layer,

with the mean values found for granites and for basalts; (3) no heat is generated below these two layers. These conditions suffice to determine the problem, and the thicknesses found, 11 and 22 km., are of the order found from the seismic study of near earthquakes. Later work (Jeffreys, 1941) leaves these conclusions essentially unaltered. In its general form, however, the thermal problem is indeterminate, since the only quantities known, even approximately, are the flow of heat at the surface and the conductivities and rates of heat production for certain samples of rock.

Although the details of the vertical distribution of the heat-producing elements in and below the crust are unknown, it has been demonstrated that granitic rocks are usually richer in the radioactive elements than basaltic rocks and that these, in turn, are far more radioactive than ultrabasic rocks. The formation of a root of relatively low density under mountains thus requires the thickening of the most radioactive components of the crust, and there should result, as Jeffreys points out (1927; 1929, p. 298), "an increase in the local output of radioactive heat"; but although this change should be "capable of observational test, the existing data suffer from ambiguities of interpretation." The last remark may be applied to all indications of mountain roots. A determination of this difference of local output of heat would, however, enable us to estimate the radioactivity of the root, and hence to reduce the uncertainty with respect to the vertical distribution of radioactivity in the crust.

In a preliminary survey of the feasibility of finding a difference of thermal output between mountains and lowlands, some estimates were given for the Front Range of Colorado (Birch, 1947a). These estimates were based on the simplest assumptions: a regional root of the Airy type, sufficient to compensate the present mountain range, formed at the time of Laramide folding in this region, perhaps 50 million years ago; uniform radioactive content and heat production throughout the thickened upper layers, of the order found by laboratory measurements; uniform thermal properties; density differences for the upper and lower layers as assumed in recent isostatic studies (Heiskanen, 1939). On this basis, it appeared that an appreciable difference might be expected, and a search was begun for measurements, or the possibility of obtaining measurements, adequate for a determination of the flow of heat in the Front Range.

The construction of the Alva B. Adams Tunnel by the Bureau of Reclamation of the U. S. Department of the Interior afforded an opportunity for the measurement of temperature through the central portion of the Front Range. This great tunnel, 13 miles long, passes under Rocky Mountain National Park at a mean altitude of 8300 feet, with a maximum vertical cover of nearly 4000 feet. Except for patches of glacial drift, the rocks of this area are Precambrian granites, gneisses, and schists. Some 70 determinations of temperature, spaced at 1000-foot intervals along the tunnel, were obtained as the work progressed by geologists of the Bureau of Reclamation; the tunnel was minutely mapped, and about 1000 samples of rock were collected and described. Thus there already existed a formidable accumulation of data, in a favorable region, having only to be analyzed and correlated with laboratory measurements of conductivity.

Like observations of gravity, observations of temperature acquire their full significance only after certain kinds of "reduction." Reduction has, in general, the purpose of removing the effects of known, disturbing elements, and of correcting to some standard datum at which measurements for different localities may be compared. For gravity, reduction has the purpose of eliminating the effects of known masses above sea level and of the departure of station level from this datum. The reduced observations then reflect, in the form of the Bouguer anomalies, variations of density below sea level.

Similarly, in thermal studies, we begin by recognizing that the total amount of heat coming to the surface over a wide area is not dependent upon surface irregularities or surface temperature; but at any particular point near the irregular surface, both the temperature and the vertical gradient of temperature may depart considerably from the values which would be found at the same depth below a smooth horizontal surface at uniform temperature, with the same mean flow of heat. The problem arises of passing from observed temperatures, at known positions below an irregular surface

over which the temperature is more or less well known, to the temperatures as function of depth below a plane surface on which the temperature is uniform and constant. Whereas the gravitational corrections depend only upon the distribution of masses at the present time, the thermal corrections depend to some extent upon the whole climatic and geological history of the region. Uplift and erosion lower the surface temperature and increase the apparent vertical gradient. Thus, not only the present topography but also the physiographic history are important elements in the reduction of thermal data for mountain regions.

Many studies have been devoted to the temperatures of the great Alpine tunnels and to the effects of the topography, the ground water, the schistosity of the formations, and, to some extent, the conductivity of the rocks. Perhaps the most important objective of the early work was the prediction of maximum temperatures to be encountered in such tunnels, a matter of great technical interest when, as in the Simplon Tunnel, this temperature reached 55°C (131°F). It appeared that a satisfactory prediction could be based on a value for the "normal" gradient of temperature borrowed from the observations made in wells or mines in relatively flat country, corrected for a schematic topography resembling the mountain to be traversed. The analysis was not directed to the question of finding the best value of the gradient from observations in the tunnels, and no corrections were applied for the topographic evolution. The technique of topographic correction used in the older work was inadequate for making full use of the copious observations, though probably satisfactory for estimating the maximum temperature.

Surprisingly little geological or geophysical use has been made of the Alpine measurements, although Osmond Fisher (1889) estimated the depth to a molten substratum by a rather primitive use of the uncorrected gradient observed in the St. Gothard Tunnel. Stapff (1883–1884), who carried out the observations of temperature in the St. Gothard Tunnel, obtained a value for the flow of heat by combining a "corrected" gradient with Everett's "mean conductivity of rock"; with his weakness for superfluous digits, he gives 1.837×10^{-6} cal/cm²-sec, a plausible value, but his method is scarcely acceptable. Other writers have wished to account for the "high" temperatures found in the tunnels by mechanical action during mountain formation, unknown sources of heat, hot springs, and so on. Koenigsberger (1908) is on firmer ground when he insists (p. 523): "Für die Temperatur ist in erster Linie die Gestalt der Oberfläche massgebend"; it appears, moreover, that he had commenced, shortly before his death, to consider the general geophysical significance of the tunnel temperatures, and certain results, though no details, may be obtained from several letters to the late A. C. Lane (1942, p. 44–48). Anderson (Kennedy and Anderson, 1938) reviewed the Alpine studies, in connection with a discussion of the origin of magmas, but was unable to decide whether the flow of heat in the mountains was more or less than the "normal" flow.

Because of the "ambiguities" and other deficiencies of the earlier work, the writer has given more attention to details of correction and to sources of error than might otherwise appear justifiable. Some of this material may find useful application in other geothermal studies.

Acknowledgments

The analysis presented here rests on the observations and collections obtained by the geologists and engineers of the U. S. Bureau of Reclamation at Denver, and clearly would have little substance apart from their studies. I am heavily indebted to many members of the Bureau: to Mr. Michael W. Straus, Commissioner, for his permission to obtain and publish this material; to Mr. Walker R. Young, formerly Chief Engineer, Mr. Robert F. Blanks, Chief, Research and Geology Division, Dr. Roger Rhoades, Chief Geologist, Mr. Douglas McHenry, Mr. Ross L. Heaton, Mr. K. L. Dickey, and other members of the staff at Denver and Estes Park for their co-operation and interest in the problem, which was expressed in the tangible form of reports, maps, and an appreciable fraction of their magnificent collection of samples.

A grant from the Rumford Fund of the American Academy of Arts and Sciences defrayed in part the expense of preparing the many specimens for measurements of con-

ductivity and for petrographic study. The exacting work of grinding the discs of rock was carried out by Mr. Harold J. Ames, who introduced a number of improvements of technique. Rosiwal analyses of about a dozen samples were performed by Mr. Eugene Robertson.

My debt to many colleagues is also great: to Professor Ernest E. Wahlstrom of the University of Colorado for details concerning the physiographic history of the Front Range; to Dr. P. M. Hurley of the Massachusetts Institute of Technology for unpublished determinations of radioactivity and for helpful discussion of this troublesome subject; and to Professors R. A. Daly, Kirk Bryan, C. F. Brooks, L. C. Graton, and Marland P. Billings for discussion and criticism of many aspects of the work. Professors Billings and Graton read the manuscript and suggested many improvements.

Notation and Abbreviations

For convenient reference, a few of the symbols and abbreviations used in the text are collected below:

α	vertical gradient of temperature in the rock, in units of °F/kft or °C/km, corrected to "standard" conditions
α'	rate of change of surface (soil) temperature with decrease of altitude (units as for α).
c	specific heat, cal/gm·deg.
cal	calorie
e	base of natural logarithms, 2.7182 . . .; also strain.
$\dot{e}$	time derivative of strain, de/dt, or strain velocity.
$\exp \beta$	e^{β}
K	thermal conductivity, cal/cm·sec·deg·C.
$K_{\parallel}$	thermal conductivity, with flow of heat parallel to schistosity
$K_{\perp}$	thermal conductivity, with flow of heat normal to schistosity
k	thermal diffusivity, $K/\rho c$, in cm²/sec or km²/My.
kft	kilofoot or kilofeet, 1000 feet.
mg	milligal, 10^{-3} cm/sec².
microcalorie	10^{-6} calorie (microcal)
millicalorie	10^{-3} calorie (millical)
My	million years
P	radioactive heat production, cal/gm·My or cal/cm³·sec.
ρ	density, gm/cm³.
σ	standard deviation of a single observation.

The following mathematical functions are of frequent use in the theory of heat conduction; for discussion of their properties and numerical tables, *see* Carslaw and Jaeger (1947, p. 370–373); tables of the exponential integral are found in Jahnke and Emde (1938, p. 6).

$$\operatorname{erf} \beta = \frac{2}{\sqrt{\pi}} \int_0^{\beta} e^{-x^2}\, dx, \quad \text{the error function, or probability integral}$$

$$\operatorname{erfc} \beta = 1 - \operatorname{erf} \beta$$

$$\operatorname{ierfc} \beta = \int_{\beta}^{\infty} \operatorname{erfc} x\, dx = e^{-\beta^2}/\sqrt{\pi} - \beta \operatorname{erfc} \beta$$

$$\operatorname{i^2erfc} \beta = \int_{\beta}^{\infty} \operatorname{ierfc} x\, dx = \tfrac{1}{4}[\operatorname{erfc} \beta - 2\beta \operatorname{ierfc} \beta]$$

$$-Ei(-\beta) = \int_{\beta}^{\infty} x^{-1} e^{-x}\, dx, \quad \text{the exponential integral.}$$

Special functions developed for the topographical correction, in two and three dimensions, are:

$$G(\beta) = \beta^2\, Ei(-\beta^2) + e^{-\beta^2}$$
$$E(\beta) = 2 \operatorname{erfc} \beta - 4 \operatorname{i^2erfc} \beta$$

These functions are tabulated in Table 6 for a few values of the argument.

Field Studies

Description of Adams Tunnel

The Adams Tunnel connects Grand Lake, on the west side of the Divide, with the Wind River, a tributary of the Thompson River, on the east (Fig. 1). For the exact location, and for all details concerning the location of temperature stations, the writer is indebted to the members of the Office of the Chief Engineer of the Bureau of Reclamation at Denver, in particular to Mr. Ross L. Heaton. The invert elevation at the west end is 8356.99 feet; at the east end, 8249.66 feet; and the length from portal to portal, 68,810 feet. The tunnel was driven from both ends between 1940 and 1944, to a junction about 27,000 feet from the west end. Geologic mapping and measurement of temperature proceeded concurrently with the construction. (*See also* Heaton, 1940.)

The tunnel was mapped on 140 sheets, on a scale of 10 feet to the inch. Each sheet covers 500 feet of tunnel and shows three views of the interior: North Side, South Side, and plan of

FIGURE 1.—TOPOGRAPHIC MAP OF ROCKY MOUNTAIN NATIONAL PARK

arch. Of these sheets, 67, covering 33,500 feet have been incorporated in *Progress Reports* (dated March 26, 1941, Ross L. Heaton and Horace N. Goodell, 13 sheets; April 16, 1942, 24 sheets; March 15, 1944, Ross L. Heaton and C. Phillip Wagner, 34 sheets) in which the important features are discussed. The other sheets, though completed, have not been assembled in a report, but a log of the rock types for this missing portion was kindly furnished. The care and effort expended on these sheets gives them a high value, and the additional work of preparing them for publication would be amply justified.

The contacts, faults, joints, shear zones, and occurrences of water are shown on these sheets in great detail; the original location and a general description of each sample are also given. There is a geologic section of the eastern third of the tunnel, based on both surface and tunnel geology. The only geologic section for the whole tunnel, dated December 22, 1936, is based on a reconnaissance map prepared by Heaton before the tunnel exposures were available. The section of Figure 2 is based on Heaton's original section, slightly modified to agree with the tunnel mapping, and with the information obtained from two holes drilled near the East Portal.

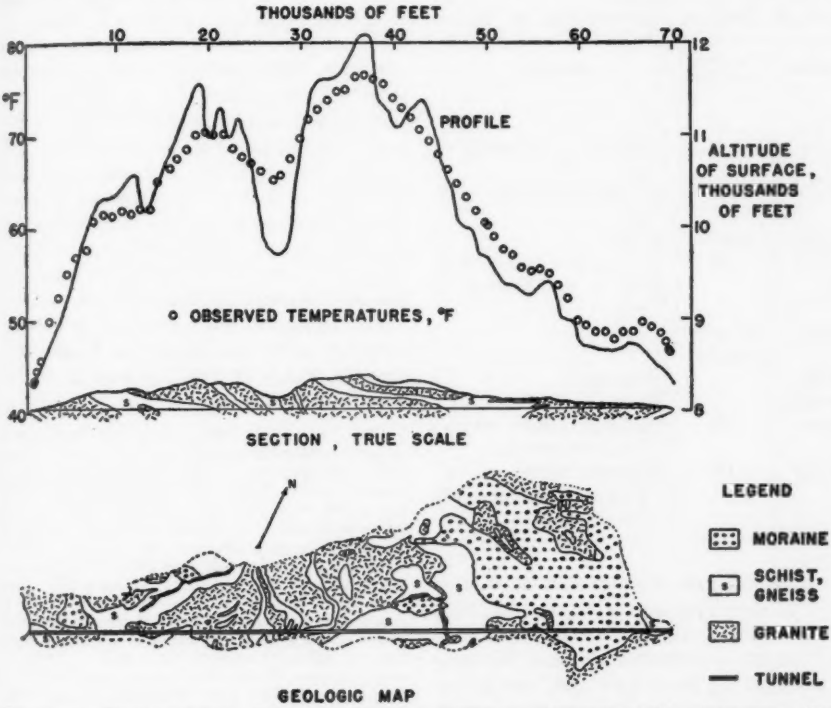

FIGURE 2.—TEMPERATURES, PROFILE (TENFOLD VERTICAL EXAGGERATION), STRUCTURE (TRUE SCALE), AND GEOLOGIC RECONNAISSANCE MAP

The tunnel position is shown by a single line on the section and by a double line on the map.

Positions in the tunnel are measured from station zero, which is 595 feet west of the West Portal, close to Grand Lake, The original station numbers were given in units of hundreds of feet, following the use of a 100-foot steel tape for determining positions inside the tunnel; for brevity, 1000-foot units are used hereafter. The completed tunnel is 434 feet shorter than its estimated length, and hence there is a sec-

tion, between stations 26 and 27, which, instead of 1000 feet, measures only 566 feet. This adjustment has been made in fixing the position of stations on the map.

TABLE 1.—PRINCIPAL OCCURRENCES OF WATER

Station	Maximum flow gal/min	Remarks
0–2.5	80	Total to 2.5
2.5–7.0	75	Total to 7.5, including 40 gpm to 2.5
8.177	300	Diminished in 2 weeks to 30 gpm
8.581	(2500)	See text
12.767	100	Reduced to trickle in week
14		Total at this heading, 45 gpm
14–48	no report available	
48–58		"Very dry"
58–65.5		Average total, 15 gpm
65.686	170	Diminished rapidly; 30 gpm for several months
65.820	150	Decreased rapidly to one-half; stopped when 65.680 was encountered

Rocky Mountain National Park appears on a U. S. Geological Survey topographic map, edition of 1919, reprinted in 1947, with a scale of 1/125,000 and 100-foot contours. This map is too small for the present work, and photographic enlargements to two and to four times the original scale have been used. The scale in the central region of these enlargements was determined from the known length of the carefully plotted tunnel line. This line was then marked off into 1000-foot intervals (except for the short interval adjacent to station 27), and station numbers of even thousands of feet have been used for most of the following work. The errors of position on the map probably do not exceed 100 feet; the actual positions in the tunnel were, of course, established to a fraction of a foot.

In some circumstances the circulation of water rivals conduction in the transport of heat. Some of the Alpine tunnels, notably the Simplon, were invaded by very large flows, which in a short time depleted important surface springs. Schardt (1905) postulated a continuous circulation from surface to a considerable depth, principally in open fissures or cavities in the limestones. The low temperatures in one section of the Simplon Tunnel were attributed to this circulation. Fortunately, this complication does not reach serious proportions for the Adams Tunnel. As against the flows averaging 1000 litres per second for several years (16,000 gal/min) for the Simplon, the total amount flowing from the Adams Tunnel was usually of the order of 100 gal/min, and most of the length was remarkably free from flows greater than a few gallons per minute. The principal occurrences are listed in Table 1; except for the fairly large flow at Station 8.581, they are all minor, temporary, and incapable of seriously affecting the temperatures.

The account of the exceptional flow is interesting, and is reproduced from Progress Report III, March 15, 1944, by Ross L. Heaton and C. Phillip Wagner.

"On January 5, 1942, water was encountered under considerable pressure at the bottom of three 9-foot drill holes on the right side of the face, which was at Station 8.581. The flow was estimated at 400 g.p.m. A 20-foot pilot hole was drilled on the left side of the face, striking the water course at 16 feet. The pressure was estimated at 150 psi since it was forced out through the drill steel against 120 pounds of air pressure. Four more pilot holes were drilled and capped. All encountered water at 9 to 16 feet and were drilled to 35 feet in hard rock. Three of these were connected to the main water line and delivered water to the portal . . . under its own pressure. The pressure was gauged at 48 psi on January 7. At 8 a.m. on January 8, water was barely flowing from holes in the top of the face while the lower holes were still making about 400 g.p.m. A maximum of 2500 g.p.m. was estimated to be flowing from the tunnel at 11:00 p.m. on January 6. The pressure and flow diminished rapidly and work was resumed at 8:00 a.m. January 8. After the water course was shot, the flow was about 200 g.p.m. and reduced to 100 g.p.m. the next day. The water came from a zone of closely spaced gouge seams which broke out to 1 to 1½ feet deep on the right and in the arch and 3 feet deep one foot above right spring line . . . The total delay in connection with this incident was 78 hours . . ."

This appears to have been the only serious flow in the part of the tunnel covered by the first three Progress Reports. With respect to the general occurrence of water, Heaton and Goodell remark (Progress Report, March 26, 1941):

"Most of the water comes from flat seams and joint planes, although there are no evident differences between those systems of flat joints that

TABLE 2.—ORIGINAL ROCK TEMPERATURES

Date	Station	Temperature, °F
	(feet)	
(East Portal)	69,839	
28 Aug. 1940	69,739	46.4
4 Sept.	69,639	46.6
4 Sept.	69,339	47.5
4 Sept.	68,839	48.4
4 Sept.	67,839	49.1
4 Oct.	66,839	49.6
29 Oct.	65,839	48.6
22 Nov.	64,839	48.6
8 Jan. 1941	63,800	47.8
18 Jan.	62,824.5	48.6
17 Apr.	61,825	48.6
30 Apr.	60,750	49.3
20 May	59,839	49.8
16 June	58,818	52.2
2 July	57,735	53.6
11 Aug.	56,819.4	54.9
11 Aug.	55,838.5	55.4
3 Sept.	54,839	55.2
26 Sept.	53,838	55.6
20 Oct.	52,840	57.0
12 Nov.	51,839	57.6
3 Dec.	50,839	59.0
30 Dec.	50,100	60.3
30 Dec.	49,839	60.5
23 Jan. 1942	48,839	61.8
16 Feb.	47,839	63.3
18 Mar.	46,831	64.8
9 Apr.	45,842.6	66.4
5 May	44,836.6	68.0
28 May	43,839.8	69.4
16 June	42,834.6	70.7
13 July	41,841.3	72.0
4 Aug.	40,822.7	73.0
1 Sept.	39,833	74.1
25 Sept.	38,840.5	75.6
26 Oct.	37,839.5	76.1
18 Nov.	36,826	76.6
11 Dec.	35,837.5	76.4
5 Oct. 1943	34,838.7	75.0
10 Nov.	33,825.8	74.8
17 Dec.	32,838.4	73.9
14 Jan. 1944	31,832.8	73.0
16 Feb.	30,831	72.0
28 Mar.	29,839	69.8
29 Apr.	28,821.8	67.6
30 May	27,832.5	65.8
9 June	26,912.5	65.3
8 May 1944	25,568	66.2
6 Apr.	24,614	67.1
14 Feb.	23,606.1	67.8
24 Jan.	22,603	68.7
24 Jan.	21,600	70.2
4 Dec. 1942	20,633.5	70.2
22 Oct.	19,595	70.5
15 Sept.	18,595	70.2
15 Sept.	17,660	68.7
30 July	16,595	67.6
30 July	15,848	66.6
23 May	14,612	65.1
23 May	13,608	62.1
23 May	12,601	62.1
2 Apr.	11,598	61.5
12 Mar.	10,607	61.9
3 Feb.	9,609	61.3
3 Feb.	8,625	61.5
3 Feb.	7,600	60.8
June, 1941	6,610	57.7
May	5,609	56.8
Apr.	4,595	55.0
Feb.	3,590	52.5
1 Feb.	2,605	50.0
2 Dec. 1940	1,596	45.7
1 Nov. 1940	1,092	44.6
1 Nov. 1940	800	43.5
1 Nov. 1940	695	43.3
(West Portal)	595	

TABLE 2.—*Concluded*

are wet and those that are dry. The same is true of gouge seams, some of which furnish small amounts of water, others being tight and dry. More than half of them are wet, and the proportion is about the same regardless of the direction of dip. Generally speaking, the more prominent seams are wet and the narrow ones dry."

In all cases, the maximum flow was of short duration, and the flows usually subsided to mere drips in a few weeks. There is probably little circulation of this water, which in its undisturbed condition merely stagnates in the poorly connected seams and joints. The greatest pressure observed, of the order of 150 psi, corresponds to a head of water of only about 350 feet; the depth of rock above Station 8.5 is about 2000 feet. It seems likely that this water also moves, if at all, principally in a horizontal direction, along seams of low dip.

Measurement of Temperature in the Adams Tunnel

The original determinations of temperature of the rock are given in Table 2 and Figure 2.

TABLE 3.—VARIATION OF ROCK AND AIR TEMPERATURES WITH TIME

Degrees Fahrenheit

Station (feet)	Distance from portal, feet		Oct. 7 1940	Oct. 29 1940	Nov. 22 1940	Dec. 9 1940	Jan. 8 1941	Jan. 18 1941
			East End					
69,739	100	Rock	46.4	45.7	44.2	44.2	43.2	
		Air			40.1			
69,639	200	Rock	47.1	46.8	45.9	45.7	45.1	
		Air			45.1			
69,339	500	Rock	48.0	47.7	47.5	47.3	47.1	
		Air			49.6			
68,839	1,000	Rock	48.7	48.6	48.2	48.2	48.0	
		Air			50.4			
67,839	2,000	Rock	49.5	49.5	48.9	48.7	48.7	
		Air			51.3			
66,839	3,000	Rock	49.6	49.3	49.1	49.1	49.1	
		Air	52.3		51.1			
65,839	4,000	Rock		48.6	48.4	48.4	48.4	
		Air		50.0	50.7			
64,839	5,000	Rock			48.6	47.8	47.8	
		Air			50.4			
63,800	6,039	Rock					47.8	
		Air					51.1	
62,824	7,015	Rock						48.6
		Air						50.4
			Nov. 1 1940	Dec. 2 1940	Jan. 3 1941	Feb. 1 1941		
			West End					
695	100	Rock	43.3	41.7	39.4	39.6		
		Air	45.3			41.0		
800	205	Rock	43.5	42.1	39.9	41.0		
1,092	497	Rock	44.6	43.9	43.2	43.2		
		Air		46.0		44.1		
1,596	1,001	Rock		45.7	45.3	44.6		
		Air		47.1	46.8			
2,605	2,010	Rock				50.0		
		Air				50.0		

The method of measurement is described in the Progress Report dated March 26, 1941, by Ross L. Heaton and Horace N. Goodell, as follows:

"For taking rock temperatures, sloping holes were drilled 6 to 10 feet into the wall of the tunnel and filled with water. After the water reached rock temperature, readings were taken after immersing a mercury thermometer, graduated to 0.2°C. Temperatures were taken at points 100, 200, 500 and 1000 feet from the portal, and at points 1000 feet apart thereafter. When new distances were reached, and another temperature station established, readings were repeated at the old stations and comparisons made with former readings."

Mr. Heaton has kindly supplied some additional details concerning this procedure. The thermometer was fixed to a wooden strip long enough to reach the bottom of the 10-foot holes. After the hole was filled with water, readings were made at intervals until a steady temperature was reached. This value is taken as the "original rock temperature." The slow changes found thereafter, over some weeks or months, are shown for some of the stations near the portals in Table 3 (extracted from the Progress Report cited above). Temperatures were read to the nearest 0.1°C with the aid of a flashlight. They were converted to Fahrenheit temperatures, which are consequently used in the present work up to the final stage of results.

In this tunnel, the air temperature was generally close to the rock temperature at the time of exposure, so that important subsequent changes are not to be expected. The rock temperatures of Table 3 generally tended to decrease at stations near the portals, even though the air temperatures were in most instances higher than the rock temperatures. The downward drift may therefore be caused by seepage of water or other effects unrelated to air temperature, though conceivably there are fluctuations of air temperature which have not been recorded.

For a rough upper limit of the effect of ventilation, we use the solution for the temperature in a half-space resulting from a sudden change ΔT_o on the surface. The change at depth x after a time t is $\Delta T = \Delta T_o \operatorname{erfc}(x/\sqrt{4kt})$ (Carslaw and Jaeger, 1947, p. 43). With $x = 2$ meters, $k = 0.02$ cm²/sec, and $t = 3$ months or 8.10^6 sec, $\Delta T = 0.7\ \Delta T_o$. Thus in three months, nearly the whole surface change is transmitted

to this depth. About one-tenth of the surface change is reached at 2 meters in 110 hours. At 3 meters, the corresponding times are $(3/2)^2$ or 2.25 times as long. There is much to be gained by drilling deeper holes, perhaps to 20 feet.

In the present case, it is doubtful whether the air was consistently either warmer or cooler than the rock; with oscillation of surface temperature, the net effect is of course reduced.

The record (Table 2) indicates that at a few points (Stations 7.6, 12.6, 15.8, 17.6, 21.6, and close to the East Portal) several weeks of exposure must have preceded the first determinations of temperature. At some of these, the readings do appear to be too low, by about 2° at Stations 12 and 15, less at the others, but the trend of values of Table 3 suggests that this delay would not be of importance except perhaps close to the portal.

The change of temperature horizontally along the tunnel rarely exceeded 1°F/1000′; thus the temperatures at the 1000-foot stations may be found by linear interpolation with errors no greater than those of the original observations, about 0.2°F. With the estimated allowance for the effect of disturbances such as ventilation and drilling, the temperatures at the "even" stations are probably known to better than 1°F.

A preliminary value for the mean vertical gradient of temperature may readily be found by plotting, as in Figure 3, the observed temperatures of Table 2 as function of the vertical cover—that is, the depth of rock vertically above the station. As this plot does not take into account the unevenness of the surface, the points are badly scattered, but they determine a line having a slope of 8.3 ± 0.2°F/kft (kft = kilofoot = 1000 feet); the standard deviation of a single point from this line is 2°F. A preliminary value for the gradient in the rock of 10.8°F/kft is obtained by adding to this the rate of change of surface temperature with altitude, 2.5°F/kft. (*See* Section on Surface Temperature.)

It is convenient to adjust the temperature at "even" stations to a common altitude, as the tunnel falls about 100 feet from the West to the East portals, enough to introduce a difference of about 1°F. Hence the temperatures at these stations have been corrected to a level of 8300 feet; the maximum correction is 0.6°F. These adjusted values, at 1000-foot intervals, are used throughout the following work.

Surface Temperature

The observations of temperature in the tunnel lead to the difference between two gradients;

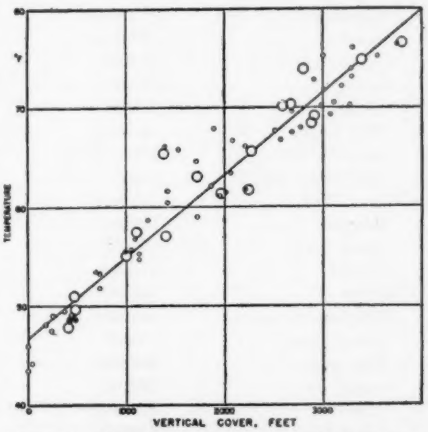

FIGURE 3.—OBSERVED TEMPERATURES AS FUNCTION OF VERTICAL COVER

The stations designated by the larger circles are those selected for detailed topographic correction in later figures.

(1) the gradient of temperature in the rock, and (2) the gradient (measured downward) of the temperature at the surface of the ground, or the rate of change of surface temperature with (negative) altitude. It is a fact of common experience that the temperature decreases as the altitude increases, and a considerable amount of information relative to the variation of air temperatures is found in the publications of the Weather Bureau and in treatises on meteorology. The mean soil temperature usually differs from the mean air temperature, however, and the temperature at zero depth obtained by prolonging the temperature-depth curves for wells or mines ordinarily exceeds the mean air temperature, sometimes by as much as 10°F (Van Orstrand, 1934a), or even more. A number of studies, particularly in the Alps, have shown that the soil is increasingly warmer than the air as the altitude increases; little has been done with this problem in the United States,

TABLE 4.—MEAN ANNUAL TEMPERATURES

Station	County	Altitude feet	Temperature, °F		Reference*
			Air	"Soil" (estimated, *see* text)	
Fort Collins	Larimer	5,000	47.0	48	1947
Waterdale	Larimer	5,200	47.9	48	1947
Boulder	Boulder	5,350	50.6	51	1946
Edgewater	Jefferson	5,450	50.0		1947
Kassler	Jefferson	5,500	51.5	51	1947
Colorado Springs	El Paso	6,100	47.8		1944
Alford	Larimer	6,320	44.5		1930
Cheesman	Jefferson	6,890	46.5	47	1947
Fry's Ranch	Larimer	7,500	42.1		1930
Idaho Springs	Clear Creek	7,540	43.3	44	1947
Blue Valley Ranch	Lake	7,600	38.2	43	1930
Estes Park	Larimer	7,750	42.3		1947
Moraine	Larimer	7,780	40.7		1930
Buena Vista	Chaffee	7,960	41.7		1945
Walden	Jackson	8,050	37.8		1947
Spicer	Jackson	8,300	36.9	41	1947
Red Feather Lakes	Larimer	8,360	37.8		1942–1946
Grand Lake	Grand	8,370	36.4	41	1940–1947
Allenspark	Boulder	8,500	40.2		1945–1947
Fraser	Grand	8,570	32.7	39	1947
Dillon	Summit	8,900	33.8		1947
Longs Peak	Larimer	8,960	37.3	40	1930
Frances	Boulder	9,300	39.9	42	1930
Victor	Teller	9,370	40.2		1924
Cripple Creek	Teller	9,510	39.4		1943–1947
Breckenridge	Summit	9,530	33.4		1930
Leadville	Lake	10,180	35.7	40	1947
Alma	Park	10,230	32.8	38	1930
Lake Moraine	El Paso	10,270	35.6	39	1947
Echo Lake	Clear Creek	10,600	32.2	38	1930
Climax	Lake	11,300	28.6		1912
Corona	Grand	11,660	26.2		1926
Pikes Peak	El Paso	14,110	19.3	33	1912

* All references are to the designated years of the *Climatological data of the United States*, Weather Bureau, U. S. Depart. Agric., or the equivalent; the title has varied.

though excellent opportunities exist. It is necessary to review this material briefly with the object of selecting the best value for the present purpose.

Though not useful directly, the mean annual air temperatures are relatively abundant and probably afford a fair estimate of the kind of variation from a simple, uniform dependence on altitude to be expected for the soil temperatures. Mean annual air temperatures for 33 stations in the mountains or foothills of Northwestern Colorado are given in Table 4, and plotted against altitude in Figure 4. The least-squares straight line through these points has a slope of -3.3 ± 0.2°F/kft, or -6.0°C/km. The standard deviation of a single point is 2.6°F. The gradient is close to the "saturated adiabatic lapse rate" for free air and to corresponding figures for other mountain regions (Hann-Süring, 1939, p. 166–168). The scatter is not surprising, as the stations occupy a variety of sites with respect to exposure to sun and wind, proximity to peaks, valleys, forests, and to other factors which affect temperature.

Probably variations of the same order would be found within Rocky Mountain National Park.

One factor which causes a difference between air and soil is snow cover. Except where swept by winds, the surface in the mountains is likely to be covered with snow for half the year or more, and in general the snow comes earlier and stays later as the altitude increases. In this area, the prevailing winds are from the west or northwest, and the western slopes tend to be somewhat colder than the eastern slopes. The thickest accumulations of snow are likely to be east of the ridges, and patches in sheltered ravines near the Divide last through the summer. Under a thick cover of snow, the soil temperature remains close to 32°F, even when the air temperature is much lower, provided the snow comes before very cold weather (Fitton and Brooks, 1931). Thus a fair estimate of mean annual soil temperature can often be obtained by taking 32°F for the months in which the mean air temperature is below 32°, and the actual mean air temperature for the other months (Lane, 1923; Hotchkiss and Ingersoll, 1934). In this way, "soil" temperatures have been estimated for a few stations (Table 4). Clearly the rate of decrease of this temperature is smaller than for air temperature, but these estimates should not be taken too seriously. For example, the surface rock temperature at Grand Lake may be found, by extrapolation of the tunnel temperatures near the West Portal, to be 43.5°F, to be compared with the "estimated surface temperature of 41°F, and with the mean annual air temperature (1940–1947) of 36.4°F. The temperature estimated in this way can evidently not fall below 32°F and may be too high for bare, wind-swept surfaces at high altitude. For lower surfaces, the mean monthly air temperature may never fall below 32°F, and yet the mean soil temperature ordinarily exceeds the mean air temperature.

The kind of soil or surface cover is also a factor. The temperature of interest in geothermal work is the surface temperature which would be found by extrapolation of "rock" temperatures to zero depth. Since the conductivity of soil or of slide rock is usually lower than that of the bedrock, the gradient will increase close to the surface. As a result, the rock temperature found by extrapolation to zero depth is likely to be greater, not only than the mean air temperature, but also than the mean soil temperature near the surface. Unless the soil is very deep, this latter difference will probably not exceed a degree or so. Larger differences may arise from the effects of flowing ground water.

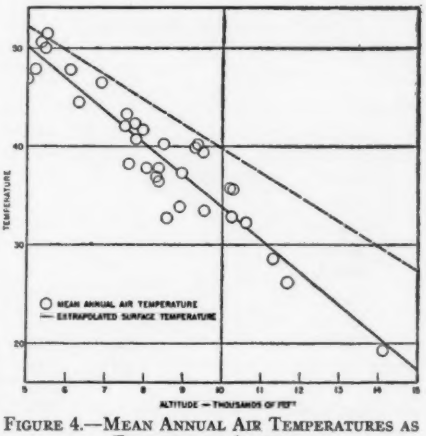

FIGURE 4.—MEAN ANNUAL AIR TEMPERATURES AS FUNCTION OF ALTITUDE

The solid line is the least-squares straight line fitted to the mean annual air temperatures. The broken line gives the variation of surface rock temperature with altitude adopted in this work.

The results of the studies of soil temperature are summarized in Table 5. Many of the values are in good agreement. There is evidently room for further work on this subject, and measurements at some standard depth at established weather stations in the mountains would be of value. It is here assumed that the best value for the rate of decrease of surface temperature is 4.5°C/km, or 2.5°F/kft. Probably this figure is in error by no more than 1°C/km, and it is probably too low rather than too high. As this is very nearly additive in the final value for the gradient, a correction may easily be applied when a better value is obtained. In Figure 4 (broken line), a line with this slope has been drawn through the temperature of 44°F at 8300 feet; this is the surface rock temperature at mean tunnel level found from the whole set of measurements in the tunnel. (*See* Figures 8, 9, 10, 11.) This line defines the surface temperatures, as function of altitude, implied in the following reduction. Deviations from this

line may be as great as the deviations of the mean air temperatures shown in Figure 4. The topographic correction is based on an integration over the surface in circular zones over which some of the deviations may be expected to compensate one another, but a considerable part of the remaining deviations of corrected temperatures probably arises from deviations of the surface temperature from the assumed linear dependence on altitude.

TABLE 5.—RATE OF DECREASE OF MEAN ANNUAL SOIL TEMPERATURE WITH ALTITUDE

Region	Depth of measurement meters	Rate of decrease °C/km	Author
Alps, Gothard	(Shallow springs)	4.3	Stapff, 1883
Central Tyrol	(Shallow springs)	4.4	Kerner, 1905
North Tyrol (Kalkalpen)		8.0	Kerner, 1905
Alps		4.4	Koenigsberger, 1908
Simplon	1–1.5	4.57	Niethammer, 1910
Simplon	1	5 ?	Schardt, 1914
Alps		4.3	Mezger, 1915
Alps		4.3	Maurer, 1916
Arizona (summer only)	0.1	7	Shreve, 1924
Central Alps	(springs)	3.5–4	Jäckli and Kleiber, 1943

GEOLOGIC HISTORY

As the processes of geology are continuous, there is seldom a clearly defined situation resembling the "initial conditions" of mathematical physics. Though an element of vagueness is necessarily present, it need not deter us from seeking a useful approximate solution. The greatest depth of cover above the Adams Tunnel is about 1 kilometer, so we are not seriously concerned with the surface history prior to, say, Pliocene time. On the other hand, the present temperatures near the surface are not materially affected by changes at depths greater than 30 or 40 kilometers which may have taken place later than Miocene time. The widespread igneous activity of Oligocene or Miocene time appears to have had minor and localized expression in the region of interest, and for the moment corrections for such disturbances are neglected.

The most important corrections to the observed temperatures depend upon the surface history of the Pleistocene and Pliocene. The principal factors are general uplift, erosion, and climatic variation. We require a reconstruction of the topography at the beginning of the Pliocene, some account of the rate of development to the present surface forms, and a rough calendar of Pleistocene climatic change.

The physiographic history of the Front Range and of neighboring mountain provinces has been discussed by a number of authorities with a striking diversity of opinion, particularly with respect to those elements of most importance for our present purpose. A geophysicist would be rash to attempt to choose among these conclusions; instead, the various proposed physiographic histories will be examined only with the intention of setting upper and lower limits for the implied corrections to the thermal gradient. Attention must thus be given chiefly to the most divergent proposals, rather than to a larger number among which the differences bear on points less relevant to the present issue.

Representing one extreme of the range of conclusions is the work of Wahlstrom (1947), whose views are stated succintly in his abstract:

> "The multiple peneplain hypothesis for the Front Range of Colorado is rejected as unsatisfactory. Re-examination of all available types of evidence indicates that remnants of only one extensive pre-Pleistocene old-age surface are present. This surface probably reached its maximum development in late Pliocene or early Pleistocene. Uplifts initiated in late Pliocene or early Pleistocene accelerated erosional processes which resulted in deep dissections of the uplifted surface during later Pleistocene to produce the modern canyons and valleys."

Wahlstrom has been kind enough to suggest

figures for the maximum amount of uplift which may have taken place since the development of this old-age surface, which, in Rocky Mountain National Park, now lies at about

Though with a shorter time scale, Wahlstrom's view in general outline resembles the earlier conclusions of Davis (1911), Atwood and Atwood (1938a; 1939b), and Powers (1935),

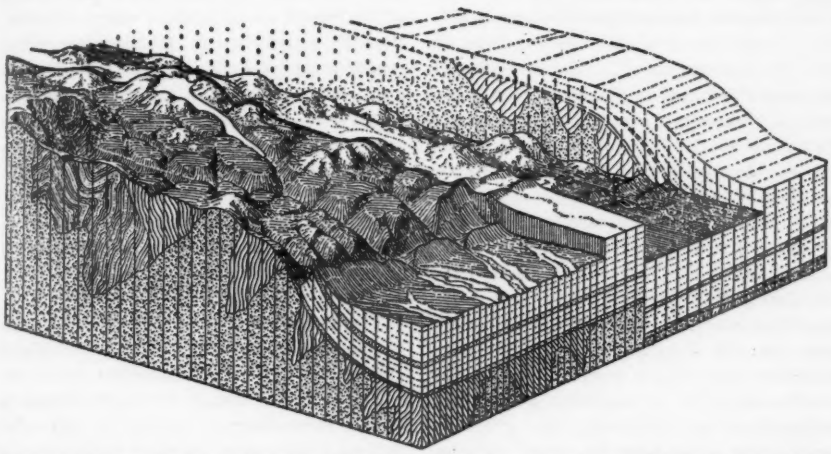

FIGURE 5.—BLOCK DIAGRAM SHOWING "TWO-CYCLE" EVOLUTION OF THE FRONT RANGE, AFTER W. M. DAVIS

12,000 feet. Following his ideas, we have the following account of late Cenozoic history:

(1) Early Tertiary folding and uplift was followed by a long period of erosion; by late Pliocene or early Pleistocene, there had developed a widespread old-age surface, lying perhaps as low as 5000 to 6000 feet above sea-level, "locally interrupted by 2000-foot monadnocks," and continuing east with little change of slope onto the High Plains.

(2) Beginning in late Pliocene or early Pleistocene, a series of uplifts raised this surface to about 12,000 feet along the Continental Divide, by faulting or upwarping or both, so that different parts of the original surface were raised to different present altitudes.

(3) During the uplifting, and as a result of the new elevation, the present canyons and valleys were excavated "subsequent to the deposition of pre-Wisconsin till by an ice sheet moving over a relatively flat surface."

The uplift along the Divide may be as great as 6000 or 7000 feet, accomplished since "late Pliocene or early Pleistocene", a time which we may estimate as between 1 million and 4 million years.

and appears to be consistent with the recent work on South Park (Stark *et al.*, 1949, p. 146–149).

At the other extreme with respect to the age of the surfaces are the conclusions of Van Tuyl and Lovering (1935), who find evidence for from five to eight peneplans, the youngest of Miocene age, plus a number of minor surfaces. On this view, the present altitude of the Front Range was reached by more gentle stages, with the total uplift since the last general planation distributed over the 15 or 20 million years since Miocene time.

The views of other writers are intermediate between the extreme positions of Wahlstrom, on the one hand, and of Van Tuyl and Lovering on the other, as indicated by a comparison given by the latter (1935, Fig. 2) of the ages assigned to various surfaces by earlier writers. Nearly all accept a long period of planation resulting in the "Flat Top" surface, which is regarded as reaching maturity at different times, in all cases somewhat earlier than the period assigned by Wahlstrom.

For definiteness, let us take this "Flat Top" surface, now at roughly 12,000 feet and existing

only as a remnant, as initially a peneplain of considerable extent at some lower level. If the uplift since this initial state is distributed over 15 million years, the correction for uplift is negligible, and the range may for this purpose be considered to have possessed its present altitude (though not necessarily its form) for all time. On the other hand, uplift of 7000 feet uniformly distributed over 1 million years would result in an apparent mean gradient near the surface about 0.8°F/kft, or 1.4°C/km, too high. For the same amount over 4 million years, the effect is one-half, or 0.7°C/km. For 16 million years, this is again halved and becomes negligible. These estimates are based on the assumption that the uplift is proportional to the time during these intervals, evidently a drastic simplification of a process which probably comprises intervals of rapid uplift, perhaps even of subsidence; but if the total amount of rise and the total duration are correct, the approximation should be sufficiently close, and there seems to be little basis for more elaborate computations.

The correction for general uplift is not the only one which depends on the dating of the last peneplanation; erosion of the present landscape from this initial surface also may be assigned to the interval since this stage. Again, if the time is as long as post-Miocene time, there is a close approach to the "steady state"; but there are appreciable corrections for a time of 1 million years, which will be described and applied in subsequent sections. In the end, the difference between the steady-state solution, which leads to an upper limit for the thermal gradient, and the lower limit, which I suppose to be given by the most extreme form of Wahlstrom's conclusion (7000 feet uplift in 1 million years), is about 20 per cent of the gradient, the largest uncertainty in the determination of the corrected gradient and of the flow of heat.

Thermal Gradient

Historical Review

The underground temperatures in mountainous regions are closely related to the topography, and the isothermal surfaces, though smoother, tend to follow the broad trends of the ground surface, rising under peaks and falling under valleys. The situation is complicated by the fact that the surface temperature also depends upon altitude, so that the ground surface is not an isothermal surface, and the first "continuous" isotherm is encountered only at the bottom of the deepest valleys. The isothermal surfaces are in general more widely spaced under peaks than under valleys, or in other words the vertical gradient of the temperature is lower under the peaks than under the valleys. Thus, the temperature at a given distance below a peak will be lower than at the same depth below a plane surface, other conditions being equal, and similarly, at a given depth below the bottom of a valley, the temperature will be higher than for an equal depth below a plain.

These relationships became clear as a result of the observations carried out in the Alpine tunnels. It is useful to examine a few of the principal studies, though no attempt is made to give a comprehensive account of this voluminous literature; an excellent bibliography is given in the review by Stiny (1933). The methods developed for these studies, though of interest, are not adequate for the present purpose.

Although Giordano made a few measurements of temperature in the Mt. Cenis Tunnel, Stapff (1877) made the first systematic study of this kind during the penetration of the St. Gothard massif. A number of writers, including Stapff, Osmond Fisher, Prestwich, Thoma, Koenigsberger, Anderson, and others, have discussed these measurements. On the basis of these observations Stapff predicted the high temperatures later found in the Simplon Tunnel, where a number of authorities, including Lommel and Heim (Schardt, 1914, p. 3), believed much lower temperatures would be encountered. The extensive measurements by Schardt in the Simplon Tunnel have also been discussed by Koenigsberger and Thoma (Koenigsberger, 1908), by Niethammer (1910–1912), and by Somigliano and Vercelli (1913). Observations in a number of lesser tunnels have been briefly summarized by Koenigsberger (1937). Van Orstrand (1934b) has given a short account of some measurements in the Moffat Tunnel in Colorado.

In this work are several levels of analysis. In the first, mean gradients are found by

schemes of averaging the surface altitudes along and across the tunnel line for arbitrarily selected distances. It is recognized that the vertical distance from tunnel to surface is not the determining factor for the temperature at tunnel level, but no use is made of the theory of conduction of heat in finding the appropriate method of averaging. This intuitive approach is used by Stapff, Osmond Fisher, and Niethammer.

On the next level, the problem of the distribution of temperatures is considered in terms of Fourier's theory, as a steady-state distribution satisfying certain boundary conditions. In its general form, this is a problem in potential theory known as Dirichlet's problem, for which closed solutions are available when the boundaries have certain simple forms. The first attempt along these lines was by Thoma (1906), who obtained a particular solution for a corrugated boundary of infinitely extended parallel ridges and valleys. By fitting one of the theoretical ridges to the major dimensions of the profile along the St. Gothard Tunnel, Thoma found that he could account for the rise of temperature with the assumption that the gradient approached a limit at great depth equal to 27°C/km, a value often found in wells in flat country. Thoma's method was later applied to the Simplon observations by Koenigsberger with fair success, though the differences between observed and calculated temperatures are frequently several degrees (Centigrade). Some improvement was obtained by introducing corrections for the effects of schistosity upon thermal conductivity and of flowing water. The first factor was of minor importance, and the second of consequence only in a portion of the Simplon Tunnel where exceedingly large flows occurred (more than 1000 litres per second). The correction for water circulation, of an empirical nature, is not of general applicability.

Thoma's work has been critically reviewed by Volterra (1912) and by Somigliano and Vercelli (1913); the latter proposed a more general form of solution in terms of sums of products of exponentials and sines or cosines with coefficients determined by the shape of the surface. Though in principle this form of solution might be applied to a three-dimensional problem, the determination of the coefficients requires the solution of a great number of simultaneous equations, a thoroughly impractical procedure. In the end, Volterra dismisses the problem as "practically insoluble," while Somigliano and Vercelli are content with a two-dimensional treatment of the Simplon, which, in spite of a laborious computation, leads to a calculated profile of temperature at least as generalized and unrelated to the details of the topography as Thoma's, with deviations reaching 5°C or more. As we shall see, a good two-dimensional approximation may be obtained with much less effort.

The methods discussed thus far depend upon periodic solutions—that is, it is assumed that there is some unit of "mountain" which is repeated indefinitely in either one or two dimensions. A more useful solution, for a single isolated ridge of infinite length on the surface of which change of temperature is proportional to the altitude, was given by Lees (1910). This solution is derived from the logarithmic potential and is composed of a uniformly increasing temperature, plus the field of a "line doublet." By placing this doublet at different distances from the surface of the "plain," it is possible to obtain surfaces of different shapes on which the boundary conditions are satisfied, and hence to fit the solution to single ridges of simple symmetrical cross section. Van Orstrand has applied this treatment to several localities, including the Moffat Tunnel. The solution is exact for a particular profile, assumed to be the same for all parallel sections; an approximation enters in fitting this mathematical profile to irregular real profiles. We shall employ this solution to estimate the accuracy of the method adopted for the present work.

A much more flexible method, on which the corrections applied below are based, has been proposed by Jeffreys (1938) and further developed by Bullard (1938). Jeffreys derives the correction from a result of potential theory, known as the Poisson integral, for the potential in the interior of a sphere on whose surface the potential satisfies given continuous boundary values. By considering depths small with respect to the radius, Jeffreys transforms this to a formula for a semi-infinite region with a plane boundary on which the potential (in this case,

the temperature) is known. The effect of irregular terrain at an interior point is then treated as equivalent to a distribution of temperature over a plane near or at the surface above the point, proportional to the distance from the plane to the true surface and to the difference of (undisturbed) gradients in rock and air. This correction is therefore approximate, as the true temperature on this plane differs from the assumed temperature because the true gradient differs from the undisturbed gradient. Jeffreys restricts this treatment to the case where the relief is small by comparison with the depth, but Bullard has applied it to one point in the Simplon Tunnel. It is of interest to evaluate the error involved in this approximation for a few examples where the exact solution is known (Appendix A). Even rough topography can be treated with fair success.

With this form of correction we are no long limited to two-dimensional shapes, but may take account of as much of the irregularity of the terrain as we wish, within the limits of accuracy of this approximation. Furthermore, by deriving the correction from the theory of the conduction of heat, instead of from potential theory, we can investigate the effect of the rate of development of the topography—that is, allow for a finite time of uplift and erosion of the present range. The difference between the assumption of finite and of infinite age is appreciable, but entering as a moderate correction it need not be determined with high accuracy. Though at first sight the introduction of the time seems to complicate the problem, in practice an important simplification is thereby effected; for whereas in the potential problem the effect of "all" topography must be computed, in a finite time, say a million years or so, only the topography within a few tens of miles can have a perceptible influence, and the amount of map reading is reduced.

Another possible approach to the present problem is the "relaxation method" (Emmons, 1943; 1944), either in the three- or two-dimensional form. The three-dimensional problem is extremely cumbersome, however, and in any case it is necessary, in the process of reaching a solution, to find the temperatures at a whole network of points of no interest for our purpose. The two-dimensional method developed below is much simpler for problems involving a half-space with an irregular boundary of relatively broad curvature.

Theory of Thermal Effects of Topographic Evolution

In this section we take up the mathematical treatment of the changes of temperature in the interior of a mountain range as it is uplifted and dissected. The theory of the conduction of heat is a well-developed subject, rich in solutions of particular problems and in methods for attacking new ones. Several excellent texts are available and are drawn on freely in the interest of brevity. For the nonmathematical reader, the basic assumptions, rather than the analytical details, are of principal interest, and these will be first set forth. The assumptions are given a very definite form, which cannot be justified in detail; however, the results are to a large extent independent of these assumptions: with a considerable variation of premise the conclusions would remain unaltered.

It is first assumed that the whole mass of material forming the Front Range in the neighborhood of the Adams Tunnel is thermally uniform, possessing a single value of thermal diffusivity k. This assumption is supported by the measurements of conductivity and density described below, a fortunate circumstance, for with a variable diffusivity the theory would become extremely complicated. There are, of course, irregular variations on a small scale, and also systematic variations depending upon temperature and stress. Such variations, if sufficiently large, should give rise to observable deviations from the theoretical conclusions. It is also supposed that the transfer of heat is by conduction only.

The evolution of the topography is assumed to have taken place as follows: At some time in the past, there existed a plane, horizontal surface in this region, beneath which the temperature was so adjusted that the isothermal surfaces were also plane and horizontal with a uniform vertical gradient of temperature. Beginning at a certain moment, this surface moved upward at a uniform rate and began to be carved into its present shape. The upward movement and the erosion proceeded simultaneously, the latter at a rate variable, from point to

point, but independent of time, just sufficient to produce the present relief at the present time. The calculations are carried out for different values of the amount of uplift and of the interval since the time of the "initial" plane surface. As a special case, the topography is supposed to have had its present shape and altitude for all time; this "steady-state" assumption leads to the largest value for the corrected thermal gradient. The corrections for uplift and for erosion both lower the corrected gradients, by amounts depending upon the times of development and amount of uplift.

In Appendix B it is shown that the actual shape of the "initial surface" is of little consequence; even topography as rough as at present would have an unimportant effect upon the result. Thus the assumption that the initial surface was plane is not necessary, but it is convenient and definite.

The evolution of the surface has now to be translated into variations of temperature. Uplift has the effect of cooling the surface, according to a linear decrease of surface temperature with altitude. Erosion exposes regions, originally blanketed by some thickness of rock, to the lower surface temperatures. At every stage, the temperatures in the interior are adjusting to the changing surface temperatures, and equilibrium is reached only in the limiting "steady-state" or standstill solution.

The solution finally obtained is an approximation, in that the effects of changes of temperature on the true surface are considered equivalent to the effects of the same changes on horizontal planes near the surface. The validity of this approximation is examined for a few cases where exact solutions can be obtained (Appendix A). Furthermore, it is supposed that the changes of temperature on the surface are proportional to the time, measured from the initial "instant", at which uplift and erosion commenced. This is not quite equivalent to the assumption that the rates of uplift and erosion are proportional to the time (*see* Benfield, 1949a; 1949b), but, for the slow rates of these processes, the difference is inappreciable; the real history was undoubtedly more complex.

The result of the analysis is that the present temperature T at a point in the tunnel at a vertical distance z below the present surface is given by a relation of the form

$$T = To + \alpha' Laz + (\alpha - \alpha')[z - \bar{h}(t) + as(D - z)]$$

where α is the thermal gradient in the rock in the "initial" state—that is, with a plane horizontal surface; α' is the rate of increase of surface temperature downward; L the amount of uplift; D the distance of the tunnel level below the original plane surface; T_o the present surface temperature at tunnel level; a and $\bar{h}(t)$ functions of the time, to be calculated below. The topographic correction appears as a correction to z, principally $\bar{h}(t)$. A plot of $T - \alpha' Laz$ versus the "corrected depth," $[z - \bar{h}(t) + az(D - z)]$ should thus give a straight line with the slope $(\alpha - \alpha')$; from this, by adding α', we obtain the required α. These quantities are plotted for various times of evolution in Figures 8–11.

Our starting point for the calculation of the topographic correction is the solution for the temperature produced by a "point doublet" (Carslaw and Jaeger, 1947, p. 228). The temperature at the point (x, y, z) due to an "instantaneous point doublet" of strength Q, parallel to the axis of z and located at the point (x', y', z') is

$$(1) \qquad v(x, y, z, t) = \frac{2Q(z - z')}{\pi^{3/2}(4kt)^{5/2}} \exp(-R^2/4kt),$$

where $R^2 = (x - x')^2 + (y - y')^2 + (z - z')^2$, and t is the time since the initiation of the doublet; this result holds for a continuous medium of uniform thermal diffusivity k.

If, instead of an instantaneous, there is a "continuous" doublet at (x', y', z') of strength $Q(t)$ varying with time, the temperature becomes

$$(2) \qquad v(x, y, z, t) = \frac{2(z - z')}{\pi^{3/2}} \times \int_{t'=0}^{t} \times \cdot \frac{Q(t')\,dt'}{[4k(t - t')]^{5/2}} \exp[-R^2/4k(t - t')]$$

It is further demonstrated (Carslaw and Jaeger, 1947, p. 230) that the boundary, $z = O$, of a semi-infinite body or half-space may be maintained at the varying temperature $f(x', y', t)$ by means of a distribution of continuous doublets over this surface, with their axes parallel to the z-axis, and strength

$Q(x', y', t) = 2k\, f(x', y', t)dx'dy'$, integrated over the surface ($z = O$).

Then the temperature at an interior point (x, y, z), produced by the distribution of temperature $f(x', y', t)$ on the surface, for $t > O$, is (Carslaw and Jaeger, 1947, p. 229, 308):

$$v(x, y, z, t,) = \frac{4kz}{\pi^{3/2}} \int_{-\infty}^{\infty}\int_{-\infty}^{\infty}\int_{0}^{t} \cdot \frac{f(x', y', t')}{[4k(t - t')]^{5/2}} \exp\left[-\frac{R^2}{4k(t - t')}\right] dx'\, dy'\, dt' \tag{3}$$

The element of surface, $dx'dy'$, produces the disturbance:

$$dv(x, y, z, t) = \frac{4kz}{\pi^{3/2}} \int_{0}^{t} \cdot \frac{f(x', y', t')}{[4k(t - t')]^{5/2}} \exp\left[-\frac{R^2}{4k(t - t')}\right] dt'\, dx'\, dy' \tag{4}$$

If we assume that the temperature of this element of surface varies linearly with the time, so that $f(x', y', t') = t'\, F(x', y')$, we can perform the integration with respect to t'. After a standard change of variable, with $\xi = R/\sqrt{4k(t - t')}$, this integral (omitting the factor $4kz/\pi^{3/2}$) becomes

$$\frac{1}{2kR^3} \int_{\beta}^{\infty} [t - R^2/(4k\xi^2)] e^{-\xi^2} \xi^2\, d\xi = \pi^{1/2} t E(\beta)/4. \tag{5}$$

Here we have put $\beta = R/\sqrt{4kt}$, and introduced the function:

$E(\beta) = 2$ erfc $\beta - 4$ i^{2}erfc β (*see* Notation and Abbreviations).

The effect of the element of surface $dx'dy'$ thus becomes

$$dv(x, y, z, t = \frac{zt}{2\pi R^3} F(x', y') E(\beta)\, dx'\, dy' \tag{6}$$

and the effect of the whole surface is to be found by integration with respect to x' and y'. For the three-dimensional case, it is convenient to substitute the cylindrical polar coordinates r and ϕ for x' and y', where $r^2 = (x - x')^2 + (y - y')^2$, and ϕ is an angle measured in the (x, y) plane, with vertex at (x, y, z). In these variables, (6) becomes:

$$dv(x, y, z, t) = \frac{zt}{2\pi R^3} F(r, \phi) E(\beta) r\, dr\, d\phi; \tag{7}$$

the effect of the whole surface at the interior point (x, y, z) is

$$v(x, y, z, t) = \frac{z}{2\pi} \int_{0}^{\infty}\int_{0}^{2\pi} \cdot f(r, \phi, t) E(\beta) r\, dr\, d\phi / R^3 \tag{8}$$

since at the present time, t, we have $t\, F(r, \phi) = f(r, \phi, t)$, the present temperature at the point (r, ϕ) on the surface, $z = O$. If we suppose that the present distribution of temperature has persisted for an infinite time ($t = \infty$), the function $E(\beta)$ becomes unity, and we find the steady-state correction function of Jeffreys and Bullard. For near-by elements of surface, or R small, $E(\beta)$ is nearly equal to 1 but the effect of more distant points is appreciably reduced even when times of the order of several million years are considered.

In the present application, the integration of (8) is numerical, and the introduction of the function $E(\beta)$ presents no difficulty. This function is given for a few values of β in Table 6 and plotted as function of R for several values of t in Figure 6. A different correction function would be required for a different assumption regarding the dependence of surface temperature upon time.

For a change affecting the whole surface by the same amount, so that $F(r, \phi) = A$, a constant, we can integrate at once with regard to r and ϕ; we have

$$\frac{Azt}{2\pi} \int_{0}^{\infty}\int_{0}^{2\pi} E(\beta) \frac{r\, dr\, d\phi}{R^3} = Azt \int_{0}^{\infty} E(\beta) \frac{r\, dr}{R^3} \tag{9}$$

since $E(\beta)$ is independent of ϕ. Now $R^2 = r^2 + z^2$; for a fixed depth z, $r\, dr = R\, dR$, and with $\beta = R/\sqrt{4kt}$, as above, the integral is

$$\frac{Azt}{\sqrt{4kt}} \int_{\gamma}^{\infty} \frac{E(\beta)\, d\beta}{\beta^2} = At \cdot 4i^2\text{erfc } \gamma; \tag{10}$$

$$\gamma = z/\sqrt{4kt}.$$

The same result is found directly by using the theorem giving the disturbance of temperature in a uniform half-space by a uniform surface temperature varying with time (Carslaw and Jaeger, 1947, p. 45).

We shall require this result only for small

values of the argument γ, for which $4i^2\text{erfc}\,\gamma$ becomes approximately $1 - 4\gamma/\sqrt{\pi} + 2\gamma^2 + \ldots$, or nearly enough, $1 - 4\gamma/\sqrt{\pi} = 1 - 2z/\sqrt{\pi kt}$. We notice that the gradient of this quantity (with respect to z) is $-2/\sqrt{\pi kt}$, or just twice the value for a sudden change of surface temperature at the time $t = O$ (Carslaw and Jaeger, 1947, p. 45 (i)).

TABLE 6.—CORRECTION FUNCTIONS FOR SURFACE CHANGE PROPORTIONAL TO TIME(t)

$\frac{R}{\sqrt{4kt}}$	$E\left(\frac{R}{\sqrt{4kt}}\right)$	$G\left(\frac{R}{\sqrt{4kt}}\right)$	R (miles)	
			t = 1 My	t = 4 My
			(k = 0.02 cm²/sec)	
0	1.000	1.000	0	0
.1	.982	.950	1	2
.2	.932	.854	2	4
.3	.860	.741	3	6
.4	.773	.627	4	8
.5	.679	.518	5	10
.6	.583	.426	6	12
.7	.490	.332	7	14
.8	.404	.259	8	16
.9	.326	.198	9	18
1.0	.258	.149	10	20
1.1	.200	.110	11	22
1.2	.152	.079	12	24
1.3	.115	.057	13	26
1.4	.083	.040	14	28
1.5	.060	.027	15	30
2.0	.009	.003	20	40

For $\frac{R}{\sqrt{4kt}} = 0.1$, $k = .02$ cm²/sec and $t = 1$ My, we have: $R = 1.587$ km $= 0.986$ miles, or closely enough 1 mile.

The solution (8) may be interpreted geometrically as follows: the quantity $z\,r\,dr\,d\phi/R^3$ is the element of solid angle, $d\Omega$, subtended at the point (x, y, z) by the element of surface $r\,dr\,d\phi$ of the plane $z = O$. This element of surface is bounded by the concentric circles having the center (x, y, O) and radii r and $r + dr$, and by the axial planes of azimuth ϕ and $\phi + d\phi$. The steady-state solution is

$$(11) \qquad v(x, y, z, \infty) = \frac{1}{2\pi}\int_0^{2\pi} f(r, \phi)\, d\Omega,$$

the integration being extended over the whole plane, $z = O$. This is a known result for the potential of a "double distribution" on an infinite plane surface (Kellogg, 1929, p. 243). When the surface temperature depends linearly on the time, the function $E(\beta)$ gives the corresponding correction for each element of solid angle.

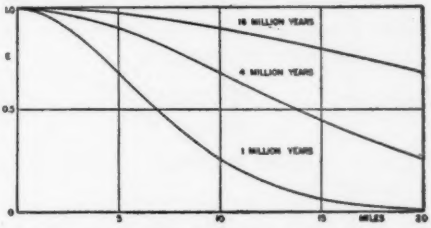

FIGURE 6.—CORRECTION FUNCTION E (R/4kt) FOR VARIOUS TIMES t (k = 0.02 cm² sec)

This function is equal to 1 for all values of R in the steady-state case (t = infinite).

This interpretation is especially useful in two-dimensional problems. Suppose, for example, that the surface temperature varies only with the x-coordinate. Then the steady-state integral becomes:

$$(12) \qquad v(x, z, \infty) = \frac{1}{2\pi}\int_0^{2\pi} f(x')\, d\Omega,$$

but now the element $d\Omega$ is the dihedral angle subtended by the strip of width dx' at the point (x, z); if $d\Psi$ is the plane angle (in the (x, z) plane) subtended by dx', and ψ is measured from the vertical (z axis), we have $d\Omega = 2d\Psi$, and

$$(13) \qquad v(x, z, \infty) = \frac{1}{\pi}\int_{-\pi/2}^{\pi/2} f(x')\, d\psi.$$

This integral is readily calculated approximately by graphical methods.

For a surface temperature $f(x', t)$, a correction function similar to $E(\beta)$ can be computed by using "line" instead of "point" doublets. If, in particular, $f(x', t) = t\,F(x')$, it can be shown that the temperature is given by:

$$(14) \qquad v(x, z, t) = \frac{1}{\pi}\int_{-\pi/2}^{\pi/2} f(x', t) G(R, t)\, d\psi$$

with $G(R, t) = (R^2/4kt)\ Ei\ (-R^2/4kt) + \exp\ (-R^2/4kt)$, $R^2 = (x - x')^2 + z^2$, and $-Ei(-x) = \int_x^\infty z^{-1} e^{-z}\, dz$, the "exponential

ntegral." The function $G(R, t)$ is given in Table 6 for a few values of the argument, $iR/\sqrt{4kt}$.

In the application of (8) to three-dimensional problems in which $f(r, \phi)$ must be determined from a map, it is convenient to effect a further transformation. Consider a ring between two radii r_1 and r_2, centered at the point (x, y). The contribution of this ring is

$$(15)\quad \Delta v(x, y, z, t) = \int_{r_1}^{r_2} E(\beta)\frac{r\,dr}{R^3}\int_0^{2\pi} f(r, \phi, t)\,d\phi$$

Let $\bar{f}(r, t)$ be the mean value of $f(r, \phi, t)$ in this ring; then

$$(16)\quad \Delta v(x, y, z, t) = z\bar{f}(r, t)\int_{r_1}^{r_2} E(\beta)r\,dr/R^3 = \bar{f}(r, t)E_r\Delta\Omega r/2\pi$$

where $\Delta\Omega_r$ is the solid angle subtended by the ring at (x, y, z) and E_r is a mean value of $E(\beta)$ for this ring. The "weight" of this ring, $\Delta\Omega_r/2\pi$ is given by

$$(17)\quad \Delta\Omega_r/2\pi = z\int_{r_1}^{r_2} r\,dr/R^3 = (r_1^2/z^2 + 1)^{-1/2} - (r_2^2/z^2 + 1)^{-1/2}.$$

For approximate numerical computation, the integral (8) is replaced by a summation for a finite number of rings, and we have finally,

$$(18)\quad v(x, y, z, t) = \Sigma\bar{f}(r, t)E_r\Delta\Omega_r/2\pi$$

The "weights," $\Delta\Omega_r/2\pi$, as given by (17) are conveniently found by using tables of squares, square roots and reciprocals, such as Barlow's Tables, or trigonometrical tables, since, if $r/z = \tan\theta$, $(r^2/z^2 + 1)^{-1/2} = \cos\theta$. A template, divided into rings and sectors by suitably spaced circles and radii, is useful here as in the computation of terrain corrections for gravity, but, as the depth z commonly varies from point to point, the weights of the compartments also vary and must be computed for each point.

In the reduction of the integral to a finite sum, fine points with regard to the mean values have been neglected, but as the variation of $E(\beta)$ is relatively small until the outer rings are reached, no serious error is to be anticipated from this source.

It is also possible to plot the integrand of (8) as a function of r and to obtain the integral by graphical quadrature. The method of summation is somewhat more flexible and less laborious for a large number of points and for a variety of assumptions with respect to the time of development t, particularly when a computing machine is available. This method is illustrated in detail in Table 10.

We have found the effect at an interior point of a changing distribution of temperature on a plane boundary, when the change is everywhere proportional to the time elapsed since some initial condition. In the form (8), this is an exact solution, subject to the assumptions made. We have now to adapt this solution to an approximate treatment of the problem in hand.

For the initial condition, imagine a plane boundary, on which the temperature has been uniform and constant for some millions of years. The material is supposed to be uniform, with a uniform rate of increase of temperature downward, the gradient near the surface being designated α. We now think of this plane as uniformly uplifted by a total amount L and, at the same time, as eroded into the shape of the present surface. Our problem is to find the changes of temperature at points in the interior. It is useful to consider several points, as shown in Figure 7, and to form the initial and final temperatures and the differences.

Let the temperature on the original surface be T_s. This surface is uplifted by an amount L; with a linear decrease of surface temperature with altitude, with gradient α' (positive downward), the temperature on the uplifted surface will be $T_s - \alpha' L$, and the change, $-\alpha' L$. Consider a point P_3, originally at a depth d below the surface, but now, because of erosion, on the surface. The original temperature was $T_s + \alpha d$, the present temperature is $T_s - \alpha' L + \alpha' d$, and the change, $-\alpha' L - (\alpha - \alpha')d$. Let us take the horizontal plane through P_3 as a plane of reference, and measure relief h from this plane, with h positive for points below P_3. Then at P_3 (for which h is negative), the original temperature was $T_s + (d + h)\alpha$, the present temperature is $T_s - \alpha' L + \alpha'(d + h)$, and the change, $-\alpha' L - (\alpha - \alpha')(d + h)$. At P_4, vertically under P_3, but at the level of P_3, the initial temperature was $T_s + \alpha d$, but the present temperature is $T_s - \alpha' L + \alpha(d + h) - \alpha'' h$, where α'' is the present mean

gradient between P_3 and P_4. Finally, at P_5, at tunnel level, the original temperature was $T_s + \alpha D$, the present temperature, which has been measured, is T, and the change, $T - T_s - \alpha D$. These quantities are summarized in Table 7.

The approximation to be adopted consists in replacing the gradient α'', which varies from point to point over the plane through P_2 in an unknown way, by the constant gradient α, also unknown. This is also equivalent to distributing over the reference plane the changes found for the true surface; that is, the change found for P_3 is considered to act at P_4, vertically below P_3 but at the level of P_2. This substitution enables us to obtain an approximate solution for $(\alpha - \alpha')$. Imagine the whole space below the plane through P_2 filled in, with the temperatures (or changes of temperature) prescribed over the whole plane in accordance with this approximation. The problem of finding the resulting change at P_5 has been solved above for the special case where the changes are proportional to the time elapsed since the initial state. For the general point on the plane of reference, such as P_4, the present value of the change is $-\alpha' L - (\alpha - \alpha')[d + h(x, y)]$, when α is substituted for α''. All terms are independent of position on the surface except $h(x, y)$, which must be found from the map. This change of

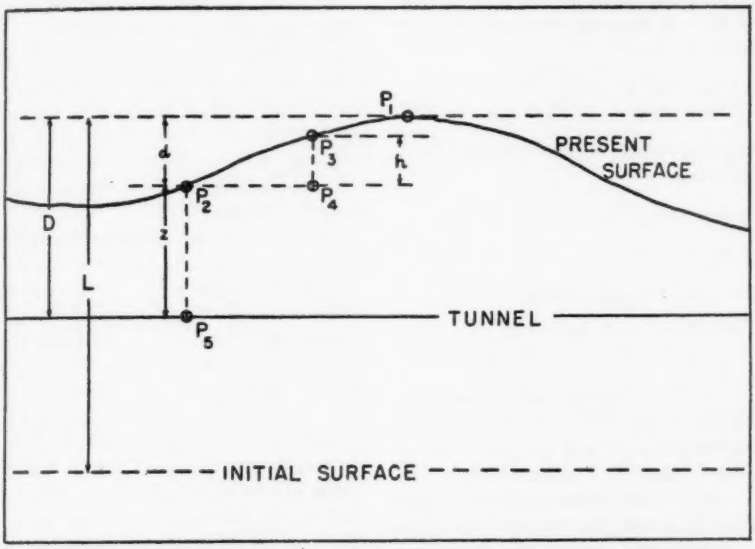

FIGURE 7.—REFERENCE DIAGRAM FOR DISCUSSION OF TOPOGRAPHIC CORRECTION

The "initial surface" indicated by the lower broken line is supposed to have risen by the amount L to the upper broken line; during this time, erosion reduces the initial surface to the heavy irregular "present surface". For the changes of temperature, *see* Table 7.

TABLE 7.—THEORETICAL TEMPERATURES AT VARIOUS POINTS DURING UPLIFT AND EROSION

Point	Initial	Present	Change
P_1	T_s	$T_s - \alpha' L$	$-\alpha' L$
P_2	$T_s + \alpha d$	$T_s - \alpha' L + \alpha' d$	$-\alpha' L - (\alpha - \alpha') d$
P_3	$T_s + \alpha(d + h)$	$T_s - \alpha' L + \alpha'(d + h)$	$-\alpha' L - (\alpha - \alpha')(d + h)$
P_4	$T_s + \alpha d$	$T_s - \alpha' L + \alpha'(d + h) - \alpha'' h$	$-\alpha' L + \alpha'(d + h) - \alpha'' h - \alpha d$
P_5	$T_s + \alpha D$	T	$T - T_s - \alpha D$

temperature is substituted for $f(x, y, t)$ in equation (8), and the integral then gives the change of temperature at P_s.

Let z be the distance measured downward from the reference plane to the point P_s, so that $d = D - z$. Then the change at P_s may be written:

$$T - T_s - \alpha D = -\alpha' L - (\alpha - \alpha')(D - z)\, F(z, t) - (\alpha - \alpha')\bar{h}(t) \tag{24}$$

where $F(z, t)$ and $\bar{h}(t)$ are functions which have been calculated

$$F(z, t) = 4i^2\mathrm{erfc}(z/\sqrt{4kt}) \approx 1 - 2z/\sqrt{\pi k t},$$

$$\bar{h}(t) = \Sigma h_r E_r \Delta\Omega_r / 2\pi.$$

With $a = 2/\sqrt{\pi k t}$, (24) becomes

$$T - \alpha' L a z = T_s + \alpha'(D - L) + (\alpha - \alpha')\,[z - \bar{h}(t) + az(D - z)] \tag{25}$$

Now $T_s + \alpha'(D - L)$ is the surface temperature at mean tunnel level, say T_o. Using the measured temperatures and the map, we can form pairs of values, $T - \alpha' L a z$ and $[z - \bar{h}(t) + az(D - z)]$ for every station along the tunnel. On plotting the former, the "corrected temperature", against the latter, the "corrected depth", we expect to find a straight line with slope $(\alpha - \alpha')$ and intercept at zero depth T_o, if the observations are consistent with our assumptions. The slope α finally obtained is corrected for topographic irregularity, for erosion, and uplift.

The correction for general uplift appears in the term $-\alpha' L a z$. For $t = 1$ My and $k = 0.02$ cm²/sec or 63 km²/My, this gives a correction to the temperature of about $0.8\, z$ °F/kft, for $L = 7000$ feet; thus for $z = 3000$ feet, the correction is 2.4°F. The effect on the slope $(\alpha - \alpha')$ is about 0.8°F/kft for $t = 1$ My, and half of this, 0.4°F/kft, for $t = 4$ My, again with $L = 7000$ feet. This correction is easily varied or omitted. The effect on the slope of a sudden rise of 7000 feet, 1 My ago, is just half the effect calculated above for a gradual rise of this amount, distributed over the whole period.

The correction for erosion to the reference level appears in the term $az(D - z)$; this vanishes for $z = O$ and for $z = D$, and is greatest for $z = D/2$. For $D = 4000$ feet—that is, with the "original" plane surface at a present altitude of 12,300 feet—the maximum is about 170 feet, for $t = 1$ My, and 85 feet for 4 My.

For the steady state, the terms in a vanish, and we have only

$$T = T_o + (\alpha - \alpha')\,[z - \bar{h}(\infty)].$$

This treatment of the topographic correction is approximate, and it is important to obtain an estimate of the errors to be expected. This point is considered in Appendix A, where exact and approximate steady-state solutions are compared for a few simple forms resembling the major topographic features in the neighborhood of the Continental Divide.

A discussion of various other departures from the assumed conditions is given in Appendix B.

It may be helpful at this point to recall the significance of the "corrected gradient", α. This quantity was introduced as the uniform gradient under a plane horizontal surface at a steady uniform temperature, the "standard" conditions. It is tacitly assumed that during the evolution of the present topography from such ideal conditions the mean flow of heat to the surface has not varied appreciably. The assumptions can be justified in terms of the geologic history of the Front Range, where the modern high relief has apparently developed from a relatively subdued landscape in no more than a few million years. The corrected gradient α is, therefore, the gradient beneath the old-age surface of Pliocene time.

Calculation of Corrected Gradient, Adams Tunnel

By means of the interpolation and adjustment described above we obtain 71 "observed" temperatures, all at an altitude of 8300 feet, and at 1000-foot intervals (with the single exception of the 26–27 interval). From these 71 points, 20 nearly evenly spaced points (marked with large circles in Fig. 3) have been selected for detailed topographic correction. Finally, it is possible to use all 71 points by obtaining the necessary corrections by interpolation between the 20 fully corrected points.

Most of the labor is in making the map readings which determine the function $\bar{h}(t)$ for the 18 stations. It is convenient to divide the whole surface so that the individual sectors are of roughly equal, and sufficiently small weight (solid angle divided by 2π). It is also con-

venient to use a single set of zones for all station but, since the depth varies, the weight of zones of fixed radii also varies. As a compromise, the radii of the zones are selected so that, with a depth of 2000 feet, the weight of each ring is about 0.1, except for the outer rings where further subdivision reduces the difficulty of estimating mean altitude. Each ring is divided into 12 or 24 equal compartments each having a weight of 0.01 to 0.005. The mean altitude of the surface in each compartment is then estimated from the map with the aid of a transparent template ruled to define the limits of the compartments and centered on the station of interest.

In many compartments the error in estimating mean altitude does not exceed the probable map error, perhaps of the order of the contour interval, 100 feet. In others, particularly the distant ones, the error of the estimate may reach 1000 feet. With 100 or more individual readings, the error on the mean or on $\bar{h}$ is much reduced, and aside from systematic errors may be as low as 20 feet. This is probably smaller than the error inherent in the form of approximation for the topographic correction, and a smaller number of readings would have sufficed.

The radii and weights of the rings for a few typical depths are shown in Table 8. The outer rings are more important than would be judged from their weights, as in the nature of the topography the departure from the plane of reference becomes larger as we leave the mountains and pass onto the plains. For the rings of radius greater than 20 miles, however, the mean altitudes differ little for the different stations, and there is no serious error in using the same figures for these rings for all stations. An error of 1000 feet for one of these outer rings means an error of less than 15 feet on $\bar{h}$, even for the deepest point. The correction for finite time of development (1 My or 4 My) nearly eliminates the region beyond 20 miles.

The sector readings for a given ring are averaged to give the mean altitude for the whole ring. The mean altitudes of the rings out to 22 miles are shown in Table 9 for 18 selected stations. Beyond 22 miles, the altitudes adopted for all stations are: 22 to 40 miles, 8000 feet; 40 to 100 miles, 7500 feet; 100 miles on, 5000 feet. With the experience gained in this work, a better choice of ring diameters could be made, with a smaller number of rings within 1 mile and several additional ones between 2 and 20 miles.

TABLE 8.—WEIGHTS OF RINGS FOR VARIOUS DEPTHS

Radius of ring, miles		Weight of ring at depth z (feet)		
Inner	Outer	$z = 1000$	$z = 2000$	$z = 3000$
0	0.125	0.165	0.165	0.084
0.125	.25	.231		
0.25	.375	.153	.124	.081
0.375	.5	.097	.107	.084
0.5	.75	.109	.153	.147
0.75	1.0	.059	.097	.110
1.0	1.25	.036	.064	.080
1.25	1.75	.042	.078	.105
1.75	2.75	.039	.075	.098
2.75	5.0	.031	.061	.098
5	10	.019	.038	.056
10	22	.010	.021	.031
22	40	.004	.005	.012
40	100	.003	.008	.009
100	∞	.002	.005	.006

The mean altitude is multiplied by the weight of the ring, and by the correction factor (E) depending upon the time assumed for the development. The "weighted" mean altitudes are then summed for all rings to give $\bar{h}(t)$. The details of this work are given for station 37 in Table 10. This is the station with deepest cover and hence for which the outer rings are most important. For this station, most of the correction depends upon the topography between 1 and 20 miles away. The "effective depth," $z - \bar{h}(t)$, for $t = 1$ My, is more than 10 per cent greater than for t infinite.

In the corrections which depend upon t for material between the surface and tunnel level at a mean temperature of about 10°C, a value, 0.02 cm²/sec = 63 km²/My for the thermal diffusivity k has been adopted. This is slightly greater than the value (0.019 cm²/sec) which we obtain from the measured mean conductivity and density (*see* below), and a mean value, 0.16 cal/gm.deg. for the specific heat. The constant k enters as a factor of the time t, which

TABLE 9.—MEAN SURFACE ALTITUDES FOR RINGS
(kilofeet)

Station	Ring diameters, miles											
	0–¼	–¼	–½	–¾	–¾	–1	–1¼	–1½	–2¾	–5	–10	–22
3	8.80	8.85	8.87	8.87	8.89	8.86	8.98	9.29	9.84	9.90	10.24	9.50
6	9.75	9.69	9.62	9.48	9.31	9.09	9.06	9.30	9.84	9.90	10.24	9.52
9	10.30	10.30	10.22	10.07	9.81	9.53	9.48	9.59	9.97	9.98	10.24	9.52
12	10.50	10.44	10.37	10.36	10.31	10.15	10.00	9.88	9.90	10.25	10.16	9.50
15	10.70	10.75	10.75	10.81	10.87	10.72	10.43	10.24	10.27	10.56	10.08	9.48
20	11.20	11.36	11.36	11.36	11.20	11.00	10.60	10.27	10.34	10.62	10.06	9.49
23	11.05		10.88	10.76	10.70	10.66	10.64	10.70	10.94	10.72	10.01	9.49
27	9.70	9.80	9.98	10.18	10.47	10.71	10.84	11.18	11.18	10.81	10.07	9.33
30	10.90	10.81	10.66	10.54	10.62	10.90	11.10	11.16	11.26	10.92	10.07	9.50
34	11.70	11.74	11.75	11.75	11.70	11.68	11.35	11.07	11.14	10.78	10.10	9.29
37	12.04		12.02	12.03	11.83	11.62	11.41	11.43	11.15	10.75	10.12	9.40
40	11.10	11.35	11.57	11.58	11.48	11.50	11.60	11.52	11.16	10.73	10.15	9.52
44	11.10	10.95	10.77	10.69	10.66	10.89	11.04	11.15	10.99	10.66	10.10	9.54
48	10.00	9.91	9.99	9.98	10.07	10.25	10.40	10.65	10.76	10.58	10.04	9.56
52	9.40	9.42	9.42	9.49	9.65	9.89	10.01	10.22	10.50	10.44	10.05	9.56
55	9.30	9.36	9.42	9.39	9.36	9.59	9.77	9.82	10.15	10.30	10.05	9.55
60	8.80	8.88	8.91	8.96	9.09	9.24	9.33	9.43	9.28	9.82	9.89	9.08
64	8.68	8.72	8.75	8.76	8.82	8.96	9.07	9.20	9.28	9.82	9.89	9.08

TABLE 10.—DETAILS OF CORRECTION FOR STATION 37
z = 3800 feet

Ring diameters, miles	Weight of ring	Mean diff. of altitude feet	Correction factor		Weighted diff. of altitude, feet		
			t = 4 My	t = 1 My	t = ∞	t = 4 My	t = 1 My
0 – 0.25	.0554	60	1	1	3.3	3.3	3.3
0.25 – 0.375	.0578	80	1	1	4.6	4.6	4.6
0.375– 0.500	.0656	70	1	1	4.6	4.6	4.6
0.50 – 0.75	.1287	270	1	1	35	35	35
0.75 – 1.0	.1085	480	1	1	52	52	52
1.0 – 1.25	.0852	690	1	.99	59	59	59
1.25 – 1.75	.1184	670	1	.96	79	79	76
1.75 – 2.75	.1271	950	.97	.91	121	117	110
2.75 – 5.0	.1108	1350	.93	.77	150	139	115
5 – 10	.0707	1980	.80	.51	140	112	71
10 – 22	.0390	2700	.49	.084	105	52	9
22 – 40	.0147	4000	.087	—	59	5	—
40 –100	.0108	4600	—	—	50	—	—
100 –	.0072	7100	—	—	51	—	—
				$\bar{h}(t)$ =	910	660	540
				$z - \bar{h}(t)$ =	2890	3140	3260

is in any case assumed. A small change in k is equivalent to a corresponding proportional change of t. In later computations involving deeper parts of the crust, k is taken as 0.01 cm²/sec, since the conductivity diminishes and the specific heat rises with increase of temperature.

According to the theory developed above, a plot of $(T - az\alpha' L)$ versus $[z - \bar{h}(t) + az(D - z)]$ should determine a straight line

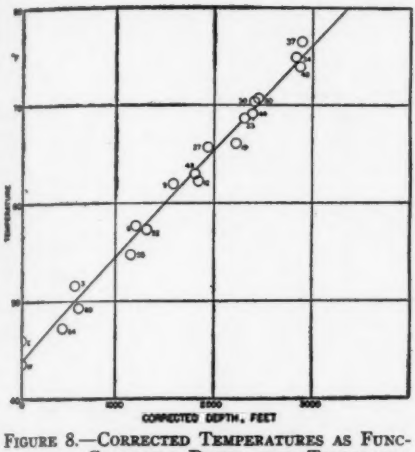

FIGURE 8.—CORRECTED TEMPERATURES AS FUNCTION OF CORRECTED DEPTH, WITH TOPOGRAPHY PERMANENTLY AS AT PRESENT (STEADY-STATE SOLUTION)

The station number is given beside each point. The circles have a diameter of about 1°F. The slope of the line is 10.76 ± 0.28°F/kft (Table 13).

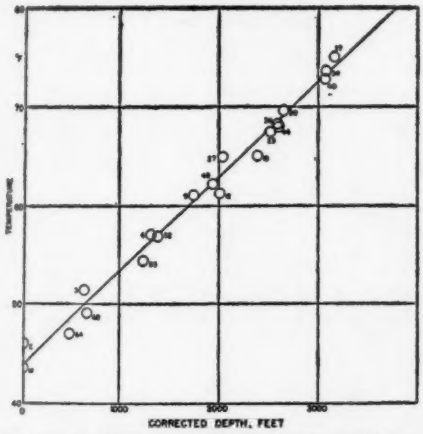

FIGURE 9.—CORRECTED TEMPERATURE AS FUNCTION OF CORRECTED DEPTH, FOR LINEAR EVOLUTION IN 4 MILLION YEARS

The slope of the line is 9.52 ± 0.25°F/kft (Table 13).

of slope $(\alpha - \alpha')$ and intercept T_0. These parameters are determined for each solution by the method of least squares, and the "fit" is evaluated in terms of the standard deviations from the straight lines. If σ_i denotes the difference between the calculated and observed (adjusted) temperatures for the ith point, then the standard deviation of a single observation, σ, is,

for n points,

$$\sigma = \sqrt{\frac{\Sigma\sigma_i^2}{n}}$$

and the mean-square error of the slope is

$$\sigma\sqrt{\frac{n}{n\Sigma\bar{z}_i^2 - (\Sigma\bar{z}_i)^2}}$$

where $\bar{z}$ is written for $[z - \bar{h}(t) + az\,(D - z)]$.

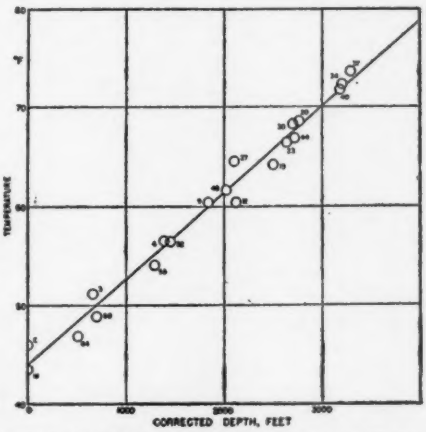

FIGURE 10.—CORRECTED TEMPERATURE AS FUNCTION OF CORRECTED DEPTH, FOR LINEAR EVOLUTION IN 1 MILLION YEARS (20 POINTS)

The slope of the line is 8.72 ± 0.26°F/kft (Table 13).

The corrected data for the steady state, and for the assumptions, t = 4 My and t = 1 My, are shown in Table 11 and plotted in Figures 8, 9, and 10. For the steady state, the function $a = 2/\sqrt{\pi kt}$ vanishes, and the values of $T - aza'L$ are simply the observed temperatures, adjusted to even station numbers and a common altitude of 8300 feet. The parameters of the least-squares straight lines are collected in Table 13. In all cases, the standard deviation of a single point is about 1.2°F. The standard error of the slope $(\alpha - \alpha')$ lies between 0.2 and 0.3°F/kft, or between 2 and 3 per cent of the slope. The differences afford no basis for discriminating among the assumptions regarding length of time of development, or amount of uplift.

The whole body of temperatures may be used by finding $\bar{h}(t)$ for the intermediate points by interpolation. In this way, data are found for 51

additional points, for $t = 1$ My (Table 12). With the 71 points, the parameters of the least-squares straight line are found to be: intercept

TABLE 11.—CONDENSED RESULTS FOR SELECTED STATIONS

Station	z kft	$T - \alpha\alpha' L$			$z - \bar{h}(t) + \alpha z(D - z)$			
					$t = \infty$			
		$t = \infty$	$t = 4$ My	$t = 1$ My	3-dim.	2-dim.	$t = 4$ My	$t = 1$ My
W	0	43.5	43.5	43.5	0	0	0	0
3	.50	51.6	51.4	51.2	.58		.64	.66
6	1.45	57.7	57.1	56.6	1.21	1.37	1.32	1.39
9	2.00	61.9	61.1	60.4	1.59		1.75	1.84
12	2.30	62.2	61.3	60.4	1.84	2.04	2.01	2.12
15	2.30	66.0	65.1	64.2	2.22		2.39	2.50
20	2.70	70.7	69.6	68.6	2.45	2.51	2.65	2.77
23	2.90	68.6	67.5	66.4	2.31		2.52	2.64
27	1.40	65.6	65.0	64.5	1.94	1.93	2.04	2.10
30	2.60	70.3	69.3	68.3	2.41		2.59	2.70
34	3.40	74.9	73.6	72.3	2.83	2.73	3.08	3.21
37	3.80	76.5	75.0	73.6	2.89		3.16	3.29
40	2.80	73.9	72.8	71.8	2.87	2.68	3.07	3.18
44	2.90	69.1	68.0	66.9	2.39	2.29	2.60	2.72
48	1.70	62.9	62.2	61.6	1.81		1.94	2.02
52	1.10	57.3	56.9	56.5	1.32	1.21	1.39	1.45
55	.95	54.8	54.4	54.1	1.16		1.24	1.29
60	.50	49.3	49.1	48.9	.62	.56	.67	.70
64	.38	47.2	47.0	46.9	.45		.49	.51
E	0	46.0	46.0	46.0	0	0	0	0

Other data: $D = 4.00$ kft
$L = 7.00$ kft
$\alpha' = 2.5$ °F/kft
$a = 2/\sqrt{\pi k t} = 0.0434/\sqrt{t}$ per kft, with t in My, if
$k = 0.02$ cm²/sec = 63 km²/My = 678 kft²/My

at zero depth, 43.98°F; slope 8.77 ± 0.12°F/kft, $\sigma = 1.03$°F. This is in substantial agreement with the result for 20 points, and the procedure has not been repeated for the other cases.

In Figure 11, 71 consecutive points are joined to show the trend of the deviations; the corrections are based upon an assumed time of development of 1 million years, but the results would be similar for the other assumptions. With respect to the least-squares straight line, the temperatures at the west end gradually rise, and between stations 3 and 8 are about 1°F too high; between 8 and 12, there is little change of temperature, though the depth in-

TABLE 12.—CORRECTED TEMPERATURES AND DEPTHS FOR INTERMEDIATE STATIONS BY INTERPOLATION
($t = 1$ My, $L = 7000$ feet)

Station	$T - \alpha\alpha' L$ °F	$z - \bar{h}(t) + \alpha z(D - z)$ kilofeet
1	44.7	0.11
2	47.9	0.39
4	53.5	0.91
5	55.5	1.15
7	58.3	1.54
8	60.2	1.68
10	60.4	1.93
11	60.5	2.03
13	61.2	2.24
14	62.3	2.27
16	65.2	2.55
17	66.3	2.59
18	67.3	2.62
19	68.2	2.66
21	68.1	2.70
22	67.7	2.69
24	65.5	2.57
25	65.3	2.41
26	64.8	2.20
28	65.1	2.18
29	66.6	2.50
31	69.9	2.80
32	70.7	2.93
33	71.6	3.07
35	72.5	3.27
36	73.5	3.28
38	73.5	3.33
39	73.0	3.27
41	70.5	3.06
42	69.4	2.94
43	68.0	2.82
45	65.7	2.46
46	64.3	2.38
47	63.2	2.20
49	60.3	1.87
50	59.1	1.74
51	57.4	1.59
53	55.8	1.40
54	54.4	1.34
56	54.1	1.19
57	53.5	1.08
58	52.4	0.94
59	50.9	0.83
61	48.3	0.63
62	47.8	0.59
63	47.7	0.55
65	47.7	0.52
66	47.9	0.52
67	48.7	0.45
68	48.2	0.29
69	47.4	0.18

creases; between 12 and 16, the temperatures are too low. The points under the valley of the North Inlet (26, 27, 28) fall above the line. by acting as an aquifer for water from the higher slopes (between 59 and 65). Most of these deviations are not greater than 1°, occasionally

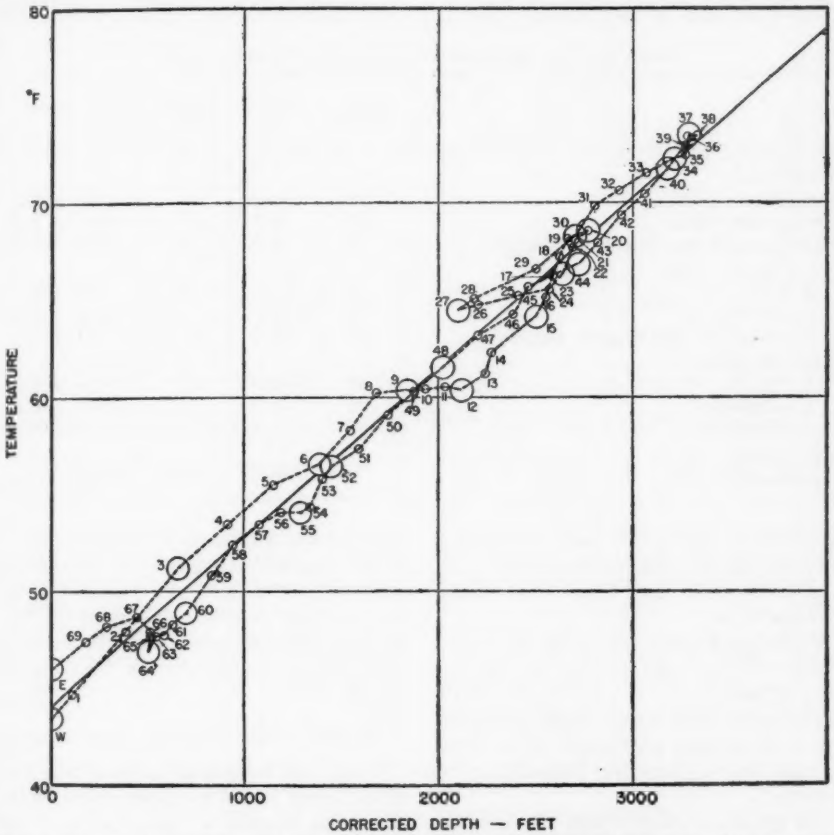

FIGURE 11.—CORRECTED TEMPERATURE AS FUNCTION OF CORRECTED DEPTH FOR LINEAR EVOLUTION IN 1 MILLION YEARS (71 POINTS)

All the observations are plotted in this figure; the numbers are the station numbers, in thousands of feet. The slope of the line is 8.77 ± 0.14 °F/kft (Table 13).

For the 30,000 feet between 29 and 59, the temperatures are close to the line; between 60 and 65, they are again too low, crossing over between 66 and 67 and remaining high to the East Portal.

The disturbance between stations 8 and 12 has the appearance of an effect of recent faulting (Appendix B). East of station 59, much of the cover is glacial till, which may raise the temperature because of its poorer conductivity (as between 69 and 67), or lower the temperature reaching 2°F; much more information would be required for convincing detailed explanation. On the whole, these observations, extending horizontally for 13 miles, are remarkably consistent with the simplest interpretation, in terms of uniform conductivity, uniform variation of surface temperature, and topographic irregularity.

The "correlation coefficient," r, has been computed for one case; with t = 1 million years, and L = 0, r = 0.933, r^2 = 0.986. The inter-

pretation of this result (Hoel, 1947, p. 84) is that 98.6 per cent of the variance of the temperature is accounted for by the linear relationship between temperature and corrected depth.

TABLE 13.—PARAMETERS OF LEAST-SQUARES STRAIGHT LINES

	No. of points	Intercept T_0 °F	Standard Deviation °F	Slope $(\alpha - \alpha')$ F°/kft
Adams Tunnel				
Steady-state, 3-dim.	20	43.8	1.2	10.76 ± 0.28
Steady-state, 2-dim.	11	44.0	1.4	10.80 ± 0.45
Steady-state, 2-dim. (rejecting Station 12)	10	44.1	1.0	10.95 ± 0.31
t = 4 My. 3 − dim.				
L = 0	20	—	—	9.90 ± 0.3
L = 7000 feet	20	43.9	1.1	9.52 ± 0.25
L = 7000 feet, with "glacial" correction	20	44.5	1.1	9.51 ± 0.24
t = 1 My. 3-dim.				
L = 0	20	43.9	1.2	9.53 ± 0.25
L = 7000 feet	20	44.0	1.2	8.72 ± 0.26
L = 7000 feet	71	44.0	1.0	8.77 ± 0.14
Moffat Tunnel				
Steady-state, 2 dim.	8	44.5	1.3	11.4 ± 0.8

Thus there is little to be explained in other ways. Though this coefficient has not been computed for the other cases, it is certainly nearly the same for all.

The standard deviation for all these solutions is about 1°F, as compared with 2.6°F for the mean air temperatures (Fig. 4). It seems likely that the relationship between mean surface soil or rock temperature and altitude is more regular than that between air temperature and altitude.

The collected results (Table 13) show the magnitudes of the various corrections. The correction for uniform uplift of 7000 feet, as given above, is 0.8°F/kft if accomplished in 1 million years, 0.4°F/kft if in 4 million years, and vanishes in the steady-state correction. Nearly all the remaining difference between the corrections for finite times and for the steady state results from the difference in the topographic correction, or "differential erosion." This difference is 1.2°F/kft for 1 million years, 0.9°F/kft for 4 million years, in both cases larger than the correction for uniform uplift of probably the maximum acceptable figure. It is thus important to introduce the time-dependent corrections [$E(R, t)$ or $G(R, t)$] in the calculation of the topographic correction; on the other hand, it is not necessary to know this time of evolution with high precision. A reliable assignment of the last peneplanation to a definite epoch of the Cenozoic would suffice to limit the uncertainty in the topographic correction to a few tenths of a degree per 1000 feet, with similar errors for the correction for uplift. The removal of "ambiguities" from the thermal studies of mountains consequently requires definitive physiographic studies.

Two-Dimensional Solution, Adams Tunnel

Strictly, the topography in the neighborhood of the Adams Tunnel is without symmetry, but the tunnel direction is nearly normal to the axis of the Continental Divide, and many of the features are prolonged for some distance normal to the tunnel line. It is thus of some interest to see what errors are introduced by the assumption that the topography is cylindrical, with every normal cross section identical with the vertical profile along the tunnel. Where such an assumption can be justified, the work of computing the topographic correction is evidently enormously reduced, as we have then to deal only with the profile and with plane angles. The two-dimensional case can be rapidly solved by graphical methods.

The two-dimensional computation has been made for 9 points, for the steady-state case.

Angular elements of 10° were used, except between 80° and 90° from the vertical, where further subdivision aids in limiting the errors due to poorly determined distant topography. The two-dimensional and three-dimensional

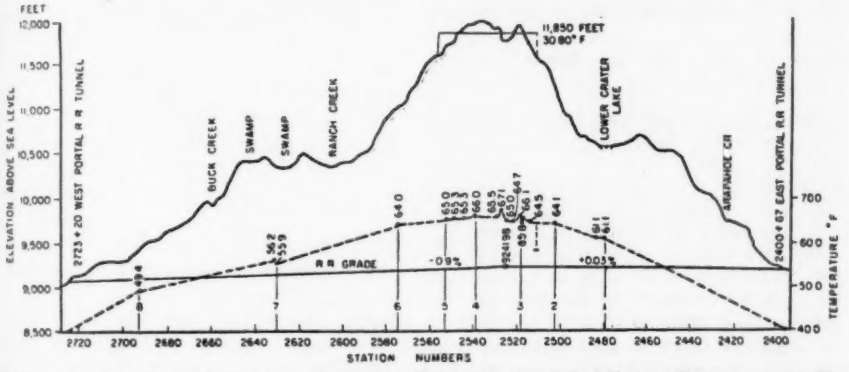

FIGURE 12.—SURFACE PROFILE AND OBSERVED TEMPERATURES FOR MOFFAT TUNNEL, AFTER VAN ORSTRAND

The station numbers are in hundreds of feet. The points numbered from 1 to 8 have been used in the present work.

values of $z - h(\infty)$ are compared in Table 11. The greatest difference is about 200 feet, equivalent to about 2°F. A least-squares solution for these 11 points (9 plus the two ends) gives a slope of 10.80°F/kft, compared with 10.76 for the three-dimensional solution. The deviation for one point (Station 12) is much greater, 3.3°F, than any found with the three-dimensional values and is 2.4 times the standard deviation (1.4). Without this point, the standard deviation becomes 1.0°F, nearly the same as for 20 points in the three-dimensional case. The slopes are not significantly different. It thus appears that the two-dimensional treatment is valid for this topography; it will generally be advisable, however, to treat a few points by both the two- and three-dimensional methods before concluding that the two-dimensional treatment is adequate.

Two-Dimensional Solution, Moffat Tunnel

Temperatures were measured in the Moffat Tunnel, about 27 miles south of the Adams Tunnel, by Van Orstrand (1934b). Of the original data, nothing remains except a profile showing temperatures and positions of measurement. The writer is indebted to the Director of the U. S. Geological Survey for a copy of this profile (Fig. 12), which was enlarged and formed the basis of the following treatment. Twenty measurements are plotted, but 12 are grouped in one 5000-foot interval near the center of the tunnel. The Moffat Tunnel is 32,253 feet long and lies mostly in the Central City quadrangle; the West Portal and about 3000 feet lie in the Frazer quadrangle. The maps of these two quadrangles, both on a scale of 1/62,500, were joined as accurately as possible, and the line of the tunnel, which is not shown on the only available edition of the Central City quadrangle, was established by using the known length and the altitude of the East Portal. The vertical profile was then constructed for this line; it differs only slightly from the profile drawn by Van Orstrand.

This region departs from two-dimensional symmetry rather more than does the region of the Adams Tunnel, but a comparison for two points (4 and 7) showed little difference between the two- and three-dimensional effective depths. Consequently 8 stations, spaced as evenly as possible over the whole length, are treated for the steady state only, by the two-dimensional method. The tunnel altitude is about 9200 feet, or 900 feet higher than the Adams Tunnel, while the surface of the Divide is at nearly the same altitude in both regions. The effective depths and the rise of temperature are thus smaller in the Moffat Tunnel. As the observa-

tions are fewer and less well distributed, the gradient is less accurately determined; the mean-square error reaches 0.8°F/kft, as against 0.25°F/kft for the Adams Tunnel.

A temperature of 40°F is shown on the chart (Fig. 12) for both ends of the tunnel, but this

TABLE 14.—DATA FOR THE MOFFAT TUNNEL

Point No.	Station kft	Altitude of Station kft	Altitude of Surface kft	T_{obs} °F	T_{max} °F	$z - h(\infty)$, kft (measured from 9243 ft.) 2-dim.	3-dim
1	248	9.243	10.55	61.1	61.1	1.41	
2	250.25	9.243	11.25	64.1	64.1	1.65	
3	251.8	9.242	11.95	66.1	66.1	1.83	
4	253.8	9.230	11.97	66.0	65.9	1.83	1.83
5	255.2	9.218	11.70	65.0	64.7	1.86	
6	257.45	9.197	11.00	64.0	63.4	1.64	
7	263.1	9.147	10.36	56.0	54.8	1.15	1.08
8	269.25	9.091	9.45	49.4	47.6	0.21	

was found by use of air temperatures instead of by measurement in the rock. If this point is rejected, the least-squares straight line has a slope of 11.4°F/kft, with a standard deviation of 1.25°F (Fig. 13). Only one point deviates more than 1°F from this line, and this is so far off as to suggest a local disturbance. If the point at zero depth is used, the slope is 12.8°F/kft, and the standard deviation 1.6°F. Four points have large deviations, three greater than 2°F. It thus seems likely that 40°F is too low for the extrapolated surface-rock temperature, which cannot be found here, as in the Adams Tunnel, by using tunnel measurements within 500 feet of the portals. The gradient 11.4 ± 0.8 is to be compared with the steady-state gradient for the Adams Tunnel, 10.8 ± 0.3°F/kft. The difference is less than its standard error. The true gradient, found by adding the "surface" gradient, 2.5°F/kft, is 13.9°F/kft or 25.3°C/km for the Moffat Tunnel.

The rocks of the Moffat Tunnel region are described as injection gneiss, pegmatite, schist, granite, and quartz monzonite (Lovering, 1928), in general character resembling those of the region farther north. The Ranch Creek fault, about 2 miles each of the West Portal, separates two anticlines, with schist the major rock to the west, quartz monzonite and gneiss to the east. The low temperature at Point 7 may result from a peculiarity of location with respect to a body of schist, an explanation which also suggests itself for the similar situation of Stations 12 and 15 in the Adams Tunnel. The faulting itself

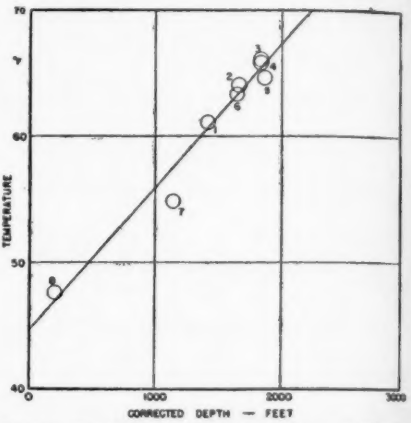

FIGURE 13.—CORRECTED TEMPERATURE AS FUNCTION OF CORRECTED DEPTH FOR MOFFAT TUNNEL (STEADY-STATE SOLUTION)

The slope of the line is 11.4 ± 0.8°F/kft (Table 13).

is probably of too great an age to have so large a residual effect (Appendix B), though it may permit access of water from the surface. Experimental work on samples from the Moffat region would be required for an independent determination of heat flow, but one might expect to find about the same conductivities as for the Adams Tunnel. There seems to be no reason for assuming different physiographic histories for the two regions, so corrections of about the same magnitude for finite duration of topography would apply to both. Though with a higher uncertainty, the results for the Moffat Tunnel thus agree wth those for the Adams Tunnel.

Van Orstrand gives an appreciably higher steady-state gradient for the Moffat Tunnel—31.4°C/km. This is based on Lees' solution for a single steady "line doublet", which fits the true profile reasonably well, and upon assumptions of definite values for the surface temperature at 11,850 feet and at the portals. As Van Orstrand uses the mean air temperatures at these altitudes, and also takes for α' the "air

gradient", 3.4°F/kft, instead of the lower value 2.5 which appears to be more nearly correct for the surface rock, his reduction does not allow for the excess of rock temperatures over air temperatures. Furthermore, it uses only the measurements under the Divide, while those at shallower depths are ignored. As we have seen, the temperature of the air at a given place may depart considerably from the mean line; the standard deviation (Fig. 4) is several degrees. On the other hand, the air *gradient* is much better determined; if we took $\alpha' = 3.3$°F/kft, the gradient α would be 14.7°F/kft, or 26.8°C/km.

By the method adopted here, the extrapolated surface rock temperature (rejecting the 40° point) is 44.5°F at 9240 feet. The implied surface rock temperature at 11,850 feet with a surface gradient of 2.5°F/kft is thus 38°F, instead of the 30.8° taken by Van Orstrand. This difference accounts for the difference of gradient between his result and the present one; it is no greater than the difference between air and soil temperatures observed by Van Orstrand in many wells in the western United States at lower altitudes.

Change of Gradient with Depth

General statement.—The corrected gradient[t] has been computed on the assumption of a linear relationship between corrected temperatures and depths. Several effects may produce a variation of gradient with depth, or a deviation from linearity of the temperature as function of depth: (1) local radioactivity; (2) variation of conductivity with depth; (3) incorrect allowance for erosion; (4) glaciation, or climatic variation in general. The magnitude of the curvature to be expected from these causes will be examined below. The "glacial" correction is the largest of these disturbances, but is still too small to have an appreciable influence on the result.

Local radioactivity.—As a result of local radioactivity, the gradient should decrease as the depth increases. Within a uniform layer, the rise of temperature with depth x from its surface due to its own radioactivity is given by $T = (PH^2/2K)[(2x/H) - (x/H)^2]$, where H is the thickness of the layer, K its conductivity, and P the heat production (cal/cm³·sec). At the base of the layer, this is $PH^2/2K$; with $K = 0.008$ cal/cm·sec·deg. and $P = 6 \cdot 10^{-13}$ cal/cm³·sec, the rise of temperature is about $0.4H^2$ °C, with H in kilometers. The greatest depth in the tunnel is about 1 kilometer, and thus the maximum rise of temperature due to the radioactivity of the rock above the tunnel is about 0.4°C, or 0.7°F. Three-quarters of this rise occurs in the first half kilometer of depth. The average rate of rise is 0.4°C/km, and the deviation from linearity at mid-point (x = 0.5 km) is 0.1°C or 0.2°F. With a standard deviation of 1°F, so small a curvature is beyond detection. The maximum correction to the gradient would be about 0.4°C/km, or roughly 2 per cent.

Variation of conductivity with depth.—For a given flow of heat, a decrease of conductivity means an increase of gradient; at depths of tens of kilometers, this becomes an important consideration in determining the temperatures. The conductivity of quartz-rich rocks generally decreases as the temperature increases (Birch and Clark, 1940); near the surface, this is partly or completely offset by the increase of conductivity with mean stress. The effects of temperature and of stress, of opposite sign as the depth increases, are both of the order of a few per cent at a depth of 1 kilometer. Within 1 kilometer of the surface, the assumption of uniform conductivity within a mass of uniform rock should be sufficiently exact. The variation with rock type is considered below.

Effect of incorrect allowance for erosion.—Curvature may result from an incorrect allowance for erosion. The correction was of the form of an addition to the depth (*see* above), $az(D - z)$, where D was taken as 4000 feet for all stations. This is equivalent to about 1°F at mid-depth. Even if the error were as large as 50 per cent, the error of the correction would be only about 0.5°F, thus of the same order as a number of other possible disturbances. (*See* also Appendix B.) Presumably the curvature from such a source might have either sign. No serious error is likely to be introduced by this correction.

Effect of glaciation.—Several episodes of mountain glaciation in this region have been recognized (Atwood and Mather, 1932; Bryan and Ray, 1940; Ray, 1940; Jones and Quam,

1944; Antevs, 1945), and it is at least plausible that they are to be correlated with the continental glaciations of the Middle West and East. An attempt to calculate the geothermal effects of glaciation is at once enmeshed in the uncertainties of the Pleistocene time scale. This problem has been discussed in terms of a "schematic" glacial history, with the conclusion that in glaciated regions near the limit of glaciation the net effect of the correction for climatic oscillations may be a reduction of the apparent gradient by not more than 3°C/km (Birch, 1948). Farther north or farther south, smaller effects might be expected. This conclusion appears to be consistent with the observations of temperature in mines and wells.

The former discussion was restricted to a consideration of the temperatures below a plane surface on which the mean temperature decreased when the surface was covered with ice. The temperatures cannot adjust immediately to changes of surface temperature, and thus, if the last change of sufficient duration was a warming of the surface, the deep temperatures remain too low for a period depending upon the depth and the thermal diffusivity.

A different situation exists for a tunnel under high mountains. Little or no correction is required for the shallow stations near the ends of the tunnel. The deepest stations lie near the center, but the mean surface temperature above these stations is likely to be close to the freezing point (at least in Colorado) even in interglacial times, so long as the altitude is nearly as at present. Thus correction for these points is small. At the intermediate depths, say at 1600 feet or 0.5 km, glaciation might lower the surface temperature by perhaps 8°F below its present mean. With a lowering of 8°F for all the glacial stages, and the "schematic" chronology of the former work, we find a present lag of about 1°F at 0.5 km, with values gradually diminishing toward the greater and smaller depths. We might expect to find the corrected temperature-depth plot slightly concave toward the temperature axis.

This curvature was sought by finding the least-squares solution of the form $T = a + bx + cx^3$, where T is the corrected temperature and x the corrected depth. For the 4-My solution, we find:

$$a = 44.38 \pm 0.63°\text{F}$$
$$b = 8.50 \pm 0.87°\text{F/kft}$$
$$c = 0.32 \pm 0.26°\text{F/kft}^3$$

The standard deviation, for 20 points, is 1.04°F; thus even with an additional adjustable parameter the fit is not significantly better than for the straight line. The parameter c, which determines the curvature, is only slightly greater than its standard error. There is no positive evidence for curvature, though it is interesting that the deviation of this curve at midpoint ($x = 1.6$ kft) from the straight line between the points at zero and at maximum (3.2 kft) depths is 0.8°F, or roughly the "predicted" amount.

For completeness, let us introduce the theoretical correction for glaciation and solve again for the parameters of the best straight line. The correction is a term to be added to the temperature, having a maximum value of 1°F at a depth of 1.6 kft, and zero for depths of 0 and 3.2 kft. For simplicity, this may be taken as parabolic in the corrected depth, say $Cz(3.2 - z)$, with $C = 0.39$. The straight line adjusted to these corrected temperatures ($t = 4$My) has an intercept 44.5°F and a slope 9.51 ± 0.24°F/kft, with a standard deviation of 1.06°F. Both the mean slope and the standard deviation are unchanged by this correction (*see* Table 13) though there is an insignificant increase of 0.6°F in the intercept. It seems unnecessary to repeat this calculation for the other cases. The theoretical correction is consistent with the present measurements, but no positive confirmation of the correction can be claimed. The correction to the gradient as a result of the glacial history may probably be neglected for these circumstances.

Thermal Conductivity

Introduction

In the determination of the flow of heat, the thermal conductivity is of equal importance with the thermal gradient, and in certain respects presents greater difficulties. The temperature at a point depends not simply upon the conductivity in the immediate neighborhood but upon a mean value for a large and indeterminate volume around the point. The rocks pierced by the Adams Tunnel have been minutely mapped, but much less detail is avail-

able for the surface, and the cross-section or three-dimensional relationships are largely hypothetical. On the other hand, the details of the structure are important only if the different rocks have appreciably different conductivities. Thus the first step is to examine the variations within and among the principal types; the second, to analyze the variations along the tunnel; and, finally, to inquire whether significant deviations of temperature are likely to result from the observed deviations of conductivity from its mean value.

No method of approaching this problem has yet been devised other than by measurement of the conductivity of individual samples, although this procedure necessarily leaves certain questions unanswered. It is not possible to determine, for example, the effects of the innumerable large-scale discontinuities, such as faults, joints, or veins, but even the most perfect rock is a composite structure, with discontinuities on a still finer scale between individual crystals. The effect of the fine-scale structure is included in the measurement on small samples, and the smaller number of large-scale discontinuities probably have a minor effect upon the conductivity of large volumes of rock. This consideration is common to all determinations of geothermal flow, though not necessarily always of the same importance.

Method of Measurement

The conductivity was measured in a special apparatus, remodeled from an older form used by Clark (1941) for a number of sedimentary rocks. The specimen, a circular disc 1.5 inches in diameter, and about ½ inch thick, with flat, parallel faces, is inserted between copper discs of the same diameter, $\frac{1}{16}$ inch thick (Fig. 14). On each side of this unit are discs of pyrex glass, capped at the ends by two more copper discs. This "stack" is surmounted by a heating element and assembled in a hydraulic press between special hemispherical thrust bearings. The press is shielded by a heavy steel cylinder.

Three differential thermocouples of copper-constantan are used to measure the differences of temperature across the three poor conductors, two of pyrex and one of rock. These couples are made by soldering short lengths of No. 30 enameled constantan wire between longer lengths of No. 30 copper wire, with the junctions soldered in copper bushings about ⅛ inch long by $\frac{1}{16}$ inch in diameter, which fit closely in wells drilled in the copper discs.

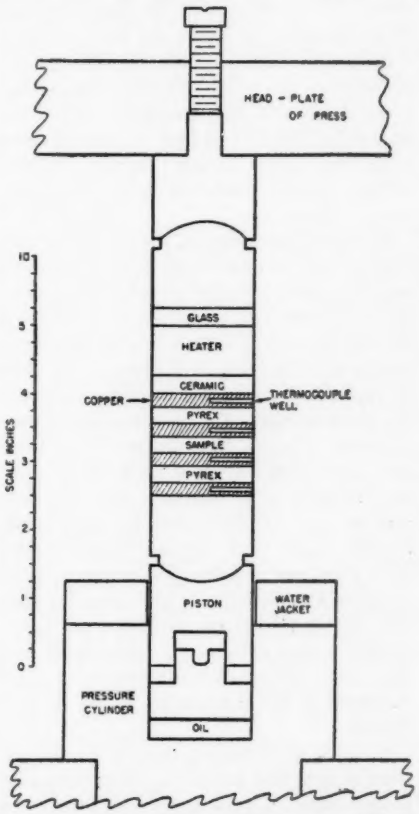

FIGURE 14.—DIAGRAM OF APPARATUS FOR MEASUREMENT OF RELATIVE CONDUCTIVITY

Three differential thermocouples, not shown, give differences of temperature across the two discs of pyrex glass and the sample. The stack of discs is compressed by the action of a pump, not shown, which raises the pressure of the oil in the pressure cylinder. The head-plate is held in place by tie-rods, omitted from the figure.

The external circuits are entirely of copper and manganin. The thermoelectric potentials are measured with a Leeds and Northrup Type K potentiometer and a galvanometer giving a deflection of 2 mm/microvolt at 1 meter.

There are two heating coils, one in the small

heater above the sample, one wound on the external shield. A circulation of cold water is provided for the lower end of the system. The heaters are adjusted so that there is a drop of about 7°C across each of the glass samples. As the conductivity of the rocks varies between 2 and 3 times that of pyrex, the difference of temperature across the sample is usually between 2° and 3°C, corresponding to 80 to 120 microvolts. The shield is kept at about the mean temperature of the sample. Thyratron regulators are used to maintain both heaters at constant temperatures.

To a first approximation, the ratio of conductivity of rock to pyrex is the ratio of the mean potential across the glass samples to the potential across the rock. A correction of about 3 per cent is found by substituting another pyrex specimen for the rock; this includes the effect of temperature on the thermoelectric output of the thermocouples. The absolute conductivity of pyrex is known from former work (Birch and Clark, 1940) to be 0.00296 cal/cm·sec·deg. at 30°C; other materials have also been used to verify the calibration, including single-crystal quartz (flow normal to optic axis), silica glass, and obsidian. The conductivity of of the rocks falls between the values for glass and quartz. The lateral heat losses are nearly proportional to difference of temperature, and the ratios are nearly independent of small variations of the temperature of the external shield.

A single measurement consists of observations of potential across the three discs with potentiometer current direct and reversed, 6 readings in all; small parasitic potentials are thus eliminated. Readings are made to 1 microvolt, and ratios are reproducible to about 2 per cent or better.

All interfaces between glass or rock and copper were thinly coated with a high-temperature silicone stop-cock grease before assembly. After alignment, the stack of discs was compressed with an initial load of 500 psi, and then 2500 psi for most of this work. Many of the rocks show reversible changes of conductivity of several per cent with this change of load; conductivity always increases with compression.

Some advantages of this equipment are as follows:

(1) Samples are quickly changed, with little alteration of the temperature of the heavy parts of the apparatus. The temperature of the heater is unaffected, and it is necessary to wait for redistribution of temperature only across the specimen and the glass; measurements may be made rapidly, probably within 15 minutes after inserting a specimen, though in the present work much longer intervals were allowed, at least several hours or often overnight, as the limiting factor was the time required for preparing the specimens.

(2) Thermocouples are easily replaced, interchanged, or compared by insertion across the same sample. This is an important step in avoiding systematic error.

(3) Absolute temperatures are not required, except for an approximate determination of the mean temperature of the sample; thus no closely controlled cold junction is needed.

(4) With the relatively heavy loading, contact resistance is virtually eliminated. This may be checked in various ways, such as by observing the potential with the sample removed, leaving copper discs in contact, or by inserting two samples in series.

(5) An approach to natural conditions of stress is realized with loads up to several thousand pounds per square inch, equivalent to the weight of rock columns several thousand feet deep.

Sampling

Samples of the major types of rock were selected from the large collections stored by the Bureau of Reclamation at Denver and at Estes Park. The samples represented the whole tunnel except for a section between Stations 21 and 35 (14,000 feet) for which the samples had been mislaid. The rocks for this section are probably well enough represented by the similar rocks from other parts of the tunnel. In the selection, rocks present in small volumes were omitted; there are few samples of pegmatite, basic dikes, or altered varieties present only at contacts, but otherwise the choice was designed to obtain a fairly uniform distribution of samples. Nearly all are classified as granite, injection biotite schist or gneiss, or quartz diorite gneiss; the last named appears only in the western-

most 10,000 feet; all the rest, except for narrow veins and dikes, is granite and schist or gneiss.

The distribution of the 80 samples selected for measurement of conductivity, according to position of origin in the tunnel, is as follows:

Between Stations	0 and 10	14 samples
	10 and 20	15 samples
	20 and 21.3	4 samples
	35 and 40	7 samples
	40 and 50	17 samples
	50 and 60	12 samples
	60 and 70	11 samples

In many instances, several specimens were made from a given sample, particularly for the schistose rocks where measurements in different directions were desired. Conductivity was determined for a total of 123 specimens.

Though this number seems large as a laboratory chore, it amounts after all only to one sample for 900 feet of tunnel, a density of sampling which might be inadequate were it not for the relatively uniform properties of the rocks.

The measurements of conductivity and density are assembled in Table 15; in all cases, the mean temperature is about 33°C, with a load parallel to the direction of flow of heat of about 2500 psi.

Rosiwal analyses for a few samples are given in Table 16. In the granites, the quartz content ranges from 30 to 40 per cent; there is from 6 to 12 per cent of dark minerals, mostly biotite; the feldspar usually includes a considerable fraction of plagioclase (An_{30}–An_{38}) which is untwinned and difficult to distinguish from the quartz. Probably many of these "granites" would be more accurately classified as quartz monzonites or granodiorites; the proportion of plagioclase is frequently about half of all the feldspar. The schist is extremely variable in thin sections; it is possible to select pieces consisting almost exclusively of biotite, or with almost no biotite. This variability is also reflected in the densities, and with greater sensitivity, in the conductivities.

Variation of Conductivity with Rock Type

Let us first examine the variation of conductivity within the three major groups—granite, quartz diorite gneiss, and injection schist and gneiss. The third group, which includes a number of relatively massive rocks as well as true schists, might have been further subdivided. It is the least homogeneous, and there are also definite differences for the directions parallel and normal to the planes of schistosity. A few rocks escape these categories: the dolerite from the principal dike (No. 142, Station 59.-853); a sample of pegmatite (No. 198, Station 54.3905); a sample of biotite-sillimanite schist, considerably altered (No. 13, Station 69.275). No one of these represents an appreciable fraction of the volume.

Table 15 includes measurements on 59 samples of "granite" from 43 locations. The mean conductivity is 7.89 ± 0.05 millical/cm·sec·deg. (1 millicalorie = 10^{-3} calorie. This unit will be used henceforth without repetition of its dimensions.), and the standard deviation of a single observation is 0.4. There are two deviations from the mean of nearly 3 times the standard deviation, but, if these are rejected, the mean is 7.93 ± 0.04, an insignificantly different value. Even with these, the deviations have roughly a normal distribution. The difference between samples cut from the same hand specimen is occasionally greater than the standard deviation. It seems likely that much of the variation is random, perhaps resulting partly from the small dimensions of the samples.

There are 17 samples of quartz diorite gneiss from 9 locations. Eleven are oriented with the heat flow parallel, 4 with the flow normal, to the foliation. The mean ratio, $K_{\parallel}/K_{\perp}$, is 1.16 for the four localities for which this can be found. The mean of all samples is 7.75 ± 0.13, with a standard deviation of 0.54. This mean is weighted by the predominance of parallel-flow samples in about the right proportion to give the conductivity for random orientation of foliation. Though by no means random, the direction of foliation in the tunnel is variable, and such a mean value is probably as suitable as any other.

Of the 41 samples of injection schist and gneiss from 24 locations, there are 9 pairs, for which the mean ratio, $K_{\parallel}/K_{\perp}$, is 1.20. The mean of all the parallel-flow samples (17) is 8.55; of 15 normal-flow samples, 6.95. The ratio of these means is 1.23. There are 8 massive samples for which the mean is 7.24. The mean of all 41 is

TABLE 15.—THERMAL CONDUCTIVITY AND DENSITY
In 10^{-3} calories/cm·sec·deg. C at 30°C and 2500 psi

Station	General description of rock		Density	Conductivity, K
2.739	Quartz diorite gneiss, fine, soft, altered	parallel	2.592	7.7
		45°	2.564	6.6
2.793	Quartz diorite gneiss, medium, hard	parallel	2.646	7.8
		45°	2.638	8.0
3.031	Quartz diorite gneiss, hard, fine-grained	parallel	2.70	8.5
		normal	2.69	7.3
4.644	Quartz diorite gneiss, hard, medium-grained	parallel	2.654	8.4
		normal	2.656	7.7
4·984	Granite, hard, medium, pink		2.609	8.4
			2·609	
5.380	Granite, hard, coarse, gray, flow alignment		2.607	
			2.612	8.0
5.757	Granite, hard, coarse, gray gneissoid		2.63	7.2
6.308	Quartz diorite gneiss, hard, dark gray		2.70	7.8
			2.71	7.6
7.363	Granite gneiss, medium-grained, gray		2.649	7.5
			2.634	
7.689	Quartz mica schist, hard, fine-grained	parallel	2.853	8.7
		parallel	2.850	8.4
8.498	Quartz diorite gneiss, tiny garnets	parallel	2.712	8.0
			2.647	
8.922	Quartz diorite gneiss	parallel	2.68	8.3
			2.68	7.8
9.261	Quartz diorite gneiss	normal	2.68	6.7
		parallel	2.71	8.2
9.9025	Quartz diorite gneiss, hard, fine-grained, gray	parallel	2.701	8.2
		normal	2.706	7.1
10.025	Granite gneiss, hard, fine-grained gray		2.673	8.2
11.0302	Inj. biotite schist	normal	2.690	6.8
11.506	Inj. biotite schist	parallel	2.722	8.6
		normal	2.718	6.7
11.887	Inj. biotite schist, contorted	parallel	2.734	8.3
		parallel	2.70	7.9
13.3275	Granite, reddish		2.61	8.3
			2.61	8.0
13.658	Granite, medium-grained, light gray		2.609	7.7
14.566	Inj. biotite schist	parallel	2.732	9.7
15.083	Inj. biotite schist	normal	2.69	6.9
		normal	2.65	7.0
15.688	Inj. biotite schist	normal	2.966	6.2
			2.930	
16.085	Inj. biotite schist	normal	2.797	5.4
16.781	Inj. biotite schist		2.78	6.5
			2.82	7.3
17.7627	Inj. biotite schist	parallel	2.806	11.0
		parallel	2.810	10.4
		normal	2.594	8.0
		normal	2.655	8.6
18.0095	Biotite gneiss		2.729	7.8
19.149	Inj. biotite gneiss	parallel	2.730	9.2
			2.746	

TABLE 15.—*Continued*

Station	General description of rock		Density	Conductivity, K
19.780	Granite		2.613	7.9
20.080	Inj. biotite schist		2.58	
		normal	2.613	9.1
20.528	Inj. biotite schist	parallel	2.759	10.0
21.0425	Granite, fine, gray		2.62	7.3
			2.62	7.5
21.360	Granite		2.610	7.6
			2.643	
35.3086	Granite		2.654	7.9
			2.658	
35.8152	Granite		2.623	8.2
			2.641	7.5
36.0176	Granite		2.620	7.8
			2.63	8.1
36.8525	Granite, coarse		2.64	8.2
			2.65	8.6
37.147	Granite, gneissoid		2.60	8.1
			2.60	7.5
38.490	Granite		2.62	7.9
38.886	Granite, coarse		2.635	8.4
			2.632	
40.0164	Granite and gneiss	parallel	2.71	10.2
		parallel	2.70	9.5
40.4684	Granite, coarse		2.62	7.5
41.2343	Granite, coarse		2.62	7.3
41.4035	Granite		2.660	7.7
			2.639	7.3
42.0696	Granite		2.636	8.3
			2.64	8.0
42.373	Granite		2.635	8.3
			2.645	8.3
42.681	Granite		2.63	7.8
			2.63	7.8
42.834	Granite, gneissoid		2.63	7.7
			2.62	7.6
44.407	Granite, pink		2.620	7.9
			2.618	
45.0275	Inj. biotite gneiss		2.610	6.8
45.5655	Granite, fine, gray		2.64	7.3
			2.64	6.9
46.164	Biotite inj. gneiss	parallel	2.69	8.4
		normal	2.69	6.6
46.7167	Biotite inj. gneiss	parallel	2.75	7.2
		normal	2.75	6.4
47.2175	Schist	parallel	2.76	9.8
		normal	2.71	8.6
48.058	Inj. biotite gneiss massive	parallel	2.75	5.9
		normal	2.74	5.3
48.2194	Inj. biotite gneiss massive	parallel	2.643	7.2
			2.663	9.3
49.7128	Biotite, sillimanite inj. schist	normal	2.694	6.2
		normal	2.690	6.6

TABLE 15.—*Concluded*

Station	General description of rock		Density	Conductivity, K
52.5754	Massive biotite inj. gneiss		2.73	7.3
			2.70	6.7
52.431	Quartz mica inj. schist	normal	2.65	6.6
		parallel	2.68	8.3
53.3267	Massive biotite gneiss with garnets		2.828	7.8
			2.821	7.7
54.3905	Pegmatite with large crystals of sillimanite		2.711	5.4
			2.722	
55.085	Massive biotite inj. gneiss, chloritized, slickensided surface		2.660	8.4
			2.652	
55.3325	Granite, coarse red, thin vein of fluorite		2.631	8.5
			2.631	8.4
56.610	Granite, banded pink and gray		2.64	7.6
			2.63	
57.050	Granite, coarse gray		2.65	8.0
			2.65	
57.655	Granite, coarse, reddish gray		2.610	7.7
			2.618	
58.692	Granite, coarse pink		2.603	8.1
			2.621	8.1
59.853	Dolerite, main dike		2.970	5.9
			2.969	6.0
59.9675	Granite, coarse red, heated by dike		2.59	8.0
			2.590	
60.661	Granite, red		2.611	8.3
			2.610	
62.4545	Granite, red		2.611	8.1
			2.610	8.0
62.9765	Granite, coarse pinkish gray		2.631	8.0
			2.631	
64.2562	Granite, pink		2.609	8.3
			2.611	
65.353	Granite, coarse gray		2.632	7.8
			2.634	
66.150	Granite, red, biotite		2.605	8.3
67.264	Granite, pink bands of biotite		2.642	8.5
			2.632	
67.528	Granite, gray		2.661	7.2
			2.640	6.7
67.989	Granite		2.616	8.1
			2.628	
68.565	Granite, gray		2.633	7.9
			2.624	
69.275	Biotite stillimanite schist with garnets		2.498	4.0
			2.580	

7.74 ± 0.21, with a standard deviation of 1.35. A "weighted" mean, with the parallel orientation taken twice and the normal once, is 8.02. These rocks do not form a homogeneous group; the effect of the schistosity is to produce two overlapping groups, with the parallel-flow group displaced toward higher values than the normal-flow group. The range is nearly two-to-one within each group, a ratio much larger than $K_{\parallel}/K_{\perp}$. Schistosity is probably a much

less important factor than variation of composition, and corrections for schistosity are of little value unless the more important correction for change from place to place can first be applied.

Variation of Conductivity with Location

We now examine the variation from place to place along the tunnel. Grouping the rocks over intervals of about 5000 feet, we find the figures of Table 18. It appears that low values tend to be concentrated between Stations 45 and 55, especially between 45 and 50, where the means are probably significantly lower than for the other intervals. The interval 55–60 is slightly high. There is also a notable concentration of high values between Stations 17.7 and 20.5, where the mean for 9 samples is 9.1. If these values continued up-dip toward the west, they might account for the low temperatures in the neighborhood of Stations 12 to 15.

We do not know, of course, to what extent

TABLE 16.—COMPOSITION AND CONDUCTIVITY

Station	Classification	Mineral proportions, %			Conductivity $\times 10^{-3}$ cal/cm·sec·deg.
		Quartz	Feldspar	Mafic	
4.984	Granite	34	60	6	8.4
10.025	Granite gneiss	39	49	12	8.2
21.0425	Granite	41	49	10	7.4
35.4086	Granite	31	59	10	7.9
42.373	Granite	39	55	6	8.3
57.655	Granite	31	62	7	7.7
64.2562	Granite	36	57	7	8.3
3.031	Quartz-diorite gneiss	29	57	14	8.5, 7.3
7.689	Quartz mica schist	24	68	8	8.7, 8.4
11.506	Injection biotite schist	50	15	35	8.6, 6.7
15.688	Injection biotite schist	19	—	81	6.2
17.7627	Injection biotite schist	49*	9†	42**	8.0 to 11.0
46.7167	Biotite injection gneiss	32	60	8	7.2, 6.4
53.3267	Biotite gneiss with garnets	28	49	23	7.8
59.853	Dolerite (dike)	3	52	45	6.0

* Includes plagioclase (An_{25})

† Microcline only

** Altered biotite and sillimanite

TABLE 17.—VARIATION OF CONDUCTIVITY AND DENSITY WITH ROCK TYPE

Classification	No. of samples	No. of localities	Mean conductivity (millical/cm·sec·deg.	Standard deviation	Mean density
Granite and quartz monzonite	59	43	7.89 ± 0.05	0.41	2.628
Quartz diorite gneiss	17	9	7.75 ± 0.13	0.54	2.671
Injection schist and gneiss	41	24	7.74 ± 0.21	1.32	2.728
Mean, 117 samples			7.82 ± 0.08	0.84	
Mean, 123 samples (all)			7.77 ± 0.09	1.0	

The mean values for these three groups are summarized in Table 17. The means do not differ significantly from one another, and the mean for 117 samples, 7.82 ± 0.08, is probably the best single value. There are six other samples including two of diabase, which do not fall clearly into these categories; the mean for all 123 samples is 7.77 ± 0.09. In these means, each sample has been given unit weight; if, instead, each locality is given unit weight, the values are but little affected.

the low value for the interval 45–50 is characteristic of the whole region vertically above this interval: (1) we are not sure of the structure, in a quantitative sense; (2) similar samples of gneiss and schist at other places have about the mean value of conductivity. Suppose, however, that the whole section above this interval has a conductivity of 7.2. Then, at most, the temperatures in this section would be about 3°F too high, if we assume the same flow of heat as elsewhere. This estimate is too high, as a region of low conductivity tends to be "shunted" by adjacent regions of high conductivity; the difference to be expected would not exceed a degree or so. As this is about equal to the standard deviation of the observations, it is unlikely that a definite indication would be found. The observations for this interval are, in fact, very close to the best straight line. On the whole, the assumption of thermal uniformity appears to be remarkably well justified by these measurements.

TABLE 18.—VARIATION OF CONDUCTIVITY AND DENSITY ALONG THE TUNNEL

Interval (Station numbers)	No. of locations	No. of samples	Predominant rock	Mean conductivity (millical/cm·sec·deg.)	Mean density
0– 5	5	9	Quartz diorite	7.82 ± 0.19	2.636
5–10	9	14	Quartz diorite	7.82 ± 0.14	2.691
10–15	7	10	Inj. schist, gneiss	8.02 ± 0.26	2.679
15–21.3	12	18	Inj. schist, gneiss	7.98 ± 0.24	2.717
35–40	7	11	Granite	8.02 ± 0.09	2.631
40–45	9	15	Granite	8.08 ± 0.20	2.642
45–50	8	15	Inj. gneiss	7.23 ± 0.32	2.694
50–55	3	6	Inj. gneiss	7.40 ± 0.25	2.730
55–60	7	9	Granite	8.09 ± 0.10	2.626
60–69	10	12	Granite	7.93 ± 0.14	2.624
	77	119			2.667

A small correction may be made for the difference between the temperature of the laboratory measurements, about 33°C, and of the rocks in place. Near the ends of the tunnel, the temperature is about 45°F or 7°C. Under the Divide the tunnel temperature is about 76°F (24°C), and at the surface the mean surface temperature is about at the freezing point. Thus the mean temperature may be taken as about 10°C. At this temperature the conductivity of these quartz-rich rocks will be about 2 per cent higher than at 33°C (Birch and Clark, 1940), and as a corrected mean conductivity the round figure, 8.0 millical/cm·sec·deg. is adopted, with an uncertainty of 2 or 3 per cent.

Density

These samples also afford an opportunity for a determination of the mean density of the Continental Divide in this region. The granites vary little, the schists and gneisses a great deal. By types, the mean values are: granite (78 samples) 2.628; quartz diorite gneiss (18) 2.671; schist and gneiss (48) 2.728. The mean for 144 samples is 2.667, exactly the mean value found by Daly (1933, p. 47) for 155 samples of granite, though the range is smaller for the present group. This value is also close to the density, 2.67, taken by Hayford, Bowie and others for the mean density of the normal crust. There is no indication of abnormal "lightness" of surface rock for this high-standing region, though the mean density of the granites alone is somewhat below the usual figure.

FLOW OF HEAT

In the foregoing sections, it has been shown that the temperatures observed in the Adams Tunnel are consistent with the assumption of uniform corrected gradient and uniform conductivity, and that the best value for the conductivity is 0.008 cal/cm·sec·deg. The mean flow of heat to the surface is now found as the

product of this conductivity (K) by the corrected thermal gradient (α); as the latter depends upon the assumptions with respect to topographic evolution, there are several correspondingly values for the flow of heat (Table 19). The significance of these values emerges on comparison with the determinations for other regions.

Table 19.—Corrected Gradients and Flow of Heat in Mountains

	$\alpha - \alpha'$ °C/km	α °C/km	Flow of heat $K\alpha$ in 10^{-6} cal/cm²·sec
Front Range, Colorado			
Adams Tunnel			
Steady state*	19.6 ± 0.4	24.1 ± 1	1.93 ± 0.1
Erosion in 4 My, no uplift	18.0	22.5	1.80
Erosion and uplift of 7000 feet in 4 My	17.3	21.8	1.74
Erosion in 1 My, no uplift	17.3	21.8	1.74
Erosion and uplift of 7000 feet in 1 My	16.0	20.5	1.64
"Best value"			1.7 ± 0.2
Moffat Tunnel			
Steady state*	20.8 ± 1.5	25.3 ± 2	2.0 ± 0.2
Central Alpine tunnels (Koenigsberger)			
Steady state*			2.0 ± 0.5

* This refers only to the assumption on which the topographic correction is based.

To establish a difference, we must first assess the errors of the various measurements. For the Adams Tunnel, the error on the mean conductivity is probably no greater than 3 per cent. The uncertainty with respect to the flow of heat arises mainly from the gradient. The mean-square error of the "apparent" gradient ($\alpha - \alpha'$) is about 2 per cent for each case, but the error on α' may be as much as 1°C/km. The different physiographic assumptions lead to corrected gradients with a maximum difference of about 20 per cent. The steady-state solution affords an upper limit, within the other errors, and a lower limit is probably given by the solution for 1 million years, with 7000 feet of uplift. Thus the major uncertainty results from the difficulty in specifying the physiographic history within sufficiently narrow limits. The "best" value is considered to be 1.7 ± 0.2 microcal/cm²·sec; (1 microcal = 10^{-6} calorie); the estimate of uncertainty is necessarily subjective and may be somewhat high.

Large as this uncertainty may seem, there are surprisingly few determinations for "normal" regions of comparable precision. In Table 20 are assembled the available results, including a number of estimates of uncertain value. The "best determinations" are the studies in South Africa, Great Britain, Persia, and California, all based on measurements of conductivity of a number of samples from the wells or boreholes in which the temperatures were measured. For most of these, the statistically determined errors are of the order of 5 to 10 per cent. In some instances, there may be larger systematic errors, such as may arise from glacial or other geological "corrections"; the values of Table 20 for Great Britain and Persia are smaller than the published figures as a consequence of rediscussion of the correction for glaciation (Birch, 1948). Excellent studies of temperature in deep Canadian mines have recently appeared (Misener, 1949); from the preliminary report, it appears likely that the heat flow will be close to 1 microcal/cm²·sec.

Of the "estimates" of heat flow, some are based on good observations of temperature but on estimates, or too few measurements, of conductivity; for others, there are too few

TABLE 20.—FLOW OF HEAT IN VARIOUS REGIONS

1. *Best Determinations*

Place	Surface altitude, feet	Rock	No. of wells	Flow of heat in 10^{-6} cal/cm²·sec.	
				Range	Mean
South Africa (Bullard, 1939)					
Witwatersrand	4200–5500	quartzite, lava	5	0.95–1.28	1.09 ± 0.05
Carnarvon	4060	granite	1		1.52 ± 0.04
Great Britain (Benfield, 1939)	—	sandstone, shale, marl salt	5	0.8–1.6	1.1 ± 0.1
Persia (Coster, 1947)	1000–1900	limestone, salt, anhydrite	18	0.7–1.3	1.0 ± 0.04
California (Benfield, 1947)	680	shale	1		1.3 ± 0.1
Mean, 30 wells					1.06
Mean, 4 regions (*see* text)					1.14
Mean, 5 regions					1.20

2. *Estimates* (*see* Birch, 1947b, for references)

Place	Surface altitude, feet	Rock	α °C/km	K in 10^{-3} cal/cm·sec·°C	$K\alpha$ in 10^{-6} cal/cm²·sec.	Remarks
Michigan, Calumet and Hecla mine	1200	trap	18	5	0.9	mean conductivity of 20 samples.
Texas, Big Lake 1-B	2700	dolomitic limestone	24	8	2.0	depends on correlation of samples from other wells
Colorado, Red Creek	6200	arkose, granite	20	6–8	1.2–1.6	conductivity estimated
Georgia, Griffin, LaGrange	1000	gneiss	17–22	7	1.4	conductivity estimated
Kansas, Syracuse	3460	limestone	28	5–6	1.4–1.7	conductivity estimated
Scotland, Boreland Bore (Anderson, 1939)	200	sandy shale	23	4.7	1.1	conductivity estimated
England, (Anderson, 1939)						
Durham	—	sandstone	17	10?	1.7	conductivity estimated
Wigan	—	shale, sandstone	36	3.2	1.2	conductivity estimated

observations of temperature. A careful study of the geologic column for some of the large number of wells where reliable temperatures have been obtained (by Van Orstrand, for example) might lead to reasonably good estimates of conductivity, and thence to a considerable increase in the number of estimates of heat flow, for which the individual errors would be reduced in the error of the mean.

The value for Michigan is based on the measurements of temperature by Hotchkiss and Ingersoll (1934; Birch 1948) and new, unpublished measurements of conductivity of 20 samples of the basic flows. For these samples, the writer is indebted to Dr. Walter S. White, of the U. S. Geological Survey. The figure for heat flow is listed with the estimates because a complete analysis of the distribution of con-

ductivity has not yet been completed, but it is probably nearly as accurate as the best determinations.

In view of the probable errors, the estimates of Table 20 are in fair agreement with the determinations of greater precision. Of the British values, Anderson (1939) remarks: "At present it can hardly be said with confidence that most of the results arrived at are accurate within about 10 per cent." The writer would put the uncertainty at a higher figure where the conductivities are estimated, perhaps at 30 per cent or more. For example, the heat flow at Durham depends upon a value for the conductivity of "sandstone" taken from the British Association Reports of 0.010 cal/cm·sec·deg. But even quartzites with more than 95 per cent quartz may have conductivities as low as 0.008, and sandstones with 80 per cent quartz may range as low as 0.005. The use of typical values for sedimentary rocks is often unavoidable, but the large uncertainties inherent in this procedure are not always recognized. Another procedure which may introduce error is the use of samples from correlated formations at some distance from the point of temperature measurement, as for the Texas (Big Lake 1-B) determination. The samples had to be selected from cores from wells in Crane and Upton counties, and these samples (dolomites) may possess higher conductivities than the rocks at the Big Lake field; it is known that the conductivity of "limestone" increases appreciably with increase of dolomite (Birch and Clark, 1940; 1945).

For comparison with the Front Range, a mean value for the normal crust has been formed from the "best determinations." There are several ways of combining them: (1) assigning unit weight to each well, we find a mean of 1.06 microcal/cm²·sec, reflecting the low mean of the 18 Persian wells; (2) weighting the four regions equally, we find 1.14; (3) distinguishing two regions in South Africa of equal weight (Witwatersrand and Carnarvon), we find 1.20. A mean of from 1.1 to 1.2 is indicated as the best value. There is reason to believe that the lower value is more typical of a "normal" or sea-level crust (Birch, 1947a). The apparently high value at Carnarvon may be nearly normal for this altitude, while the lower values at Witwatersrand, at about the same altitude, approach the figure for a sea-level crust as a result of the great thickness in this locality of quartzites, dolomites, and lavas, presumably of lower radioactive content than granite.

The means, as well as nearly all of the individual values, are thus smaller than the flow for the Front Range; with 1.1 ± 0.1 and 1.7 ± 0.2 respectively as the best values, the difference is 0.6 ± 0.2, or about half the normal flow. Although the uncertainties are not statistically determined, this difference is considered significant.

Table 19 includes a figure for the heat flow in the Central Alps, given in the letter from Koenigsberger to Lane cited above. As there is no mention of a correction for erosion or uplift, it is assumed that this is based on the steady-state correction for topography, probably according to Thoma's method. This value is close to the steady-state figures for Colorado. The corrections for a finite time of development would also be comparable; on the other hand, the conductivities given by Koenigsberger in published studies seem to be low, and the number of samples small. The details of the work thus require examination, but, on its face, this result for heat flow in the Alps supports the thesis that high values are to be expected in mountainous regions.

Though the present data are inadequate to determine a line with precision, a plot of heat flow as function of surface altitude does show a fair correlation. The measurements in the Rand are the only ones of high reliability which deviate widely; a possible reason for this has been suggested above. The correlation should be most significant between the "equilibrium" heat flow and altitude; the difference between present flow of heat and the "equilibrium" flow is presumably small for stable regions at low altitude, but may be appreciable for the mountain regions. Let us suppose, however, that the equilibrium flow for the Front Range is 1.7 microcal/cm²·sec. The "normal" variation of heat flow with mean altitude would be given by a straight line starting at 1.1 at sea level, reaching 1.7 at 3 km. The slope is 0.2 microcal/cm²·sec per kilometer of mean altitude. This is a reasonable rate of increase in terms of a thickening of a layer of granitic or intermediate rock. Deviations from such a

line of "normal heat flow", or "thermal anomalies", are of course to be expected. The prolongation of this continental line toward the ocean basins remains as one of the outstanding geothermal problems, of which investigation has just begun (Pettersson, 1949).

Discussion

Introduction

Taken together, the hypotheses of mountain roots and of concentration of radioactivity in the upper part of the crust lead to an expectation of an increased flow of heat in mountainous regions. This expectation has been verified in the Front Range, and probably also in the Alps. The most natural conclusion is that both hypotheses are at least qualitatively confirmed; the observed excess of geothermal flow may then be used for a determination of the mean radioactivity of the root, and this in turn for a calculation of the temperatures within the crust. There are, of course, alternatives to this straightforward interpretation, some of which will be briefly examined.

It cannot be argued that abnormally high heat flow is associated *only* with mountain roots. In well-known areas—Yellowstone Park, Iceland, New Zealand, and elsewhere—conspicuous volcanic and thermal activity is reasonably ascribed to local magmatic bodies, probably relatively recent and shallow. Many kinds of observations support such an explanation for these regions, which are exceptional at present. For the Front Range, however, the hypothesis of a recent intrusion to a high level in the crust would have no basis other than the observed increment of thermal flow. An effort will be made to narrow the possibilities of this form of interpretation.

Of other special explanations, perhaps the most plausible is that the crust in this region is not thicker but merely more radioactive than normal. This proposal cannot be definitely refuted, and there is even a suggestion that it may be partly correct. We shall begin, therefore, with an examination of the available information on the distribution of radioactivity.

Distribution of Radioactivity

Since the compilations of Holmes (1933) and Jeffreys (1929; 1936), new studies, especially those of Piggot, Evans and Goodman, Hurley, Keevil and Davis, have greatly increased our knowledge concerning the distribution of the radioactive elements among different kinds of rocks, among different regions, within individual batholiths and magma series, and among the different mineral species. Nearly all this work deals with North American rocks. In precision, in the number of samples, and in scope of investigation, these recent studies so far outweigh the earlier work that rejection or retention of the latter has become of minor importance. A discussion of this material is planned for another occasion; a brief summary must suffice for the present purpose.

The greatest quantity of information bears on the radioactivity of granitic rocks; this classification often includes quartz monzonites and other rocks which might also be termed intermediate. There are a considerable number of determinations for intermediate and for basaltic rocks, and a few reliable measurements for ultrabasic rocks. Metamorphic rocks, though they probably form a large proportion of the "granitic layer," and sedimentary rocks have been little studied.

Among igneous rocks, the radioactive content usually decreases as the density increases, approaching the limit of reliable detection for ultrabasic rocks (dunite). Within petrologic categories, the range of activity is broad; many individual samples of basalt are more radioactive than many granites. Within individual batholiths or magma series, the range may be relatively narrow (Billings and Keevil, 1946). Significant regional variations, emphasized by Jeffreys (1942), appear to exist.

The mean rates of heat production for various groups of rocks are assembled in Table 21. The following values have been used for the rates of energy release of the different radioactive series: for the uranium series (U^{238} and U^{235}) $2.2 \cdot 10^{6}$ cal per year per gm of radium, or 0.72 cal per year per gm of uranium; for the thorium series, 0.20 cal per year per gm of thorium; for potassium, $20 \cdot 10^{-6}$ cal per year per gm of potassium (Gràf, 1948a; 1948b; Borst and Floyd, 1948; Ahrens and Evans, 1948). With this value, still somewhat uncertain, potassium contributes about 10 per cent of the total present energy release of the gran-

TABLE 21.—RADIOACTIVITY AND HEAT PRODUCTION OF ROCKS
(Numbers in parentheses are numbers of samples)

Authority	Radioactive elements Proportion by weight (gm/gm)			Heat generation (recalculated) in 10^{-13}cal/cm^3·sec
	Ra·10^{13}	Th·10^{6}	K	
Granitic rocks				
Jeffreys (1936) "all"	2.4 (122)	18 (60)	[0.028]†	7.9
"North America, Ireland, Etc."	1.6 (53)	8.1 (30)	[0.028]†	4.8
Evans and Goodman (1941)	1.37 (43)	13 (26)	[0.028]†	5.2
Billings and Keevil (1946) New Hampshire granites, (55)				6.3**
Senftle and Keevil (1947) North American granites	1.4 (1287)	13.5 (1287)	[0.028]†	5.1
Intermediate rocks				
Jeffreys (1936)	1.9 (36)	19 (4)	[0.02]†	7.4
Evans and Goodman (1941)	0.51	4.4	[0.02†]†	2.1
Senftle and Keevil (1947)	0.92 (297)	10 (297)	[0.02]†	3.9
Basaltic rocks				
Jeffreys (1936)	0.95 (106)	6.9 (55)	[.014]†	3.7
Evans and Goodman (1941)	0.38 (54)	3.9 (34)	[.014]†	1.8
Hurley (11 samples of Keweenaw basalt and diabase)				1.5**
Keevil *et al.* (1943) (170)*				1.3**
Ultrabasic rocks				
Davis (1947) (Dunite)	0.0046 (6)		[.0004]†	~0.03

* This compilation probably includes the values of Evans and Goodman, and Hurley.
† Estimated
** Calculated from α-activity

itic rocks, and about 20 per cent for the basaltic rocks. The best mean values for large samples are probably about $5 \cdot 10^{-13}$cal/cm^3·sec for granitic rocks, $4 \cdot 10^{-13}$ for intermediate rocks, between $1 \cdot 10^{-13}$ and $2 \cdot 10^{-13}$ for basaltic rocks, and less than $0.1 \cdot 10^{-13}$ for dunite.

The best indications of regional variation are to be found in the measurements of Senftle and Keevil (1947), who reported means for large numbers of samples, divided into 10 geographic groups. Radium and thorium were determined for composite samples made by mixing material from many different rocks; the corresponding values of heat production are given in Table 22. The range within each group cannot be found by this method, but an upper limit for the error of the mean may be estimated with the assumption that the stand-

ard deviation of a single observation would be equal to the mean value. The standard errors of the means of Table 22 are computed in this way and are probably too high. Even so, there are significant differences among the groups; the greatest departure from the mean of all groups, however, is only about 35 per cent. It is possible to find larger variations for smaller groups of samples or for smaller regions.

TABLE 22.—HEAT PRODUCTION FROM URANIUM AND THORIUM
After Senftle and Keevil
P(cal/gm · My)

Region	Granitic rocks		Intermediate rocks	
	No. of rocks	P	No. of rocks	P
1. Outside North America	30	6.4 ± 1.2		
2. Ontario and Quebec	396	4.0 ± 0.2	72	3.2 ± 0.4
3. New England, etc.	123	7.8 ± 0.7	31	4.7 ± 0.9
4. Eastern States	143	4.8 ± 0.4	20	2.3 ± 0.5
5. Central States	76	5.4 ± 0.6	17	3.8 ± 0.9
6. Southwestern States	50	5.9 ± 0.8	10	4.2 ± 1.3
7. West Coast States	52	4.6 ± 0.6	23	4.2 ± 0.9
8. Rocky Mountain States	199	7.6 ± 0.5	52	4.7 ± 0.7
9. Central Canada	126	5.9 ± 0.5	23	5.4 ± 1.1
10. British Columbia and Alaska	92	5.2 ± 0.5	49	3.5 ± 0.5
Mean (samples)	1287	5.5 ± 0.2	297	3.9 ± 0.2
Mean (regions)		5.8 ± 0.4		4.0 ± 0.3

Note: The standard errors have been computed on the assumption of a proportional scatter equal to one. *See* text.

The figures of Table 22 suggest that the granitic rocks of the Rocky Mountain States are, on the average, 30 per cent more radioactive than the mean for all North America; the corresponding figure for intermediate rocks is 20 per cent. This is insufficient to account for the observed excess of heat in the Front Range in terms of a normal thickness of the granitic layer. The excess is about half the total normal flow, of which the granitic layer alone may be expected to produce about half. Thus the heat production in the granitic layer below the Front Range would have to be roughly twice as high as for average granite. So high a mean value for a large sample is not supported by the results of Table 22, or by any other evidence.

An attempt to obtain the additional heat from deeper layers of normal thickness leads to a still sharper conflict with the data, unless the deeper material is assumed to have an activity approaching that of granitic or intermediate rocks. In this way, we return to the "granitic root." As will be shown below, even with a substantial granitic root, a mean rate of heat production somewhat higher than that of average granite may be required. To account for the excess of heat in terms of abnormal radioactivity of a normal crust involves a considerable, if not impossible, stretching of the data. This interpretation also ignores the gravitational evidence that the crust in this region is far from normal. A more rational approach, therefore, is to accept the probability of crustal thickening and to compute the radioactivity required to produce the excess of heat.

Estimated Radioactivity of Root

An increment of thermal flow of 0.6 microcal/cm²·sec is produced in a layer 15 km thick with a mean rate of heat production of $4 \cdot 10^{-13}$ cal/cm³·sec, or 10 km thick with a mean rate of $6 \cdot 10^{-13}$, and so on. These are rates consistent with measured values for granites and intermediate rocks (Tables 21, 22), but there

are two further points: (1) what is the probable root thickness in this area; and (2) what is the relation between the currently generated heat and the present surface flow of heat?

(Table 23) show isostatic anomalies only one-tenth or less as large as the Bouguer anomalies. Of these stations, however, only Pikes Peak is actually in the mountains, and its position is

TABLE 23.—GRAVITY ANOMALIES IN COLORADO

Station	*H* meters	Anomalies, mg.		
		Bouguer	Hayford 113.7 km	Airy-Heiskanen 40 km
44 Denver	1638	−216	−18	−10
42 Colorado Springs	1841	−219	−8	−5
273 Boulder	1630	−232	−15	−4
274 Lafayette	1595	−222	−21	−12
275 Brighton	1511	−197	−7	0
43 Pikes Peak	4293	−215	+19	+8
45 Gunnison	2340	−243	+18	+25
46 Grand Junction	1398	−184	+22	+32
276 Idaho Springs	2303	−229	+20	+21
(300, Woollard) Loveland Pass	(3660)	−289	−30	

Much of the isostatic reduction of the Airy-Heiskanen type has been based on an assumed difference of density of 0.6 between a light upper layer and a dense lower layer, with compensation determined as if every surface feature possessed its own complete local "root" (Heiskanen, 1939). Although this scheme is generally recognized as artificial, it has the advantage of simplicity and is usually as successful in reducing the anomalies as more realistic assumptions. The extra thickness of root, T, below the normal sea-level crust is given at once for any height H above sea level by $T = \rho H/0.6$; with $\rho = 2.67$, this becomes $T = 4.45H$. The total additional thickness of the crust is then $5.45H$. The Front Range altitudes are between 2 and 4 km, with a mean in the neighborhood of the Adams Tunnel of about 3 km. The extra thickness of root on this assumption of densities is thus between 9 and 19 km, with a mean of about 13 km; the addition to the normal crust is on the average about 16 km. The root thicknesses are doubled if the density difference is taken as 0.3.

Determinations of gravity in Colorado are too few to support a detailed analysis of root structure, but it appears that compensation is nearly complete. Data for nine stations occupied by the U. S. Coast and Geodetic Survey exceptional. Woollard (1943) has occupied a number of stations on a traverse which cuts across the Front Range between Denver, Loveland Pass, and Grand Junction. The measurements are not tabulated, but Woollard's curve (Pl. 1) of isostatic (Hayford, 113.7 km) anomalies shows no value greater than 30 mg over the Front Range. The Bouguer anomalies reach nearly 300 mg and may be used, with various assumptions, for a direct estimate of root thicknesses. The region over which the (negative) Bouguer anomaly is 200 mg or more is about 300 km wide, so to a first approximation we treat the root as a horizontal sheet of great width and obtain the thickness from the simple relation for the attraction of a uniform plate of infinite extent. This attraction is $42\Delta\rho$ mg per kilometer of thickness; $\Delta\rho$ here is the difference of density between root and the material normally at the same level. With $\Delta\rho = 0.6$, this becomes 25 mg per km; thus to give an anomaly of 200 mg, a root of 8 km is required. This thickness will be increased by 50 per cent where the anomaly reaches 300 mg; an allowance for finite width of the root will increase it further. These figures are of the same order as those computed on the assumption of complete compensation.

The simplest imaginable "root" is obtained

by replacing a single uniform underlying material by the downward extension of uniform "crustal" material of lower density. Because of the general relation between radioactive content and density, this replacement of denser material by lighter should increase the local radioactive generation of heat. If we suppose that the present surface flow of heat is equal to the equilibrium flow, then a simple proportion furnishes a rough value for the radioactivity of the root.

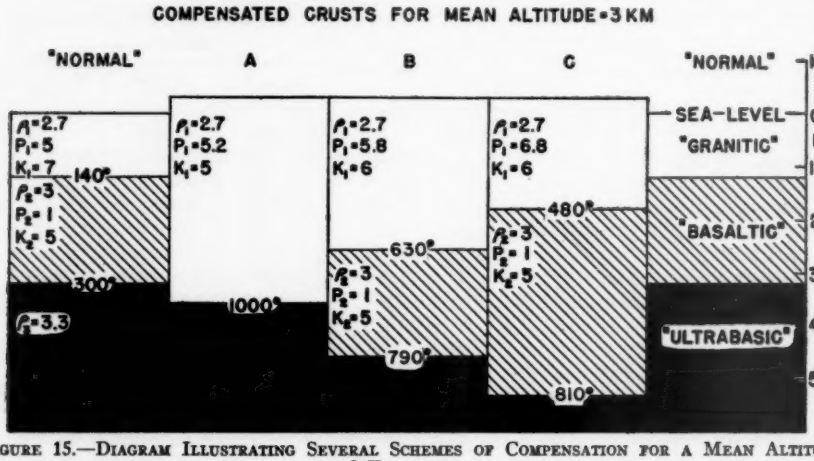

FIGURE 15.—DIAGRAM ILLUSTRATING SEVERAL SCHEMES OF COMPENSATION FOR A MEAN ALTITUDE OF 3 KILOMETERS

Also shown are estimates of equilibrium temperatures at the base of the several layers; these are computed for the values of conductivity K, and heat production P, given on the diagram. (*See also* Table 26 for other estimates.)

Let ρ be the density of the root, ρ_N the density of the replaced underlayer, P the heat generation (per cm³) of the root, P_N, of the underlayer. The increase of thickness of the "crust" for a mean surface altitude H is $\Delta T = H\rho_N/(\rho_N - \rho)$. The increase of surface heat flow is $\Delta Q = \Delta T\ (P - P_N) = H\rho_N\ (P - P_N)/(\rho_N - \rho)$. We have estimated above that $\Delta Q/H$ is equal to about 0.2 microcal/cm²·sec per kilometer; with this value, the relation becomes $20 \cdot 10^{-13} = (P - P_N)\rho_N/(\rho_N - \rho)$, with P and P_N in cal/cm³·sec.

For example, let "granite" replace basalt; $\rho_N = 3.0$, $\rho = 2.7$, $P - P_N = 2 \cdot 10^{-13}$. With P_N between 1 and 2 (times 10^{-13}), as suggested by Table 21, we find P between 3 and 4 (times 10^{-13}), a range more characteristic of "intermediate" rocks than of "granite." If "granite" replaces ultrabasic rock, we may take $\rho_N = 3.3$, $P_N = 0$, and find $P = 3.6 \cdot 10^{-13}$ for the "granite." If basalt replaces ultrabasic rock, then $P = 1.8 \cdot 10^{-13}$ for the basalt. All these values are acceptable in terms of the measured radioactivities of surface rocks.

The real distribution of compensation is of course not known, but it is possible to show, by treating somewhat more elaborate schemes, illustrated in Figure 15, that the conclusions are nearly independent of the assumed details of compensation. A "normal" sea-level crust is also shown in Figure 15 (*see also* Table 26); for the sake of consistency, the normal layers are assigned thicknesses such that, with average values for heat production, the total flow of heat will have the value $1.1 \cdot 10^{-6}$ selected as the best value for a "normal" crust. This flow is derived from: 12 km of granitic rock with a mean energy release of $5 \cdot 10^{-13}$ cal/cm³·sec, plus 20 km of "basaltic" rock, with mean energy release of $1 \cdot 10^{-13}$ cal/cm³·sec, plus a flow of $0.3 \cdot 10^{-6}$ cal/cm²·sec from beneath these layers, from all other sources. These thicknesses are comparable with those found in various regions by seismologists. The "normal" crust plays little part in schemes A and B, except to

determine the absolute depth of the root, and hence the correction for defect of equilibrium between surface heat flow and heat production in the root. In scheme C, the thickness of the root depends to some extent upon the original thickness adopted for the upper layer.

flow, 0.6 microcal/cm²·sec. Second, the mean heat production of the whole granitic layer is calculated from the *total* heat flow, 1.7 microcal/cm²·sec. In each case, three different values for the mean heat production P_2 of the basaltic layer are assumed: 0; $1 \cdot 10^{-13}$; and $2 \cdot 10^{-13}$cal/

TABLE 24.—ESTIMATED MEAN HEAT PRODUCTION

Units of 10^{-13} cal/cm²· sec; *see* Table 22.

	Scheme of compensation								
	A			B			C		
P_2 =	0	1	2	0	1	2	0	1	2
"Equilibrium"									
Granitic root only, by difference (±30%).....	2.3	3.0	3.7	—	3.6	—	6.7	4.7	2.7
Whole granitic layer, by total flow (±10%).....	—	3.6	—	4.9	4.2	3.5	6.7	5.0	3.3
"50 million years"									
Granitic root only, by difference (±30%).....	3.5	4.2	5.0	5.0	5.3	5.6	8.8	7.9	7.1
Whole granitic layer, by total flow (±10%).....	4.8	5.2	5.7	5.9	5.8	5.8	7.5	6.8	6.1

In scheme A, it is supposed that the granitic layer is thickened at the expense of the basaltic layer, which disappears under heights exceeding 2.2 km, and then by displacement of the lower layer. Such a situation might be imagined if the basaltic layer were forced from its position to issue at the surface or to intrude into or beneath the upper layer in another area. (*See* for example, Jeffreys, 1927; Lawson, 1948.)This is nearly equivalent to the assumption of a density difference of 0.3 between crust and substratum. In scheme B, the basaltic layer is simply pushed down, with no change of thickness (Kennedy and Anderson, 1938, p. 63); this is merely an assumption intermediate between A and C. In C, granitic and basaltic layers are thickened in the same ratio (1.75 for a mean height of 3 km and the supposed densities). These examples serve only to illustrate the effect of different root structures and do not, of course, exhaust the possibilities.

Calculations for each of these three imaginary structures have been carried out in several ways. First, the mean heat production P_1 of the granitic root, that is the thickness added to the "normal" granitic layer, or the excess over 12 km, is found from the *difference* of heat

cm²·sec. (*See* Table 2.) The heat production of the underlying material is taken as zero, but a value of $0.1 \cdot 10^{-13}$ would have an imperceptible effect on the present calculation. Of the total flow of heat, a value of 0.3 microcal/cm²·sec is again used for the flow from the interior.

If the heat produced in the thickened layers is supposed to be in *equilibrium* with the present surface flow, the mean heat production of the root, P_1, is given at once, by the first method, by the following relation, for scheme B:

$$0.6 \cdot 10^{-6} = 3 \cdot 10^{5} P_1 + 13.5 \cdot 10^{5} (P_1 - P_2) + 13.5 P_2,$$

$$\text{whence } P_1 = \frac{60 \cdot 10^{-13}}{13.5} = 3.6 \cdot 10^{-13} \text{ cal/cm}^2 \cdot \text{sec}.$$

In this case, P_1 is independent of P_2.

By the second method, we have

$$1.7 \cdot 10^{-6} = 0.3 \cdot 10^{-6} + 28.5 \cdot 10^{5} P_1 + 20\ P_2, \text{ or}$$
$$140 \cdot 10^{-13} = 28.5\ P_1 + 20\ P_2.$$

The values for P_1 thus found for various assigned values of P_2 are shown in Table 24.

To improve upon the simple assumption of equilibrium, it will be necessary to trace out the thermal history of the thickened crust for the last 50 million years. The initial thick-

ness, rates of erosion, and radioactivity of the sedimentary cover must be taken into account. This problem is complex, and much of the essential data uncertain; further elaboration is left for another occasion.

TABLE 25.—THE QUANTITY Erfc $L/\sqrt{4kt}$ FOR VARIOUS VALUES OF L AND t, FOR k = 0.01 cm²/sec = 32 km²/My

Depth L km	Erfc $L/\sqrt{4kt}$		
	t = 50 My	12.5 My	3.13 My
0	1.000	1.000	1.000
10	.860	.724	.480
20	.724	.480	.157
30	.596	.289	.034
40	.480	.157	.005
50	.377	.077	.001
60	.289	.034	—
70	.216	.013	—
80	.157	.005	—
90	.112	.001	—
100	.077	—	—

It is possible to find "upper limits" for the radioactivity of the crust, however, by ignoring such effects as initial heat, and erosion and uplift prior to Pliocene time, all of which tend to increase the present flow of heat. We may suppose that the present flow is equal to the sum of the heat production of the original "normal" crust plus that fraction of the heat production of the root now arriving at the surface. The values of mean radioactivity so computed will be too high, but it is of interest to find the difference between these and the "equilibrium" values. Even the latter may be slightly high as a result of the neglect of "initial heat," but rough computations suggest that, by an accidental balance between the residue of initial heat and of defect of equilibrium with the heat generation of the root, the present flow of heat approaches very nearly the equilibrium value for the present structure.

Suppose, then, that the root was formed 50 million years ago, in a time short by comparison with this interval. We obtain an approximate solution for the present contribution to flow at the surface by using the result for a steady plane source of heat (Carslaw and Jaeger, 1947, p. 222). The fraction of the current heat production of a steady plane source at depth L which reaches the surface at a time t after initiation of the source is erfc $L/\sqrt{4kt}$. Values of this function for a few depths and times, with k = 0.01 cm²/sec = 31.5 km²/My, are given in Table 25. It will suffice to take the value for the mean depth of the various layers.

With t = 50 My, the equation for the radioactive heat generation in the root becomes, for scheme B:

$$0.6\cdot10^{-6} = 3\cdot10^{5}(0.81)\,P_1 + 13.5\cdot10^{5}(0.70)(P_1 - P_2) + 13.5\cdot10^{5}(0.47)\,P_2,$$

whence $60\cdot10^{-13} = 11.9\,P_1 - 3.1\,P_2$. Similar calculations give the mean heat generation for the whole crust in terms of the total flow of heat. These values are given in Table 24 under the caption "50 million years."

In assessing the results of Table 24, we must bear in mind that the uncertainty of the values found "by difference" is at least as great as that of the difference of heat flow, or about 30 per cent; similarly, the uncertainty for the values found from the total flow is at least 10 per cent. Thus there are scarcely any significant differences between the comparable figures for the mean heat production of the root alone and for the whole granitic layer. Furthermore, nearly all the values fall within the range of the measurements for granitic or intermediate rocks. As P_2 is unlikely to be zero, the columns under P_2 = 1, and P_2 = 2, are most significant. These solutions satisfy the requirements with respect to gravitational compensation and heat flow and are consistent with the assumption of uniform distribution of radioactivity, on a large scale, of the same order found by laboratory determinations for granitic and intermediate rocks. As the figures of Table 24 do not vary greatly with moderate changes of the assumed thickness of the normal layers, and as the schemes of compensation which have been considered are fairly representative, these conclusions possess a high degree of general validity.

Other Hypotheses

General statement.—Let us now examine briefly a few of the other conceivable explanations for an abnormally high flow of heat: (1) mechanical compression; (2) initial heat of

TABLE 26.—CHARACTERISTIC OF SEVERAL SCHEMES OF COMPENSATION

(*See* Figure 15)

	"Normal crust"	Scheme of compensation for 3-km mean altitude		
		A	B	C
Density				
Granitic layer	2.7	for all schemes		
Basaltic layer	3.0			
Ultrabasic layer	3.3			
Thickness, km				
Granitic	12	38.6	28.5	21
Basaltic	20	0	20	35
Assumptions for estimates of temperature				
Mean conductivity K (millical/cm · sec · deg)				
Granitic	7	5	6	6
Basaltic	5	—	5	5
Mean flow of heat from the interior, all cases, 0.3 microcal/cm² · sec.				
Assumption 1. Equilibrium values (*see* Table 24)				
Mean heat production P, in 10^{-13} cal/cm³ · sec.				
Granitic	5	3.6	4.2	5.0
Basaltic	1	1	1	1
Equilibrium flow at surface, in microcal/cm² · sec	1.1	1.7	1.7	1.7
Equilibrium temperatures, °C, at base of				
Granitic	140	770	520	410
Basaltic	300	—	680	750
Assumption 2. "50 My" values (Table 24; *see also* Figure 15)				
Mean heat production P, in 10^{-13} cal/cm³ · sec.				
Granitic	5	5.2	5.8	6.8
Basaltic	1	1	1	1
Equilibrium flow at surface, in microcal/cm² · sec	1.1	2.3	2.2	2.1
Equilibrium temperatures, °C, at base of				
Granitic	140	1000	630	480
Basaltic	300	—	790	810

a nonradioactive root; (3) subcrustal currents; (4) intrusion of magma. We shall attempt to define the conditions under which an appreciable fraction of the observed flow of heat may be expected; but the demonstration of a possible effect from these hypothetical sources does not mean that they actually are present. Needless to say, highly idealized treatments of these questions must suffice; most of them are based on simple applications of the theory of the conduction of heat, and the derivations have been omitted.

Mechanical compression.—Since we are concerned with a phenomenon presumably observable over a large area, as indicated by the agreement between the results for the Adams and Moffat tunnels, local heating on widely spaced faults hardly recommends itself as a serious factor. We may postulate, however, that a wide prism, as thick as the crust, is at

present being slowly crushed by a compression normal to the strike of the mountains, and that this process generates heat uniformly throughout the crushed region. We estimate the proportion of the currently generated heat which reaches the surface at any time after the beginning of compression.

TABLE 27.—STRAIN AND STRAIN RATES FOR DIFFERENT DURATIONS OF CRUSHING
(H = 40 km)

β	$\phi(\beta)$	t(My)	Q = 0.6		Q = 0.06	
			$\dot{e}$ per My	e	$\dot{e}$ per My	e
0	1	∞	0.020	∞	0.002	∞
1	0.51	13	.039	0.50	.0039	0.05
2	.28	3.2	.071	.23	.0071	.023
4	.14	.8	.142	.11	.0142	.011
8	.07	.2	.284	.06	.0284	.006

For an approximation to the rate of heat production per unit volume, we assume that the crushing takes place at a constant stress F, as in ideal plastic flow. Let e be the strain, and $\dot{e} = de/dt$, the strain rate, or strain velocity, supposed constant. Then the rate of heat production per cm³ is $F\dot{e}$, and the rate per cm² of surface, $HF\dot{e}$, where F is a mean value for the whole thickness H of the crushed layer. The flow of heat Q at the surface at time t (measured from the beginning of crushing) is $Q = HF\dot{e}\,\phi(\beta)$, with $\beta = H/\sqrt{4kt}$, and $\phi(\beta) = (1/\sqrt{\pi} - \text{ierfc } \beta)/\beta$. We solve for $\dot{e}$ for various values of Q, F, H, and t. The total strain in the time t is $e = \dot{e}t$; in this form, the theory will be meaningful only for small values of strain.

As an example, let H = 40 km, $F = 10^4$ bars $= 10^{10}$ dyne/cm². Then $\dot{e} = 0.02/\phi(\beta)$ per My, for Q = 0.6 microcal/cm²·sec; a few values are given in Table 27. If we take Q equal to one-tenth of the observed excess of heat flow, the relation is $\dot{e} = 0.002/\phi(\beta)$ per My, and so on.

We now have to decide how great a strain or strain velocity is consistent with other information. It seems highly probable that the shortening required for Q = 0.6 microcal/cm²·sec is excessive. Whether any of the values under Q = 0.06 are acceptable is more questionable. Even 2 per cent in 3 million years, or 1 per cent in 0.8 million years seems high, though in terms of geodetic measurements the changes would be too small to be observed. With a strain rate of 0.01/My, the two sides of a belt 100 km wide approach one another at 1 mm/year or 10 cm/century. The change in a century is one part per million. Few present-day geodetic arcs have this precision, and none of a century ago. Over a million years, the shortening becomes a kilometer, with this rate, and might perhaps find geological expression.

The value assumed for F is probably too high, and consequently e and $\dot{e}$ may be too small. The results are not sensitive to changes of H; for β greater than about 2, $\phi(\beta)$ is very nearly $1/\beta\sqrt{\pi}$, and $\dot{e}$ is independent of H.

To summarize, mechanical compression is rejected as a major source of heat, but a contribution of the order of 10 per cent of the excess is perhaps not inconsistent with the available information.

Initial heat of a nonradioactive root.—At the time of Laramide folding, a considerable compression presumably occurred, and not only the root, but the whole mountain belt may have been heated above the normal temperature. In the following, we wish to determine the present flow of heat from such a source; the calculation is the same, of course, whatever process is held responsible for the initial heat, so long as continued generation of heat, as by radioactivity, is excluded.

Consider first a surface layer of thickness H, in which the temperature is everywhere raised by an amount ΔT above the normal temperature, whatever this may be. Then the contribution to the flow of heat at the surface, after a time t, is

$$\frac{K\Delta T}{\sqrt{4kt}} \cdot \frac{2}{\sqrt{\pi}} (1 - e^{-H^2/4kt}).$$

For t = 50 My, $\sqrt{4kt}$ = 80 km (with k = 0.01 cm²/sec = 32 km²/My). If we suppose that this flow equals 0.6 microcal/cm²·sec, we find ΔT for various values of H and t, as follows:

H (km) =		16	32	48	64	80
ΔT (°C)	t = 50My	13,500	3600	1800	1100	840
	t = 12.5My	1800	560	350	290	270

For t = 50 My, such increases of temperature would evidently imply melting; we conclude that no amount of mere heating, short of fusion, 50 million years ago, can account for the whole observed excess of heat flow. If the heating is supposed to have been more recent, the required temperatures, for a given thickness H, are much reduced, though even with t = 12.5 My it is doubtful whether the full amount of heat flow could be obtained without fusion.

The effect of a single convective overturn below a depth H can also be found from this solution. We imagine that a deep mass of material arrives beneath the layer of thickness H with an excess of temperature above the normal distribution everywhere equal to ΔT, and thereafter cools by conduction. At the time t after this event, the flow of heat at the surface will be increased by $K\ \Delta T\ e^{-H^2/4kt}/\sqrt{\pi kt}$. The values of ΔT required to give the total present excess of flow for t equal to 50 My and to 12.5 My are as follows:

H(km) =		16	32	48	64	80
ΔT (°C)	t = 50 My	550	620	760	1000	1500
	t = 12.5 My	310	500	1120	3500	14,500

Again, these temperatures imply fusion, except perhaps in the case of a relatively recent overturn bringing heated material to within 16 km of the surface, over a wide area.

To account for a fraction of the whole excess by these mechanisms, the required excess of temperature is of course correspondingly reduced, and acceptable solutions become possible, though the fraction must be very small in some cases.

To summarize, initial heat of a surface layer cannot supply the required flow at the surface without the assumption of temperatures in the range of fusion, unless the heating was relatively recent; the same conclusion is reached for heating by a single convective overturn, unless the crust is taken to be improbably thin.

Subcrustal currents.—The single overturn may be considered a special case of convection with low velocity. At the other extreme is a rate of overturn high enough to "maintain" an abnormally high temperature at or near the base of the crust. The effect at the surface depends upon the depth at which this temperature is maintained H, the amount of excess ΔT, and its duration t. The additional flow at the surface for this case is

$$\frac{K\Delta T}{H}\,(\operatorname{erfc}\beta + 2\beta e^{-\beta^2}/\sqrt{\pi}$$

with $\beta = H/\sqrt{4kt}$. We calculate ΔT required to produce the whole excess of heat flow for several values of H and t:

H(km) =		16	32	48	64	80
ΔT (°C)	t = 50 My	120	240	360	480	600
	t = 12.5 My	125	330	880	2900	13,000

With a crust of the order of 30 km thick, and t greater than 12 My, the required excess of temperature is moderate. On the other hand, the problem of obtaining a movement of material so close to the surface sufficiently rapid to maintain this temperature has not been dealt with. The velocity is necessarily small near the base of the crust, so the depth at which an excess of temperature can be maintained must be greater than the thickness of the crust. Thus we are again in doubt whether the condition can be met without recourse to fusion.

Magma.—Finally, we shall consider the effect of a single intrusion of magma, possessing latent heat. This problem is complicated, not only by the presence of latent heat, but also by ambiguity as to the details of crystallization. There are two relatively simple hypotheses: (1) We may suppose that the magma remains at a uniform temperature throughout until completely crystallized; in this case the time required for extraction of the latent heat can readily be estimated, and thereafter we have merely a problem of cooling from an initial temperature, similar to those considered above; (2) we may suppose that crystallization proceeds inward from the boundaries, the frozen material remaining in place; this case is more difficult, but useful solutions have been found (Jeffreys, 1927; Lightfoot, 1950; Ingersoll *et al.*, 1948, p. 190; Carslaw and Jaeger, 1947, p. 71, 227). In either case, the initial loss of heat is rapid, and a layer as thick as 20 km would freeze within a few millions of years. The contribution of the latent heat to the surface flow would rise to its maximum value in about the same time, and thereafter decline. By a time of 20 My after an intrusion which came to within

10 km of the surface, the effect of the latent heat would be minor.

To raise the present gradient by the observed amount, a non-radioactive magma would have to be either very large (thicker than some 20 km) or else relatively recent and near the surface. The latest important volcanism in the Front Range is assigned to Oligocene or Miocene time (Wahlstrom, 1947, p. 557), probably more than 20 million years ago, and it seems to have been localized along rather definite lines. A substantial contribution to the present flow of heat from this source seems unlikely, but an intrusion which would produce the present effect can unquestionably be "designed" if sufficient freedom is allowed for adjustment of depth, thickness, and time of intrusion.

Concluding Remarks

As we have seen, a number of explanations can be "adjusted" to satisfy the thermal observations alone. Most of these explanations lack the simplicity and freedom from special assumptions which characterize the interpretation in terms of mountain roots; furthermore, they leave the gravitational observations to be accounted for by still another and possibly conflicting set of special assumptions. Airy's conception of mountain roots affords a straightforward interpretation of the thermal as well as the gravitational and seismological data. It is necessary to assume only that the roots are approximately as radioactive as surface samples of granitic or intermediate rocks.

It is possible that a number of processes have contributed to the observed excess of heat, and that the estimates of the radioactivity of the root may consequently require some reduction, depending upon the proportion attributed to other sources. For the moment, refinements of this kind would be premature.

These conclusions have little bearing on the problem of the heat production in the deep interior of the earth. The flow of heat at the surface sets an upper limit to the amount of heat produced in the outer few hundred kilometers, but as yet it can be but little affected by conduction of heat generated either in the core or in the deeper parts of the mantle (Slichter, 1941). No distribution of radioactivity yielding a present contribution to the surface flow of less than, say, 0.2 microcal/cm²·sec can be rejected as incompatible with our present thermal data, whatever objections may be raised on other grounds. If currents are of importance in the transport of heat from the interior, then the limitation on the total amount of radioactivity is more severe.

Table 26 and Figure 15 show estimates of the "equilibrium" temperatures at the base of the various layers for several distributions of radioactivity; P_2 has been taken as $1 \cdot 10^{-13}$ cal/cm²·sec, and the flow from the interior as $0.3 \cdot 10^{-6}$cal/cm²·sec for all cases. A moderate increase in the mean radioactivity of the basaltic layer leads to considerably higher temperatures for schemes, such as C, involving thickening of this layer. The temperature at the base of a crust 50 km thick is also increased by about 100°C for every increment of $0.1 \cdot 10^{-6}$ cal/cm²·sec of the flow from the interior. The temperatures are inversely proportional to the thermal conductivities, for a given flow of heat; since assumed conductivities may be in error by perhaps 20 per cent, particularly at the higher temperatures, a similar uncertainty must be ascribed to the temperatures. Clearly, however, the temperatures beneath all these compensated crusts must eventually exceed the temperatures at corresponding depths beneath the normal crust; temperatures adequate for the formation of magmas may conceivably occur within the thickened crust.

As a result of this increase of temperature, the compensation, which has been assumed to be of the Airy type, gradually acquires some of the characteristics of the Pratt-Hayford type. With a Hayford depth of compensation of 100 km, a 3-km altitude requires a mean decrease of density of 3 per cent, for the whole 100-km column. To obtain such a decrease of density by variation of temperature alone, a mean difference of temperature of the order of 1000°C would be needed. This exceeds the mean differences of temperature of Table 26 by a considerable margin; nevertheless, with the gradual rise of temperature within the roots, there is an appreciable change of density which contributes to the elevation of the mountains. This effect may ultimately be offset by the increase of temperature and decrease of density

of the underlying medium. The natural consequence of the Airy scheme of compensation, in combination with the concentration of radioactivity in the upper layers, is thus an approach toward the apparently quite different scheme of Pratt and Hayford; such a combination of varying thickness and varying density has been employed by Heiskanen. Study of the variations of temperature and of density within thickened sections of the crust might be of value in the analysis of the history of mountains and of volcanism; although there have been a few such studies (*see* Lee, 1923, with papers by Van Orstrand and Lambert), it appears that the subject might be profitably reopened.

References Cited

Ahrens, L. H., and Evans, R. D. (1948) *Radioactive decay constants of K^{40} as determined from the accumulation of Ca^{40} in ancient minerals*, Phys. Rev., vol. 74, p. 279–285.

Anderson, E. M. (1938) See Kennedy and Anderson.

—— (1939) *The loss of heat by conduction from the earth's crust in Britain*, Roy. Soc. Edinburgh, Pr., vol. 60, p. 192–209.

Antevs, Ernst (1945) *Correlation of Wisconsin glacial maxima*, Am. Jour. Sci., vol. 243-A, p. 1–39.

Atwood, W. W., and Atwood, W. W., Jr. (1938a) *Opening of the Pleistocene in the Rocky Mountains of the United States*, Jour. Geol., vol. 46, p. 239–247.

—— —— —— (1938b) *Working hypothesis for the physiographic history of the Rocky Mountain region*, Geol. Soc. Am., Bull., vol. 49, p. 957–980.

—— and Mather, K. F. (1932) *Physiography and Quaternary geology of the San Juan Mountains, Colorado*, U. S. Geol. Survey, Prof. Paper 166, 176 pages.

Benfield, A. E. (1939) *Terrestial heat flow in Great Britain*, Roy. Soc. London, Pr., vol. A 173, p. 428–450.

—— (1947) *A heat flow value for a well in California*, Am. Jour. Sci., vol. 245, p. 1–18.

—— (1949a) *A problem of the temperature distribution in a moving medium*, Quart. App. Math., vol. 6, p. 439–443.

—— (1949b) *The effect of uplift and denudation on underground temperatures*, Jour. App. Phys., vol. 20, p. 66–70.

Billings, M. P., and Keevil, N. B. (1946) *Petrography and radioactivity of four Paleozoic magma series in New Hampshire*, Geol. Soc. Am., Bull., vol. 57, p. 797–828.

Birch, Francis (1947a) *Crustal structure and surface heat flow near the Colorado Front Range*, Am. Geophys. Union, Tr., vol. 28, p. 792–797.

—— (1947b) *Temperature and heat flow in a well near Colorado Springs*, Am. Jour. Sci., vol. 245, p. 733–753.

—— (1948) *The effects of Pleistocene climatic variations upon geothermal gradients*, Am. Jour. Sci., vol. 246, p. 729–760.

—— and Clark, Harry (1940) *The thermal conductivity of rocks and its dependence upon temperature and composition*, Am. Jour. Sci., vol. 238, p. 529–558, 613–635.

—— —— —— (1945) *An estimate of the surface flow of heat in the West Texas Permian basin*, Am. Jour. Sci., vol. 243-A, p. 69–74.

Borst, L. B., and Floyd, J. J. (1948) *The radioactive decay of K^{40}*, Phys. Rev., vol. 74, p. 989.

Bryan, Kirk, and Ray, L. L. (1940) *Geology of the Lindenmeier Site, Colorado*, Smithson. Misc. Coll., vol. 99, p. 85–105.

Bullard, E. C. (1938) *The disturbance of the temperature gradient in the earth's crust by inequalities of height*, Mon. Not. Roy. Astr. Soc., Geophys. Supp. vol. 4, p. 360–362.

—— (1939) *Heat flow in South Africa*, Roy. Soc. London, Pr., vol. A 173, p. 473–502.

Byerly, Perry (1939) *Near earthquakes in central California*, Seismol. Soc. Am., Bull., vol. 29, p. 427–462.

Carslaw, H. S., and Jaeger, J. C. (1947) *Conduction of heat in solids*, Oxford, 386 pages.

Clark, Harry (1941) *The effects of simple compression and wetting on the conductivity of rocks*, Am. Geophys. Union, Tr., pt. II, p. 543–544.

Coster, H. P. (1947) *Terrestrial heat flow in Persia*, Mon. Not. Roy. Astr. Soc., Geophys. Supp., vol. 5, p. 131–146.

Daly, R. A. (1933) *Igneous rocks and the depths of the earth*, McGraw-Hill, New York.

Davis, G. L. (1947) *Radium content of ultramafic rocks*, Am. Jour. Sci., vol. 245, p. 677–693.

Davis, W. M. (1911) *The Colorado Front Range*, Assoc. Am. Geog., Ann., vol. 1, p. 21–84.

Emmons, H. W. (1943) *The numerical solution of heat conduction problems*, Am. Soc. Mech. Eng., Tr., vol. 65, p. 607–615.

—— (1944) *The numerical solution of partial differential equations*, Quart. Appl. Math., vol. 2, p. 173.

Evans, R. D., and Goodman, Clark (1941) *Radioactivity of rocks*, Geol. Soc. Am., Bull., vol. 52, p. 459–490.

Fisher, Osmond (1889) *Physics of the Earth's Crust*, Macmillan, London.

Fitton, Edith M., and Brooks, C. F. (1931) *Soil temperatures in the United States*, Monthly Weather Rev., vol. 59, p. 6–16.

Grâf, T. (1948a) *Significance of the radioactivity of potassium in geophysics, II*, Phys. Rev., vol. 74, p. 831.

—— (1948b) *On the total half-life period of K^{40}*, Phys. Rev., vol. 74, p. 1199.

Gutenberg, B. (1943) *Seismological evidence for roots of mountains*, Geol. Soc. Am., Bull., vol. 54, p. 473–498.

Hann-Süring (1939) *Lehrbuch der Meteorologie*, Leipzig.

Heaton, Ross L. (1940) *Geological aspects of the Colorado-Big Thompson project*, Mines Mag., vol. 30, p. 257–264.

Heiskanen, W. (1939) *Catalogue of the isostatically reduced gravity stations*, Ann. Acad. Sci. Fennicae, Ser. A., vol. 51, 140 pages.

Hoel, Paul G. (1947) *Introduction to Mathematical Statistics*, Wiley, New York.

Holmes, Arthur (1933) *The thermal history of the earth*, Washington Acad. Sci., Jour., vol. 23, p. 169–195.

Hotchkiss, W. O., and Ingersoll, L. R. (1934) *Postglacial time calculations from recent geothermal measurements in the Calumet copper mines*, Jour. Geol., vol. 42, p. 113–122.

Ingersoll, L. R., Zobel, O. J., and Ingersoll, A. C. (1948) *Heat conduction*, McGraw-Hill, New York.

Jäckli, H., and Kleiber, K. (1943) *Temperaturstudien an Gebirgsquellen*, Eclog. geol. Helv., vol. 36, p. 8–15.

Jahnke, E., and Emde, F. (1938) *Tables of functions*, Teubner, Leipzig.

Jeans, J. H. (1927) *The mathematical theory of electricity and magnetism*, Cambridge University.

Jeffreys, Harold (1927) *On the earth's thermal history and some related geological phenomena*, Beitr. Geophys., vol. 18, p. 1–29.

—— (1929) *The Earth*, Cambridge Univ., 2d ed.

—— (1936) *On the radioactivities of rocks*, Beitr. Geophys., vol. 47, p. 149–170.

—— (1938) *The disturbance of the temperature gradient in the earth's crust by inequalities of height*, Mon. Not. Roy. Astr. Soc., Geophys. Supp., vol. 4, p. 309–312.

—— (1941) *The thermal state of the earth*, Am. Jour. Sci., vol. 239, p. 825–835.

—— (1942) *On the radioactivities of rocks*, Mon. Not. Roy. Astr. Soc., Geophys. Supp., vol. 5, p. 37–40.

Jones, W. D., and Quam, L. O. (1944) *Glacial land forms in Rocky Mountain National Park, Colorado*, Jour. Geol., vol. 52, p. 217–234.

Keevil, N. B., Keevil, A. R., Ingham, W. N., and Crombie, G. P. (1943) *Causes of variations in radioactivity data*, Am. Jour. Sci., vol. 241, p. 345–365.

Kellogg, O. D. (1929) *Foundations of Potential Theory*, Springer, Berlin.

Kennedy, W. Q., and Anderson, E. M. (1938) *Crustal layers and the origin of magmas*, Bull. Volcanologique, vol. 3, p. 1–80.

Kerner von Marilaun, F. (1905) *Über die Abnahme der Quellentemperatur mit der Höhe*, Meteor. Zeitschr., vol. 22, p. 159–164.

Koenigsberger, J. (With E. Thoma and H. Golz) (1908) *Versuche über primäre und sekundäre Beeinflussung der normalen geothermischen Tiefenstufe, und über die Temperaturen im Albula-, Arlberg-, Simplon-, Ricken-, Tauern-, und Bosrucktunnel*, Eclog. geol. Helv., vol. 10, p. 508–526.

—— (1937–1939) *Geothermische Messungen in Bergwerken und Übersicht über die Ergebnisse der Geothermik*, Beitr. angew. Geophys., vol. 7 p. 68–83.

Lane, A. C. (1923) *Geotherms of the Lake Superior copper country*, Geol. Soc. Am., Bull., vol. 34, p. 703–720.

——, *Chairman* (1942) *Report of the Committee on the measurement of geologic time*, Nat. Res. Council, Washington.

Lawson, A. C. (1948) *Some further implications of the doctrine of isostasy*, Geol. Soc. Am., Bull., vol. 59, p. 197–210.

Lee, W. T. (1923) *Building of the southern Rocky Mountains*, Geol. Soc. Am., Bull., vol. 34, p. 285–308.

Lees, C. H. (1910) *On the shape of the isogeotherms under mountain ranges in radio-active districts*, Roy. Soc. London, Pr., vol. A 83, p. 339–346.

Lightfoot, N. M. H. (1930) *The solidification o molten steel*, London Math. Soc., Pr., vol. 31, p. 97–116.

Lovering, T. S. (1928) *Geology of the Moffat Tunnel, Colorado*, Am. Inst. Min. Metall. Eng., Tr., vol. 76, p. 337–346.

Maurer, J. (1916) *Bodentemperatur und Sonnenstrahlung in den Schweizer Alpen*, Meteor. Zeitschr., vol. 33, p. 193–198.

Mezger, C. (1915) *Über die Temperatur der Erdrinde und ihre Beziehungen zum Luftdrucke*, Gluck auf, p. 1019.

Misener, A. D. (1949) *Temperature gradients in the Canadian Shield*, Canad. Min. Metall., Bull., Tr., vol. 52, p. 125–132.

Niethammer, G. (1910–1912) *Die Wärmeverteilung im Simplon*, Eclog. geol. Helv., vol. 11, p. 96–121.

Pettersson, Hans (1949) *Exploring the bed of the ocean*, Nature, vol. 164, p. 468–470.

Powers, W. E. (1935) *Physiographic history of the upper Arkansas Valley and the Royal Gorge, Colorado*, Jour. Geol., vol. 43, p. 184–199.

Ray, L. L. (1940) *Glacial chronology of the southern Rocky Mountains*, Geol. Soc. Am., Bull., vol. 51, p. 1851–1918.

Rayleigh, *see* Strutt.

Schardt, H. (1905) *Les resultats scientifiques du percement du tunnel du Simplon*, Bull. techn. de la Suisse romande, p. 1–46.

—— (1914) *Die geothermischen Verhältnisse des Simplongebirges in der Zone des grossen Tunnels*, Zurich, 20 pages.

Senftle, F. E., and Keevil, N. B. (1947) *Thorium-uranium ratios in the theory of genesis of lead ores*, Am. Geophys. Union, Tr., vol. 28, p. 732–738.

Shreve, Forrest (1924) *Soil temperature as influenced by altitude and slope exposure*, Ecology, vol. 5, p. 128–136.

Slichter, L. B. (1941) *Cooling of the earth*, Geol. Soc. Am., Bull., vol. 52, p. 561–600.

Somigliano, C., and Vercelli, F. (1913) *Sulla previsione matematica delle temperatura nei grandi trafori alpini*, Mem. R. Accad. Sci., Torino, vol. 63, p. 327–375.

Stapff, J. (1877) *Studien über die Wärmeverteilung im Gotthard*, Berne.

—— (1883–1884) *Some results of the observations on underground temperature during the construction of the St. Gotthard Tunnel*, North of England Inst. Min. Mech. Eng., Pr., vol. 33, p. 19–34.

Stark, J. T., Johnson, J. H., Behre, C. H., Jr., Powers, W. E., Howland, A. L., Gould, Don B., and Others (1949) *Geology and origin of South Park, Colorado*, Geol. Soc. Am., Mem. 33.

Stiny, J. (1933) *Zur Vorausbestimmung der Erdwärme im Bauwesen, besonders in Stollen und Tunneln*, Geol. Bauwesen, vol. 5, p. 77–123.

Strutt, R. J. (1906–1907) *On the distribution of radium in the earth's crust*, Roy. Soc. London, Pr., vol. 78, p. 150–153.

Thoma, Eugen (1906) *Über das Wärmeleitungsproblem bei wellig begrenzter Oberfläche und dessen Anwendung auf Tunnelbauten*, Inaug. dissert. Karlsruhe.

Van Orstrand, C. E. (1934a) *Temperature gradients, Problems of Petroleum Geology*, Am. Assoc. Petrol. Geol., p. 989–1021.

—— (1934b) *Some possible applications of geo-*

thermics to geology, Am. Assoc. Petrol. Geol., Bull., vol. 18, p. 13–38.

Van Tuyl, F. M., and Lovering, T. S. (1935) *Physiographic development of the Front Range*, Geol. Soc. Am., Bull., vol. 46, p. 1291–1350.

Volterra, V. (1912) *Sulle temperature nell' interno delle montagne*, Nuovo Cimento, vol. 4, p. 111–127.

Wahlstrom, Ernest E. (1947) *Cenozoic physiographic history of the Front Range, Colorado*, Geol. Soc. Am., Bull., vol. 58, p. 551–572.

Woollard, G. P. (1943) *Transcontinental gravitational and magnetic profile of North America and its relation to geologic structure*, Geol. Soc. Am., Bull., vol. 54, p. 747–790.

DUNBAR LABORATORY, HARVARD UNIVERSITY, CAMBRIDGE, MASS.

MANUSCRIPT RECEIVED BY THE SECRETARY OF THE SOCIETY, MAY 25, 1949

Paper No. 108. Published under the auspices of the Committee on Experimental Geology and Geophysics and the Division of Geological Sciences at Harvard University.

APPENDIX A

VALIDITY OF APPROXIMATE TREATMENT OF TOPOGRAPHY

Probably the best method of determining the degree of approximation achieved by the treatment of surface irregularity adopted above is by comparison with the exact solutions for a few simple cases. In general, the success to be anticipated depends upon the curvature of the surface, with the approximation improving as the surface becomes flatter; at shallow depths, under sharp angularities, the approximation is sure to be poor. It is important, therefore, that the curvatures of the surfaces in these examples bear some resemblance to those of the real topography. Only the steady state, for which the temperature satisfies Laplace's equation, will be considered.

As a first example, let us take a hemispherical depression in an otherwise plane surface. The solution for the steady-state temperature in the interior, when the surface, including that of the "bowl", is maintained at the uniform and constant temperature C, is known to be (Jeans, 1927, p. 194):

$$V = C + \alpha z(1 - a^3/r^3),$$

where z is the distance below the plane, r the radial distance from the center of the bowl, a the radius of the bowl, and α the vertical component of the thermal gradient at a great distance from the depression. This solution is the sum of the uniformly increasing temperature αz, and the field of the "point doublet" of strength $-\alpha a^3$, located at the center of the bowl, parallel to the z axis. At the point $z = r = 2a$, for example, the temperature is $C + 1.75\ \alpha a$. If the depression were filled up to the plane $z = 0$, level with the rest of the surface, the steady temperature at depth $2a$ would be $C + 2\alpha a$. The effect of the depression is to reduce the temperature at this point by $0.25\ \alpha a$, as compared with its value at the same place with the depression filled (the limiting gradient remaining equal to α); or we may say that the effective depth is seven-eights of the vertical distance below the plane surface. The depression has less and less effect at increasingly deeper points: for $z = r = 3a$, the effective depth is $3a\ (1 - \frac{1}{27})$; for $4a$, $4a(1 - \frac{1}{64})$, and so on.

By the approximate method, we calculate this temperature as follows: The effect of the depression is considered equivalent to a distribution of temperature over the horizontal plane through the bottom of the depression, such that the temperature at each point is proportional to the distance h from this plane to the actual surface, and to the gradient α. The effect of the part of the system above the plane $z = a$, at the point $z = r = 2a$, is then given approximately by the integral, $\frac{\alpha a}{2\pi}\int \frac{h}{a}\, d\Omega$ where $d\Omega$ is the element of solid angle subtended at the point $z = r = 2a$ by an element of surface of the plane $z = a$ distant by h from the true surface. In this simple case of symmetry about the z axis, the solid angle for a cone of half-angle ψ is $2\pi(1 - \cos\psi)$, and we divide the plane, $z = a$, into concentric rings determined by increments of ψ. The integral is evaluated as a sum, in the form,

$$\alpha\, a(1/a)\, \Sigma\, [h_1(\cos\psi_1 - \cos\psi_0) + h_2(\cos\psi_2 - \cos\psi_1) + \cdots],$$

where h_1, h_2, etc. are the mean values of h in the appropriate rings. The values, found graphically, are given below. The result of the summation is $0.78\ \alpha a$; to this must be added αa, for the effect of the layer between $z = a$ and $z = 2a$. The result is $1.78\ \alpha a$, instead of the exact value, $1.75\ \alpha a$.

This point was at a distance below the bottom of the depression equal to the radius. At greater depths the approximation should be better, and at shallower depths, worse.

ψ	$\cos\psi$	$\Delta(\cos\psi)$	h/a	$(h/a)\,\Delta(\cos\psi)$
0	1.0000	0.0152	0.006	0.0001
10°	.9848	.0451	.038	.0018
20°	.9397	.0737	.121	.0088
30°	.8660	.1000	.302	.0300
40°	.7660	.0589	.631	.0370
45°	.7071	.7071	1.000	.7071
90°	0			
				.7848

In this example, we used a uniform gradient plus the field of a point doublet centered at the surface $z = 0$. The shape of the isothermal surfaces may be altered by shifting the doublet up or down, though they remain symmetrical about the axis of the doublet. Surfaces resembling simple mountain ranges more closely are obtained by passing to two-dimensional cases, next to be considered.

In two dimensions, the "point doublet" becomes a "line doublet," derivable from the "line source" (or logarithmic potential in the steady state) by partial differentiation. The potential of the steady point source is A/r, with $r^2 = x^2 + y^2 + z^2$; of the point doublet with axis parallel to z, by $A\frac{\partial}{\partial z}(\frac{1}{r}) = -Az/r^3$. Similarly, in two dimensions, with $r^2 = x^2 + z^2$, the potential of the line source is $A\ log\ (1/r)$, and of a line doublet parallel to z by $A\frac{\partial}{\partial z}(log\ 1/r) = -Az/r^2$. For a simple example, analogous to the three-dimensional one treated above, we find the effect of an infinitely long valley of semicircular cross section by combining a uniform field with the field of a line doublet (Fig. 16A): say, $V = \alpha z\,[1 - a^2/(x^2 + z^2)]$. This is zero for $z = 0$, and for $x^2 + z^2 = a^2$. Temperatures are easily computed by the exact and approximate methods; a few values for the plane of symmetry are:

z/a	$V/\alpha a$		Ratio Approx./Exact
	Exact	Approx.	
1.5	0.833	0.885	1.062
2	1.500	1.586	1.056
3	2.667	2.764	1.036
4	3.750	3.838	1.024

The approximation becomes relatively better as the depth increases, but the absolute error remains between 0.05 αa and 0.09 αa for these depths. With a = 3000 feet (about like the North Inlet) and α = 10°F/kft, αa = 30°F, and these errors would be between 1.5° and 3.0°F. At Station 27, 1400 feet below the surface, an error of about 1.5°F might be expected.

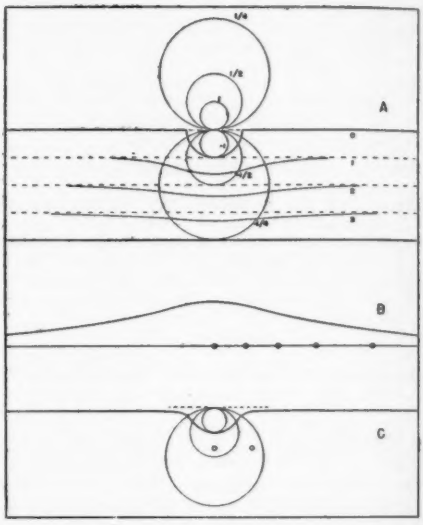

FIGURE 16.—COMBINATIONS OF A UNIFORM FIELD WITH THE FIELD OF A LINE DOUBLET

In (A), the center of the doublet is at the surface of the plane, with the negative part of the field downward; in (B), the center of the doublet is above the contour, with the positive part of the doublet field downward; in (C), the negative doublet field is turned downward, but the center of the doublet is above the surface of the plane. The small circles indicate the positions for which comparative calculations have been made.

The solution for an infinitely long symmetrical ridge, on which the surface temperature varies linearly with altitude, was given by Lees in 1910. Aside from a term for local heat production, Lees' solution is

$$V = V_0 + \alpha z + A(z + a)/[x^2 + (z + a)^2]$$

for a ridge of contour defined by

$$0 = (\alpha - \alpha')z + A(z + a)/[x^2 + (z + a)^2]$$

On the surface, the temperature is $V = V_0 + \alpha' z$, with z positive downward. The term A

$(z + a)/[x^2 + (z + a)^2]$ is the potential of a line doublet of strength A at the point $x = 0, z = -a$. Here α is the gradient of temperature in the rock, at great depth, α' the gradient on the surface. There are two adjustable parameters, A and a, for determining the shape of the ridge.

The field of the line doublet may also be written, $V = A \cos \theta/R$, where $R^2 = x^2 + (z + a)^2$, and $\cos \theta = (z + a)/R$. Thus the equations of equipotentials for the line doublet are $R = (A/V) \cos \theta = \rho \cos \theta$, where ρ is a constant for any given equipotential. In the x, z plane, the equipotentials determine two families of circles, all tangent at the center of the doublet, with radii $\rho/2$. On one side the values are positive, on the other negative (Fig. 16A). The center is a singular point and must be located outside the space in which we wish to find the potential.

We obtain a "valley" by taking the negative part of the doublet downward, in the direction of increasing z and increasing temperature. In this case, the center is always outside the region of interest. For a "ridge", the positive part is taken downward, but the center of the doublet must be a certain distance above the plane $z = 0$ if equipotentials with cusps at $x = 0$ are to be avoided. Without entering into details, we state the following conclusions: (1) if $\alpha' = 0$, so that the temperature is constant on the free surface, then, in order to avoid equipotentials with cusps, we must have $A/\alpha a^2$ less than $\frac{1}{4}$. If $A/\alpha a^2 = \frac{1}{4}$, the surface contour alone will have a cusp; (2) if α' is not zero, then, in order to avoid a cusp at $x = 0$, we must have $\dfrac{(\alpha - \alpha')}{\alpha} \cdot \dfrac{A}{\alpha a^2}$ less than $\frac{1}{4}$.

Let us apply this theory to a rounded ridge resembling the main mass of the Continental Divide (Fig. 16B). The height of the peak is taken to be 4000 feet above the "plain". The other dimensions are shown below. To calculate temperatures, let us assume the following values for α and α': $\alpha = 12°F/kft$, $\alpha' = 2.4°F/kft$. These are close to the actual gradients for the Adams Tunnel. The temperatures have been calculated by the exact method and by the approximate method for several points on the plane $z = 0$; these points are indicated in Figure 16B.

Contour of ridge, feet		Temperature, °F on plane, $z = 0$, at x	
x	$-z$	exact	approximate
0	4,000	27.79	27.2
2,802	3,618	26.78	27.1
5,789	2,894	23.95	24.4
9,275	2,171	19.69	19.8
14,400	1,447	13.96	14.3

By the approximate method, the "disturbance" of temperature at a point P resulting from the departure of the surface from a reference plane through the surface point directly above P is taken as $(\alpha - \alpha')hd\Omega/2\pi$. For the two-dimensional case, the element of solid angle becomes a dihedral angle, numerically equal to twice the element of plane angle, in the plane normal to the vertex of the dihedral angle. The values in the table have been found by computing the integral as a sum, with 10-degree increments of plane angle. The errors in this case are generally less than 0.5°F.

A "valley" much like the North Inlet in cross section (Fig. 16C) is obtained by placing a doublet of suitable strength slightly above a plane surface, with the negative part of the field downward. The dimensions are as follows:

x (feet)	0	720	1577	2049	2491
z (feet)	2000	1889	1416	944	472

With the thermal gradients as before, the temperature at $z = 3400$ feet, $x = 0$, 1400 feet below the bottom of the valley, is 20.7°F (exact), as compared with 21.8°F by the approximate method, applied graphically. For $z = 3400$ feet, $x = 3400$ feet, the temperatures are 26.3°F (exact), 28.4 approximate. (These temperatures have been adjusted with respect to those beneath the "ridge", so that the stations are all at the same level.) The curvature of the surface above this last point is evidently sharp, but not much more so than that of the real surface in the neighborhood of the North Inlet.

The real problem presents itself differently, in that we have measured temperatures and computed depths, $z - \bar{h}$, and wish to find $\alpha - \alpha'$. The comparisons of exact and approximate temperatures just given suggest that errors of determination of corrected depths

will rarely exceed 100 feet, equivalent to about 1°F. Uncertainty of about the same order arises from many other disturbances, and the standard deviation actually found is close to 1°F. With a distribution of 20 observations over a depth of 3000 feet, the statistical error on the slope turns out to be only a few per cent. The principal uncertainties are the systematic ones, which are not included in the estimate of error. It does not appear, however, that a significant systematic error is introduced by the method of computing the topographic correction, except insofar as the age of the topography is uncertain.

Appendix B

Effect of Departures from Assumed Conditions

When the observed temperatures and depths are corrected as described above, in terms of an assumption of uniform uplift and uniform initial temperature at each depth below an initially plane surface, deviations at the expected linear relation, amount at most to several degrees (F). Some part of these deviations is probably to be traced to the approximate treatment of the topography, discussed in Appendix A, and to other disturbances which have been considered. Still other sources of error are departures of the initial conditions from the simple uniformity postulated for the calculation of the corrections.

The "initial" surface was not a plane, but at best a rolling surface with hills and valleys reaching perhaps several thousand feet above or below the general level. As a consequence, the initial temperature was not uniform at what is now tunnel level, but was affected by the topography of that time; furthermore, the erosion to the present surface is not equal to the difference between present altitude and, say, 12,300 feet, but to the difference between present altitude and original altitude plus uplift. There may also have been differential uplift (faulting or warping) of some sections with respect to the rest. The thermal consequences of these effects depend upon the time which is taken as the initial time, or the time at which faulting occurred, and diminish as these times increase. The present temperatures are, however, fairly closely adjusted to the present topography. The correction to the steady-state gradient for a period of development of one million years (Table 13), without uplift, is only 1.2°F/kft or about 10 per cent of the gradient. Thus the original topography cannot have a very considerable residual effect, and a rough estimate will suffice.

The effect of an initial temperature $f(x, y, z)$ in the uniform half-space bounded by the plane $z = 0$, which is maintained at zero temperature, is (Carslaw and Jaeger, 1947, p. 308; there is an obvious misprint here, the function $f(x', y', z')$ appearing twice under the integral sign)

$$V(x, y, z, t) = (4\pi kt)^{-3/2} \int_{-\infty}^{\infty}\int_{-\infty}^{\infty}\int_{0}^{\infty} \cdot f(x', y', z') \exp\left[-\frac{(x-x')^2}{4kt}\right] \cdot \exp\left[-\frac{(y-y')^2}{4kt}\right]\left\{\exp\left[-\frac{(z-z')^2}{4kt}\right] - \exp\left[-\frac{(z+z')^2}{4kt}\right]\right\} dx'\, dy'\, dz'$$

As a simple form of initial temperature, consider $f(x, y, z) = A \cos ny$, a disturbance depending on the single coordinate y, parallel to the surface. This would be approximately true near the surface under a topography consisting of parallel and equal ridges and valleys of "wave length" $2\pi/n$. Then the triple integral given above is the product of three integrals, I_1, I_2, and I_3:

$$I_1 = (4\pi kt)^{-1/2}\int_0^{\infty} dz'\left\{\exp\left[-\frac{(z-z')^2}{4kt}\right] - \exp\left[-\frac{(z+z')^2}{4kt}\right]\right\} = \operatorname{erf}(z/\sqrt{4kt})$$

$$I_2 = (4\pi kt)^{-1/2}\int_{-\infty}^{\infty} dx' \exp\left[-\frac{(x-x')^2}{4kt}\right] = 1$$

$$I_3 = (4\pi kt)^{-1/2}\int_{-\infty}^{\infty} dy' \cos ny' \exp -\left[\frac{(y-y')^2}{4kt}\right].$$

The quantity I_3 is greatest for $y = 0$, at the center of a ridge or valley, for which it becomes $A \exp(-n^2kt)$. Thus the temperature at $(x, 0, z, t)$ is $V(x, 0, z, t) =$

$$A \exp(-n^2kt) \operatorname{erf}(z/\sqrt{4kt}).$$

For $t = 1$ My, and $z = 1$ km, with $k = 63$ km²/My, $z/\sqrt{4kt} = 0.063$, and erf (0.063) = 0.07. Thus the initial temperature A at this point would be reduced to 0.07 A by this factor alone. This would be the result for a uniform initial temperature. The other factor depends also upon the wave length $2\pi/n$, $= \lambda$, say; we have to evaluate exp $(-4\pi^2kt/\lambda^2)$. With the above values for t and k, this is exp $-(50/\lambda)^2$, with λ in kilometers. The whole length of the tunnel is about 21 km; if we regard this as about one half wave length, the exponential attenuation factor is about $\frac{1}{3}$, and the whole residual effect about 0.02 A. The present amplitude of the disturbance is 30°F; thus even with an initial relief as great as the present one, one million years ago, there might remain an effect of about 0.6°F. The lateral variation would be small over most of the central part of the tunnel, and the whole effect would be smaller near the ends where the depth z is smaller. For shorter wave lengths, there would be relatively greater variation along the tunnel, but the exponential attenuation would reduce the magnitude still further. Thus deviations from this source are probably beyond possible recognition.

The same sort of approximation may be used for investigating the consequence of differential uplift. Imagine a prism, indefinitely extended in the x direction, with vertical sides determined by the planes, $y = \pm a$, uplifted relatively to the material outside these planes by the distance H. In the interior, the prism will be momentarily warmer than material outside at the same level by the amount αH. Ignoring the projection of the upper surface of the prism above the general level, we have for the disturbance of temperature at (x, y, z, t):

$$V(x,y,z,t) = \alpha H\, I_1 I_2 I_4\,,$$

where I_1 and I_2 are given above, and

$$I_4 = (4\pi kt)^{-1/2} \int_{-a}^{+a} dy' \exp\left[-\frac{(y-y')^2}{4kt}\right]$$

$$= \frac{1}{2}\left[\operatorname{erf}\frac{y+a}{\sqrt{4kt}} - \operatorname{erf}\frac{y-a}{\sqrt{4kt}}\right]$$

At $y = 0$, the center of the prism, the disturbance is greatest, and is given by

$$V(x,0,z,t) = \alpha H \operatorname{erf}(z/\sqrt{4kt}) \operatorname{erf}(a/\sqrt{4kt}.$$

Deviations of one sign seldom persist for more than a few kilometers along the tunnel; in such a region, between Stations 10 and 16, say, the observed temperatures are about 2°F too low. We may inquire how great a downthrow of a block 2 km wide would be required to account for this difference of temperature, for various assumed times of faulting. We assume t, solve for αH, and thence for H, taking $a = 12$°F/kft; the depth z is about 0.7 km.

t, My	1.0	0.25	0.0625	0.0156	0
H, feet	47,000	12,000	3100	840	170

Evidently, if faulting is responsible for these deviations, it must be very recent, within the last 10,000 years. There is in fact a valley about 800 feet deep, described by Heaton (Progress Report III, p. 38), which crosses the tunnel line between Stations 12 and 14. "The west side of the valley is very steep cliff, with evidence of faulting and shearing on and at the foot of the cliff." There is little reason to suppose, however, that this feature is as young as 15,000 years, and a more likely explanation of the low temperatures might be percolation of water along the fault.

Another possibility is relative vertical movement on a single fault plane. Let a of the case just considered become large, and consider points $y = a + w$, where w is of the order of a few kilometers. We have

$$V = \frac{\alpha H}{2} \operatorname{erf}(z/\sqrt{4kt}\left[\operatorname{erf}\frac{2a+w}{\sqrt{4kt}} - \operatorname{erf}\frac{w}{\sqrt{4kt}}\right]$$

or, for a very large (compared with $\sqrt{4kt}$),

$$V = (\alpha H/2)\operatorname{erf}(z/\sqrt{4kt})[1 - \operatorname{erf}(w/\sqrt{4kt})].$$

With $z = 1$ km, the values of vertical differential movement required to give a difference of 2°F at the fault ($w = 0$) for various times of faulting are as follows:

t, My	1.0	0.25	0.0625	0.0156	0
H, feet	4700	2400	1200	640	333

The variation laterally away from the fault is also of interest. For $t = 0.25$ My, and a throw of 2400 feet, there is a variation of about 2.5°F between points 5 km from the fault, on opposite sides. The same difference would take place in half this distance for $t = 0.0625$ My and a throw of 1200 feet, and so on. Faulting

during the Pleistocene uplift may thus conceivably be responsible for some of the deviations, but there is little systematic difference between points at the same corrected depths on opposite sides of the Divide, at least in the central region. There are probably no recent faults with large vertical displacements in the central region, and very possibly none anywhere across the tunnel line.

The effect of gradual erosion of a uniform layer of thickness d is a steepening of the gradient of the order $2(\alpha - \alpha') d/\sqrt{\pi kt}$. With $k = 63$ km²/My, $t = 1$ My, and $\alpha - \alpha' = 18$°C/km = 10°F/kft, this is 2.55 d°C/km, with d in km, or 0.434 d°F/kft, with d in thousands of feet. If the initial surface possessed hills or valleys departing 1000 feet from the assumed level, then points immediately under such fearures might be in error by a maximum of 1.5°F, for a present cover of 3500 feet. The actual value would be less than this, depending upon the extent of the hill or valley. Features with dimensions of the order of a mile or so would produce only a fraction of the full effect. Most of the present hills are smaller than this. For peaks such as Longs Peak, the departure from the general level is about 2000 feet at the crest, but the area above 14,000 feet is negligible. Even the area above 13,000 feet is scarcely a mile across and, if centered on a tunnel station, would subtend less than one-fifth of the solid angle subtended by the whole surface. Actually, Longs Peak is 3 miles from the tunnel line, and its effect in this respect is negligible. This is the nearest of the present 14,000-foot peaks. On the other hand, so pronounced a feature as the valley of the North Inlet may have had some expression in the old-age topography, perhaps of the order of 1000 feet. Here the depth to the tunnel is less, and the solid angle subtended by the valley at Station 27 is roughly half of the whole angle. The indicated correction is still less than 0.5°F and if applied would increase the deviation of this point.

The smallness of all these second-order disturbances is reassuring with respect to the determination of gradient. A corollary is that information about the degree of planation at some earlier time, derivable from the study of the temperatures, is limited to statements of somewhat vague upper limits for relief and for differential movements.

INDEX TO VOLUME 61 (JANUARY–JUNE)*

Adirondack garnet deposits, Genesis of some. By S. B. Levin..... 519
Age determinations by lead ratios. By O. B. Muench.... 129
Alberta, Correlation of the Cretaceous-Tertiary transition in. By L. S. Russell..... 27
Analyses
  Petrofabric
    Storm King granite at Bear Mountain, New York. By K. E. Lowe..... 137
  – for age by lead ratios. By. O. B. Muench..... 129
Andes at about parallel 33° (Argentina-Chile), Geologic cross section of the Cordillera de los. By Félix González-Bonorino..... 17
Argentina, Geologic cross section of the Cordillera de los Andes at about parallel 33°. By Félix González-Bonorino..... 17
Arizona
  Cenozoic gravels on the rim of Sycamore Canyon. By W. E. Price, Jr..... 501
  Lava flows in Grand Canyon of Colorado River. By J. H. Maxson..... 9
Athens limestone at Riverton, Virginia, Conjugate sets of en echelon tension fractures in. By V. E. Shainin..... 509
Atlantic basement rocks. By L. D. Leet..... 411

Barton deposit, Gore Mountain, Adirondacks, Garnet deposits of. By S. B. Levin..... 519
Basement rocks, Atlantic. By L. D. Leet..... 411
Basin Ranges
  Panamint Range, California. By J. H. Maxson..... 99
  Tectonic theory viewed from. By C. R. Longwell..... 413
Bear Mountain, New York, Storm King granite at. By K. E. Lowe..... 137
BILLINGS, M. P.: Stratigraphy and the study of metamorphic rocks..... 435
Biogeochemistry
  Gold and silver content of some trees and horsetails in British Columbia. By H. V. Warren and R. E. Delavault..... 123
BIRCH, FRANCIS: Flow of heat in the Front Range, Colorado..... 567
Black Eagle sandstone member (new name). By L. S. Russell..... 27
Block faulting in western Montana, Late Cenozoic. By J. T. Pardee..... 359
British Columbia, Gold and silver content of some trees and horsetails in. By H. V. Warren and R. E. Delavault..... 123
Buckhorn conglomerate, Pediment concept applied to. By W. L. Stokes..... 91

California
  Moraine and shoreline relationships at Mono Lake. By W. C. Putnam..... 115
  Physiographic features of Panamint Range. By J. H. Maxson..... 99
  Volcanic geology of Toowa Valley, southern Sierra Nevada. By R. W. Webb..... 349
Cap rock, eastern New Mexico. By Sheldon Judson..... 253
Cenozoic block faulting in western Montana, Late. By J. T. Pardee..... 359
–gravels on the rim of Sycamore Canyon, Arizona. By W. E. Price, Jr..... 501
CHAPMAN, R. W.: Contact-metamorphic effects of Triassic diabase at Safe Harbor, Pennsylvania..... 191
Chile, Geologic cross section of the Cordillera de los Andes at about parallel 33°. By Félix González-Bonorino..... 17
Colorado, Flow of heat in Front Range. By Francis Birch.. 567
Comments on Taconic sequence in Pennsylvania. By G. W. Stose..... 133
Conjugate sets of en echelon tension fractures in the Athens limestone at Riverton, Virginia. By V. E. Shainin..... 509
Contact-metamorphic effects of Triassic diabase at Safe Harbor, Pennsylvania. By R. W. Chapman..... 191
Copper
  Hydrothermal alteration at Santa Rita, New Mexico. By P. F. Kerr *et al.*..... 275
Cordillera de los Andes at about parallel 33 (Argentina-Chile), Geologic cross section of. By Félix González-Bonorino..... 17
Correlation of the Cretaceous-Tertiary transition in Saskatchewan and Alberta. By L. S. Russell..... 27
Cretaceous-Tertiary transition in Saskatchewan and Alberta, Correlation of. By L. S. Russell..... 27

Dakota sandstone, Pediment concept applied to. By W. L. Stokes..... 91
DELAVAULT, R. E. (With H. V. WARREN): Gold and silver content of some trees and horsetails in British Columbia..... 123
Depressions of the northern portion of the Southern High Plains of eastern New Mexico. By Sheldon Judson..... 253
Diabase at Safe Harbor, Pennsylvania, Contact-metamorphic effects of. By R. W. Chapman..... 191
Dilatation as factor in ore localization, Lead, South Dakota. By J. A. Noble..... 221
Distribution of radioactivity in granites and possible relation to helium age measurement. By P. M. Hurley..... 1

Euxenite
  Analyses for age. By O. B. Muench..... 129

Faulting in Panamint Range, California. By J. H. Maxson 99
– –western Montana, Lake Cenozoic block. By J. T. Pardee..... 359
Flow of heat in the Front Range, Colorado. By Francis Birch..... 567
FREEDMAN, JACOB: Stratigraphy and structure of Mt. Pawtuckaway quadrangle, southeastern New Hampshire.. 449
Front Range, Colorado, Flow of heat in. By Francis Birch. 567

Gabbro, Adirondack garnetiferous. By S. B. Levin..... 519
Garnet deposits, Genesis of some Adirondack. By S. B. Levin..... 519
Genesis of some Adirondack garnet deposits. By S. B. Levin..... 519
Geochemistry
  Distribution of radioactivity in granites and possible relation to helium age measurement. By P. M. Hurley..... 1
Geologic cross section of the Cordillera de los Andes at about parallel 33° (Argentina-Chile). By Félix González-Bonorino..... 17
Geomorphology
  Cenozoic gravels on the rim of Sycamore Canyon, Arizona. By W. E. Price, Jr..... 501

* Full title of papers are in **boldface** type

Geophysics
Atlantic basement rocks. By L. D. Leet 411
Flow of heat in Front Range, Colorado. By Francis Birch 567
Gold and silver content of some trees and horsetails in British Columbia. By H. V. Warren and R. E. Delavault 123
— mine, Lead, South Dakota, Ore mineralization in Homestake. By J. A. Noble 221
GONZÁLEZ-BONORINO, FÉLIX: Geologic cross section of the Cordillera de los Andes at about parallel 33° (Argentina-Chile) 17
Gore Mountain, Garnet deposits of. By S. B. Levin 519
Grand Canyon of the Colorado River, Arizona, Lava flows in. By J. H. Maxson 9
Granite at Bear Mountain, New York, Storm King. By K. E. Lowe 137
Granites and possible relation to helium age measurement, Radioactivity in. By P. M. Hurley 1

HEALD, M. T.: Structure and petrology of Lovewell Mountain quadrangle, New Hampshire 43
Heat in the Front Range, Colorado, Flow of. By Francis Birch 567
HEIM, ARNOLD: Northwest of Lake Titicaca: critical remarks 407
Helium age measurement, Possible relation of radioactivity in granites to. By P. M. Hurley 1
High Plains, eastern New Mexico, Depressions in Southern. By Sheldon Judson 253
HOLTEDAHL, OLAF: Supposed marginal fault lines in shelf area off some high northern lands 493
Homestake gold mine, Lead, South Dakota, Ore mineralization in. By J. A. Noble 221
Horsetails in British Columbia, Gold and silver content of. By H. V. Warren and R. E. Delavault 123
HURLEY, P. M.: Distribution of radioactivity in granites and possible relation to helium age measurement 1
Hydrothermal alteration at Santa Rita, New Mexico. By P. F. Kerr, J. L. Kulp, C. M. Patterson, and R. J. Wright 275

Igneous rocks
Lava flows in the Grand Canyon of the Colorado River, Arizona. By J. H. Maxson 9

JUDSON, SHELDON: Depressions of northern portion of Southern High Plains of eastern New Mexico 253

KERR, P. F., *et al.*: Hydrothermal alteration at Santa Rita, New Mexico 275
Knickpoints
Physiographic features of Panamint Range, California. By J. H. Maxson 99
KULP, J. L. (With P. F. KERR *et al.*): Hydrothermal alteration at Santa Rita, New Mexico 275

Lake Russell, California. By W. C. Putnam 115
Lake Titicaca: critical remarks, Northwest. By Arnold Heim 407
Late Cenozoic block faulting in western Montana. By J. T. Pardee 359
Lava flows in the Grand Canyon of the Colorado River, Arizona. By J. H. Maxson 9
Leaching as cause of depressions of Southern High Plains, New Mexico. By Sheldon Judson 253
Lead, South Dakota, Ore mineralization in Homestake gold mine. By J. A. Noble 221
Lead ratios, Analyses for age by. By O. B. Muench 129
LEET, L. D.: Atlantic basement rocks 411
LEVIN, S. B.: Genesis of some Adirondack garnet deposits 519
LONGWELL, C. R.: Tectonic theory viewed from the Basin Ranges 413
Lovewell Mountain quadrangle, New Hampshire, Structure and petrology of. By M. T. Heald 43
LOWE, K. E.: Storm King granite at Bear Mountain, New York 137

MAXSON, J. H.: Lava flows in the Grand Canyon of the Colorado River, Arizona 9
—: Physiographic features of the Panamint Range, California 99
Metamorphic rocks, Stratigraphy and the study of. By M. P. Billings 433
Mineralization in the Homestake gold mine, Lead, South Dakota. By J. A. Noble 221
Mineralogy
Homestake gold mine, Lead, South Dakota. By J. A. Noble 221
— of Santa Rita area, New Mexico. By P. F. Kerr *et al.* 275
Monazite
Analyses for age. By O. B. Muench 129
Mono Lake, California, Moraine and shoreline relationships at. By W. C. Putnam 115
Montana
Late Cenozoic block faulting in western. By J. T. Pardee 359
Moraine and shoreline relationships at Mono Lake, California. By W. C. Putnam 115
Mt. Pawtuckaway quadrangle, southeastern New Hampshire, Stratigraphy and structure of. By Jacob Freedman 449
MUENCH, O. B.: Recent analyses for age by lead ratios 129

New Hampshire
Stratigraphy and structure of the Mt. Pawtuckaway quadrangle. By Jacob Freedman 449
Structure and petrology of the Lovewell Mountain quadrangle. By M. T. Heald 43
New Mexico
Depressions of Southern High Plains. By Sheldon Judson 253
Hydrothermal alteration at Santa Rita. By P. F. Kerr *et al.* 275
New York
Storm King granite at Bear Mountain. By K. E. Lowe. 137
NOBLE, J. A.: Ore mineralization in the Homestake gold mine, Lead, South Dakota 221
Northwest of Lake Titicaca: critical remarks. By Arnold Heim 407

Ore deposits
Ore mineralization in Homestake gold mine, Lead, South Dakota. By J. A. Noble 221
Stages of mineralization in Homestake gold mine, Lead, South Dakota. By J. A. Noble 221
Structural control of mineralization, Homestake gold mine, Lead, South Dakota. By J. A. Noble 221
— **mineralization in the Homestake gold mine, Lead, South Dakota.** By J. A. Noble 221

Panamint Range, California, Physiographic features of. By J. H. Maxson 99
PARDEE, J. T.: Late Cenozoic block faulting in western Montana 359
PATTERSON, C. M. (With P. F. KERR *et al.*): Hydrothermal alteration at Santa Rita, New Mexico 275

Pediment concept applied to Shinarump and similar conglomerates. By W. L. Stokes 91
Pennsylvania
Comments on Taconic sequence. By G. W. Stose 133
Contact-metamorphic effects of Triassic diabase at Safe Harbor. By R. W. Chapman 191
Peru, Northwest of Lake Titicaca: critical remarks. By Arnold Heim 407
Petrofabric analyses of Storm King granite at Bear Mountain, New York. By K. E. Lowe 137
Petrology
Genesis of some Adirondack garnet deposits. By S. B. Levin 519
– of Lovewell Mountain quadrangle, New Hampshire. By M. T. Heald 43
Physiographic features of the Panamint Range, California. By J. H. Maxson 99
Physiography
Late Cenozoic block faulting in western Montana. By J. T. Pardee 359
Pitchblende
Analyses for age. By O. B. Muench 129
Pleistocene, Mono Lake, California. By W. C. Putnam 115
– climate and depressions of Southern High Plains, New Mexico. By Sheldon Judson 253
Pliocene "cap rock," eastern New Mexico. By Sheldon Judson 253
PRICE, W. E., JR.: Cenozoic gravels on rim of Sycamore Canyon, Arizona 501
Profiles of canyons in Panamint Range, California. By J. H. Maxson 99
PUTNAM, W. C.: Moraine and shoreline relationships at Mono Lake, California 115

Radioactivity in Front Range, Colorado, Distribution of. By Francis Birch 567
– – granites and possible relation to helium age measurement. By P. M. Hurley 1
Recent analyses for age by lead ratios. By O. B. Muench 129
Riverton, Virginia, Conjugate sets of en echelon tension fractures in Athens limestone at. By V. E. Shainin 509
RUSSELL, L. S.: Correlation of the Cretaceous-Tertiary transition in Saskatchewan and Alberta 27

Safe Harbor, Pennsylvania, Contact-metamorphic effects of Triassic diabase at. By R. W. Chapman 191
Santa Rita, New Mexico, Hydrothermal alteration at. By P. F. Kerr *et al.* 275
Saskatchewan, Correlation of the Cretaceous-Tertiary transition in. By L. S. Russell 27
Scandinavian peninsula
Supposed marginal fault lines in shelf area off some high northern lands. By Olaf Holtedahl 493
Sedimentation
Cenozoic gravels on rim of Sycamore Canyon, Arizona. By W. E. Price, Jr. 501
Seismology
Atlantic basement rocks. By L. D. Leet 411
SHAININ, V. E.: Conjugate sets of en echelon tension fractures in the Athens limestone at Riverton, Virginia 509
Shinarump conglomerate, Pediment concept applied to. By W. L. Stokes 91
Shoreline relationships at Mono Lake, California, Moraine and. By W. C. Putnam 115
Sierra Nevada, California, Volcanic geology of Toowa Valley, southern. By R. W. Webb 349
Silver
Hydrothermal alteration at Santa Rita, New Mexico. By P. F. Kerr *et al.* 275
– content of some trees and horsetails in British Columbia. By H. V. Warren and R. E. Delavault 123
South Dakota, Ore mineralization in Homestake gold mine, Lead. By J. A. Noble 221
STOKES, W. L.: Pediment concept applied to Shinarump and similar conglomerates 91
Storm King granite at Bear Mountain, New York. By K. E. Lowe 137
STOSE, G. W.: Comments on the Taconic sequence in Pennsylvania 133
Stratigraphy
Northwest of Lake Titicaca: critical remarks. By Arnold Heim 407
– **and structure of the Mt. Pawtuckaway quadrangle, southeastern New Hampshire.** By Jacob Freedman 449
– – **the study of metamorphic rocks.** By M. P. Billings 435
Structural control of mineralization
Cross folds as control in ore localization, Lead, South Dakota. By J. A. Noble 221
Dilatation as factor in ore localization, Homestake gold mine, Lead, South Dakota. By J. A. Noble 221
Structure
Conjugate sets of en echelon tension fractures in Athens limestone at Riverton, Virginia. By V. E. Shainin 509
Contact-metamorphic effects of Triassic diabase at Safe Harbor, Pennsylvania. By R. W. Chapman 191
Late Cenozoic block faulting in western Montana. By J. T. Pardee 359
Northwest of Lake Titicaca: critical remarks. By Arnold Heim 407
Storm King granite at Bear Mountain, New York. By K. E. Lowe 137
Stratigraphy and the study of metamorphic rocks 435
Tectonic theory viewed from the Basin Ranges. By C. R. Longwell 413
– **and petrology of the Lovewell Mountain quadrangle, New Hampshire.** By M. T. Heald 43
– of Mt. Pawtuckaway quadrangle, southeastern New Hampshire. By Jacob Freedman 449
– – Panamint Range, California. By J. H. Maxson 99
Submarine geology
Atlantic basement rocks. By L. D. Leet 411
Supposed marginal fault lines in shelf area off some high northern lands. By Olaf Holtedahl 493
Supposed marginal fault lines in the shelf area off some high northern lands. By Olaf Holtedahl 493
Sycamore Canyon, Arizona, Cenozoic gravels on the rim of. By W. E. Price, Jr. 501

Taconic sequence in Pennsylvania, Comments on. By G. W. Stose 133
Tahoe glacial stage, Mono Lake, California. By W. C. Putnam 115
Tectonic theory viewed from the Basin Ranges. By C. R. Longwell 413
Tertiary transition in Saskatchewan and Alberta, Correlation of Cretaceous-. By L. S. Russell 27
Tioga glacial stage, Mono Lake, California. By W. C. Putnam 115
Toowa Valley, southern Sierra Nevada, California. By R. W. Webb 349
Trees and horsetails in British Columbia, Gold and silver content of some. By H. V. Warren and R. E. Delavault. 123
Triassic diabase at Safe Harbor, Pennsylvania, Contact-metamorphic effects of. By R. W. Chapman 191

Virginia
Conjugate sets of en echelon tension fractures in Athens limestone at Riverton. By V. E. Shainin..... 509
Volcanic geology of Toowa Valley, southern Sierra Nevada, California. By R. W. Webb..... 349
Vulcanism
Volcanic geology of Toowa Valley, southern Sierra Nevada, California. By R. W. Webb..... 349

WARREN, H. V., AND DELAVAULT, R. E.: Gold and silver content of some trees and horsetails in British Columbia..... 123
WEBB, R. W.: Volcanic geology of Toowa Valley, southern Sierra Nevada, California..... 349
Wind
Cause of depressions of Southern High Plains, New Mexico. By Sheldon Judson..... 253
WRIGHT, R. J. (With P. F. Kerr *et al.*): Hydrothermal alteration at Santa Rita, New Mexico..... 275

Zinc
Hydrothermal alteration at Santa Rita, New Mexico. By P. F. Kerr *et al.*..... 275